



Title	Studies on the Eukaryotic Ribosomal Exit Tunnel Function in Nascent Peptide-Mediated Ribosome Stalling
Author(s)	高松, 世大
Citation	北海道大学. 博士(生命科学) 甲第13953号
Issue Date	2020-03-25
DOI	10.14943/doctoral.k13953
Doc URL	http://hdl.handle.net/2115/78088
Type	theses (doctoral)
File Information	Seidai_TAKAMATSU.pdf



[Instructions for use](#)

Doctoral Dissertation

**Studies on the Eukaryotic Ribosomal Exit Tunnel Function
in Nascent Peptide-Mediated Ribosome Stalling**

新生ペプチド鎖が司るリボソーム停滞における
真核生物リボソーム出口トンネル機能の研究

Seidai Takamatsu

高松 世大

Graduate School of Life Science

Hokkaido University

March, 2020

Synopsis	ii
Abbreviations	v
1. Introduction	1
1.1. Structure and function of ribosomes	2
1.2. Translational regulation by ribosome stalling	5
1.3. Roles of ribosomes in plant developmental control	20
1.4. Tables	23
1.5. Figures	26
2. Characterization of regulatory nascent peptides that cause programmed ribosome stalling in eukaryotes using Arabidopsis cell-free extract for <i>in vitro</i> translation	31
Abstract	31
2.1. Introduction	32
2.2. Materials and Methods	34
2.3. Results	38
2.4. Discussion	43
2.5. Tables	45
2.6. Figures	47
3. Reverse genetics-based biochemical studies of the ribosomal exit tunnel constriction region in eukaryotic ribosome stalling: spatial allocation of the regulatory nascent peptide at the constriction	59
Abstract	59
3.1. Introduction	60
3.2. Materials and Methods	62
3.3. Results	66
3.4. Discussion	73
3.5. Tables	75
3.6. Figures	77
4. General discussion	98
References	102
Acknowledgements	119
List of publications	120

Synopsis

Historically, the ribosome has been described as a protein synthesis machinery in the cell rather than intrinsic regulator of mRNA translation. However, emerging studies revealed that ribosomal activity is highly regulated. Translational regulation is involved in a range of biological processes including metabolism, development, and stress responses.

A feature of polypeptide might have a strong influence on translational status. Regulatory nascent peptides have been identified to cause nascent peptide-mediated ribosome stalling (NPmRS) during translation on either the main open reading frame (ORF) or an upstream ORF (uORF), which is a small ORF present upstream of the main ORF of eukaryotic mRNAs. In both cases, the stalled ribosome inhibits translation of the succeeding ribosomes, either by blocking ribosomal scanning for initiation or blocking translation elongation, and thus down-regulates the translation of the mRNA. In eukaryotes, however, molecular mechanisms underlying how the nascent peptide works with the translating ribosome for the NPmRS induction is not fully understood. In this doctoral thesis, I conducted reverse genetics-based biochemical studies to obtain insights into the involvement of the ribosomal constriction region in mediating NPmRS.

For the NPmRS systems to be tested, I selected five genes from divergent eukaryotes, including virus, fungus, mammals, and plants, of which four have their relevant amino acid residues >20 from the stalling site. I also tested another NPmRS system, in which only six amino acids are encoded and is the shortest among the NPmRS systems thus far identified. Lastly, I tested the shortest possible uORF, AUG-stop. This minimum uORF codes for only one amino acid, methionine, and is not actually an NPmRS, but was included as a negative control.

To know whether these amino acid sequences could function in *Arabidopsis* ribosomes, I first investigated their stalling using an *Arabidopsis* cell-free extract (ACE) *in vitro* translation system prepared from wild-type *Arabidopsis* (Chapter 2). In all cases, I observed accumulation of peptidyl-tRNA, a translation intermediate, and, in cases when the 5'-UTR carrying the relevant uORF was placed before a reporter gene, down-regulation of expression was observed. These results showed that all NPmRSs to be tested are recapitulated in ACE *in vitro* translation system.

During translation, new peptide bonds are formed at the peptidyltransferase center in the ribosomal large subunit, and the growing peptide passes through the ribosomal exit tunnel that penetrates the large subunit before emerging from the ribosome. The exit tunnel is approximately 100 Å long and holds 30–40 amino acid residues of the nascent peptide. Since regulatory peptides are usually 20–30 amino acids long, they exert their function while residing inside the

exit tunnel. In the midst of the tunnel, there is a constriction region, where the tunnel narrows. This region has been suggested to function as a discriminating gate by interacting with the nascent peptide, and this is supported by recent structural studies of stalled ribosomes using cryo-electron microscopy. In contrast to bacteria, however, genetic evidence showing that the physical contacts of the nascent peptides and the constriction are the cause, and not the result, of eukaryotic NPmRS is still elusive. Therefore, I investigated contributions of the constriction region on the NPmRS induction (Chapter 3).

Among the ribosomal components that constitute the constriction region, I focused on ribosomal protein uL4. The uL4 protein contains two β -loop structures, both of which protrude into the exit tunnel to form the constriction in coordination with ribosomal protein uL22. Two types of mutant uL4s were used: a point mutation [uL4D(*R77A*)] and a small deletion [uL4D(Δ TV)]. The latter would alter the geometry around the constriction region. In Arabidopsis, cytosolic uL4 protein is encoded by two paralogous genes, *uL4A* and *uL4D*. Since double-*knockout* mutant of *uL4A* and *uL4D* is lethal, the mutant plants carry modified *uL4D:FLAG* gene in the genetic background of *uL4D knockout* mutant, in which endogenous *uL4A* is kept intact.

To know the functionality of mutant uL4D proteins, I first tested the association of FLAG-tagged uL4D proteins with 80S ribosomes with immunoblot analyses. The results showed that mutant uL4D proteins are efficiently incorporated into translating ribosomes, and the mutant uL4D-containing ribosomes can all achieve active translation. To confirm this, I then performed complementation analyses. The results showed that both *R77A* and Δ TV mutant uL4Ds complement the ribosome-deficient phenotypes, further supporting the functionality of mutant ribosomes *in vivo*. Therefore, I next examined effects of the two uL4D mutations on ribosome stalling using ACE prepared from transgenic lines carrying mutant uL4D-containing ribosomes.

Translation analyses showed that uL4D(Δ TV) mutant ribosomes reduced the ribosome stalling of the four eukaryotic systems, in which the nascent peptide is long enough to cross over the constriction region. Among these, two were also reduced in uL4D(*R77A*) mutant ribosomes. The difference is consistent with structural data obtained using cryo-electron microscopy. In contrast, NPmRS caused by the six-amino-acid uORF and the AUG-stop were unaffected. The results indicate that NPmRS is indeed affected by mutation of uL4 residues, but not all are affected in the same way.

In this doctoral thesis, I clearly showed that the constriction region of the ribosomal exit tunnel is crucial for most of the NPmRS systems that have their functional amino acids >20 amino

SYNOPSIS

acids. The results also explained the difference in spatial allocation of the nascent peptides in the constriction region that have been solved by the structural analyses. In contrast to these stalling systems in which the regulatory nascent peptide >20 amino acids, the one in which the relevant nascent peptide is too short to reach the constriction region uses a distinct mechanism for the induction of ribosome stalling. These findings provide new insights into regulatory mechanisms underlying the commonality and the specificity involved in eukaryotic NPmRS systems.

Abbreviations

AAP	arginine attenuator peptide
ACE	<i>Arabidopsis</i> cell-free extract
AdoMet	S-adenosyl-L-methionine
AMD	AdoMet decarboxylase
CGS	cystathionine γ -synthase
Col-0	<i>Arabidopsis thaliana</i> ecotype Columbia
cryo-EM	cryo-electron microscopy
DP	dipeptidyl-aminopeptidase B
gp48	glycoprotein gpUL4
GST (tag)	glutathione S-transferase
HA (tag)	human influenza hemagglutinin
hCMV	human cytomegalovirus
IP	immunoprecipitation
KO	<i>knockout</i>
LUC	firefly (<i>Photinus pyralis</i>) luciferase
MifM	membrane protein insertion and folding monitor
NIP5;1	nodulin 26-like intrinsic protein 5;1
NMD	nonsense-mediated mRNA decay
NPmRS	nascent peptide-mediated ribosome stalling
ORF	open reading frame
PTase	peptidyltransferase
PTC	peptidyltransferase center
RF	release factor
RLUC	sea pansy (<i>Renilla reniformis</i>) luciferase
r-protein	ribosomal protein
SecM	secretion monitor
SD sequence	Shine-Dalgarno sequence
Spd	spermidine
uORF	upstream ORF
UTR	untranslated region
VemP	<i>Vibrio</i> protein export monitoring polypeptide
WGE	wheat germ extract
XBP1	X-box binding protein 1

CHAPTER 1.

Introduction

ABSTRACT: Historically, the ribosome has been viewed as a ribozyme that converts the genetic information into an amino acid sequence of polypeptides rather than an intrinsic regulatory machinery that controls mRNA translation in response to cellular conditions. Recently, a number of regulatory nascent peptides have been shown to regulate gene expression by causing programmed ribosome stalling during translation. In this chapter, I summarize translational regulation by nascent peptide-mediated ribosome stalling. I first provide an overview of the structure and function of ribosomes (1.1). Then, I introduce several examples of translational regulations from bacteria to higher organisms including plants and mammals (1.2). Finally, I also introduce important roles of plant ribosomes in developmental control (1.3).

1.1. Structure and function of ribosomes

- 1.1.1. Protein synthesis
- 1.1.2. The peptidyltransferase center
- 1.1.3. The ribosomal exit tunnel

1.2. Translational regulation by ribosome stalling

- 1.2.1. Regulatory nascent peptides
- 1.2.2. Ribosome stalling on uORFs
- 1.2.3. Classification of regulatory nascent peptides
- 1.2.4. Biological aspects of programmed ribosome stalling
- 1.2.5. Genetic studies for programmed ribosome stalling

1.3. Roles of ribosomes in plant developmental control

- 1.3.1. Molecular organization of plant ribosomes
- 1.3.2. Phenotypes of ribosomal protein loss-of-function mutants
- 1.3.3. Roles of ribosomes in plant development
- 1.3.4. Differences and similarities between plants and animals

1.4. Tables

1.5. Figures

1.1 STRUCTURE AND FUNCTION OF RIBOSOMES

The ribosome is a macromolecular machine that is responsible for protein synthesis in all living organisms. All ribosomes are composed of two subunits, both of which are built from RNA and proteins; however, their composition and size differ significantly among the organisms (Figure 1.1) (Melnikov *et al.* 2012). Bacterial small and large ribosomal subunits have sedimentation coefficients of 30 and 50 Svedberg units (S), respectively, and together form the complete ribosome with a sedimentation coefficient of 70S. In contrast to their bacterial counterparts, the sedimentation coefficients for eukaryotic ribosomal small and large subunit is 40S and 60S, respectively, with a sedimentation coefficient of 80S for the whole eukaryotic ribosome particle. The eukaryotic 80S ribosome is much larger and more complex due to additional rRNA as well as eukaryote-specific ribosomal proteins (r-proteins) and their extension sequences (Figure 1.1) (Melnikov *et al.* 2012, Wilson and Cate 2012). In spite of these differences, all ribosomes possess a conserved core that is necessary for the basic functions of translation.

Each subunit has three binding sites for three different states of tRNA molecules: the A-site that is responsible for the recognition of aminoacyl-tRNA, the P-site that binds to peptidyl-tRNA, and the E-site that holds deacylated tRNA before it dissociates from the ribosome. Both subunits have different functions during protein synthesis. The small subunit contains the mRNA exit site (5'-end of the mRNA) and the decoding center, where codon and anticodon are paired to ensure the fidelity of translation. The large subunit contains the peptidyltransferase center (PTC), where peptide bond formation is catalyzed.

1.1.1 Protein synthesis

Protein synthesis is carried out on the ribosome in a series of reactions, termed the translation cycle. The translation cycle proceeds in three steps: initiation, elongation, and termination. In each of these steps, additional protein factors are required, many of which are GTPase that are activated by the ribosome itself.

Initiation of translation

Bacterial and eukaryotic ribosomes use different strategies to recruit an mRNA during initiation. In bacteria, an initiator tRNA is loaded onto the ribosomal small subunit along with three initiation factors. This ternary complex (preinitiation complex) binds to the first initiation codon of the

mRNA template, and then associates with the large subunit to form an initiation complex of translation. A nucleotide sequence, called the Shine-Dalgarno sequence (SD sequence), plays an important role to anchor the small subunit at the correct location on mRNA. The initiator tRNA is bound to the P-site of the ribosome while the A-site is empty. In eukaryotes, a similar complex is formed by the small subunit, initiation factors, and the initiator tRNA. Instead of the SD sequence, the preinitiation complex recognizes the 7-methylguanosine cap, to which several initiation factors are bound, at the 5'-end of mRNA. This preinitiation complex then moves forward (5' to 3') along the mRNA, searching for an initiation codon. Additional eukaryotic initiation factors are involved in this process.

Elongation of translation

In both bacteria and eukaryotes, elongation is conservative and contains three steps, namely decoding, peptide bond formation, and translocation. During the first step, an aminoacyl-tRNA with an anticodon complementary to the mRNA codon binds to the A-site of the ribosome. The decoding center is located on the ribosomal small subunit. In the second step, the aminoacyl-tRNA in the A-site reacts with a peptidyl-tRNA bound to the P-site to form a peptide bond, resulting in a deacylated tRNA in the P-site and the peptidyl-tRNA in the A-site that is extended by one amino acid. The reaction takes place at the PTC of the large subunit. The cycle of elongation is completed by peptidyl-tRNA translocation from the A-site to the P-site; during this movement, the deacylated tRNA moves to the E-site and dissociates from the ribosome. For the first and the third steps, GTP hydrolysis of elongation factors is required.

Termination of translation

Termination occurs when one of three termination codons (UAA, UAG, or UGA) reaches the A-site in the decoding center of the ribosomal small subunit. Termination codons are recognized by a release factor that promotes peptidyl-tRNA hydrolysis in the P-site, releasing completed polypeptides. Ribosome recycling factor binds together with the elongation factor to the post-termination ribosome, leading to the dissociation of the ribosome into two subunits to prepare for the next round of translation.

1.1.2 The peptidyltransferase center

New peptide bonds are formed at the PTC during translation. This reaction involves a nucleophilic

attack of the α -amino group of aminoacyl-tRNA on the ester carbonyl carbon of peptidyl-tRNA in the P-site. This reaction leads to formation of peptidyl-tRNA in the A-site and the peptide is extended by one amino acid residue and deacylated tRNA in the P-site (Figure 1.2). Another chemical reaction at the PTC is peptidyl-tRNA hydrolysis, which is required for the release of fully assembled polypeptides from the ribosome during translation termination (Figure 1.2). In this reaction, water molecule attacks the ester carbonyl carbon of peptidyl-tRNA bound to the P-site, leading to the transfer of nascent peptide to the water molecule.

The PTC is located on the ribosomal large subunit and is almost all organized by the domain V of rRNA (Nissen *et al.* 2000). Therefore, the ribosome is regarded as a ribozyme with the rRNA being responsible for peptide bond formation (Morgan *et al.* 2000, Nissen *et al.* 2000). The ribosome utilizes an induced-fit mechanism in which substrates and active site residues are repositioned to facilitate the peptidyltransferase (PTase) reaction (Sievers *et al.* 2004). The PTC core is comprised of the universally conserved rRNA nucleotides including C2063, A2451, C2452, U2506, U2585, and A2602 of 23S rRNA (*E. coli* numbering of rRNA nucleotides is used unless otherwise stated) (Nissen *et al.* 2000). Upon peptide bond formation, proper accommodation of an aminoacyl-tRNA in the A-site induces specific movements of 23S rRNA nucleotides and reorients the ester group of the peptidyl-tRNA for a nucleophilic attack (Schmeing *et al.* 2005b). Accumulating biochemical studies have demonstrated the fundamental importance of these rRNA residues. Indeed, their mutations are dominantly lethal in *E. coli* (Thompson *et al.* 2001, Sato *et al.* 2006).

1.1.3 The ribosomal exit tunnel

The growing nascent peptide passes through the ribosomal exit tunnel that penetrates the ribosomal large subunit before emerging from the ribosome. The exit tunnel is approximately 100 Å in length and the diameter is 10–20 Å in both bacteria and eukaryotes (Morgan *et al.* 2000, Nissen *et al.* 2000). The tunnel holds 30–40 amino acid residues of a nascent peptide provided that the nascent peptide adopts an extended conformation (Malkin and Rich 1967, Blobel and Sabatini 1970, Morgan *et al.* 2000, Nissen *et al.* 2000). The tunnel walls are primarily formed by the 23S/28S rRNA. At approximately 80 Å from the PTC, there is a vestibule near an exit port where the tunnel widens (Lu and Deutsch 2008, Kosolapov and Deutsch 2009). Formation of short α -helix and β -hairpin structures are observed in the last 20 Å of the tunnel (Nilsson *et al.* 2015). The exit tunnel also contains a constriction region located 30–40 Å from the PTC (Morgan

et al. 2000, Nissen *et al.* 2000). The β -loop structures of two r-proteins, uL4 (formerly L4; Ban *et al.* 2014) and uL22 (formerly L17 in eukaryotes and L22 in prokaryotes; Ban *et al.* 2014), protrude into the exit tunnel to form the constriction, where the tunnel narrows (Morgan *et al.* 2000, Nissen *et al.* 2000). This region has been suggested to function as a discriminating gate by interacting with growing nascent peptides in programmed ribosome stalling (Nakatogawa and Ito 2002).

In eukaryotes, the constriction is narrower than in bacteria because of additional insertions in uL4. Although the significance of this difference between bacteria and eukaryotes is unclear, it has been suggested that the narrower size of the constriction in eukaryotes may block the access of several macrolide antibiotics to the PTC (Tu *et al.* 2005, Zaman *et al.* 2007). Genetic studies showed that an insertion of six amino acids in the β -loop of uL4 endows the *E. coli* ribosome with a resistance to macrolides, which is similar to eukaryotic ribosomes (Lawrence *et al.* 2008).

On the solvent side, the rim of the exit tunnel contains several bacteria- or eukaryote-specific r-proteins and extensions: bL17 and bL32, and an insertion in uL24 in bacteria and eL19 and eL31 in eukaryotes (Ban *et al.* 2014). These differences are partly associated with N-terminal processing of nascent peptide. In bacteria, nascent peptides contain formyl group at the N-terminus as a result of the special modification of initiator tRNA. During protein synthesis, the formyl group is cleaved by the bacteria-specific deformylase through the interaction with bL32 (Bingel-Erlenmeyer *et al.* 2008). Since initiator tRNA is not formylated in eukaryotes, the corresponding positions to bL17 and bL32 on the ribosomal large subunit are occupied by other eukaryote-specific r-protein, eL31. In yeast, eL31 is associated with eukaryote-specific chaperone ZUO1 and is involved in co-translational folding of growing peptides (Peisker *et al.* 2008).

1.2 TRANSLATIONAL REGULATION BY RIBOSOME STALLING

Features of nascent peptide could affect the rate of translation or even direct the ribosome to stall during translation. Some of the nascent peptides, or the regulatory nascent peptides, contain an amino acid sequence that specifically interacts with the exit tunnel components, including the PTC and the constriction. Such programmed ribosome stalling is involved in translation regulation in both bacteria and eukaryotes as described below (Ito and Chiba 2013).

1.2.1 Regulatory nascent peptides

Nascent peptide-mediated ribosome stalling (NPmRS) is caused by the functional amino acid sequences of regulatory nascent peptides, but is independent of mRNA features, such as codon usages (Sørensen *et al.* 1989, Plotkin and Kudla 2011), local secondary structures (Doma and Parker 2006, Tholstrup *et al.* 2012), and complementary interaction of SD sequence with 16S rRNA (Li *et al.* 2012). Regulatory peptides act in *cis* on the ribosome during their own translation to induce ribosome stalling. Generally, these peptides are 20–30 amino acids long to interact with the exit tunnel component (Table 1.1a); however, it should be noted that some of them are long enough to have their N-terminus emerge from the ribosome. The nascent peptide outside the ribosome might also affect the stability of ribosome stalling (Yang *et al.* 2015, Fujiwara *et al.* 2018).

Regulatory nascent peptides have been found in a variety of organisms (Ito and Chiba 2013). Functional sequences are divergent in amino acids, whereas functional amino acid residues essential for the stalling are located near the PTC and constriction (Figure 1.3). Translation elongation can be inhibited at either the peptidyltransfer or the translocation step, leaving peptidyl-tRNA in the P-site or the A-site, respectively. Other stalling occurs during termination with a stop codon in the A-site of stalled ribosomes. Thus, both elongation and termination have a potential to be interfered in the NPmRS systems.

1.2.2 Ribosome stalling on uORFs

The translation status of the uORF regulates translation of the downstream ORF, including the main ORF (Kozak 1986, von Arnim *et al.* 2014, Hinnebush *et al.* 2016). The presence of uORF is not exceptional because 40–50% of mRNAs in mammals and 30–40% of mRNAs in higher plants have one or more of them (Crowe *et al.* 2006, von Arnim *et al.* 2014). Many of the uORFs are actually translated, as evidenced by ribosome profiling analyses that showed the presence of 80S ribosomes on the uORFs (Juntawong *et al.* 2013, Wethmar 2014). Translation of a uORF generally down-regulates the translation of the main ORF because those ribosomes that have translated the uORF will be dissociated from the mRNA (Hinnebush *et al.* 2016) (Figure 1.4A). The uORF may occasionally be overlooked and then translation starts at the start codon of the main ORF by a mechanism termed leaky scanning (Kozak 1999, 2002). The nucleotide sequence around the start codon, known as the Kozak sequence (Kozak 1986, Joshi *et al.* 1997), of uORF plays a major role in determining the frequency of leaky scanning (Figure 1.4B). When a very short

uORF is translated, the ribosome may not be fully dissociated at the termination codon and the small subunit may remain on the mRNA. The small subunit re-scans for the downstream start codon and reinitiates translation there (Kozak 1987, von Arnim *et al.* 2014, Wethmar 2014) (Figure 1.4C). If the ribosome stalls on the uORF, translation of the downstream ORF is severely inhibited by blocking the succeeding ribosomes (Hinnebush *et al.* 2016). The ribosome stalling on uORF can occur either during translation elongation or at translation termination, while most of the known stalling events in eukaryotes occur at the termination (Figure 1.4D).

1.2.3 Classification of regulatory nascent peptides

Regulatory nascent peptides can be classified into two categories (Table 1.1b). The inducible class of regulatory peptides senses a specific small molecule in conjunction with the translating ribosome. The known effector molecules include amino acids (tryptophan and arginine), a derivative of amino acid (S-adenosyl-L-methionine), polyamines, and antibiotics (erythromycin and chloramphenicol). This class of regulatory peptides directs the ribosome to stall only when the effector is present at a significant concentration. In contrast, the intrinsic class of regulatory peptides halts translation autonomously without any assistance by a metabolite or a drug; however, this class of ribosome stalling is subject to resumption of translation under physiological conditions.

1.2.4 Biological aspects of programmed ribosome stalling

Regulatory nascent peptides control gene expression by causing NPmRS at a specific position on mRNA. Therefore, the robust ribosomal occupation could affect cellular states of the mRNA, leading to repression of target genes (Figure 1.5), as well as mRNA degradation (Chiba *et al.* 2003; Onouchi *et al.* 2005, Tanaka *et al.* 2016), altered mRNA localization in the cell (Yanagitani *et al.* 2011), and mRNA recoding (Kurian *et al.* 2011).

The SecM system

E. coli *sec* operon encodes two different proteins: the 170-amino-acid leader peptide of SecM and an ATPase encoded by *secA*, which is involved in protein export. SecM is one of the most characterized examples of bacterial regulatory peptides that cause ribosome stalling autonomously. When the protein translocation activity is impaired, SecM stalling persists for a long time, which, in turn, leads to activation of the downstream *secA* expression (Nakatogawa

and Ito 2001). The stalled ribosome alters the mRNA structure to make the SD sequence of *secA* accessible to ribosomes (Nakatogawa and Ito 2001).

The C-terminal amino acid sequence of SecM, ¹⁵⁰FSTPVWISQAQGIRAGP¹⁶⁶ (important residues are underlined), is the *cis* element for autonomous stalling that occurs at Gly-165 (Nakatogawa and Ito 2002, Muto *et al.* 2006, Yap and Bernstein 2009). The stalled complex has peptidyl-tRNA in the P-site and Pro-tRNA^{Pro} in the A-site of the ribosome and is thus stalled during peptide bond formation (Muto *et al.* 2006). Genetic analyses identified essential residues of ribosomal components located in the mid-tunnel region (A751 and A2058 of 23S rRNA and Gly-91 and Ala-93 of uL22) and in the vicinity of the PTC (A2503 and A2062) (Nakatogawa and Ito 2002, Vázquez-Laslop *et al.* 2010). These results suggest that interactions between the nascent peptide and the exit tunnel are essential features of the SecM stalling mechanism.

Structural analyses of the SecM-stalled ribosomes using cryo-electron microscopy (cryo-EM) identified physical contacts of critical residues of nascent peptide with the exit tunnel components (Bhushan *et al.* 2011, Zhang *et al.* 2015). Near the PTC, the P-site-bound peptidyl-tRNA was found to be shifted away from its canonical position, as a consequence of interaction between Arg-163 of SecM and A2062 of 23S rRNA. Since precise positioning of the A-site and P-site tRNA substrates is required for peptide bond formation, even slight shifts of relative positions of the either substrate reduce the efficiency of peptide bond formation (Simonović and Steitz 2009). Therefore, this orientation of A2062 might trigger a relay of conformation changes around the PTC, leading to blockage of PTC activity. Mid-tunnel contacts are also observable between Trp-155 and A751 of 23S rRNA as well as between the N-terminal region of SecM and the β -loop of uL22. These interactions might assist in positioning Arg-163 in contact with A2062.

The TnaC system

E. coli tna operon encodes three proteins: the 24-amino-acid TnaC leader peptide, tryptophanase encoded by *tnaA*, and tryptophan permease encoded by *tnaB*. TnaC is another well-documented example of bacterial regulatory peptides that directs the ribosome to stall in the presence of high concentrations of L-tryptophan (Gong and Yanofsky 2002). The stalled ribosome precludes the access of a transcription termination factor ρ by covering its binding site on the mRNA to ensure transcription of the downstream *tnaA/B* (Gong *et al.* 2001). Elevated levels of free L-tryptophan inhibit peptide release by the release factor 2 (RF2) (Gong *et al.* 2001).

Thus, the ribosome stalls with Pro-24 codon in the P-site and a stop codon in the A-site (Gong and Yanofsky 2002).

TnaC uses the critical residue of Pro-24 for L-tryptophan-induced stalling (Gong and Yanofsky 2002), similar to the hCMV system (see below). Mid-tunnel residues Trp-12 and Asp-16 of TnaC are also shown to be essential for stalling (Cruz-Vera *et al.* 2005, Cruz-Vera and Yanofsky 2008). These residues might contact with different ribosomal components as evidenced by mutation, cross-linking, and methylation-protection experiments (Gong and Yanofsky 2002, Cruz-Vera *et al.* 2005, Cruz-Vera and Yanofsky 2008). Mid-tunnel mutations, which includes β -loops of uL4 and uL22, were identified by genetic screening for suppressors of L-tryptophan-induced stalling (Cruz-Vera *et al.* 2005). It has been suggested that the nascent peptide of TnaC and the exit tunnel cooperate in monitoring free L-tryptophan levels.

The cryo-EM analysis of the TnaC-stalled ribosomes provides structural insight into L-tryptophan-induced stalling (Bischoff *et al.* 2014). First, a number of critical residues of TnaC were in a defined conformation inside the exit tunnel and exhibited physical contacts to the tunnel wall, which is consistent with their importance shown by genetic studies. Second, two L-tryptophan molecules were shown to bind to the hydrophobic pockets formed by TnaC and 23S rRNA residues. Finally, compared with the crystal structure of release factor RF2-bound ribosome (Jin *et al.* 2010), the PTC adopted a conformation that would clash with the GGQ motif of RF2, which is required for peptidyl-tRNA hydrolysis (Zavialov *et al.* 2002, Mora *et al.* 2003). Taken together, the nascent peptide of TnaC cooperates with the ribosome to create specific binding sites for L-tryptophan molecules inside the exit tunnel. Stabilization of TnaC directs the PTC to be an unfavorable geometry, which precludes productive accommodation of the A-site-bound RF2.

The MifM system

In *Bacillus subtilis*, a leader peptide, MifM, is located upstream of a gene encoding YidC2, which is involved in membrane protein biogenesis. The 95-amino-acid nascent peptide of MifM causes ribosome stalling autonomously during translation elongation (Chiba *et al.* 2009, Chiba and Ito 2012). As is the case in the SecM system, *B. subtilis* ensures translation of sufficient levels of YidC2 to direct membrane protein insertion and folding by programmed ribosome stalling (Chiba *et al.* 2009).

MifM contains a functional C-terminal region, ⁶⁹RITTWIRKVF~~RM~~N~~SPV~~N~~DEED~~⁸⁹ (important

residues are underlined), which is critical for autonomous stalling. Remarkably, the ribosome stalls at four consecutive codons, namely Asp-89, Ala-90, Gly-91, and Ser-92 (Chiba and Ito 2012); however, the molecular mechanism of multisite stalling remains to be investigated. Mutational studies have identified six residues (Arg-69, Ile-70, Trp-73, Ile-74, Met-80, and Asn-81) of MifM located in the mid-tunnel region as well as the negatively charged DEED sequence (residues 86–89) as essential residues for ribosome stalling (Chiba *et al.* 2009, Chiba and Ito 2012). Despite the high conservation of the exit tunnel, MifM-induced stalling occurs on *B. subtilis* ribosomes, but not efficiently on *E. coli* ribosomes (Chiba *et al.* 2011).

The cryo-EM analysis of the MifM-stalled ribosomes provides structural insight into MifM-induced autonomous stalling in addition to its species-specificity (Sohmen *et al.* 2015). First, nascent peptide adopts a predominantly extended conformation and makes extensive interactions with exit tunnel components, including uL4 and uL22. Of all the contacts observed, only Lys-90 of uL22 is less conserved in *E. coli* and thus modulates the species-specificity of MifM stalling in *B. subtilis*. Second, conformation of the side chain of Glu-87 of MifM, part of the DEED motif, inhibits the PTC, in particular U2506 and U2585 of 23S rRNA, from adopting the conformations required for tRNA accommodation in the A-site. These rotated conformations might contribute to inhibition of peptide bond formation by perturbing accommodation of aminoacyl-tRNA at the A-site, which results in ribosome stalling.

The VemP system

VemP of *Vibrio alginolyticus* is one of the recently discovered examples among bacterial regulatory peptides. Similar to both the SecM and MifM systems mentioned above, the 159-amino-acid nascent peptide of VemP causes ribosome stalling autonomously in response to impaired protein export (Ishii *et al.* 2015). The stalled ribosome destabilizes an mRNA secondary structure that hinders the SD sequence for the downstream *secD/F*, both of which encode components of the protein targeting machinery, and allows *V. alginolyticus* to adapt to changes in salinity by modulating the SecDF expression (Ishii *et al.* 2015).

Ribosome stalling occurs at Gln-156 with peptidyl-tRNA at the P-site of the stalled ribosome (Ishii *et al.* 2015). A C-terminal region (residues 138–156) of VemP is highly conserved among *Vibrio* species and important for efficient ribosome stalling (Ishii *et al.* 2015, Mori *et al.* 2018). VemP-mediated regulation of SecDF expression is similar to other NPMRS systems including SecM and MifM (Nakatogawa and Ito 2001, Chiba *et al.* 2009), but the functional sequence of

VemP and release mechanism appears to be completely distinct (Ito and Chiba 2013, Ishii *et al.* 2015). Two mutations of uL22 (G91D and A93T) were previously isolated as stalling-defective mutants for SecM-induced ribosome stalling (Nakatogawa and Ito 2002), and these mutations showed distinct effect on VemP stalling; the former mutation dramatically decreased stalling efficiency, whereas the latter mutation did not (Ishii *et al.* 2015). Thus, specific interactions exist between the VemP nascent peptide and the interior of the ribosomal exit tunnel, and the interaction pattern of VemP is different from that of SecM.

Recently, the cryo-EM structure of the VemP-stalled ribosome has been determined and provided structural insight into VemP-induced autonomous stalling (Su *et al.* 2017). The nascent peptide adopts a compacted conformation in the exit tunnel and forms two α -helices in the exit tunnel. The α -helix in the upper region of the exit tunnel is comprised of the C-terminal residues of VemP and is directly linked to the P-site-bound tRNA. As a result of this α -helix formation, two nucleotides of 23S rRNA, U2506 and U2585, are stabilized in a unique conformation that is incompatible with peptide bond formation and thus contributes to the PTC inactivation. α -Helix formation has also been reported in the upper tunnel of the hCMV-stalled ribosome (Matheisl *et al.* 2015), but the α -helix of hCMV did not directly extend into the PTC-proximal region as observed for VemP. The linker between the two α -helices (residues 130–146) is located adjacent to r-proteins uL4 and uL22 and forms specific interactions with the constriction region; for example, a contact between Trp-143 of VemP and Arg-92 located at the tip of uL22 β -loop was observed. Consistently, alterations in uL22 reduced the efficiency of VemP-induced ribosome stalling (Ishii *et al.* 2015). Taken together, α -helix of VemP encroaches directly on the PTC and stabilizes an inactive state of the PTC that inhibits accommodation of the incoming tRNA at the A-site and therefore promotes ribosome stalling during peptide bond formation.

The ErmCL system

Drug-induced ribosome stalling is utilized by a variety of bacteria to regulate expression of antibiotic resistance genes in response to a low-level accumulation of the drug in the cell (Ramu *et al.* 2009). One of the most characterized examples is macrolide-dependent stalling during translation of Erm-type leader peptidase ErmCL (Vázquez-Laslop *et al.* 2008). In the presence of the macrolide erythromycin, the 19-amino-acid nascent peptide of ErmCL directs the ribosome to stall, which, in turn, ensures expression of the downstream *ermC*, which encodes Erm-type methyltransferases (Vázquez-Laslop *et al.* 2008). ErmC di-methylates A2058 of 23S rRNA to

confer resistance to erythromycin by reducing their affinity to the binding site on the ribosome (Skinner *et al.* 1983). In many cases, macrolide antibiotics bind within the ribosomal exit tunnel and inhibit translation of most proteins by blocking the path of growing peptides (Arenz *et al.* 2014, 2016).

The conserved C-terminal ⁶IFVI⁹ motif of ErmCL is critical for erythromycin-induced stalling that occurs at Ile-9 (Vázquez-Laslop *et al.* 2008). Since Ser-10 of ErmCL can be substituted to any amino acids without impairing ribosome stalling (Vázquez-Laslop *et al.* 2008), a peptide bond formation of the 9-amino-acid ErmCL-tRNA to any aminoacyl-tRNA is inhibited. Although alanine substitution at residues 2–6 did not impair erythromycin binding to the tunnel wall, N-terminal truncations abolished erythromycin-induced stalling (Vázquez-Laslop *et al.* 2008). These results suggest that N-terminus of ErmCL partially contributes to ribosome stalling albeit in an amino acid sequence-independent manner and that the mid-tunnel components is less efficient for the induction of ErmCL stalling than other stalling systems.

The cryo-EM analysis of the ErmCL-stalled ribosomes in the presence of erythromycin provides structural insight into erythromycin-induced ribosome stalling and the critical role of the PTC proximal region for ErmCL stalling (Arenz *et al.* 2014). First, the IFVI motif of ErmCL forms multiple contacts to the tunnel wall in the vicinity of the PTC, in particular U2506 and U2585 of 23S rRNA. Consistent with this, mutation of A2503, which is located in close proximity of U2506, severely reduced the efficiency of ErmCL stalling (Vázquez-Laslop *et al.* 2010). Second, erythromycin binds to the ErmCL nascent peptide via interactions between Phe-7 and the cladinose sugar moiety of erythromycin. Lastly, U2585 adopts an unusual conformation in the stalled ribosome compared to its canonical position during peptide bond formation. U2585 is known to be involved in PTase reaction and binding of peptidyl-tRNA to the P-site (Schmeing *et al.* 2005a, b). The rotated conformation of U2585 might contribute to inhibiting stable binding and accommodation of aminoacyl-tRNA in the A-site, thus leading to inhibition of peptide bond formation and ribosome stalling.

The AAP system

Both *Neurospora crassa arg-2* and its *Saccharomyces cerevisiae* ortholog *CPA1* encode carbamoyl phosphate synthetase, which is involved in arginine biosynthesis. The 24-amino-acid nascent peptide encoded by *arg-2* uORF, termed the arginine attenuator peptide (AAP), causes ribosome stalling during translation termination to repress *arg-2* expression in the presence of

high concentrations of L-arginine (Wang and Sachs 1997). The stalled ribosome blocks additional ribosomes from scanning to the downstream ORF, thus reducing translation of *arg-2* (Figure 1.5A) (Wang and Sachs 1997). Moreover, in yeast, ribosome stalling at the termination codon of *CPA1* uORF triggers nonsense-mediated mRNA decay (NMD) (Gaba *et al.* 2005).

AAP orthologs contain conserved residues of Asp-12, Tyr-13, and Asp-16, but its C-terminal segment (residues 21–24) and the stop codon were not evolutionary conserved (Spevak *et al.* 2010). In the mid-tunnel region, Thr-9 and Leu-14 of AAP are essential for L-arginine-induced ribosome stalling as well as conserved Asp-12 and Tyr-13 (Spevak *et al.* 2010). AAP depends mainly on these residues to mediate the mid-tunnel interactions; AAP nascent peptide can be cross-linked to uL4 and uL22 at several residues of AAP (Wu *et al.* 2012), although there is no genetic evidence supporting the involvement of ribosomal components in AAP stalling. Additionally, peptidyl-tRNA at the P-site of the stalled ribosome exhibited low reactivity to puromycin (Wei *et al.* 2012). Puromycin is an antibiotic that is widely used to monitor the PTC activity in stalled ribosomes (Cruz-Vera *et al.* 2005, Vázquez-Laslop *et al.* 2008, Yamashita *et al.* 2014). These results suggest that AAP nascent peptide and L-arginine together cooperate to interfere the PTC activity by interacting with the constriction region.

The cryo-EM analysis of the AAP-stalled ribosomes provides structural insight into L-arginine-induced ribosome stalling (Bhushan *et al.* 2010); however the effects of L-arginine on the structure have not been investigated. A number of contacts of AAP were observed with distinct regions of the exit tunnel. At the constriction region, AAP nascent peptide was in contact with the exit tunnel components, including uL4 and uL22. Consistent with this, a number of critical residues of AAP appear to be involved in these interactions, such as Ser-6, Thr-9, Asp-12, and Asp-16. Mutations of these residues abolished L-arginine-induced stalling (Wang and Sachs 1997, Delbecq *et al.* 2000, Spevak *et al.* 2010). In the PTC-proximal region, C-terminus of AAP adopted a compact conformation. The compaction of AAP was resulted from one turn of an α -helix, although an overall change in nascent peptide compaction in response to L-arginine was not observed in a PEGylation assay (Wu *et al.* 2012). Importantly, the loop of uL16 is in contact with the CCA end of AAP-tRNA at the P-site, suggesting that AAP stabilizes a distinct conformation of the PTC, in particular A2602 of 28S rRNA, that is not conducive to peptidyl-tRNA hydrolysis by the release factor eRF1. This pattern is reminiscent of that suggested in the TnaC system; it may be important for the anti-termination mechanism of AAP.

The hCMV system

The *gp48/UL4* (*gp48*) of human cytomegalovirus (hCMV), which encodes a 48-kDa glycoprotein, is preceded by three uORFs. The 22-amino-acid nascent peptide encoded by uORF2 cause ribosome stalling autonomously to down-regulate *gp48* expression during the early stages of infection (Geballe *et al.* 1986, Degnin *et al.* 1993, Cao and Geballe 1996). Similar to the AAP system, the stalled ribosome severely represses translation of the downstream *gp48* by blocking ribosomal scanning (Figure 1.5A) (Degnin *et al.* 1993, Cao and Geballe 1996). For this autonomous stalling, no mechanism to release the ribosome from stalling is known, which therefore leads to general down-regulation under normal condition, but the biological meaning of this in viral multiplication remains unclear.

Nascent peptide of hCMV stalls the ribosome in pre-termination state with a stop codon positioned in the A-site (Cao and Geballe 1996). hCMV inhibits peptide release and thus leads to accumulation of the ribosome-bound eRF1 in the A-site (Janzen *et al.* 2002). Five amino acid residues of uORF2, ¹MEPLVLSAKKLSLLTCKYIPP²² (important residues are underlined), are critical for hCMV stalling (Degnin *et al.* 1993, Alderete *et al.* 1999). Specifically, mutations of the P-site residue Pro-22 and the penultimate Pro-21 of uORF2, but not mid-tunnel residue Ser-12, increased hydrolysis activity of eRF1 in the stalled ribosome (Janzen *et al.* 2002), while did not affect accumulation of eRF3. eRF3 binds to eRF1 and stimulates eRF1 activity in a GTP-dependent manner. Thus, it has been suggested that C-terminal region of hCMV interfere with the eRF1 function and that mid-tunnel residues of hCMV interact with other ribosomal components, such as uL4 and uL22, although there is a lack of genetic studies for the involvement of the constriction region in hCMV stalling.

The cryo-EM analysis of the hCMV-stalled ribosomes provided structural insight into autonomous stalling of hCMV (Bhushan *et al.* 2010, Matheisl *et al.* 2015). Nascent peptide of hCMV forms one turn of an α -helix inside the exit tunnel. The compacted structure contributes to several contacts with the tunnel wall: the α -helix ends at the constriction region with the most distal His-133 of uL22 β -loop in close vicinity to essential residues Ser-7 and Ala-8 of uORF2. As a result of this α -helix formation, a pair of the C-terminal proline is stabilized in a distinct conformation, which, in turn, resulting in reorientation of nascent peptide that would clash with U2585 as well as adjacent U2586 and U2609. Mutations of these residues lead to loss of termination activity of ribosomes. Taken together, the nascent peptide of hCMV adopts a distinct positioning in the exit tunnel, which, in combination with the C-terminal proline pair, results in

specific perturbation of the PTC and thus ribosome stalling.

The CGS1 system

The Arabidopsis *CGS1* encodes cystathionine γ -synthase, which catalyzes the first committed step of methionine biosynthesis in plants. Expression of *CGS1* is negatively feedback-regulated by mRNA degradation in response to *S*-adenosyl-L-methionine (AdoMet), a direct metabolite of methionine (Figure 1.5B) (Chiba *et al.* 1999, 2003). In the presence of AdoMet, ribosome stalling occurs temporarily during translation elongation prior to mRNA degradation (Chiba *et al.* 2003, Onouchi *et al.* 2005). Since the 5'-ends of 5'-truncated RNA species are separated from each other by ~30 nt (Haraguchi *et al.* 2008, Yamashita *et al.* 2014), it has been suggested that endoribonuclease digestion occurs near the 5'-edge of the stalled ribosomes including those secondarily stacked ribosomes.

The 183-amino-acid sequence of the *CGS1* exon 1 coding sequence, which contains the MTO1 region, is necessary and sufficient for the regulation (Suzuki *et al.* 2001). The MTO1 region (residues 77–87) is the *cis* element for AdoMet-induced ribosome stalling that occurs at Ser-94 (Ominato *et al.* 2002, Onouchi *et al.* 2005). *CGS1* nascent peptide stalls the ribosome at a pre-translocation state with peptidyl-tRNA positioned in the A-site (Onouchi *et al.* 2005). This is a unique feature of the *CGS1* system among the known NPmRS systems (Ito and Chiba 2013). In response to AdoMet, the nascent peptide containing the MTO1 region adopts a compacted conformation in the exit tunnel (Onoue *et al.* 2011). Thus, AdoMet induces overall compaction of nascent peptide upon AdoMet-dependent ribosome stalling; however, which part of the nascent peptide is compacted remains to be elucidated.

Although any structural information of the *CGS1*-stalled ribosome is not available, two lines of biochemical evidence obtained from wheat germ extract (WGE) *in vitro* translation system have suggested the involvement of the exit tunnel in the *CGS1* system (Onoue *et al.* 2011). First, two nucleotides A879 and A885 of 28S rRNA exhibited distinct methylation patterns in the stalled ribosome (Onoue *et al.* 2011). These nucleotides correspond to *E. coli* 23S rRNA nucleotides EcU744 and EcA750, respectively, which are adjacent to EcA749-EcA753 and constitute the constriction. Second, UV cross-link patterns changed at U2955, U2956, and U2957 (Onoue *et al.* 2011), which correspond to EcU2584, EcU2585, and EcU2586, respectively. This region is known to contribute to PTase activity and peptidyl-tRNA binding to the P-site (Schmeing *et al.* 2005a, b). Taken together, nascent peptide and AdoMet cooperate with the ribosome to adopt a

specific conformation of the tunnel wall that could contribute to ribosome stalling; however, the presumptive binding site of AdoMet has not been identified.

Genetic analysis revealed physiological importance of AdoMet-induced regulation of *CGS1*. The *mto1* mutants, which are deficient in this response, overaccumulated 10- to 40-fold more soluble methionine than wild-type plants (Chiba *et al.* 1999). Although *CGS1* is a nuclear gene, CGS protein functions after transportation to the chloroplast. The later steps in methionine/AdoMet biosynthesis are carried out predominantly in the cytosol (Wallsgrove *et al.* 1983). Therefore, to finely tune methionine/AdoMet levels in the cytosol, feedback regulation during translation in the cytosol could be a reasonable strategy for plants.

The AMD system

Both mammalian *AMD1* (*mAMD1*) and Arabidopsis *AMD1* (*AtAMD1*) encode AdoMet decarboxylase that catalyzes one of the key steps in polyamine biosynthesis. Mammalian and plant cells use a similar strategy to down-regulate expression of *AMD1* by using a uORF in a polyamine-dependent manner (Figure 1.5A), but the lengths and the amino acid sequences of the uORFs are quite different (Ito and Chiba 2013). In mammal, the 5'-UTR sequence of *mAMD1* has a regulatory uORF that encodes six amino acids, MAGDIS (Hill and Morris 1992). MAGDIS stalls the ribosome in response to high concentrations of polyamines at a termination step, inhibiting ribosomal scanning for the initiation codon of the downstream *mAMD1* (Law *et al.* 2001, Raney *et al.* 2002). C-terminal residues Asp-4, Val-5, Ser-6 as well as a stop codon are required for the regulation (Law *et al.* 2001, Raney *et al.* 2002). MAGDIS is the shortest among the NPmRS systems identified so far and the nascent peptide is too short to reach the constriction region. Thus, the mid-tunnel elements such as uL4 and uL22 do not seem to be involved in *mAMD1* stalling. Further investigation is needed to determine how 6-amino-acid MAGDIS works together with the ribosome to sense polyamine and halt translation.

In Arabidopsis, *AtAMD1* has two uORFs, Tiny uORF and Small uORF (S-uORF) in its 5'-UTR (Hanfrey *et al.* 2005). The 52-amino-acid nascent peptide encoded by S-uORF cause polyamine-induced ribosome stalling during translation termination (Uchiyama-Kadokura *et al.* 2014). Amino acid sequences of S-uORF are highly conserved among higher plants (Franceschetti *et al.* 2001), and ribosome stalling occurs in an amino acid sequence-dependent manner (Uchiyama-Kadokura *et al.* 2014); however, amino acid residues responsible for stalling function have not been identified.

Spermidine accelerates decay of the S-uORF-containing mRNA as well as efficiency of ribosome stalling (Uchiyama-Kadokura *et al.* 2014). One of the possible pathways of mRNA degradation is NMD, in which a stop codon of uORF may be recognized as a premature termination codon (Gaba *et al.* 2005, Amrani *et al.* 2006). Biochemical analysis with NMD mutants showed that NMD is responsible for the spermidine-responsive acceleration of mRNA decay (Uchiyama-Kadokura *et al.* 2014). Hou *et al.* (2016) carried out high-throughput analysis for profiling the 5'-ends of RNA degradation intermediates using Arabidopsis seedlings. In this approach, mRNA-bound ribosome protects mRNA from degradation and thus leaves ribosome footprints in the RNA degradome. Protected fragments were found at position -16 from the stop codon of S-uORF, consistent with the ribosome stalling at the stop codon (Hou *et al.* 2016).

The XBP1u system

The unfolded protein response is a central cellular response mechanism that alleviates endoplasmic reticulum (ER) stress (Walter and Ron 2011). Upon ER stress, an endoribonuclease IRE1 α splices the *XBP1u* mRNA on the ER membrane to obtain its spliced form *XBP1s*, which codes for an active transcription factor. The 261-amino-acid nascent peptide of XBP1u causes ribosome stalling during elongation (Figure 1.4B) (Yanagitani *et al.* 2011). As a result, the stalled ribosome-nascent-peptide mRNA complex is targeted to the Sec61 channel on the ER membrane, where mRNA splicing by IRE1 α is active (Kanda *et al.* 2016).

Due to an unconventional splicing, the C-terminus of XBP1u protein is completely different from that of XBP1s. The C-terminal region (residues 236–261) is important for ribosome stalling (Yanagitani *et al.* 2011, Shanmuganathan *et al.* 2019), and the ribosome stalls at Met-260 with peptidyl-tRNA located at the P-site. Intriguingly, most positions of functional amino acids are not optimized for efficient stalling. Moreover, translational analyses in the presence of microsomal membrane revealed that XBP1u-induced stalling is required for the efficient membrane targeting of XBP1u itself (Yanagitani *et al.* 2011). Therefore, the wild-type XBP1u induces only an intermediate level of ribosome stalling to allow efficient targeting by SRP without activating the Sec61 channel. Since the mid-tunnel region of XBP1u is important for stalling (Yanagitani *et al.* 2011), it has been suggested that nascent peptide of XBP1u and the exit tunnel component cooperate in alleviating the ER stress.

Recently, the cryo-EM structure of the human XBP1u-stalled ribosome has been determined and provided structural insight into XBP1u-induced ribosome stalling (Shanmuganathan *et al.*

2019). In the stalled ribosome, nascent peptide adopts an extended conformation, except in the proximity of the PTC, where XBP1u forms a unique turn in the exit tunnel. The turn is comprised of eight-consecutive amino acid residues from Trp-249 to Trp-256, six residues of which have been previously shown to be critical for stalling by alanine-scanning mutagenesis (Yanagitani *et al.* 2011). The turn begins only four residues away from the PTC, suggesting that the turn within the exit tunnel may be critical for XBP1u stalling. Nascent peptide of XBP1u makes extensive interactions with the exit tunnel wall; the turn consisted of two tryptophan residues and protrudes into a hydrophobic pocket in the exit tunnel, causing the displacement of G3904 nucleotide of 28S rRNA, whose corresponding nucleotide is EcA2058 and is critical for macrolide binding and drug-dependent ribosome stalling (Ramu *et al.* 2009). At the constriction region, Arg-71 and Ser-87 of uL4, as well as Arg-128 of uL22 make contacts with XBP1u. Taken together, the entire XBP1u contributes to ribosome stalling by interacting with the exit tunnel to form a unique turn structure.

The AUG-Stop system

The Arabidopsis *NIP5;1* encodes a boric acid channel that is required for normal growth under low boron conditions in Arabidopsis (Takano *et al.* 2006). Expression of *NIP5;1* is regulated through AUG-UAA motif present in its 5'-UTR (Tanaka *et al.* 2016). Prolonged ribosome stalling occurs during translation of AUG-stop in response to high concentrations of boric acid prior to mRNA degradation (Figure 1.5A) (Tanaka *et al.* 2016). In contrast to other NPmRS systems, AUG-stop is a minimum ORF that consists of only initiation and stop codons and thus does not produce any regulatory peptide that can interact with the ribosomal exit tunnel. At this point, how the stalled complex with AUG-stop works to sense boric acid remains to be elucidated.

Ribosome stalling through AUG-stop is accompanied by mRNA degradation. One of the possible degradation pathways is NMD as observed in the AtAMD1 system. However, NMD mutant analysis showed that NMD does not function in this response (Tanaka *et al.* 2016). Considering that induction of the uORF-dependent NMD in plant is efficient if the uORF encodes a peptide longer than 34 amino acids (Nyikó *et al.* 2009), it is reasonable to assume that a mechanism other than NMD is involved in AUG-stop-mediated mRNA degradation. A conserved sequence located near the 5'-end of the stalled ribosome is also responsible for promoting mRNA degradation. Disruption of this sequence decreased mRNA degradation intermediate, whereas did not affect efficiency of boron-induced stalling (Tanaka *et al.* 2016). Thus, it is

proposed that an endoribonuclease recognizes the upstream sequence directly or indirectly and enhances mRNA degradation at a step(s) after ribosome stalling.

Physiological analysis with transgenic *Arabidopsis* plants showed biological significance of the AUG-stop-mediated regulation of *NIP5;1*. Under high boron conditions, the root growth of transgenic plants carrying a deletion of the AUG-stop was poorer than that of wild-type plants, whereas the growth of all plants was indistinguishable under normal conditions (Tanaka *et al.* 2016). Therefore, impairment of the translational regulation of *NIP5;1* is important for avoiding the toxic effect of excess boron.

Apart from *NIP5;1*, boron-induced translational regulation is also observed in a borate transporter *BOR1* (Aibara *et al.* 2018). Despite *BOR1* has an AUG-stop (uORF1) in its 5'-UTR, uORF1 is not a major element required for boron response and this process is mainly controlled by other uORFs, which differs from the regulation mechanism of *NIP5;1*.

1.2.5 Genetic studies for programmed ribosome stalling

As mentioned above, in bacteria, the importance of the ribosomal components for the induction of programmed ribosome stalling has been extensively investigated by structural studies using the cryo-EM as well as genetic studies. Specifically, reverse genetic analyses using the known stalling-defective mutants exhibited qualitative differences depending on each stalling system, which differ totally in functional amino acid sequences (Nakatogawa and Ito 2002, Cruz-Vera *et al.* 2005, Vázquez-Laslop *et al.* 2010, Chiba *et al.* 2011, Ramu *et al.* 2011, Ishii *et al.* 2015). Thus, it is shown that the ribosome itself is responsible for the induction of NPmRS, but that interactions between the nascent peptide and ribosomal components are not identical among bacterial stalling systems. In contrast to bacteria, in eukaryotes, no genetic approach has been taken to establish ribosomal mutants since a slight defect in eukaryotic ribosomal biogenesis generally causes growth defects and developmental alterations known as ribosomal stress responses (Ohbayashi *et al.* 2017). Thus, there is a lack of genetic evidence showing the contribution of the ribosomal components to NPmRS. To date, even in bacteria, there are few studies to compare the stalling efficiencies of different NPmRS systems under the same ribosomal mutation background, which will enable us to deduce both qualitative and quantitative differences in the contribution of the ribosomal components among the stalling systems.

1.3 ROLES OF RIBOSOMES IN PLANT DEVELOPMENTAL CONTROL

Translational regulation in plants is less well understood compared to other regulatory steps, including transcription, RNA silencing, protein modification, and protein degradation. Nevertheless, a number of genetic evidence has suggested that the ribosome plays important roles in plant development, probably through translational regulation.

1.3.1 Molecular organization of plant ribosomes

The cytosolic ribosomal proteome of Arabidopsis has been studied intensively by proteomics approaches and is now one of the most characterized examples in eukaryotes. Plant cytosolic ribosomes are distinguished from other eukaryotic ribosomes by an abundance of r-proteins for which multiple paralogous genes are expressed.

Rat (*Rattus norvegicus*) liver ribosomes were the first identified eukaryotic ribosomes for which a presumed complete list of r-proteins became available (Wool *et al.* 1995). In 2001, Barakat *et al.* (2001) revealed that the Arabidopsis genome encodes 81 different types of r-proteins (48 ribosomal large subunit and 33 small subunit proteins). All r-proteins are encoded by small gene families (two to seven genes), and the amino acid sequence is highly conserved among the paralogs (Barakat *et al.* 2001, Chang *et al.* 2005). A series of proteomic studies have confirmed the presence of all of the 81 predicted r-proteins and of multiple paralogous members in Arabidopsis cytosolic ribosomes (Chang *et al.* 2005, Carrol *et al.* 2008, Hummel *et al.* 2015). Theoretically, the multiple r-protein paralogs can form more than 10^{34} different ribosomes in the cell, not including different post-translational modifications (Hummel *et al.* 2015). Therefore, high heterogeneity of ribosomes might contribute to the sessile nature of plants under changing environments; however, proving the existence of such specialized ribosomes will be extremely challenging (Xue and Barna 2012, 2015).

1.3.2 Phenotypes of ribosomal protein loss-of-function mutants

Although ribosomes are ubiquitously distributed in plant cells and are essential for plant development, a number of loss-of-function mutants of r-proteins are viable. These mutants exhibit common phenotypes including growth defects and changes in leaf morphology (Bayne *et al.* 2009, Horiguchi *et al.* 2012). A characteristic developmental phenotype, referred to as *pointed leaves*, is frequently found. Thus far, r-protein mutants have been identified for more than 20

genetic loci in *Arabidopsis* (Table 1.2). Generally, r-protein mutants share developmental abnormalities including reduced shoot growth, reduced cell proliferation, and increased nuclear ploidy in leaf cells (Horiguchi *et al.* 2011). A short root phenotype is observed in several cases (Ito *et al.* 2000, Weijers *et al.* 2001, Degenhardt and Bonham-Smith 2008, Falcone Ferreyra *et al.* 2010, Rosado *et al.* 2010, 2012), suggesting that r-protein deficiency causes growth defects in the whole plant body. There are several extreme cases; for example, mutations of r-protein genes lead to an embryonic lethality (Tzafrir *et al.* 2004).

There are several rare phenotypes in plant development. The close link between specific phenotypes and r-proteins suggests their own roles in developmental regulation. For example, *pfl2/es15b* produces trichomes with fewer branches than wild-type plants (Ito *et al.* 2000), while reduced trichome number is observed in *aml1/es7b* (van Minnebruggen *et al.* 2010). *Arabidopsis es27a* is more sensitive to a DNA-damaging drug, methyl methane sulfate, but is indistinguishable from wild-type plants under normal conditions (Revenkova *et al.* 1999). Whether these uncommon phenotypes are indeed specific to limited r-protein-defective mutants or widely shared is unclear. Since there are more than 200 genes encoding cytosolic r-proteins in the *Arabidopsis* genome as mentioned above, a more comprehensive analysis is needed to address this question.

1.3.3 Roles of ribosomes in plant development

The diverse developmental phenotypes in r-protein-defective mutants raise an intriguing question as to how the ribosome specifically controls these processes. One of the possible explanations is a ribosome heterogeneity model. In this model, multiple r-protein paralogs have a non-equivalent function during translation whereby different ribosomes could be optimized for or dedicated to the translation of specific mRNAs. Although only a few studies have compared functions of all paralogs of r-protein gene family, most mutants in *Arabidopsis* (e.g., *uL4* and *eS6*) exhibited nearly identical phenotypes (Creff *et al.* 2010, Rosado *et al.* 2010, 2012). However, a few observations might support the ribosome heterogeneity model. Some of paralogous genes are identical in amino acid sequence, but are differentially expressed during development. For example, *uL16A* is strongly expressed in dividing cells, whereas *uL16B* is expressed in cells undergoing differentiation (Weijers *et al.* 2001). The expression of *uL5B* is also high in all actively dividing cells, whereas the expression pattern of *uL5A* is tissue-specific (Williams *et al.* 1995). However, there is no direct evidence that suggests regulatory roles of ribosome heterogeneity;

detailed developmental expression patterns are not known except for uL5 and uL16 members, and whether the function of one paralog is exchangeable by another one has not been studied.

In contrast to plants, the ribosome heterogeneity model seems to hold true in yeast. Similar to the case in *Arabidopsis*, 59 out of the 79 cytosolic r-proteins are encoded by two genes in yeast (McIntosh and Warner 2007). It has been proposed that different ribosomes are specialized for diverse cellular processes in yeast. For example, deletions of at least six r-proteins, but not their paralogs, affect the localization of *ASH1* mRNA (Komili *et al.* 2007). Recently, high-resolution mass spectrometry analysis has shown that the stoichiometry among core r-proteins depends both on the growth conditions and on the number of ribosomes bound per mRNA (Slavov *et al.* 2015). These findings support the existence of specialized ribosomes with distinct protein composition and distinct physiological function in yeast.

1.3.4 Differences and similarities between plants and animals

In contrast to plants, most r-proteins in animals are usually encoded by a single gene (Sugihara *et al.* 2010). Moreover, unlike plants, which have few pseudogenes for r-proteins, mammalian genomes have a large number of r-protein pseudogenes, from 1800 in humans to 2000 in mice (Zhang *et al.* 2004, Balasubramanian *et al.* 2009). Some pseudogenes are actually expressed, but the significance of the amplified copy number in animals remains to be determined.

In both plants and animals, the defect of r-proteins leads to reduced growth, which is probably linked with reduced ribosome production and lower rates of protein synthesis. Loss-of-function mutants of r-proteins in animals are generally homozygous lethal, whereas heterozygotes with reduced levels of r-proteins are viable. Specific developmental defects and cancer formation result from reduced ribosome function in mice. For example, the *belly spot and tail* gene in mice, which encodes r-protein eL24, is characterized by skin pigmentation and skeletal abnormalities as well as a reduced adult size (Oliver *et al.* 2004). Thus, reduced ribosome function in animals could also disrupt the translation of specific targets involved in development, and this mechanism might be common to plants and animals.

1.4 TABLES

Table 1.1a. Published regulatory nascent peptides and their functions.

Stalling sequence ^a (stalled positions are underlined)	Stalling system	Organism	Gene / ORF
30 20 10 1 GYRIDYAHFTPQAK <u>F</u> STPV <u>WISQAQ</u> GIRAG	SecM	<i>Escherichia coli</i>	<i>secA</i> / leader peptide
MNILHICVTSKW <u>F</u> NI <u>DNKIVDHRP</u> *	TnaC	<i>E. coli</i>	<i>tnaA, B</i> / leader peptide
MGIFS <u>I</u> F <u>V</u> I	ErmCL ^b	<i>Staphylococcus aureus</i>	<i>ermC</i> / leader peptide
NQYTFYHFTSDHRISGW <u>K</u> ETNAMYVALNSQ	VemP	<i>Vibrio alginolyticus</i>	<i>secD2</i> / leader peptide
LIIIIYHRIT <u>W</u> IRKVF <u>R</u> MNSPVNDEED <u>AGS</u>	MifM ^c	<i>B. subtilis</i>	<i>yidC2</i> / leader peptide
MNGRPSVFTSQ <u>D</u> YLS <u>D</u> HLWRALNA*	AAP	<i>Neurospora crassa</i>	<i>arg-2</i> / uORF
MEPLVL <u>S</u> AKKL <u>S</u> LLTCKYI <u>PP</u> *	hCMV	Human cytomegalovirus	<i>gp48</i> / uORF
MAG <u>D</u> I <u>S</u> *	MAGDIS	mammal	<i>AMD1</i> / uORF
QRSTQKDPVPYQPP <u>F</u> LCQ <u>WGRHQPSWKPLM</u>	XBP1u	Human	<i>XBP1u</i> / ORF
PPNFVRQLSIKARR <u>NCS</u> NI <u>GVAQ</u> I ^u AA <u>KWS</u>	CGS1	<i>Arabidopsis thaliana</i>	<i>CGS1</i> / ORF
FMLNSTIRRR <u>THLVQ</u> S <u>F</u> SV <u>VFL</u> Y <u>WLYYVS</u> *	bZIP11	<i>A. thaliana</i>	<i>bZIP11</i> / uORF
LGYSIEDVRPNGGIKK <u>F</u> KSSVYSNCSK <u>RP</u> *	AtAMD1 ^d	<i>A. thaliana</i>	<i>AMD1</i> / uORF
<u>M</u> *	AUG-Stop	<i>A. thaliana</i>	<i>NIP5;1</i> / uORF

^a Twenty-nine amino acid sequences upstream from the stalled position are shown if the regulatory peptide is longer than 30 amino acids. Amino acid residues important for NPmRS are marked in red.

^b Drug-induced ribosome stalling has been reported in several other *erm* genes (Ramu *et al.* 2009).

^c MifM undergoes NPmRS at four consecutive codons (Chiba *et al.* 2012).

^d For AtAMD1, functional amino acids are not reported, but importance of the amino acid sequence was shown by a frame-shift mutation (Uchiyama-Kadokura *et al.* 2014).

Table 1.1b. Published regulatory nascent peptides and their functions.

Stalling system	Effector ^e	Step	Outputs
SecM	–	elongation	Up-regulation of <i>secA</i> translation
TnaC	L-tryptophan	termination	Up-regulation of <i>tna</i> operon transcription
ErmCL	erythromycin	elongation	Up-regulation of <i>ermC</i> translation
MifM	–	elongation	Up-regulation of <i>gidC2</i> translation
VemP	–	elongation	Up-regulation of <i>secD2</i> translation
AAP	L-arginine	termination	Down-regulation of <i>arg-2</i> translation
hCMV	–	termination	Down-regulation of <i>gp48</i> translation
MAGDIS	polyamine	termination	Down-regulation of <i>AMD1</i> translation
XBP1u	–	elongation	Splicing of <i>XBP1u</i> mRNA
CGS1	AdoMet	elongation	mRNA degradation and down-regulation of <i>CGS1</i> translation
bZIP11	sucrose	termination	Down-regulation of <i>bZIP11</i> translation
AtAMD1	polyamine	termination	mRNA degradation and down-regulation of <i>AMD1</i> translation
AUG-Stop	boric acid	termination	mRNA degradation and down-regulation of <i>NIP5;1</i> translation

^e "–" indicates an autonomous ribosome stalling without any effector.

Table 1.2. Published Arabidopsis r-protein mutants and their phenotypes.

r-Protein ^a	AGI code	Phenotype	Reference
uL1B	At2g27530	Pointed leaves	Pinon <i>et al.</i> 2008
uL2A	At2g18020	Embryo lethal	Tzafrir <i>et al.</i> 2004
uL3A	At1g43170	Embryo lethal	Tzafrir <i>et al.</i> 2004
uL4A	At3g09630	Vascular defects, pointed leaves, short roots	Rosado <i>et al.</i> 2010
uL4D	At5g02870	Vascular defects, pointed leaves, short roots	Rosado <i>et al.</i> 2012
uL6C	At1g33140	Pointed leaves	Pinon <i>et al.</i> 2008
uL14C	At3g04400	Embryo lethal	Tzafrir <i>et al.</i> 2004
eL15C	At1g70600	Vascular defects, pointed leaves	Szakonyi and Byrne 2011
uL16A	At1g14320	Embryo lethal	Falcone Ferreyra <i>et al.</i> 2010
uL16B	At1g26910	Pointed leaves, short roots	Falcone Ferreyra <i>et al.</i> 2010
uL18A	At3g25520	Vascular defects, pointed leaves	Yao <i>et al.</i> 2008
uL18B	At5g39740	Pointed leaves, pale green leaves,	Yao <i>et al.</i> 2008
eL19A	At1g02780	Embryo lethal	Tzafrir <i>et al.</i> 2004
uL23A	At2g39460	Vascular defects, pointed leaves, short roots	Degenhardt and Bonham-Smith 2008
uL23B	At3g55280	No visible phenotype	Degenhardt and Bonham-Smith 2008
eL24B	At3g53020	Vascular defects, pointed leaves, pale green leaves	Nishimura <i>et al.</i> 2004 Yao <i>et al.</i> 2008
eL28A	At2g19730	Vascular defects, pointed leaves, pale green leaves	Yao <i>et al.</i> 2008
uL30B	At2g01250	Pointed leaves	Horiguchi <i>et al.</i> 2011
eL38B	At3g59540	Pointed leaves	Horiguchi <i>et al.</i> 2011
eL39C	At4g31985	Pointed leaves	Horiguchi <i>et al.</i> 2011
eS6B	At5g10360	Embryo lethal	Tzafrir <i>et al.</i> 2004
eS7B	At2g37270	Vascular defects, reduced trichome number	Weijers <i>et al.</i> 2001
uS13A	At1g22780	Pointed leaves	van Lijsebettens <i>et al.</i> 1994
uS15A	At3g60770	Vascular defects, pointed leaves, short roots, trichome shape change	Ito <i>et al.</i> 2000
uS17A	At3g48930	Embryo lethal	Tzafrir <i>et al.</i> 2004
eS21B	At3g53890	Pointed leaves	Horiguchi <i>et al.</i> 2011
eS27A	At2g45710	Increased sensitivity to UV irradiation and methyl methane sulfate	Revenkova <i>et al.</i> 1999
eS28B	At5g03850	Pointed leaves	Horiguchi <i>et al.</i> 2011
eL40B	At3g52590	Embryo lethal	Tzafrir <i>et al.</i> 2004

^aA new naming system for r-proteins proposed by Ban *et al.* 2014 is used. In this system, homologous r-proteins are assigned the same name, regardless of species.

1.5 FIGURES

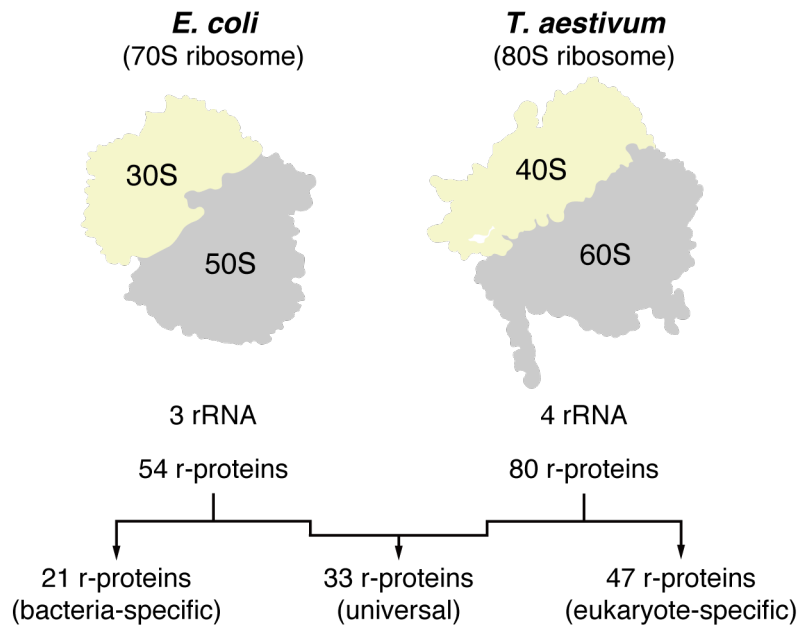


Figure 1.1. Structures and compositions of bacterial and eukaryotic ribosomes.

Bacterial (*E. coli*) and eukaryotic (*T. aestivum*) ribosomes share a common core that consists of 3-rRNA and 33-r-proteins. In addition to the universal core, ribosomes in each domain of life contain the specific r-proteins.

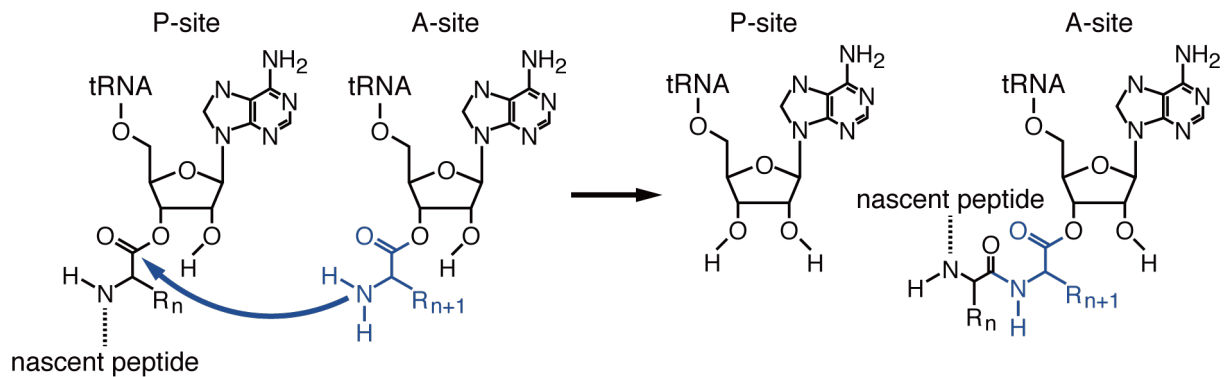
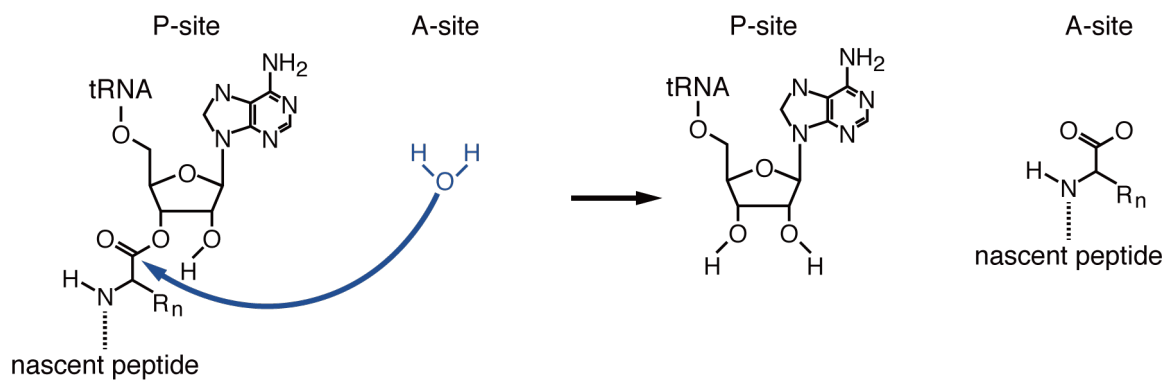
A peptide bond formation**B** peptidyl-tRNA hydrolysis

Figure 1.2. The two principal chemical reactions of protein synthesis: peptide bond formation and peptide release.

The ribosomal PTC is composed of highly conserved nucleotides of domain V of 23/28S rRNA. **(A)** During peptide bond formation, the α-amino group of aminoacyl-tRNA in the A-site attacks the carbonyl carbon of P-site-bound peptidyl-tRNA. As a result, tRNA at the P-site is deacylated and peptidyl-tRNA in the A-site is elongated by one amino acid. **(B)** During translation termination, nascent peptide at the P-site is transferred to an activated water molecule that leads to peptidyl-tRNA hydrolysis and peptide release from the ribosome.

CHAPTER 1. Introduction


Amino acid residues from PTC when stalled	Constriction region	PTC 	Stall system	Organism	Gene / ORF	Effector	Step
-50 -40 -30	-20 -10	-1					
... LALLDTLSALLTQEGTPSEKGYRIDYAHFTPQAKFSTPVWISQAQGIRAG ...	MNILHICVTSKWFNIDNKIVDHRP*		SecM	bacteria	<i>secA</i> / leader	–	elongation
	MGIFSIFVI ...		TnaC	bacteria	<i>tnaA, B</i> / leader	L-tryptophan	termination
... GEQWKSRTDEHQTVFHNRTDFLIIIIYHRITTWIRKVFMRN SPV DEED ...	MEPLVLSAKKLSLLTCKYI PP *		ErmCL	bacteria	<i>ermC</i> / leader	erythromycin	elongation
... AGISSSFTGDAGLSSRILRFPNFRQLSIKARRNCSNIGVAQI VA AKWS ...	MNGRPSVFTSQDYLS DHL WRALNA*		MifM	bacteria	<i>yidC2</i> / leader	–	elongation
	MESKGGKKKSSSSSLFYEAPLGYSIEDVRPNGGIKKFKSSVYSNCSKRPS*		CGS1	plant	<i>AtCGS1</i> / main	AdoMet	elongation
	MAGDIS*		hCMV	virus	<i>gp48</i> / uORF	–	termination
	M*		AAP	fungi	<i>Nc arg-2</i> / uORF	L-arginine	termination
			AtAMD	plant	<i>AtAMD1</i> / uORF	polyamines	termination
			MAGDIS	mammal	<i>mAMD1</i> / uORF	polyamines	termination
			AUG-Stop	plant	<i>AtNIP5;1</i> / uORF	boric acid	termination

Figure 1.3. Functional amino acid sequences of regulatory nascent peptides.

Relative position of amino acid residues important for NPmRS identified by mutational analysis. For each stalling systems, the gene and ORF in which stalling occurs, effector molecule, and translation step at which stalling occurs (elongation or termination) are shown. "–" indicates an autonomous ribosome stalling without any effector. Important amino acid residues are marked in red. For AtAMD1, functional amino acids are not reported, but importance of the amino acid sequence was shown by a frame-shift mutation (Uchiyama-Kadokura *et al.* 2014). The MTO1 region of CGS1 (Ominato *et al.* 2002) is underlined with ambiguous amino acids in dotted underline. Amino acid residues are numbered from the stalled residue (–1, marked with a clover). Approximate positions of the PTC and the constriction region are shaded, although some ambiguities in the boundaries are present because the nascent peptide may undergo compaction in the PTC proximal region.

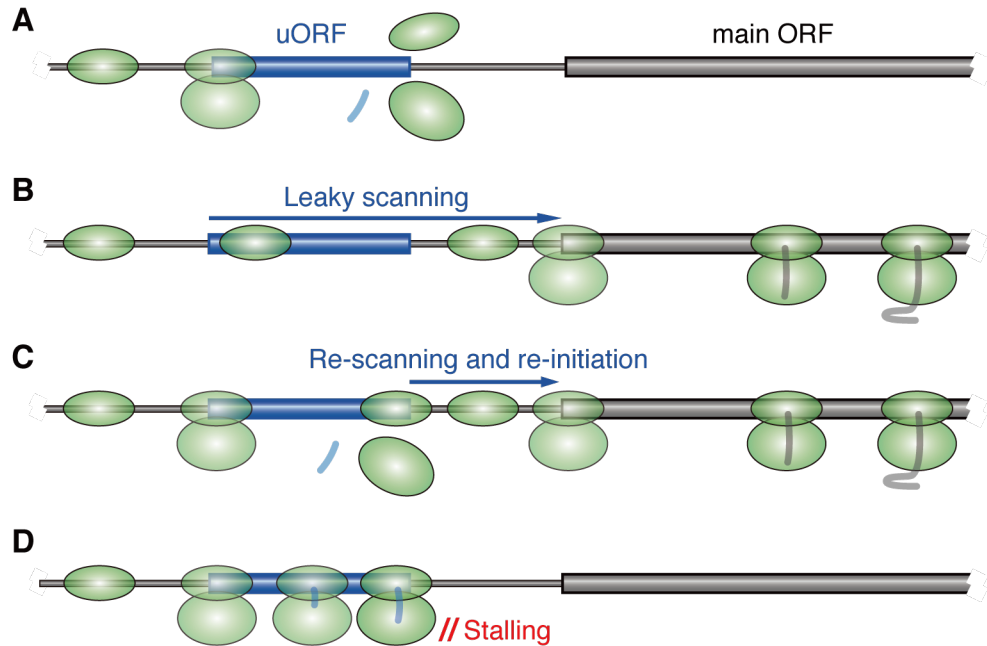


Figure 1.4. Down-regulation of the main ORF expression by uORF.

(A) Translation of a uORF generally down-regulates the translation of the main ORF. (B) The uORF may occasionally be overlooked by a mechanism termed the leaky scanning. (C) When a very short uORF is translated, the ribosome may not be fully dissociated at the termination codon and the small subunit may remain on the mRNA. (D) If the ribosome stalls on the uORF, translation of the downstream ORF is severely inhibited by blocking the succeeding ribosomes.

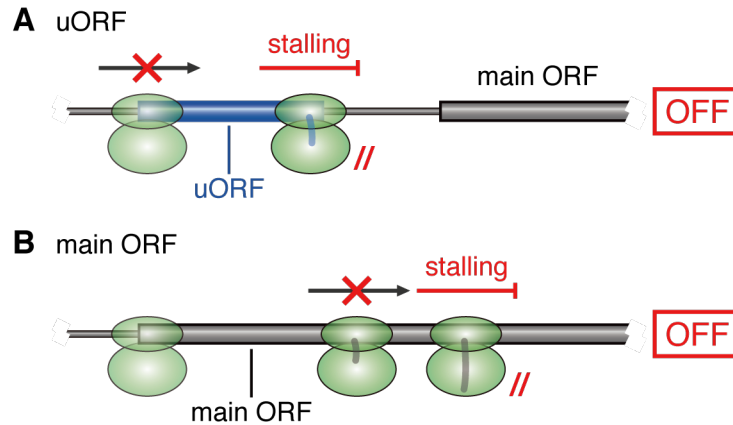


Figure 1.5. Outcomes of programmed ribosome stalling in eukaryotes.

Regulatory nascent peptides control gene expression by causing programmed ribosome stalling at a specific position on the mRNA. Blue and gray boxes indicate a uORF sequence and a main ORF sequence that induce ribosome stalling, respectively. **(A)** In eukaryotic mRNAs, the stalled ribosome on the uORF inhibits other scanning ribosomes from reaching the initiation codon of the main ORF (Degnin *et al.* 1993, Wang and Sachs 1997, Law *et al.* 2001, Hanfrey *et al.* 2005, Uchiyama-Kadokura *et al.* 2014, Tanaka *et al.* 2016, Hayashi *et al.* 2017, Yamashita *et al.* 2017). **(B)** Ribosome stalling on the main ORF occurs during translation elongation (Chiba *et al.* 2003, Onouchi *et al.* 2005, Yanagitani *et al.* 2011). The stalled ribosome inhibits other translating ribosomes from reaching the termination codon of the main ORF. For both cases, the programmed ribosome stalling results in translational repression of the main ORF.

CHAPTER 2.

Characterization of regulatory nascent peptides that cause programmed ribosome stalling in eukaryotes using Arabidopsis cell-free extract for *in vitro* translation

ABSTRACT: The ribosome has been regarded as a protein synthesis machinery rather than sophisticated regulator whose activity is highly regulated in response to cellular conditions. In eukaryotes, translational regulation is involved in a variety of biological processes including metabolism, development, and stress responses. Some of the nascent peptides can inhibit ribosomal functions during translation and thus cause programmed ribosome stalling to regulate gene expression. In eukaryotes, the stalled ribosome inhibits other ribosomes' scanning for initiation, leading to down-regulation of translation of the downstream ORF. Although a number of the regulatory nascent peptides have been identified, the mechanism by which how the nascent peptide works with the ribosome in mediating ribosome stalling is not fully understood. In this chapter, I conducted biochemical experiments using Arabidopsis cell-free translation system to investigate whether several known regulatory nascent peptides could function in Arabidopsis ribosomes. In all cases, I observed ribosome stalling and, in cases when the 5'-UTR carrying the relevant uORF was placed before a reporter gene, repression of expression was observed. The results showed that all stalling systems to be tested can be recapitulated using ACE *in vitro* translation system.

2.1. Introduction

2.2. Materials and Methods

2.3. Results

2.4. Discussion

2.5. Tables

2.6. Figures

2.1. Introduction

During the translation of mRNA, elongation process does not proceed at a uniform speed and ribosomes can transiently pause or even become stalled for prolonged periods owing to several elements in both mRNA and the nascent polypeptides. The mRNA elements include codon usage, local secondary structures, and Shine-Dalgarno-like sequences within the coding regions (Sørensen *et al.* 1989, Doma and Parker 2006, Plotkin and Kudla 2011, Li *et al.* 2012, Tholstrup *et al.* 2012). Features of a nascent peptide also can modulate translation status. A range of amino acid sequences, or the regulatory nascent peptides, is known to inhibit specific steps of translation in *cis*, leading to ribosome stalling (Ito and Chiba 2013). Nascent peptide-mediated ribosome stalling (NPmRS) is involved in biological processes including metabolism, stress responses, and protein export (Ito and Chiba 2013, Ishii *et al.* 2015, Hayashi *et al.* 2017, Yamashita *et al.* 2017). The stalled ribosome changes the translation efficiency either positively by destabilizing mRNA secondary structure in bacteria or negatively by inhibiting other ribosomes' scanning for initiation in eukaryotes.

The regulatory nascent peptides can interact with the ribosomal components at the peptidyltransferase center (PTC) on the ribosomal large subunit and/or the exit tunnel to interfere with ribosomal functions including the peptidyltransfer, translocation, and termination. Regulatory peptides are diverse in lengths and primary sequences and NPmRS is either intrinsic or is inducible in response to a specific effector. Thus, it has been thought that each regulatory peptide acts with the translating ribosome in a different way (Bhushan *et al.* 2010, Ito and Chiba 2013, Wilson *et al.* 2016). However, molecular mechanisms underlying how the nascent peptide works for the NPmRS induction is not fully understood in eukaryotic stalling systems due to a lack of biochemical studies. The aim of the present study is to determine the involvement of the constriction region in eukaryotic NPmRS. To this end, I took reverse genetics-based biochemical approaches.

For the NPmRS systems to be tested, I selected five from divergent eukaryotes including virus, fungus, mammals, and plants (Figure 2.1), of which four have their relevant amino acid residues >20 from the stalled residue, as in most NPmRS systems (Ito and Chiba 2013). These systems include *Arabidopsis CGS1* (the CGS1 system) (Chiba *et al.* 2003, Onouchi *et al.* 2005, Onoue *et al.* 2011, Yamashita *et al.* 2014), *Neurospora crassa arg-2* upstream open reading frame (uORF), termed the arginine attenuator peptide (AAP) (the AAP system) (Wang and Sachs 1997, Spevak *et al.* 2005, Wei *et al.* 2012), and human cytomegalovirus (hCMV) *gp48* uORF2

(the hCMV system) (Degnin *et al.* 1993, Cao and Geballe 1996, Alderete *et al.* 1999), and Arabidopsis *AdoMet decarboxylase 1* (*AtAMD1*) S-uORF (the *AtAMD1* system) (Hanfrey *et al.* 2005, Uchiyama-Kadokura *et al.* 2014). I also tested another NPmRS system, mammalian *AdoMet decarboxylase 1* (*mAMD1*) uORF. This uORF, encoding six amino acids, MAGDIS (the MAGDIS system) (Law *et al.* 2001, Raney *et al.* 2002), is the shortest among the NPmRS systems thus far identified (Figure 2.1) (Ito and Chiba 2013). Lastly, I tested the shortest possible uORF, AUG-stop, of *AtNIP5;1*. AUG-stop causes prolonged ribosome stalling in response to boric acid (the AUG-Stop system) (Tanaka *et al.* 2016). This minimum uORF codes for only one amino acid, methionine.

I exploited an *in vitro* cell-free translation system prepared from wild-type Arabidopsis plants, namely Arabidopsis cell-free extract (ACE) (Figure 2.2) (Murota *et al.* 2011), to elucidate whether amino acid sequences could function in Arabidopsis ribosomes. In all cases, I observed ribosome stalling activity and, in cases when the 5'-UTR carrying the relevant uORF was placed before a reporter gene, down-regulation of gene expression was observed. These results showed that all NPmRSs to be tested can be recapitulated in ACE *in vitro* translation.

2.2. MATERIALS AND METHODS

Chemicals

AdoMet and spermidine were purchased from Sigma-Aldrich (St. Louis, MO, USA), and L-arginine was purchased from Wako Pure Chemicals (Osaka, Japan). Other chemicals were obtained as described previously (Murota *et al.* 2011, Yamashita *et al.* 2014).

Construction of plasmids used for stalling assay

Plasmid pST00 (Table 2.1) carries the *M8:His:HA:DP75* sequence between the SP6 promoter and the 30-nt poly(A) in the pSP64 poly(A) vector (Promega, Madison, WI, USA). The DP75 linker was derived from the dipeptidyl-aminopeptidase B coding sequence (Matheisl *et al.* 2015, Yamashita *et al.* 2017). To construct pST00, the *His:HA:DP75* coding region was amplified by PCR from pYY105, which carries *T7::His:HA:DP75:uORF2(WT)* DNA in the pEX-A2 vector (Yamashita *et al.* 2017), using the primers DP75f and DP75r (Table 2.2). The amplified fragment was digested with XbaI and BamHI and inserted between the XbaI and BamHI sites of pYK00, which harbors *M8:CGS1(WT)* DNA in the pSP64 poly(A) vector (Onoue *et al.* 2011).

Plasmids pST55 and pST56 (Table 2.1) carry *M8:His:HA:DP75:AAP(WT)* and *M8:His:HA:DP75:AAP(D12N)*, respectively, in the pSP64 poly(A) vector. To construct these plasmids, complementary oligonucleotides AAPf/AAPr or D12Nf/AAPr (Table 2.2), encoding wild-type or mutated *N. crassa arg-2* (Wang and Sachs 1997), respectively, were annealed and filled-in using KOD-Plus-Neo DNA polymerase (Toyobo, Osaka, Japan). The amplified fragments were digested with EcoRV and BamHI and inserted between the EcoRV and BamHI sites of pST00.

Plasmids pTI5 and pTI6 (Table 2.1) carry *M8:His:HA:3xFLAG:Myc:DP75:AAP(WT)* and *M8:His:HA:3xFLAG:Myc:DP75:AAP(D12N)*, respectively, in the pSP64 poly(A) vector. To introduce the *Myc* tag sequence between the *HA* tag and the DP75 linker in pST55 and pST56, *in vitro* mutagenesis was carried out by inverse PCR using the primers MycDP75f and HAMycr (Table 2.2), followed by digestion of the plasmid DNA by DpnI (Toyobo). The amplified fragments were self-ligated using T4 DNA ligase (Wako Pure Chemicals) and T4 polynucleotide kinase (Toyobo). To construct pTI5 and pTI6, complementary oligonucleotides 3xFLAGf and 3xFLAGr (Table 2.2) were annealed and filled-in by PCR, and the amplified fragments were ligated with the PCR-amplified fragment from the *Myc* tag-fused pST55 or pST56 using Mycf and HAr primers

(Table 2.2) by the SLiCE reaction (Zhang *et al.* 2012).

Plasmids pST57 and pST58 (Table 2.1) carry *M8:His:HA:DP75:hCMV(WT)* and *M8:His:HA:DP75:hCMV(P21A)*, respectively, in the pSP64 poly(A) vector. To construct these plasmids, complementary oligonucleotides hCMVf/hCMVr or hCMVf/P21Ar (Table 2.2), encoding wild-type or mutated uORF2 of hCMV *gp48* (Schleiss *et al.* 1991, Matheisl *et al.* 2015), respectively, were annealed and filled-in by PCR. The amplified fragments were inserted into pST00 in the same way as for the construction of pST55.

Plasmids pST76 and pST77 (Table 2.1) carry *M8:His:HA:DP75:S-uORF(WT)* and *M8:His:HA:DP75:S-uORF(fs)*, respectively, in the pSP64 poly(A) vector. To construct these plasmids, the coding region of the *AtAMD1* S-uORF was amplified from pNU14 or pNU15, which carries *GST:S-uORF(WT):RLUC* or *GST:S-uORF(fs):RLUC*, respectively, in the pSP64 poly(A) vector (Uchiyama-Kadokura *et al.* 2014), using the primer sets SAMDC1f/SAMDC1r or SAMDC1fsf/SAMDC1fsr (Table 2.2), respectively. The amplified fragments were inserted into pST00 in the same way as for the construction of pST55.

Plasmids pST116 and pST117 (Table 2.1) carry *M8:His:HA:DP75:MAGDIS(WT)* and *M8:His:HA:DP75:MAGDIS(I5L)*, respectively, in the pSP64 poly(A) vector. To construct these plasmids, the *His:HA:DP75* tag sequence was amplified from pST00 using the primer sets DP75f/MAGDISr or DP75f/I5Lr (Table 2.2), respectively, and the amplified fragments were digested with XbaI and BamHI and inserted between the XbaI and BamHI sites of pST00.

Plasmids pST124 and pST125 (Table 2.1) carry *M8:His:HA:3xFLAG:Myc:DP75:MAGDIS(WT)* and *M8:His:HA:3xFLAG:Myc:DP75:MAGDIS(I5L)*, respectively, in the pSP64 poly(A) vector. To construct these plasmids, the *His:HA:3xFLAG:Myc:DP75* tag sequence was amplified from pTI5 using the primer sets DP75fMAGDISr or DP75f/I5Lr (Table 2.2), respectively, and the amplified fragments were inserted into pST00 in the same way as for the construction of pST55. For all constructs, the integrity of PCR-amplified regions was confirmed by sequence analysis.

In the Results section, *M8:His:HA* and *M8:His:HA:3xFLAG:Myc* sequences will be referred to as *TagI* and *TagII*, respectively.

Construction of plasmids used for reporter assay

Plasmids pST122 and pST123 (Table 2.1) carry *gp48 5'-UTR(WT):LUC* and *gp48 5'-UTR(P21A):LUC*, respectively, in the pSP64 poly(A) vector. To construct these plasmids,

complementary oligonucleotides hCMVf2/hCMVr2 or hCMVf2/P21Ar2 (Table 2.2), which correspond to the wild-type or mutated 5'-UTR of the hCMV *gp48* sequence (Schleiss *et al.* 1991, Cao and Geballe 1995), respectively, were annealed and filled-in by PCR. The amplified fragments were digested with HindIII and inserted at the HindIII site of pMI21, which carries *CGS1(WT):LUC* in the pSP64 poly(A) vector (Chiba *et al.* 2003).

Plasmids pST120 and pST121 (Table 2.1) carry *AtAMD1 5'-UTR(WT):LUC* and *AtAMD1 5'-UTR(fs):LUC*, respectively, in the pSP64 poly(A) vector. To construct these plasmids, the 5'-UTR of *AtAMD1* was amplified from pSY209 or pSY214, which carry *S-uORF(WT):RLUC* or *S-uORF(fs):RLUC*, respectively, in the pSP64 poly(A) vector (Uchiyama-Kadokura *et al.* 2014) using the primers SAMDC1f2 and SAMDC1r2 (Table 2.2). The amplified fragments were digested with XbaI and NcoI and inserted between the XbaI and NcoI sites of pMI21.

Plasmids pST118 and pST119 (Table 2.1) carry *mAMD1 5'-UTR(WT):LUC* and *mAMD1 5'-UTR(I5L):LUC*, respectively, in the pSP64 poly(A) vector. To construct these plasmids, complementary oligonucleotides *MAGDIS(WT)f/MAGDIS(WT)r* or *MAGDIS(WT)f/MAGDIS(I5L)r* (Table 2.2), which correspond to the wild-type or I5L mutant 5'-UTR (Hill and Morris 1992), respectively, were annealed and filled-in by PCR. pSR327 carries a chimeric 5'-UTR: -327 to -311 nt of the human *AMD1* and -310 to -1 nt of the bovine *AMD1* (Hill and Morris 1992). The amplified fragments were inserted into pMI21 in the same way as for the construction of pST120. For all constructs, the integrity of PCR-amplified regions was confirmed by sequence analysis.

Plasmid pMI27 carries the *RLUC* gene in the pSP64 poly(A) vector (Chiba *et al.* 2003). Plasmids pMT131 and pMT132 carry the wild-type or mutated 5'-UTR of *AtNIP5;1*, respectively, joined to the *LUC* gene in the pSP64 poly(A) vector (Tanaka *et al.* 2016).

***In vitro* transcription**

DNA templates in the pSP64 poly(A) vector were linearized with EcoRI and purified using the QIAquick Nucleotide Removal Kit (Qiagen), with the exception of the *M8:His:HA:DP75* and *M8:His:HA:3xFLAG:Myc:DP75* fusion constructs. DNA templates for these plasmids and nonstop RNAs were prepared by amplifying the corresponding region by PCR using KOD-Plus-Neo DNA polymerase. For PCR amplification, SP65'fP (Onoue *et al.* 2011) was used as a forward primer and the reverse primers as listed in Table 2.2 were used. *In vitro* transcription in the presence of a cap analog, m⁷G[5']ppp[5']GTP, was carried out as described previously (Chiba *et al.* 2003).

***In vitro* translation**

Preparation of ACE and *in vitro* translation reactions using ACE were carried out at 25°C as described previously (Murota *et al.* 2011). Unless otherwise stated, the template RNA was used at 50 fmol μl^{-1} . For RNase A treatment, RNase A was added at a final concentration of 0.5 mg ml^{-1} and reaction mixtures were incubated for 15 min at 37°C. For immunoblot analysis, reaction mixtures were diluted with the 1×SDS-PAGE gel sample buffer (50 mM Tris-HCl pH 6.8, 50 mM DTT, 10% (v/v) glycerol, and 1% (w/v) SDS).

Immunoblot analysis

For immunoblot analysis of *in vitro* translation products, samples were separated on a NuPAGE 4%–12% or 12% Bis-Tris Gel (Invitrogen), transferred to an Immobilon-P membrane (Millipore, Billerica, MA, USA), and immuno-reacted with either a polyclonal anti-GST antibody (Santa Cruz Biotechnology, Santa Cruz, CA, USA), a monoclonal anti-HA antibody (Santa Cruz Biotechnology), or a monoclonal anti-FLAG M2 antibody (Sigma-Aldrich). MOPS running buffer (Life Technologies, Carlsbad, CA, USA) was used for the GST tag-fusion construct. MES running buffer (Life Technologies) was used for the *M8:His:HA:DP75* or *M8:His:HA:3xFLAG:Myc:DP75* fusion constructs. The signals were detected using an Immobilon Forte Western HRP substrate (Millipore) and visualized using a LAS-3000 mini imaging system (GE Healthcare, Little Chalfont, UK). The band intensities were quantified using MultiGauge software (Fuji Photo Film, Tokyo, Japan).

Luciferase assay

Tester RNA at 2 fmol μl^{-1} carrying firefly (*Photinus pyralis*) luciferase (LUC) reporter gene and 1 fmol μl^{-1} sea pansy (*Renilla reniformis*) luciferase (RLUC) control RNA were co-translated for 120 min. LUC and RLUC activities were measured as described previously (Chiba *et al.* 2003), and the LUC activity was normalized with the control RLUC activity to obtain reporter activity.

Statistical treatments

For comparisons of stalling efficiencies or reporter activities, Welch's *t*-test was applied.

2.3. RESULTS

Ribosome stalling of the CGS1 system in wild-type ACE

When a ribosome stalls during translation, a peptidyl-tRNA species accumulates as an intermediate of translation. A tRNA moiety confers a 10- to 20-kDa gel mobility shift to the peptide, depending on the tRNA species and gel conditions. In order to preserve intact peptidyl-tRNAs, samples were electrophoresed under neutral pH conditions (Onouchi *et al.* 2005, Muto *et al.* 2006, Yamashita *et al.* 2017). Peptidyl-tRNA can be identified as an RNase-sensitive band.

The AdoMet-induced NPmRS of CGS1 has been extensively studied by using WGE (Chiba *et al.* 2003, Onouchi *et al.* 2005, Haraguchi *et al.* 2008, Onoue *et al.* 2011, Yamashita *et al.* 2014), but is only partially characterized in ACE (Murota *et al.* 2011). To further characterize the AdoMet-induced NPmRS in ACE, *GST:CGS1(WT)* RNA that carries a glutathione *S*-transferase (GST) tag sequence fused in-frame to the N-terminus of the *CGS1* exon 1 coding sequence was used (Figure 2.3A). The 183-amino-acid sequence of the *CGS1* exon 1 coding sequence is necessary and sufficient for the AdoMet-induced post-transcriptional regulation (Suzuki *et al.* 2001). The MTO1 region (residues 77–87) is the *cis* element for the AdoMet-induced NPmRS that occurs at Ser-94 (Ominato *et al.* 2002, Onouchi *et al.* 2005).

When *GST:CGS1(WT)* RNA was translated in the presence of AdoMet, immunoblot analysis using an anti-GST antibody detected RNase-sensitive 55-kDa peptidyl-tRNA in addition to a 45-kDa full-length product, whereas in the absence of AdoMet the peptidyl-tRNA was barely detectable (Figure 2.3B). *mto1-1* mutation (G84S) abolishes AdoMet-induced NPmRS of CGS1 in WGE (Ominato *et al.* 2002, Chiba *et al.* 2003, Onouchi *et al.* 2005). Translation of *GST:CGS1(mto1-1)* RNA (Figure 2.3A) in wild-type ACE in the presence of AdoMet did not show peptidyl-tRNA accumulation (Figure 2.3B). These results show that the AdoMet-induced NPmRS of CGS1 is recapitulated in wild-type ACE (Murota *et al.* 2011).

At the standard RNA concentration used in ACE (50 fmol μl^{-1}), a second ribosome is stacked behind the initially stalled ribosome (Haraguchi *et al.* 2008, Yamashita *et al.* 2014), and at least two peptidyl-tRNA species, PtR-I and PtR-II, are produced in ACE *in vitro* translation (Figure 2.3B). To determine which one of the peptidyl-tRNA bands corresponds to the initially stalled ribosome at Ser-94, increasing amounts of *GST:CGS1(WT)* RNA were translated in wild-type ACE (Figure 2.3C). By increasing the amount of input RNA to be translated, the relative intensity

of the peptidyl-tRNA that corresponds to the secondary stalled ribosome will be reduced (Haraguchi *et al.* 2008, Yamashita *et al.* 2014), because the number of ribosomes on one mRNA is reduced. Apparently, the relative intensity of PtR-II was reduced with increasing amounts of *GST:Ex1(WT)* RNA in the translation reactions (Figure 2.3D). The result indicated that PtR-I is the initially stalled ribosome at Ser-94, while PtR-II is the secondarily stalled ribosome behind the initially stalled ribosome. To confirm this, the puromycin sensitivity of the peptidyl-tRNA was analyzed (Figure 2.3E and F). Puromycin, an analog of aminoacyl-tRNA, binds to the A-site of ribosomes and reacts with peptidyl-tRNA in the P-site, and releases nascent polypeptide as a peptidyl-puromycin (Carrasco *et al.* 1976). It is previously reported that the initially stalled ribosome at Ser-94 exhibits lower reactivity to puromycin than the secondarily stalled ribosome in WGE (Yamashita *et al.* 2014). The results also indicated that PtR-I corresponds to the initially stalled ribosome at Ser-94. Therefore, PtR-I band intensities were measured for calculation of stalling efficiencies of AdoMet-induced NPmRS of CGS1 in Chapter 3.

Ribosome stalling of the hCMV system in wild-type ACE

The *gp48/UL4 (gp48)* of hCMV, which encodes a 48-kDa glycoprotein, has three uORFs in its 5'-UTR (Figure 2.4A). The 22-amino-acid nascent peptide of hCMV *gp48* uORF2 causes ribosome stalling autonomously to down-regulate *gp48* expression during the early stages of infection (Geballe *et al.* 1986, Degrin *et al.* 1993). NPmRS of hCMV is an intrinsic feature of amino acid sequence encoded by uORF2 and any effector is not required to cause ribosome stalling. This reaction occurs in WGE and the structure of the stalled ribosome in WGE has been solved by cryo-EM (Bhushan *et al.* 2010, Wilson *et al.* 2016), but has not been studied in ACE.

Autonomous ribosome stalling of the hCMV system was analyzed in wild-type ACE (Figure 2.4). *TagI:DP75:hCMV* RNA carries *M8:His:HA* tags (*TagI*) and DP75 linker fused in-frame to the N-terminus of hCMV *gp48* uORF2 (Figure 2.4B). DP75 linker (Matheisl *et al.* 2015, Yamashita *et al.* 2017) was used to facilitate the detection of short polypeptide on SDS-PAGE. After the translation of *TagI:DP75:hCMV(WT)* RNA in wild-type ACE, translation products were analyzed by immunoblotting using an anti-HA antibody, which detected 15-kDa full-length product and RNase-sensitive 37-kDa peptidyl-tRNA bands (Figure 2.4C). In contrast, the translation of *TagI:DP75:hCMV(P21A)* RNA produced only 15-kDa full-length product (Figure 2.4C). The *P21A* mutation has been reported to abolish the NPmRS (Degrin *et al.* 1993, Matheisl *et al.* 2015).

Translation of a uORF generally down-regulates translation of the main ORF, and if

ribosomes stall on the uORF, the main ORF translation is strongly repressed (Hinnebush *et al.* 2016). To know whether the nascent peptide of hCMV *gp48* uORF2 represses expression of the downstream reporter gene, 5'-hCMV:*LUC* RNA that carries the 5'-UTR of hCMV *gp48* (Figure 2.4A) fused to *LUC* reporter gene (Figure 2.4D) was constructed. After the translation of 5'-hCMV:*LUC* RNA in wild-type ACE, the LUC activity was normalized with the control RLUC activity to obtain reporter activity. The reporter activity in the *P21A* construct was ~7 times higher than that in the WT construct (Figure 2.4E). These results show that autonomous ribosome stalling of the hCMV system is recapitulated in wild-type ACE.

Ribosome stalling of the AAP system in wild-type ACE

N. crassa arg-2 codes for an enzyme involved in L-arginine biosynthesis. The 24-amino-acid nascent peptide of AAP, the sequence encoded by *arg-2* uORF (Figure 2.5A), directs the ribosome to stall in response to high concentrations of L-arginine during translation termination of AAP in WGE (Wang and Sachs 1997, Wei *et al.* 2012). This reaction occurs in WGE and the structure of the stalled ribosome in WGE has been solved by cryo-EM (Bhushan *et al.* 2010), but has not been studied in ACE.

L-Arginine-induced ribosome stalling of the AAP system was analyzed in wild-type ACE (Figure 2.5). Since an anti-HA antibody only poorly detected the translation products, the experiments were carried out using *TagII:DP75:AAP* RNA that carry *M8:His:HA:3xFLAG:Myc* tag sequences (Figure 2.5B) and the translation products were detected using an anti-FLAG antibody. Translation of *TagII:DP75:AAP(WT)* RNA in the presence of 2.08 mM L-arginine produced RNase-sensitive 40-kDa peptidyl-tRNA in addition to 25-kDa full-length product, and the peptidyl-tRNA accumulation was evidently detected at 10 min after the start of translation (Figure 2.5C). The accumulation of 40-kDa peptidyl-tRNA was also detected with 0.08 mM L-arginine, which is the basal L-arginine concentration in ACE (Murota *et al.* 2011), although the level of accumulation was lower than at 2.08 mM. This is consistent with a previous report describing that L-arginine-induced stalling was observed even at 0.01 mM (Wang and Sachs 1997). The accumulation of peptidyl-tRNA was diminished when *TagII:DP75:AAP(D12N)* RNA was translated in the presence of 2.08 mM L-arginine (Figure 2.5D). The *D12N* mutation has been reported to abolish L-arginine-induced NPmRS of AAP (Wang and Sachs 1997). The results show that L-arginine-induced NPmRS of AAP is recapitulated in wild-type ACE.

Ribosome stalling of the AtAMD1 system in wild-type ACE

The *AtAMD1* encodes an enzyme involved in spermidine and spermine biosyntheses in Arabidopsis. The 5'-UTR sequence of *AtAMD1* has two uORFs: T-uORF and S-uORF (standing for Tiny uORF and Small uORF, respectively) (Figure 2.6A) (Hanfrey *et al.* 2005). The 52-amino-acid nascent peptide of S-uORF directs ribosome to stall in response to high concentrations of polyamines during translation termination of S-uORF in WGE (Uchiyama-Kadokura *et al.* 2014). This reaction is only partially characterized in ACE (Uchiyama-Kadokura *et al.* 2014).

Polyamine-induced ribosome stalling of the AtAMD1 system was analyzed in wild-type ACE (Figure 2.6). As an effector, spermidine was used in the present study (Uchiyama-Kadokura *et al.* 2014). *Tagl:DP75:S-uORF(WT)* RNA that carries *Tagl* and DP75 linker fused in-frame to the N-terminus of *AtAMD1* S-uORF (Figure 2.6B) was translated in wild-type ACE in the presence of 0.2 or 0.7 mM spermidine and analyzed by immunoblotting using an anti-HA antibody (Figure 2.6C). In the presence of 0.7 mM spermidine, RNase-sensitive 37-kDa peptidyl-tRNA was detected in addition to 18-kDa full-length product, and the accumulation of peptidyl-tRNA was dependent on spermidine concentration (Figure 2.6D and E). The spermidine concentration for standard translation assay in ACE is 0.5 mM, which is determined by assaying a reporter expression without uORF (Murota *et al.* 2011). Introduction of a frame-shift mutation in S-uORF abolished the peptidyl-tRNA accumulation (Figure 2.6C), as previously reported in WGE (Uchiyama-Kadokura *et al.* 2014).

To confirm the stalling function of S-uORF nascent peptide, a reporter assay was carried out at a various concentrations of spermidine. For this experiment, *5'-AtAMD1:LUC* RNA that carries the 5'-UTR of *AtAMD1* fused to *LUC* reporter gene (Figure 2.6F) was used. When the RNA carrying the WT S-uORF sequence was translated in wild-type ACE, the reporter activity was reduced as the concentration of spermidine was increased, whereas the reporter activity was significantly higher if the S-uORF sequence bears a frame-shift mutation (Figure 2.6G). These results show that polyamine-induced NPmRS of AtAMD1 is recapitulated in wild-type ACE.

Ribosome stalling of the mAMD1 system in wild-type ACE

The *mAMD1* codes for an enzyme involved in spermidine and spermine biosyntheses in mammals. The six-amino-acid uORF sequence, MAGDIS, of *mAMD1* directs the ribosome to stall in response to high concentrations of polyamines in WGE (Law *et al.* 2001, Raney *et al.*

2002). The ribosome stalling occurs at the termination codon of the uORF (Law *et al.* 2001, Raney *et al.* 2002). Both *mAMD1* and *AtAMD1* genes encode AdoMet decarboxylase, and are regulated by a uORF in a polyamine-dependent manner. However, the lengths and amino acid sequences of the uORFs are quite different (Figure 2.1).

Polyamine-induced ribosome stalling of the MAGDIS system was analyzed in wild-type ACE (Figure 2.7). Since an anti-HA antibody barely detected a peptidyl-tRNA band, *TagII:DP75:MAGDIS(WT)* RNA that carries *TagII* and DP75 linker fused in-frame to the N-terminus of *mAMD1* uORF (Figure 2.7B) was translated in Col-0 ACE in the presence of 0.2 or 0.7 mM spermidine. Immunoblot analysis using anti-FLAG antibody detected double bands of ~38-kDa peptidyl-tRNA when translated in the presence of 0.7 mM spermidine, while 20-kDa full-length product predominated when translated in 0.2 mM spermidine (Figure 2.7C). The accumulation of peptidyl-tRNA was evident at 10 min of translation (Figure 2.7D) and was dependent on the spermidine concentration (Figure 2.7E and F). When *TagII:DP75:MAGDIS(I5L)* RNA, which carries an *I5L* mutation that abolishes the polyamine-dependent NPmRS of MAGDIS (Raney *et al.* 2002), was used, peptidyl-tRNA accumulation was diminished (Figure 2.7C). Although the origin of the double bands for the peptidyl-tRNA is unknown, the intensities of the two bands paralleled in each of the experiments in Figure 2.7E. Therefore, I used both bands for calculation of stalling efficiencies of polyamine-induced NPmRS of *mAMD1* in Figure 2.7F.

To confirm polyamine-induced stalling, *5'-mAMD1:LUC* RNA that carries the 5'-UTR of *mAMD1* (Figure 2.7A) fused to *LUC* reporter gene (Figure 2.7G) was used for reporter assay. When the *5'-mAMD1:LUC(WT)* RNA was translated in wild-type ACE in the presence of 0.2 or 0.7 mM spermidine, the reporter activity at 0.7 mM spermidine was reduced compared with *5'-mAMD1:LUC(I5L)* RNA (Figure 2.7H). These results show that polyamine-induced NPmRS of *mAMD1* is recapitulated in wild-type ACE.

Ribosome stalling of the AUG-stop system in wild-type ACE

The expression of Arabidopsis *NIP5;1*, encoding a boric acid transporter, is down-regulated by ribosome stalling in response to high concentrations of boric acid at the minimum uORF, AUG-stop, which is coupled with *NIP5;1* mRNA degradation in WGE (Tanaka *et al.* 2016). I used a 306-nt 5'-UTR containing uORF3 and uORF4 (Figure 2.8A) (Tanaka *et al.* 2016), of which uORF4 is the AUG-stop. In general, at both the start and the termination codons, decoding by the ribosome takes longer than at other codons, and boric acid induces prolonged ribosome

stalling at AUG-stop. This reaction has been studied in WGE (Tanaka *et al.* 2016), but not in ACE.

For this response, the AUG codon has to be directly followed by one of the stop codons, and insertion of even a single codon and joining a tag or a linker sequence is detrimental (Tanaka *et al.* 2016). Therefore, effects of boric acid-induced ribosome stalling were evaluated by a reporter assay.

When 5'-*NIP5;1(WT):LUC* RNA (Figure 2.8B) was translated in wild-type ACE, relative reporter activity was reduced in a boric acid-dependent manner (Figure 2.8C). In contrast, disruption of AUG (AUCUAA) abolished the response (Figure 2.8C). These results show that the response of AUG-Stop to boric acid is recapitulated in wild-type ACE.

2.4. DISCUSSION

In this study, I presented two lines of evidence showing that six of the NPmRS in eukaryotes, including the AUG-stop system, is reproducible in the plant ACE system. Three out of six-regulatory nascent peptides are found in the Arabidopsis genome, whereas other three peptides are from non-plant species (Figure 2.1).

In this Chapter, I found that, first, stalling assays revealed that peptidyl-tRNA, a translation intermediate, is evidently accumulated in an amino acid-sequence dependent manner during *in vitro* translation of mRNA carrying the functional amino acid sequence (Figures 2.3C, 2.4C, 2.5D, 2.6C and 2.7C). Second, reporter assays of the uORFs showed that the nascent peptide represses the reporter expression when the 5'-UTR carrying the uORF is fused to a reporter gene (Figures 2.4E, 2.6G, 2.7H and 2.8C). These results corroborate previous findings that the regulatory peptides function in wheat ribosomes (Law *et al.* 2001, Raney *et al.* 2002, Fang *et al.* 2004, Onouchi *et al.* 2005, Bhushan *et al.* 2010, Uchiyama-Kadokura *et al.* 2014, Tanaka *et al.* 2016).

Species specificity of NPmRS systems

While ribosomal components, including rRNA and r-proteins, are a common platform responsible for NPmRS induction, some of the nascent peptides may be regarded as tailor-made to fit the respective ribosomes. The nascent peptide of MifM, encoded by *Bacillus subtilis yidC2* leader region, induces ribosome stalling in *B. subtilis* but not in *E. coli* (Chiba *et al.* 2011). This species dependency is dictated by the identity of a single amino acid within the β -loop of uL22 not

because *E. coli* does not contain a corresponding gene regulated by MifM (Chiba *et al.* 2009, Sohmen *et al.* 2015). The nascent peptides of the AAP, hCMV, and MAGDIS were all capable of inducing NPmRS in a heterogeneous system of ACE. This is consistent with a cryo-EM structure of the AAP- or hCMV-stalled wheat ribosomes (Bhushan *et al.* 2010), in which all the contacts observed between the nascent peptide and the ribosomal exit tunnel are at the residues that are highly conserved among plant ribosomes. Thus, species specific factor(s) do not appear to be required in these systems. The data presented in this study would add to the repertoire of heterologous conservation of ribosome stalling mechanisms.

Establishment of NPmRS systems

For a stalling assay, the standard incubation time in WGE (30 min) (Onouchi *et al.* 2005, Haraguchi *et al.* 2008, Onoue *et al.* 2011, Yamashita *et al.* 2014, Uchiyama-Kadokura *et al.* 2014) was applied for ACE *in vitro* translation. Nonetheless, peptidyl-tRNA species was differently accumulated after the start of translation irrespective of either mRNA lengths or effector concentrations when *TagII:DP75:AAP* and *TagII:DP75:MAGDIS* constructs were used (Figure 2.5C and 2.7D). For both cases, immunoblot analysis using an anti-HA antibody detected only a faint band, and accumulation of the peptidyl-tRNA was evidently detected at 10 min after the start of translation. The result corroborates a previous report that a full-length polypeptide with AAP was observed among the major translation products between 20- and 30-min after start of translation reaction (Fang *et al.* 2004). Therefore, all the translational regulations tested in this study can be recapitulated in wild-type ACE.

The use of the ACE system in molecular genetics

A cell-free translation system derived from Arabidopsis could become a powerful tool by enabling *in vitro* studies to be used in genetics approaches. ACE has been previously applied to a cytosolic 5'-3' exoribonuclease-deficient mutant of Arabidopsis (Souret *et al.* 2004) to elucidate the molecular mechanism of mRNA degradation (Murota *et al.* 2011), overcoming a major limitation for plant translational studies that have relied almost solely on WGE, which is prepared from genetically less tractable source. As exemplified by the analysis of programmed ribosome stalling in wild-type ACE, my data obtained here would provide means by which the complex nature of the NPmRS systems can be explored.

2.5. TABLES

Table 2.1. Plasmids used in this study and primers used to construct plasmids.

Name	Construct ^a	Source	Primer ^b	
			Forward	Reverse
<i>Plasmids used for stalling assay</i>				
pST00	SP6::M8:His:HA:DP75	this study	DP75f	DP75r
pST55	SP6::M8:His:HA:DP75:AAP(WT)	this study	AAPf	AAPr
pST56	SP6::M8:His:HA:DP75:AAP(D12N)	this study	D12Nf	AAPr
pST57	SP6::M8:His:HA:DP75:hCMV(WT)	this study	hCMVf	hCMVr
pST58	SP6::M8:His:HA:DP75:hCMV(P21A)	this study	hCMVf	P21Ar
pST76	SP6::M8:His:HA:DP75:S-uORF(WT)	this study	SAMDC1f	SAMDC1r
pST77	SP6::M8:His:HA:DP75:S-uORF(fs)	this study	SAMDC1fsf	SAMDC1fsr
pST116	SP6::M8:His:HA:DP75:MAGDIS(WT)	this study	DP75f	MAGDISr
pST117	SP6::M8:His:HA:DP75:MAGDIS(I5L)	this study	DP75f	I5Lr
pTI5	SP6::M8:His:HA:3xFLAG:Myc:DP75:AAP(WT)	this study	3xFLAGf	3xFLAGr
pTI6	SP6::M8:His:HA:3xFLAG:Myc:DP75:AAP(D12N)	this study	3xFLAGf	3xFLAGr
pNU14	SP6::GST:S-uORF(WT):RLUC	Uchiyama-Kadokura <i>et al.</i> 2014		
pNU15	SP6::GST:S-uORF(fs):RLUC	Uchiyama-Kadokura <i>et al.</i> 2014		
pYF2	SP6::GST:CGS1(WT)	Haraguchi <i>et al.</i> 2008		
pYF3	SP6::GST:CGS1(mto1-1)	Haraguchi <i>et al.</i> 2008		
pYK00	SP6::M8:CGS1(WT)	Onoue <i>et al.</i> 2011		
pYY105	T7::His:HA:DP75:uORF2(WT)	Yamashita <i>et al.</i> 2017		
<i>Plasmids used for reporter assay</i>				
pST118	SP6::mAMD1 5'-UTR(WT):LUC	this study	MAGDIS(WT)f	MAGDIS(WT)r
pST119	SP6::mAMD1 5'-UTR(I5L):LUC	this study	MAGDIS(I5L)f	MAGDIS(WT)r
pST120	SP6::AtAMD1 5'-UTR(WT):LUC	this study	SAMDC1f2	SAMDC1r2
pST121	SP6::AtAMD1 5'-UTR(fs):LUC	this study	SAMDC1f2	SAMDC1r2
pST122	SP6::gp48 5'-UTR(WT):LUC	this study	hCMVf2	hCMVr2
pST123	SP6::gp48 5'-UTR(P21A):LUC	this study	hCMVf2	P21Ar2
pMI21	SP6::CGS1:LUC(WT)	Chiba <i>et al.</i> 2003		
pMI27	SP6::RLUC	Chiba <i>et al.</i> 2003		
pMT131	SP6::AtNIP5;1 5'-UTR(WT):LUC	Tanaka <i>et al.</i> 2016		
pMT132	SP6::AtNIP5;1 5'-UTR(ATCTAA):LUC	Tanaka <i>et al.</i> 2016		
pSY209	SP6::S-uORF(WT):RLUC	Uchiyama-Kadokura <i>et al.</i> 2014		
pSY214	SP6::S-uORF(fs):RLUC	Uchiyama-Kadokura <i>et al.</i> 2014		

^a Double colons indicate fusion of promoter sequence and an ORF, and single colons indicate an in-frame translational fusion (*i.e.*, *Promoter::ORF:ORF: ...*).

^b Primers used for construction. Sequences of the primers are listed in Table 2.2.

CHAPTER 2. Characterization of regulatory nascent peptides

Table 2.2. Primers used in this study.

Name	Sequence (5' to 3')	Source
<i>Plasmids construction^a</i>		
DP75f	<u>GATTCTAGACATCATCATCATCATTACCC</u>	this study
DP75r	CAT <u>GGATCC</u> GGCCATTCTGATATCCATTTCAATTTTATTGTCACT	this study
AA Pf	CAT <u>GATATC</u> ATGAACGGTCGCCCGTCAGTCTTCACTAGTCAGGATTACCTCTCA GACCATC	this study
AA Pr	CTAG <u>GATCC</u> GAGAGGCTCTCACGCGTTAAGGGCTCTCCACAGATGGTCTGAGAG G	this study
D12Nf	CAT <u>GATATC</u> ATGAACGGTCGCCCGTCAGTCTTCACTAGTCAGAATTACCTCTCA GACCATC	this study
hCMVf	CAT <u>GATATC</u> ATGGAACCGCTGGTGTGAGTGCAGAAAAACTGAGCAGCCTGCTG AC	this study
hCMVr	CTAGGATCCTCGAGTGCTTTAAGGAGGAATATATTTGCAGGTCAGCAGGC	this study
P21Ar	CTAGGATCCTCGAGTGCTTTAAGGAGCAATATATTTGCAGGTCAGCAGGC	this study
hCMVf2	<u>GATTCTAGAAATCAGTTGCCGGCCTTACCATGGAACCGCTGGTGTGAGTGC</u> GA AAAACTGAGCAGCCTGCTGACCTGC	this study
hCMVr2	CATA <u>AGCTTACCCAGACAACGGTGCTTTATAGACTCATCACTTAAGGAGGAATA</u> TATTTGCAGGTCAGCAGGC	this study
P21Ar2	CATA <u>AGCTTACCCAGACAACGGTGCTTTATAGACTCATCACTTAAGGAGCAATA</u> TATTTGCAGGTCAGCAGGC	this study
SAMDC1f	CAT <u>GATATC</u> ATGATGGAGTCGAAAGGTG	this study
SAMDC1r	CTAGGATCCTCAGGATGGCCTCTTGGA	this study
SAMDC1fsf	CAT <u>GATATC</u> ATGATGGAGCGAAAGGTG	this study
SAMDC1fsr	CTAGGATCCTCAGGATGGCCTCTTGGA	this study
SAMDC1f2	<u>GATTCTAGATCTCATTGCTTCATCATTACCA</u>	this study
SAMDC1r2	CATCCATGGCTCGCCTTGTGTGTGAG	this study
MAGDISr	CATGGATCCCTAGCTAATGTGCCGGCCATGATATCCATTTTC	this study
I5Lr	CATGGATCCCTAGCTAAGGTGCCGGCCATGATATCCATTTTC	this study
MAGDIS(WT)f	<u>GATTCTAGACTTACACAGTATGGCCGGCGACATTAGCTAGCGCTCGCTCTACTC</u> TCTCTAACGGGAAACAG	this study
MAGDIS(I5L)r	<u>GATTCTAGACTTACACAGTATGGCCGGCGACATTAGCTAGCGCTCGCTCTACTC</u> TCTCTAACGGGAAACAG	this study
MAGDIS(WT)r	CATCCATGGTGGAAATAGAGGCAGATACAGCTCAGTCTCTTGTAGTCCGCTGTT TCCCCGTTAG	this study
Myc:DP75f	TCAGAGGAGGACCTGGAAGGTGGCGAAGAAGAAGTTGAG	this study
HAMycr	GATCAGCTTCTGCTCAGCGTAATCTGGAACATCGTATGGG	this study
Mycf	GAGCAGAAGCTGATCTCAGAGGAG	this study
HAr	AGCGTAATCTGGAACATCGTATGGG	this study
3xFLAGf	GTTCCAGATTACGCTGACTACAAAGACCATGACGGTGATTATAAAGATCATGAC ATCGACTACAAAGACG	this study
3xFLAGr	GATCAGCTTCTGCTCCTTGTGTCATCGTCTTTGTAGTCGATGTCATGATC	this study
<i>Generating DNA templates for in vitro transcription</i>		
SP65'fp	CATCAGAGCAGATTGTA CTG	Onoue <i>et al.</i> 2011
poly(A)r	ACGAGCCGGAAGCATAAAG	this study

^a Restriction sites used for cloning the PCR-amplified fragments are underlined.

2.6. FIGURES

Amino acid residues from PTC when stalled	Constriction region	Stall system	Organism	Gene / ORF	Effector	Step
-50 -40 -30 -20 -10 -1		CGS1	plant	<i>AtCGS1</i> / main	AdoMet	elongation
...AGISSSFTGDAGLSSRILRFPPNFVRQLSIKARRNCSNIGVAQI VAAKWS ...		hCMV	virus	<i>gp48</i> / uORF	autonomous	termination
	MEPLVLSAKKLSLLTCKYI PP *	AAP	fungi	<i>Nc arg-2</i> / uORF	L-arginine	termination
	MNGRPSVFTSQDYLS DHLWRALNA *	AtAMD	plant	<i>AtAMD1</i> / uORF	polyamines	termination
MMESKGGKKKSSSSSFLFYEAPLGYSIEDVRP NGGIKFKSSVYSNCSKRPS *		MAGDIS*	mammal	<i>mAMD1</i> / uORF	polyamines	termination
	MAGDIS*	AUG-Stop	plant	<i>AtNIP5;1</i> / uORF	boric acid	termination

Figure 2.1. The stalling systems analyzed in this study.

For each system, the gene and ORF (main ORF or uORF) in which stalling occurs, effector molecule, and translation step at which stalling occurs (elongation or termination) are shown. Amino acid sequences relevant for stalling in CGS1 or those encoded by the uORFs are shown. Amino acid residues important for NPmRS (Alderete *et al.* 1993, Degnin *et al.* 1993, Wang and Sachs 1997, Law *et al.* 2001, Ominato *et al.* 2002, Raney *et al.* 2002, Onouchi *et al.* 2005, Spevak *et al.* 2010, Tanaka *et al.* 2016) are marked in red. For AtAMD1, functional amino acids are not reported, while importance of the amino acid sequence was shown by a frame-shift mutation (Uchiyama-Kadokura *et al.* 2014). The MTO1 region (Ominato *et al.* 2002) of CGS1 is underlined with ambiguous amino acids in dotted underline. Amino acid residues are numbered from the stalled residue (-1, marked with a clover). Approximate position of the constriction region is shaded. Since the nascent peptide may form α -helix in the PTC-proximal region as reported in AAP and hCMV (Bhushan *et al.* 2010, Wilson *et al.* 2016), residues that cross over the constriction region may be shifted to the left.

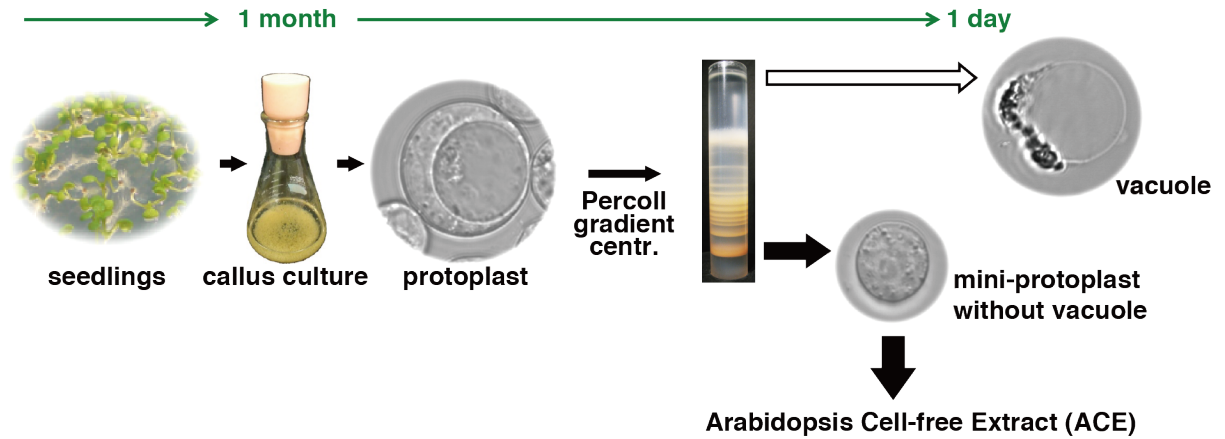


Figure 2.2. Outline of the preparation of ACE *in vitro* translation system from Arabidopsis seedlings.

One-week-old Arabidopsis seedlings were minced and were cultured with rotatory shaking in the dark. The culture medium was changed every six days. Three days after the third medium change, protoplasts were prepared. Plant cells have a large central vacuole that contains nucleases and proteases. The protoplasts were subjected to Percoll gradient centrifugation to obtain evacuated mini-protoplasts from which vacuoles were removed. The evacuated mini-protoplasts were disrupted using a Dounce homogenizer and the lysate was used to prepare an ACE *in vitro* translation cocktail. ACE can be prepared in one month after sowing Arabidopsis seeds. Note that the ACE preparation protocol (Murota *et al.* 2011) has a typographical error of m/ μ (Corrigendum: Murota *et al.* 2011).

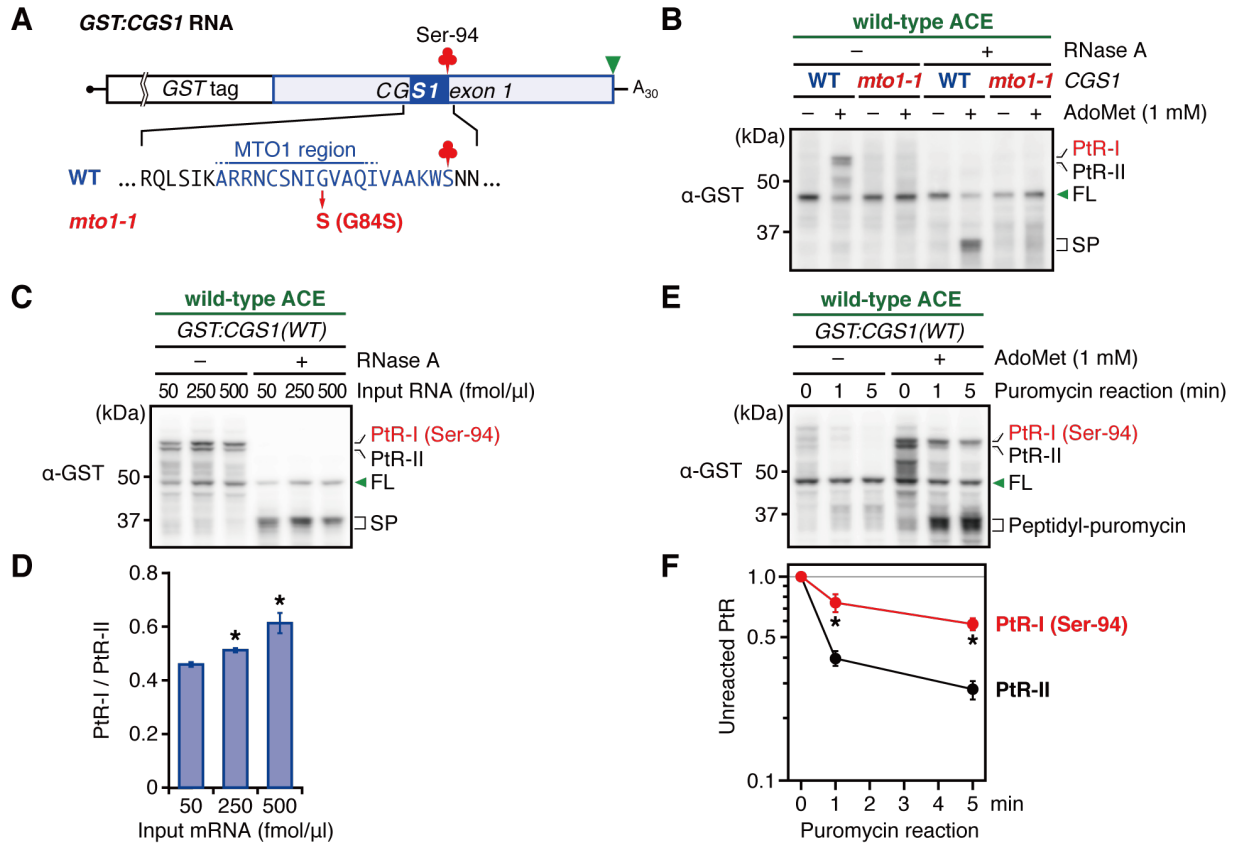


Figure 2.3. The CGS1 system in wild-type ACE.

(A) Schematic representation of *GST:CGS1* RNA for stalling assay. The RNA carries a glutathione S-transferase (GST) tag sequence fused in-frame to the N-terminus of the *CGS1* exon 1 coding sequence (Onouchi *et al.* 2005, Haraguchi *et al.* 2008). The amino acid sequences around the MTO1 region of the wild-type (WT) *CGS1* and *mto1-1* (G84S) mutation are shown. AdoMet-induced NPmRS occurs at Ser-94 (red clover). The MTO1 region (Ominato *et al.* 2002) is indicated. (B) *GST:CGS1(WT)* and *GST:CGS1(mto1-1)* RNAs ($50 \text{ fmol } \mu\text{l}^{-1}$) were translated in wild-type ACE for 30 min in the absence (–) or presence (+) of 1 mM AdoMet. In “RNase +” lanes, samples were treated with RNase A before separation by SDS-PAGE. The positions of the 45-kDa full-length product (FL), the ~55-kDa peptidyl-tRNAs (PtR-I and PtR-II), and the 35-kDa stalled peptide (SP) produced by RNase A treatment are indicated. A representative result of duplicate experiments is shown. (C) *GST:CGS1(WT)* RNA was translated in wild-type ACE at different RNA concentrations for 30 min. In “RNase +” lanes, samples were treated with RNase A before separation by SDS-PAGE. A representative result of triplicate experiments is shown. Bands are marked as in (B). (D) The immunoblot signals in (C) were quantified and relative intensity of PtR-I to PtR-II was calculated. Means \pm SD of three independent experiments are shown. Asterisks indicate significant differences compared with the standard condition at 50 fmol

μl^{-1} RNA ($p < 0.05$, Welch's t -test). **(E)** *GST:CGS1(WT)* RNA was translated in wild-type ACE. After 30 min of translation, puromycin was added at a final concentration of 2 mM and samples were withdrawn at the indicated time points. The position of the 35-kDa peptidyl-puromycin is indicated. A representative result of triplicate experiments is shown. **(F)** The immunoblot signals in (E) were quantified, and the intensity of unreacted peptidyl-tRNA was normalized to that at time 0. Means \pm SD of three independent experiments are shown. Asterisks indicate significant differences between PtR-I and PtR-II at each time point ($p < 0.05$, Welch's t -test).

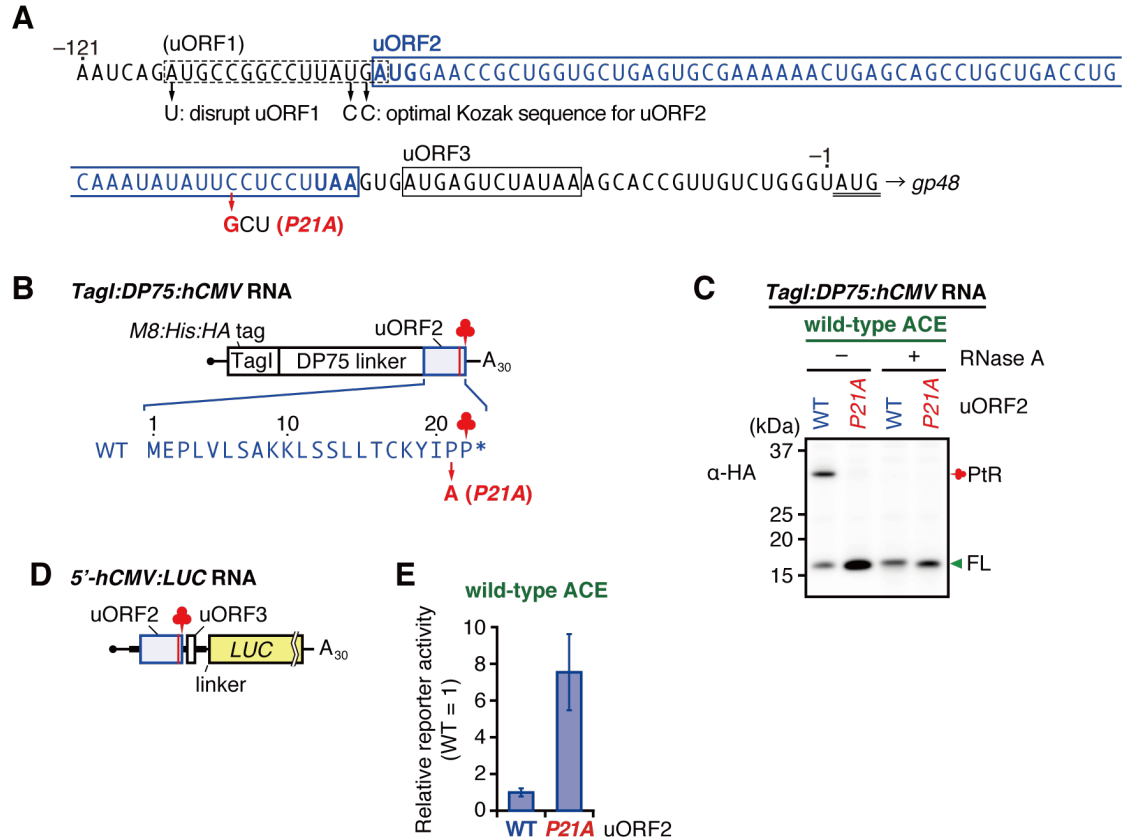


Figure 2.4. The hCMV system in wild-type ACE.

(A) 5'-UTR sequence of hCMV *gp48/UL4* (Cao and Geballe 1995). uORFs are boxed and the start codon of *gp48* is double-underlined. uORF2 is the functional uORF for NPmRS. uORF1 (dashed box) was disrupted and the Kozak sequence for uORF2 was optimized in previous studies (Alderete *et al.* 1999, Cao and Geballe 1995, 1996, Geballe *et al.* 1986), and the same sequence was used in the present study. The substituted nucleotide in Pro-21 to alanine mutation (*P21A*) in uORF2, which abolishes the NPmRS (Geballe *et al.* 1986), is indicated. (B) Schematic representation of *Tagl:DP75:hCMV RNA* for stalling assay. The uORF2 was joined in-frame to the *M8:His:HA* tags (*Tagl*) and DP75 linker. The amino acid sequences of the *gp48* uORF2 and *P21A* mutation are shown. Ribosome stalls autonomously at the stop codon of uORF2 (red clover). (C) *Tagl:DP75:hCMV(WT)* and *Tagl:DP75:hCMV(P21A)* RNAs were translated in wild-type ACE for 30 min. Translation products were separated by SDS-PAGE and analyzed by immunoblotting using anti-HA antibody. For “RNase +” lanes, samples were treated with RNase A before separation by SDS-PAGE. The positions of the 15-kDa full-length product (FL) and the 35-kDa peptidyl-tRNA (PtR) are indicated. A representative result of duplicate experiments is shown. (D) Schematic representation of *5'-hCMV:LUC RNA* used for reporter assay. The 5'-UTR sequence (-1 to -121 nt) in (A) was joined to the *LUC* reporter gene through

a linker sequence, AAGCUUUC. **(E)** *5'-hCMV:LUC(WT)* and *5'-hCMV:LUC(P21A)* RNAs were translated in wild-type ACE for 120 min. LUC activity was normalized with control RLUC activity from co-translated *RLUC* RNA, and the reporter activity relative to that in *5'-hCMV:LUC(WT)* RNA was calculated. Means \pm SD of three independent experiments are shown.

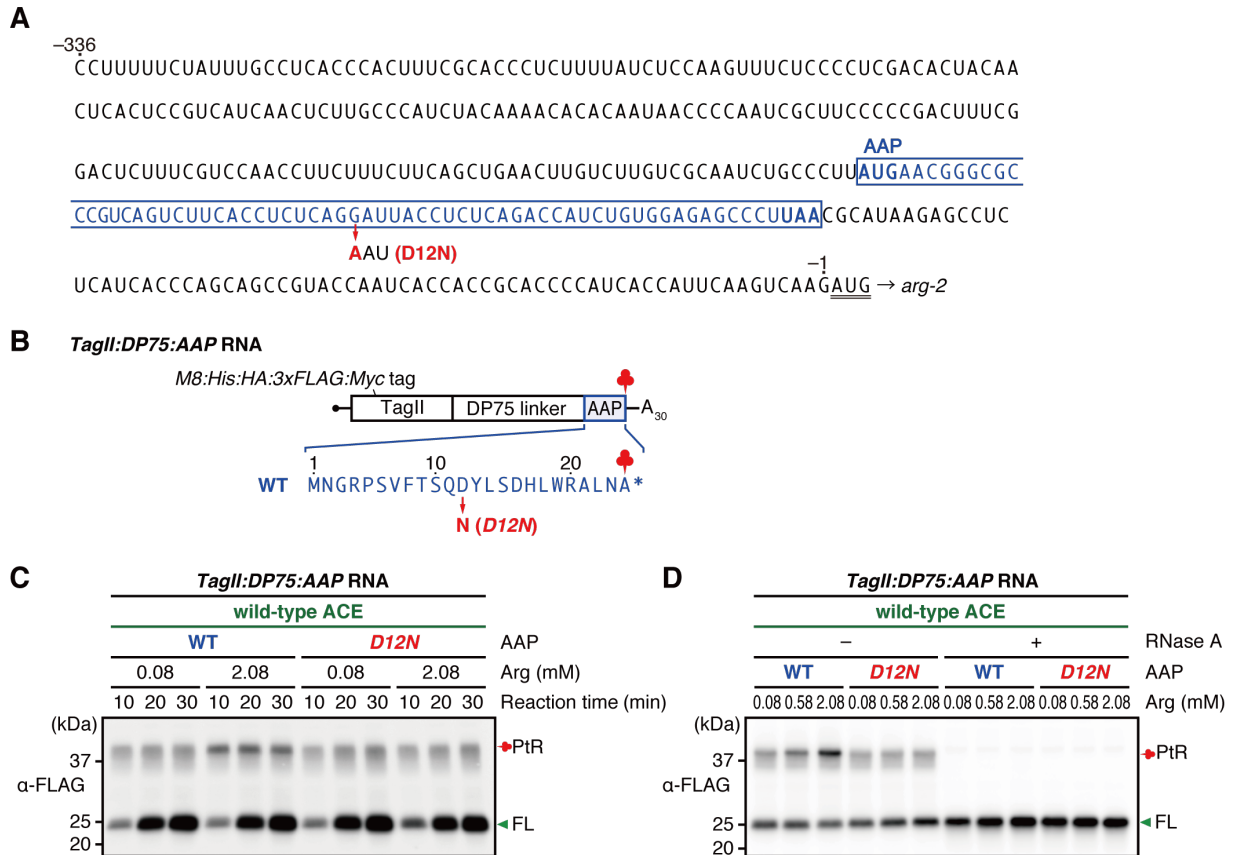


Figure 2.5. The AAP system in wild-type ACE.

(A) The 5'-UTR sequence of *N. crassa arg-2* (Wang and Sachs 1997). uORF (AAP) is boxed and the start codon of *arg-2* is double-underlined. The nucleotide substituted in Asp-12 to asparagine (*D12N*) mutation is indicated. *D12N* mutation abolishes the L-arginine-dependent NPmRS of AAP (Wang and Sachs 1997). (B) Schematic representation of *TagII:DP75:AAP RNA* used for stalling assay. The AAP sequence was joined in-frame to the *M8:His:HA:3xFLAG:Myc* tags (*TagII*) and DP75 linker. The amino acid sequences of AAP and *D12N* mutation are shown. L-Arginine-dependent NPmRS occurs at the stop codon (red clover). (C) *TagII:DP75:AAP(WT)* and *TagII:DP75:AAP(D12N)* RNAs were translated in wild-type ACE at 0.08 or 2.08 mM L-arginine (Arg). Translation products were withdrawn at the indicated time points and analyzed by immunoblotting using anti-FLAG antibody. The positions of the 37-kDa peptidyl-tRNA (PtR) and 20-kDa full-length product (FL) are indicated. A representative result of duplicate experiments is shown. (D) *TagII:DP75:AAP(WT)* and *TagII:DP75:AAP(D12N)* RNAs were translated in wild-type ACE for 10 min at different Arg concentrations. Translation products were analyzed as in (C). For “RNase +” lanes, samples were treated with RNase A before separation by SDS-PAGE. A representative result of duplicate experiments is shown.

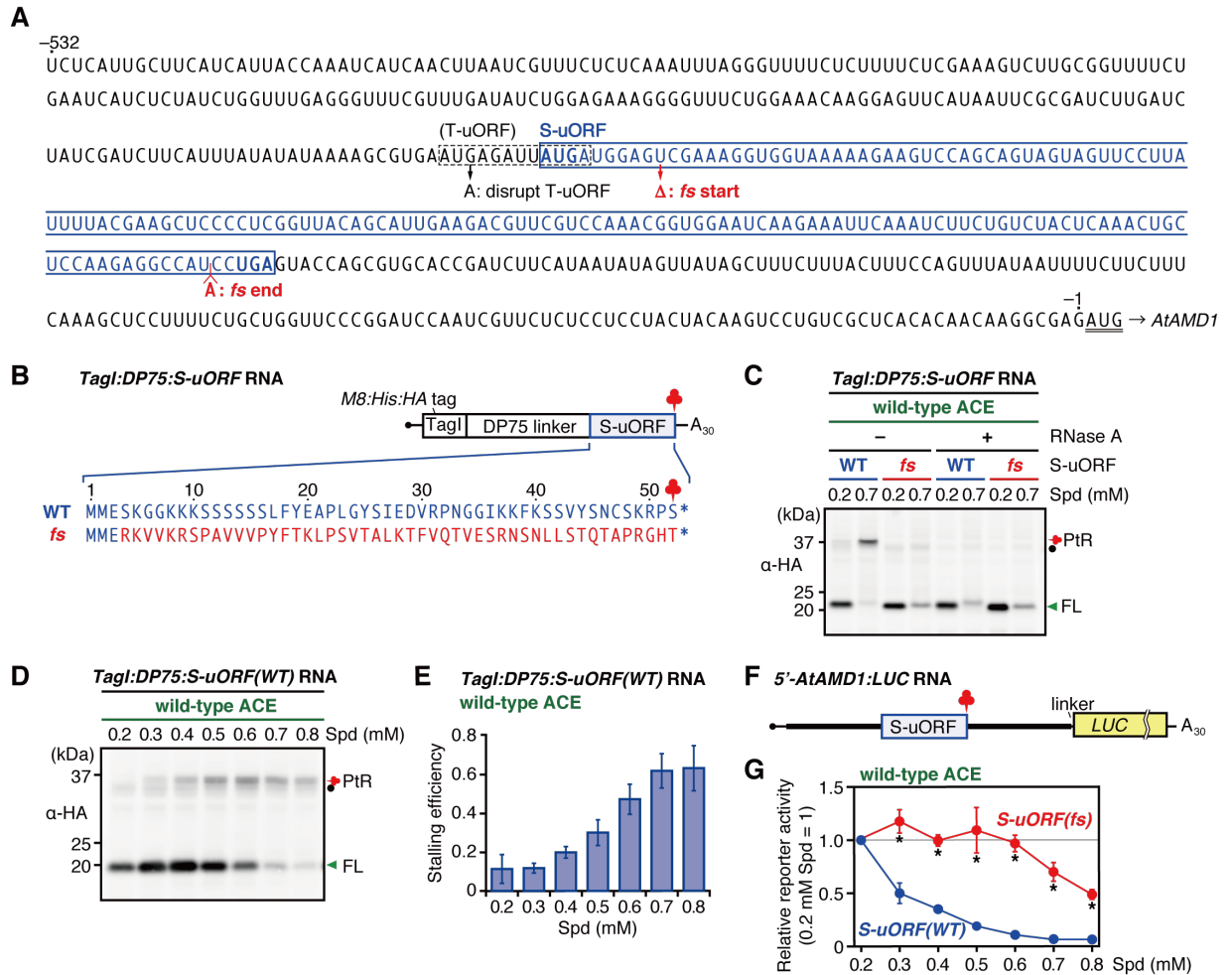


Figure 2.6. The *AtAMD1* system in wild-type ACE.

(A) The 5'-UTR sequence of *AtAMD1* (Uchiyama-Kadokura *et al.* 2014). The 5'-UTR sequence of *AtAMD1* has two uORFs, T-uORF and S-uORF (standing for Tiny uORF and Small uORF, respectively) (Hanfrey *et al.* 2005). The S-uORF is boxed and the start codon of *AtAMD1* is double-underlined. The T-uORF was disrupted as in a previous study (Uchiyama-Kadokura *et al.* 2014) and is marked with a dashed box. The nucleotides that are deleted and inserted to generate the frame-shift mutant are indicated. (B) Schematic representation of *Tagl:DP75:S-uORF* RNA used for stalling assay. The S-uORF sequence was joined in-frame to the M8:His:HA tags (*Tagl*) and DP75 linker. The amino acid sequences of *AtAMD1* S-uORF and frame-shift (*fs*) mutation are shown. Polyamine-dependent NPmRS occurs at the stop codon of S-uORF (red clover) (Uchiyama-Kadokura *et al.* 2014). (C) *Tagl:DP75:S-uORF(WT)* and *Tagl:DP75:S-uORF(fs)* RNAs were translated in wild-type ACE for 30 min at 0.2 or 0.7 mM spermidine (Spd). Translation products were separated by SDS-PAGE and analyzed by immunoblotting using anti-HA antibody. For "RNase +" lanes, samples were treated with RNase A before separation by SDS-PAGE. The positions of the 37-kDa peptidyl-tRNA (PtR) and 18-kDa

full-length product (FL) are indicated. A black dot indicates a nonspecific signal. A representative result of duplicate experiments is shown. **(D)** *Tag1:DP75:S-uORF(WT)* RNA was translated in wild-type ACE at various Spd concentrations. Translation products were analyzed as in (C). A representative result of triplicate experiments is shown. **(E)** The immunoblot signals in (D) were quantified and the stalling efficiencies were calculated. Means \pm SD of three independent experiments are shown. **(F)** Schematic representation of *5'-AtAMD1:LUC* RNA used for reporter assay. The 5'-UTR sequence (-1 to -532) in (A) was joined to the *LUC* reporter gene through a linker, CC. **(G)** *5'-AtAMD1:LUC(WT)* and *5'-AtAMD1:LUC(fs)* RNAs were translated in wild-type ACE for 120 min at various Spd concentrations. LUC activity was normalized with control RLUC activity from co-translated *RLUC* RNA, and the reporter activity relative to that at 0.2 mM Spd was calculated. Means \pm SD of three independent experiments are shown. Asterisks indicate significant differences at each Spd concentration ($p < 0.05$, Welch's *t*-test).

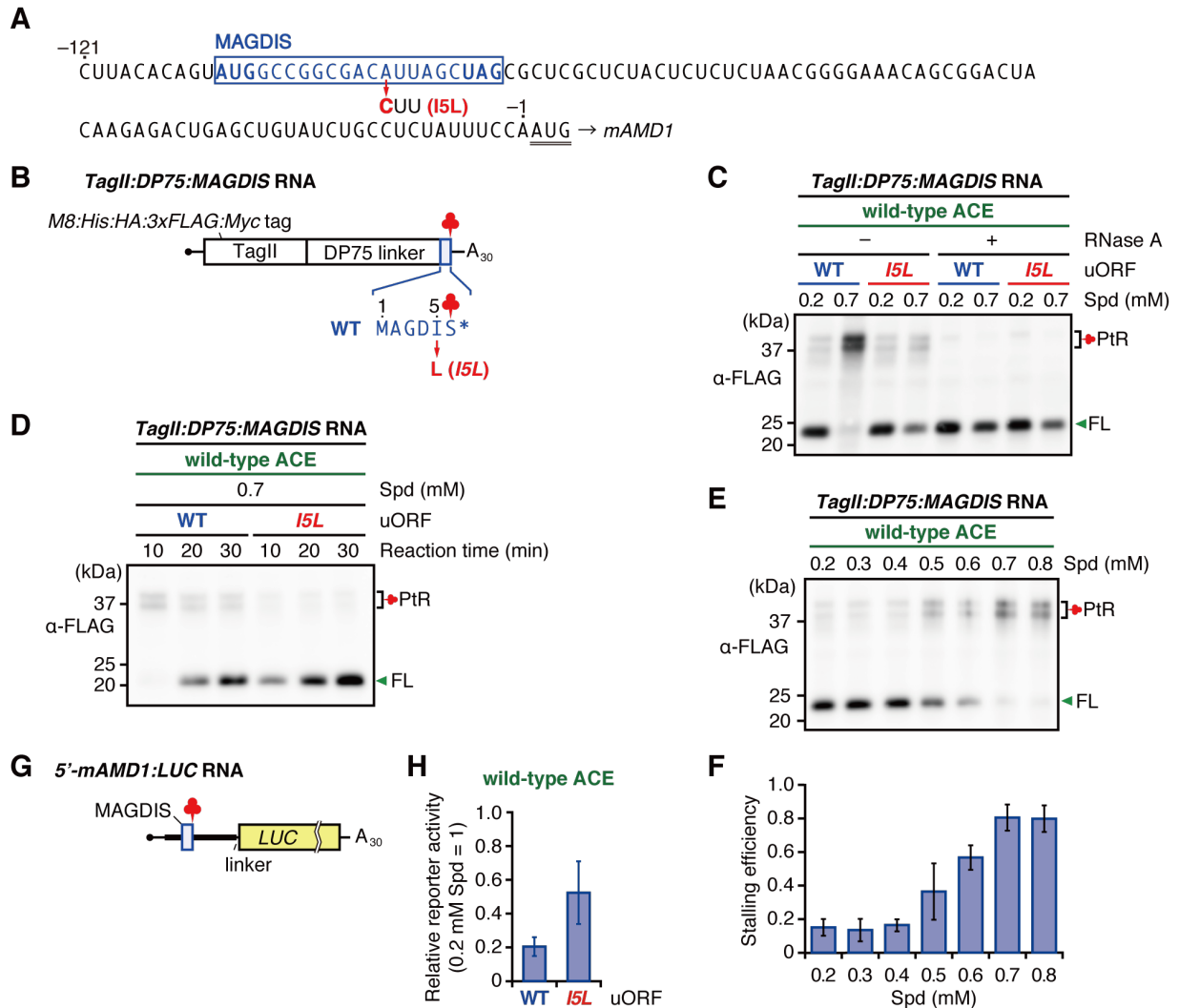


Figure 2.7. The MAGDIS system in wild-type ACE.

(A) The 5'-UTR sequence of *mAMD1* (Hill and Morris 1992, Ruan *et al.* 1996). uORF is boxed and the start codon of *mAMD1* is double underlined. The nucleotide substituted in *I5L* mutant, which abolishes the stalling (Law *et al.* 2001), is indicated. (B) Schematic representation of *TagII:DP75:MAGDIS RNA* used for stalling assay. The uORF sequence was joined in-frame to the M8:His:HA:3xFLAG:Myc tags (*TagII*) and DP75 linker. The amino acid sequences of WT and *I5L* mutation are shown. (C) *TagII:DP75:MAGDIS(WT)* and *TagII:DP75:MAGDIS(I5L)* RNAs were translated in wild-type ACE for 10 min at 0.2 or 0.7 mM spermidine (Spd). Translation products were analyzed by immunoblot analysis using anti-FLAG antibody. The positions of the 20-kDa full-length product (FL), and the 38-kDa peptidyl-tRNAs (PtR) are indicated. For "RNase +" lanes, samples were treated with RNase A before separation by SDS-PAGE. (D) *TagII:DP75:MAGDIS(WT)* RNA and *TagII:DP75:MAGDIS(I5L)* RNA were translated in wild-type ACE at 0.7 mM Spd. Translation products were withdrawn at the indicated time points and

analyzed by immunoblot analysis as in (C). **(E)** *TagII:DP75:MAGDIS(WT)* RNA was translated in wild-type ACE at various Spd concentrations. Translation products were analyzed as in (C). **(F)** The immunoblot signals in (E) were quantified and the stalling efficiencies were calculated. Means \pm SD of three independent experiments are shown. **(G)** Schematic representation of *5'-mAMD1:LUC* RNA used for reporter assay. The 5'-UTR (-1 to -121) sequence in (A) was joined to the *LUC* reporter gene through a linker, CC. **(H)** *5'-mAMD1:LUC(WT)* and *5'-mAMD1:LUC(fs)* RNAs were translated in wild-type ACE for 120 min at 0.2 mM or 0.7 mM Spd. LUC activity was normalized with control RLUC activity from co-translated *RLUC* RNA, and the reporter activity relative to that at 0.2 mM Spd was calculated. Means \pm SD of three independent experiments are shown. Asterisks indicate significant differences at each Spd concentration ($p < 0.05$, Welch's *t*-test).

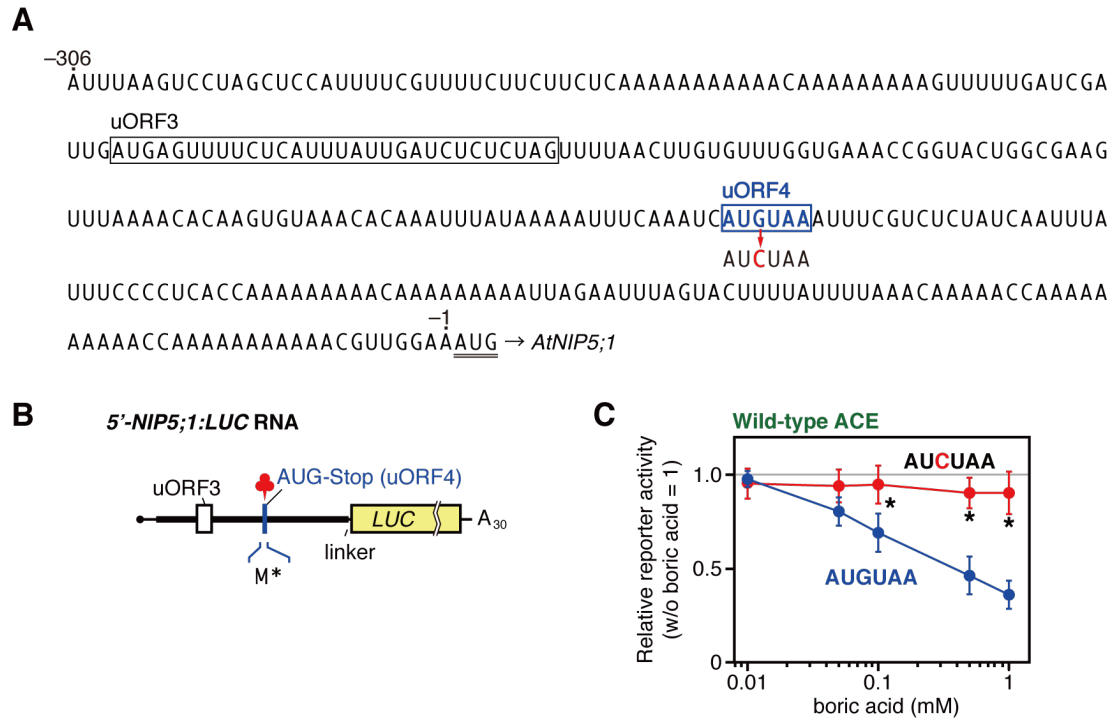


Figure 2.8. The AUG-Stop system in wild-type ACE.

(A) The 306-nt 5'-UTR sequence of *AtNIP5;1* (Tanaka *et al.* 2016). The uORFs are boxed and the start codon of *AtNIP5;1* is double-underlined. The nucleotide substituted in *AUCUAA* mutant is indicated. (B) Schematic representation of *5'-NIP5;1:LUC* RNA used for reporter assay. The 306-nt 5'-UTR sequence was joined to the *LUC* reporter gene through a linker, CC. (C) *5'-NIP5;1:LUC(AUGUAA)* and *5'-NIP5;1:LUC(AUCUAA)* RNAs were translated in wild-type ACE for 120 min at various boric acid concentrations. LUC activity was normalized with control RLUC activity from co-translated *RLUC* RNA, and the reporter activity relative to that without boric acid was calculated. Asterisks indicate significant differences at each boric acid concentration ($p < 0.05$, Welch's *t*-test).

CHAPTER 3.

Reverse genetics-based biochemical studies of the ribosomal exit tunnel constriction region in eukaryotic ribosome stalling: spatial allocation of the regulatory nascent peptide at the constriction

ABSTRACT: A number of regulatory nascent peptides have been shown to regulate gene expression by causing programmed ribosome stalling during translation. Nascent peptide emerges from the ribosome through the exit tunnel, and one-third of the way along which β -loop structures of ribosomal proteins uL4 and uL22 protrude into the tunnel to form the constriction region. Structural studies have shown interactions between nascent peptides and the exit tunnel components including the constriction region. In eukaryotes, however, there is a lack of genetic studies for the involvement of the constriction region in ribosome stalling. Here, I used transgenic Arabidopsis lines that carry mutations in the β -loop structure of uL4. Translation analyses using a cell-free translation system derived from the transgenic Arabidopsis carrying the mutant ribosome showed that the uL4 mutations reduced the ribosome stalling of four eukaryotic stalling systems, including those for which stalled structures have been solved by cryo-electron microscopy. The data obtained in the present study, which showed differential effects of the uL4 mutations depending on the stalling systems, explained the spatial allocations of the nascent peptides at the constriction that were deduced by structural studies. Conversely, the present data may predict allocation of the nascent peptide at the constriction of stalling systems for which structural studies are not done.

3.1. Introduction

3.2. Materials and Methods

3.3. Results

3.4. Discussion

3.5. Tables

3.6. Figures

3.1. INTRODUCTION

During translation, new peptide bonds are formed at the peptidyltransferase center (PTC) in the ribosomal large subunit, and the growing peptide passes through the exit tunnel that penetrates the large subunit before emerging from the ribosome. However, some of the nascent peptides, or the regulatory nascent peptides, direct the ribosome to stall during translation. This nascent peptide-mediated ribosome stalling (NPmRS) occurs either autonomously or is facilitated by an effector molecule, at either elongation or termination of translation, and on either the main open reading frame (ORF) or an upstream ORF (uORF) (Ito and Chiba 2013), which is a small ORF present upstream of the main ORF of eukaryotic mRNAs.

The ribosomal exit tunnel is approximately 100 Å long and holds 30–40 amino acid residues of the nascent peptide (Morgan *et al.* 2000, Nissen *et al.* 2000). Regulatory nascent peptides are usually 20–30 amino acids long and function while inside the exit tunnel. In both bacteria and eukaryotes, β -loop structures of two ribosomal proteins, uL4 and uL22 (Ban *et al.* 2014), which protrude into the exit tunnel, form a constriction region located 30–40 Å from the PTC (Morgan *et al.* 2000, Nissen *et al.* 2000). This region has been suggested to function as a discriminating gate by interacting with the nascent peptides (Nakatogawa and Ito 2002).

In bacteria, forward and reverse genetics studies have revealed the importance of interactions between the nascent peptide and the constriction region in mediating NPmRS (Nakatogawa and Ito 2002, Cruz-Vera *et al.* 2005, Chiba *et al.* 2011, Ramu *et al.* 2011, Cymer *et al.* 2015). This is supported by structural analyses of stalled ribosomes using cryo-electron microscopy (cryo-EM), which identified physical contacts of the nascent peptides with exit tunnel components, including the constriction region (Bhushan *et al.* 2011, Bischoff *et al.* 2014, Sohmen *et al.* 2015, Zhang *et al.* 2015).

In eukaryotes, cryo-EM studies revealed physical contacts of the nascent peptides with the constriction region in stalled ribosomes of *Neurospora crassa arg-2* uORF, termed the arginine attenuator peptide (AAP) (the AAP system), and human cytomegalovirus (hCMV) *gp48* uORF (the hCMV system) (Bhushan *et al.* 2010, Matheisl *et al.* 2015, Wilson *et al.* 2016). However, there is no genetic evidence showing the contribution of the constriction region to ribosome stalling.

In *Arabidopsis* *CGS1*, encoding cystathionine γ -synthase, the first committed enzyme of methionine biosynthesis, *S*-adenosyl-L-methionine (AdoMet), a direct metabolite of methionine, induces NPmRS during translation elongation at Ser-94 (the CGS1 system) (Onouchi *et al.* 2005, Onoue *et al.* 2011, Yamashita *et al.* 2014). The functional amino acid sequence for the response

to AdoMet is termed as MTO1 region (Chiba *et al.* 1999, 2003, Ominato *et al.* 2002). Studies using the wheat germ extract (WGE) *in vitro* translation system revealed that the nascent peptide adopts a compact conformation and 28S rRNA residues, including those near the constriction region, undergo conformation changes upon stalling (Onoue *et al.* 2011). Notably, these rRNA residues are located at or near the rRNA residues for which structural studies have identified physical contacts with the nascent peptides in bacterial TnaC, fungal AAP and viral hCMV systems (Bhushan *et al.* 2010). This suggests involvement of the constriction region in the CGS1 system, but whether the conformation changes are the cause or result of stalling remains unknown.

Here, I conducted reverse genetics-based biochemical studies to determine the involvement of the constriction region in eukaryotic NPMRS. To this end, transgenic Arabidopsis lines carrying mutant uL4-containing ribosomes were used. The uL4 protein contains a large loop structure termed the internal extended loop, at the tip of which are two smaller β -loop structures, designated here as Loops 1 and 2 (Figure 3.1A). Loops 1 and 2 protrude into the exit tunnel to constitute the constriction region (Figure 3.2A). In Arabidopsis, uL4 is encoded by two paralogous genes, *uL4A* and *uL4D* (Barakat *et al.* 2001, Hummel *et al.* 2015), sharing 95% amino acid identity. The amino acid sequences of Loops 1 and 2 are highly conserved among eukaryotes (Figures 3.1B and 3.2B).

Since double-*knockout* mutant of *uL4A* and *uL4D* is lethal (Rosado *et al.* 2010), a modified *uL4D* gene into the T-DNA insertion *knockout* mutant of *uL4D* was introduced, referred to here as the *uL4d(KO)* line, while keeping endogenous *uL4A* intact (Figure 3.2C). In the present study, transgenic Arabidopsis carrying three types of mutant *uL4Ds* were used: *uL4D(R77A)*, *uL4D(Δ TV)*, and *uL4D(Δ loop)* (Figure 3.2A–C). *uL4D(R77A)* carries an Arg-77 to alanine substitution, located near the tip of Loop 1. *uL4D(Δ TV)* carries deletions of Thr-75 and Val-79 flanking the tip, while *uL4D(Δ loop)* carries larger deletions flanking the tip (deletions of Glu-71 to Thr-75 and Val-79 to Pro-86). These mutant *uL4Ds* and the control gene, *uL4D(WT)*, were FLAG-tagged at their C-termini and placed under the control of their native promoter (Figure 3.2C) (Takamatsu *et al.*, *in press*). The C-terminus of uL4 is exposed to the ribosomal surface (Armache *et al.* 2010). A large complex of the ribosome on mRNA can be affinity-purified using a FLAG tag (Inada *et al.* 2002, Juntawong *et al.* 2013). I examined effects of the uL4 mutations on ribosome stalling using an Arabidopsis cell-free extract (ACE) *in vitro* translation system (Murota *et al.* 2011) prepared from these transgenic lines carrying FLAG-tagged mutant uL4.

For the NPmRS systems to be tested, I selected five from divergent eukaryotes (Figure 2.1), of which four have their relevant amino acid residues >20 from the stalled residue, as in most NPmRS systems, and should cross over the constriction region. These include the CGS1, AAP (Wang and Sachs 1997, Spevak *et al.* 2005, Wei *et al.* 2012), and hCMV (Degnin *et al.* 1993, Cao and Geballe 1996, Alderete *et al.* 1999) systems mentioned above, and Arabidopsis *AdoMet decarboxylase 1 (AtAMD1)* S-uORF (the AtAMD1 system) (Hanfrey *et al.* 2005, Uchiyama-Kadokura *et al.* 2014). I also tested another NPmRS system, mammalian *AdoMet decarboxylase 1 (mAMD1)* uORF. This uORF, encoding six amino acids, MAGDIS (the MAGDIS system) (Law *et al.* 2001, Raney *et al.* 2002), is the shortest among the NPmRS systems thus far identified and its nascent peptide is too short to reach the constriction region (Figure 2.1). Lastly, I tested the shortest possible uORF, AUG-stop, of *AtNIP5;1*. AUG-stop causes prolonged ribosome stalling in response to boric acid (the AUG-Stop system) (Tanaka *et al.* 2016). This minimum uORF codes for only one amino acid, methionine, and is not actually an NPmRS, but was included as a negative control. Ribosome stalling of these systems are recapitulated using ACE *in vitro* translation (see Chapter 2).

I present here biochemical evidence that the constriction region plays a crucial role in inducing NPmRS, in which nascent peptides cross over the constriction. The differential effects of the uL4 mutations explained the structural data for stalled ribosomes of the AAP and hCMV systems.

3.2. MATERIALS AND METHODS

Plant materials

Arabidopsis thaliana (L.) Heynh. ecotype Columbia (Col-0) was used as the wild-type strain. A T-DNA insertion *knockout* mutant of *uL4D* (SALK_029203) (Alonso *et al.* 2003) was obtained from the Arabidopsis Biological Resource Center (Ohio State University, Columbus, OH, USA) and is referred to as *ul4d(KO)* in this study.

For the transgenic Arabidopsis lines to be studied, two each of independent transgenic lines were used, namely uL4D(WT):FLAG lines w2 and w9, uL4D(R77A):FLAG lines r1 and r6, uL4D(Δ TV):FLAG lines d3 and d8, and uL4D(Δ loop):FLAG lines e1 and e11 (Takamatsu *et al.*, *in press*; constructed by Morimoto, K., Tajima, Y., Onoue, N., Ohashi Y., Onouchi, H. and Naito, S.).

Plant growth conditions

Standard plant growth conditions were as described previously (Suzuki *et al.* 2001). For root observations, plants were grown on vertically placed half-strength MS medium containing 1% (w/v) sucrose, 0.5% (w/v) MES (pH 5.7), and 1.5% (w/v) gellan gum for 10 days in a growth chamber at 22°C under fluorescent light with a 16 h-light/ 8 h-dark cycle. Root length was measured using RootNav software (Pound *et al.* 2013). For leaf morphology analysis, plants were grown for 21 days as described previously (Suzuki *et al.* 2001) and one of the first pair of the true leaves was dissected. Leaf index (ratio of length to width of the leaf blade) was calculated using ImageJ software (National Institutes of Health, Bethesda, MD, USA).

Chemicals

AdoMet and spermidine were purchased from Sigma-Aldrich (St. Louis, MO, USA), and L-arginine was purchased from Wako Pure Chemicals (Osaka, Japan). Other chemicals were obtained as described previously (Murota *et al.* 2011, Onoue *et al.* 2011).

Construction of plasmids used for stalling assay

See Chapter 2. In the Results section, *M8:His:HA* and *M8:His:HA:3xFLAG:Myc* sequences will be referred to as *TagI* and *TagII*, respectively.

Construction of plasmids used for reporter assay

See Chapter 2.

***In vitro* transcription**

DNA templates in the pSP64 poly(A) vector were linearized with EcoRI and purified using the QIAquick Nucleotide Removal Kit (Qiagen), with the exception of the *M8:His:HA:DP75* and *M8:His:HA:3xFLAG:Myc:DP75* fusion constructs. DNA templates for these plasmids and nonstop RNAs were prepared by amplifying the corresponding region by PCR using KOD-Plus-Neo DNA polymerase. For PCR amplification, SP65'fP (Onoue *et al.* 2011) was used as a forward primer and the reverse primers as listed in Table 3.2 were used. *In vitro* transcription in the presence of a cap analog, m⁷G[5']ppp[5']GTP, was carried out as described previously (Chiba *et al.* 2003).

***In vitro* translation**

Preparation of ACE and *in vitro* translation reactions using ACE were carried out at 25°C as described previously (Murota *et al.* 2011). Unless otherwise stated, the template RNA was used at 50 fmol μl^{-1} . For RNase A treatment, RNase A was added at a final concentration of 0.5 mg ml^{-1} and reaction mixtures were incubated for 15 min at 37°C. For immunoblot analysis, reaction mixtures were diluted with the 1×SDS-PAGE gel sample buffer (50 mM Tris-HCl pH 6.8, 50 mM DTT, 10% (v/v) glycerol, and 1% (w/v) SDS).

Immunoblot analysis

For immunoblot analysis of *in vitro* translation products, samples were separated on a NuPAGE 4%–12% or 12% Bis-Tris Gel (Invitrogen), transferred to an Immobilon-P membrane (Millipore, Billerica, MA, USA), and immuno-reacted with either a polyclonal anti-GST antibody (Santa Cruz Biotechnology, Santa Cruz, CA, USA), a monoclonal anti-HA antibody (Santa Cruz Biotechnology), or a monoclonal anti-FLAG M2 antibody (Sigma-Aldrich). MOPS running buffer (Life Technologies, Carlsbad, CA, USA) was used for the GST tag-fusion construct. MES running buffer (Life Technologies) was used for the *M8:His:HA:DP75* or *M8:His:HA:3xFLAG:Myc:DP75* fusion constructs. The signals were detected using an Immobilon Forte Western HRP substrate (Millipore) and visualized using a LAS-3000 mini imaging system (GE Healthcare, Little Chalfont, UK). The band intensities were quantified using MultiGauge software (Fuji Photo Film, Tokyo, Japan).

Total proteins from Arabidopsis callus cultures were separated by SDS-PAGE with MOPS running buffer and subjected to immunoblot analyses using a monoclonal anti-FLAG M2 antibody (Sigma-Aldrich), anti-uL22 antiserum, anti-uL4 antiserum (Proteintech, Rosemont, IL, USA), or anti- β -actin antiserum (Gene Tex, Irvine, CA, USA). The polyclonal antibody against human uL4 (accession no. BC009888) recognizes both endogenous Arabidopsis uL4A and uL4D as epitopes (Rosado *et al.* 2010). The polyclonal antiserum raised against Arabidopsis uL22 was generated by immunizing rabbit with a synthetic peptide corresponding to amino acids 4–20 of Arabidopsis uL22B (YSQEPDNQTKSCKARGS; At1g67430).

Isolation of Arabidopsis ribosomes

For ribosome isolation, liquid callus cultures were prepared from Arabidopsis seedlings as described previously (Murota *et al.* 2011) and harvested on the 21st day after callus induction.

Frozen tissues were homogenized in buffer D (Hsu *et al.* 2016). After clarification by centrifugation at $16,000 \times g$ for 30 min, crude extract (S16) was loaded on the 1.75 M sucrose cushion (100 mM Tris-HCl pH 8.0, 40 mM KCl, 20 mM $MgCl_2$, 1 mM DTT, and $100 \mu g ml^{-1}$ cycloheximide) and centrifuged at $170,000 \times g$ for 4 h at $4^\circ C$ in a TLA100.3 rotor (Beckman Coulter, Brea, CA, USA) to obtain the S170 soluble protein fraction and the P170 ribosomal pellet. The P170 fraction was suspended in the resuspension buffer (100 mM Tris-HCl pH 8.0, 40 mM KCl, 20 mM $MgCl_2$, 1 mM DTT, and $100 \mu g ml^{-1}$ cycloheximide). For immunoblot analysis, the protein concentration was measured using a Pierce 660 nm Protein Assay Reagent (Invitrogen), in accordance with the manufacturer's instructions.

Polysome profiling analysis

For the fractionation of total polysomes, ribosomes (P170) were isolated as described above. Ribosome suspension was loaded on a 15%–60% (w/v) sucrose density gradient (40 mM Tris-HCl pH 8.4, 20 mM KCl, 10 mM $MgCl_2$, and $5 \mu g ml^{-1}$ cycloheximide) and centrifuged at $275,000 \times g$ for 1.5 h at $4^\circ C$ in an SW55 Ti rotor (Beckman Coulter). The UV absorbance profile at 254 nm was recorded using an ISCO 520 gradient system (ISCO, Lincoln, NE, USA). For immunoblot analysis, fractions were analyzed as described above.

Affinity purification of FLAG-tagged ribosomes

Immunoprecipitation of FLAG-tagged ribosomes using an anti-FLAG M2 affinity resin (Sigma-Aldrich) was performed as described previously (Inada *et al.* 2002) with some modifications. All procedures were carried out at $4^\circ C$. After *in vitro* translation of 25 pmol *GST:CGS1(G183-ns)* RNA in a 50- μl reaction mixture, translation products were diluted with 50 μl of ice-cold 2 \times binding buffer (100 mM Tris-HCl pH 7.5, 24 mM $Mg(OAc)_2$, 1 mM DTT, 1 mM PMSF, $20 \mu g ml^{-1}$ cycloheximide, and $0.05 U \mu l^{-1}$ RNase inhibitor (Promega)) and 40 μl (bed volume) of anti-FLAG M2 affinity resin. After incubation with gentle shaking for 1 h, the resin was washed with ice-cold IXA-100 buffer (50 mM Tris-HCl pH 7.5, 100 mM KCl, 12 mM $Mg(OAc)_2$, 1 mM DTT, 1 mM PMSF, and $20 \mu g ml^{-1}$ cycloheximide). Bound proteins were eluted by the addition of 15 μl of the IXA-100 buffer containing $200 \mu g ml^{-1}$ FLAG peptides (Sigma-Aldrich). For immunoblot analysis, eluate was diluted with 2 \times SDS-PAGE gel sample buffer (100 mM Tris-HCl pH 6.8, 100 mM DTT, 20% glycerol, and 2% SDS).

Luciferase assay

Tester RNA at 2 fmol μl^{-1} carrying firefly (*Photinus pyralis*) luciferase (LUC) reporter gene and 1 fmol μl^{-1} sea pansy (*Renilla reniformis*) luciferase (RLUC) control RNA were co-translated for 120 min. LUC and RLUC activities were measured as described previously (Chiba *et al.* 2003), and the LUC activity was normalized with the control RLUC activity to obtain reporter activity.

Statistical treatments

For comparisons of stalling efficiencies, Welch's *t*-test followed by false discovery rate (FDR) correction of Benjamini and Hochberg (Benjamini and Hochberg 1995) was applied. The same FDR correction was also applied to comparisons of mRNA levels among the transgenic lines. For multiple comparisons of plant phenotypes, the Tukey-Kramer test was applied. For other comparisons, Welch's *t*-test was applied.

3.3. RESULTS

Nomenclature of the plants and in vitro translation extracts used in this study

In this study, I used the ACE *in vitro* translation system derived from the untransformed Arabidopsis ecotype Col-0 wild-type line, and transgenic Arabidopsis line carrying FLAG-tagged mutant uL4 as well as FLAG-tagged wild-type uL4. To avoid confusion of the two wild-types, the untransformed Arabidopsis Col-0 line will be referred to as Col-0.

Mutant uL4Ds complement the ribosome-deficient phenotypes *in vivo*, except in uL4D(Δ loop):FLAG plants

In Arabidopsis, mutations of ribosomal proteins often have multiple effects on growth and development, including narrower leaf morphology, termed the *pointed leaf*, and a short-root phenotype (Byrne 2009). *uL4d(KO)* plants also exhibited these phenotypes (Figures 3.3 and 3.4) (Rosado *et al.* 2010, 2012, Horiguchi *et al.* 2011). Both phenotypes were complemented not only in the uL4D(WT):FLAG plants but also in the uL4D(R77A):FLAG and uL4D(Δ TV):FLAG plants (Figures 3.3H and 3.4E), indicating the functionality of mutant ribosomes *in vivo*. In contrast, neither phenotype was complemented in uL4D(Δ loop):FLAG plants. Notably, the plants exhibited even narrower leaves (Figure 3.3F and H).

Mutant uL4D proteins are efficiently incorporated into translating ribosomes, except in the uL4D(Δ loop):FLAG line

To determine whether the uL4D mutant proteins are incorporated into ribosome particles, I tested the association of FLAG-tagged uL4D proteins with 80S ribosomes (Figure 3.5A). Since the ACE *in vitro* translation system is prepared from callus cultures raised from the mutant Arabidopsis seedlings (Figure 2.2) (Murota *et al.* 2011), I used the same culture system here. Crude extracts (S16) were subjected to ultracentrifugation through a sucrose cushion to obtain ribosomal pellet (P170) and post-ribosomal supernatant (S170) fractions. Immunoblot analysis of the fractions using an anti-FLAG antibody identified the ~48-kDa uL4D:FLAG proteins in the S16 and P170 fractions, but not in S170, in all mutant lines (Figure 3.5A). This indicates that the FLAG-tagged uL4D(WT), uL4D(R77A), and uL4D(Δ TV) proteins are efficiently incorporated into ribosome particles. uL4D(Δ loop):FLAG protein is also incorporated into ribosome particles; however, the antibody detected only a faint band, indicating that the mutant ribosome constitutes a very minor fraction of the total ribosomes. Since the uL4D(Δ loop):FLAG line did not seem promising for use in the present study, I excluded this line from further analyses.

To determine whether the mutant ribosomes are actively translating, I performed polysome profiling of the P170 fractions using sucrose density gradient centrifugation. Immunoblot analysis detected mutant uL4Ds in the polysome, monosome, and 60S subunit fractions, but not in the 40S subunit and free-protein fractions (Figure 3.5B). Distributions of the mutant uL4Ds in polysome fractions appeared similar to those of the total ribosome (Figure 3.5C), suggesting that the mutant uL4D-containing ribosomes can all achieve active translation *in vivo*.

Mutant ribosomes constitute substantial proportions of total ribosomes in ACE

Since the uL4D:FLAG mutant lines carry an endogenous *uL4A*, I investigated what proportion of ribosomes consisted of mutant uL4Ds in ACE (hereafter, the constitution fraction). To determine this, ACE preparations were subjected to immunoblot analysis using an anti-uL4 antiserum, to distinguish FLAG-tagged mutant uL4D from endogenous uL4A by ~1-kDa gel mobility shift (Figure 3.6A). The constitution fractions ranged from 40% to 80% (Figure 3.6B), indicating that substantial proportions of the ribosomes carry mutant uL4D in ACE.

AdoMet-induced ribosome stalling of CGS1 is reduced in uL4D(Δ TV):FLAG ribosomes

When a ribosome stalls during translation, a peptidyl-tRNA species accumulate as an intermediate of translation. A tRNA moiety confers a 10- to 20-kDa gel mobility shift on the peptide, depending on the tRNA species and gel conditions. Peptidyl-tRNA can be identified as an RNase-sensitive band.

In response to AdoMet, CGS1 nascent peptide induces ribosome stalling at the Ser-94 codon, leading to peptidyl-tRNA accumulation (Onouchi *et al.* 2005). This response was recapitulated in Col-0 ACE (Murota *et al.* 2011). To determine the effects of mutant uL4D-containing ribosomes, *GST:CGS1(WT)* RNA (Figure 3.7A) (Onouchi *et al.* 2005, Haraguchi *et al.* 2008) was translated in ACE in the presence of AdoMet. Immunoblot analysis using an anti-GST antibody detected a 55-kDa peptidyl-tRNA in addition to a 45-kDa full-length product, whereas in the absence of AdoMet the peptidyl-tRNA was barely detectable (Figure 3.7A).

To evaluate the effect of uL4D mutations, stalling efficiency was calculated, which is defined as the peptidyl-tRNA signal intensity divided by the sum of peptidyl-tRNA and full-length product signal intensities (Figure 3.8A) (Uchiyama-Kadokura *et al.* 2014, Yamashita *et al.* 2017). Since the ACE preparations contain both mutant uL4D- and endogenous uL4A-containing ribosomes, the stalling efficiency of the mutant ribosome alone have to be evaluated. To achieve this, the raw stalling efficiency was corrected for the constitution fraction of the mutant ribosomes, referred to as the corrected stalling efficiency (Figure 3.9). The corrected stalling efficiency of uL4D(ΔTV):FLAG lines d3 and d8 ACE was 63% and 56%, respectively (Figure 3.7A, shaded bar), of the raw stalling efficiency of Col-0 ACE (Figure 3.7A, open bar), while those of uL4D(WT):FLAG and uL4D(R77A):FLAG ACE were not appreciably different from the raw stalling efficiency of Col-0 ACE. These results show that uL4D(ΔTV) mutation weakens AdoMet-induced ribosome stalling, while uL4D(R77A) mutation does not.

Affinity purification of stalled ribosome confirms the corrected stalling efficiency

To validate the calculation of corrected stalling efficiencies, *GST:CGS1(G183-ns)* RNA (Figure 3.10A) was used to affinity-purify the FLAG-tagged mutant ribosomes by immunoprecipitation (IP) using an anti-FLAG antibody after translation in ACE. *GST:CGS1(G183-ns)* RNA is a *nonstop* RNA that is truncated at the Gly-183 codon and does not carry a stop codon. The use of this *nonstop* RNA is necessary to affinity-purify the stalled ribosomes because a ribosome that reached the termination codon will split into large and small subunits and the peptidyl-tRNA will be hydrolyzed into a peptide and tRNA (Figure 3.11A), while on the *nonstop* RNA, the 80S

ribosome will remain at the truncated RNA end with the peptidyl-tRNA on it (Figure 3.11A). For this experiment, the RNA concentration was increased to reduce ribosome stacking behind the initially stalled ribosome at Ser-94 (Figure 3.10C and D).

When *GST:CGS1(G183-ns)* RNA was translated in Col-0 ACE in the presence of 1 mM AdoMet (Figure 3.10B and C), ~65 kDa peptidyl-tRNA [PtR(Gly-183), green clover] that had translated to the truncated end of the nonstop RNA, 55 kDa peptidyl-tRNA [PtR(Ser-94), red clover] formed on the stalled ribosome at Ser-94, and 45 kDa full-length peptide (FL, green arrowhead) were identified. The stalling efficiency in this experiment is defined as the signal intensity of PtR(Ser-94) divided by the sum of PtR(Ser-94) and PtR(Gly-183) signal intensities. The 45-kDa full-length peptide was probably produced by spontaneous hydrolysis of PtR(Gly-183). Spontaneous hydrolysis of peptidyl-tRNA at the *nonstop* RNA end was reported (Yamashita *et al.* 2014). Since spontaneous hydrolysis of PtR(Gly-183) could occur at any step during this experiment, the signal intensity of this full-length product was not taken into account for the calculation of stalling efficiency.

After IP with an anti-FLAG antibody, an anti-uL4 antiserum detected only FLAG-tagged uL4D (Figure 3.10D), indicating that IP efficiently purified FLAG-tagged mutant ribosomes. The corrected stalling efficiencies of uL4D(Δ TV):FLAG lines d3 and d8 ACE before IP were $68\% \pm 4\%$ and $66\% \pm 8\%$, respectively, while raw stalling efficiencies after IP were $71\% \pm 6\%$ and $72\% \pm 4\%$, respectively, of that of Col-0 ACE before IP (Figure 3.10E). For all pairwise comparisons of the corrected stalling efficiency before IP and the raw stalling efficiency after IP, similar values were obtained. These results support the validity of the corrected stalling efficiency calculations.

In the experiment shown in Figure 3.7A, the corrected stalling efficiencies obtained using *GST:CGS1(WT)* RNA of the uL4D(Δ TV):FLAG lines d3 and d8 ACE were $63\% \pm 9\%$ and $56\% \pm 11\%$ (shaded bar), respectively, of that of Col-0 ACE (open bar). These values are smaller than the corrected stalling efficiencies obtained using the nonstop RNA in the above experiment. This difference may arise from the instability of PtR(Gly-183). Owing to the afore-mentioned spontaneous hydrolysis mentioned above, the amount of PtR(Gly-183) is reduced and the stalling efficiency may be overestimated.

Affinity purification of stalled ribosomes cannot be applied to NPmRS at the termination codon (Figure 3.11B). Therefore, in the present study, the corrected stalling efficiency was compared with the raw stalling efficiency of Col-0 ACE.

uL4D(ΔTV) mutation reduces autonomous ribosome stalling of the hCMV system

To further characterize the contribution of the constriction region to NPmRS, other stalling systems from different eukaryotes were tested. The 22-amino-acid uORF2 of hCMV *gp48* directs ribosomes to stall autonomously at the translation termination to down-regulate *gp48* expression (Degnin *et al.* 1993, Cao and Geballe 1996). The *gp48* uORF2-mediated stalling occurs in Col-0 ACE, and abrogation of stalling by Pro-21-to-alanine substitution (*P21A*) of uORF2 (Degnin *et al.* 1993) is reproduced in Col-0 ACE.

I tested the effects of uL4D(ΔTV) and uL4D(*R77A*) mutations. The corrected stalling efficiency in uL4D(ΔTV):FLAG ACE was estimated to be 19–30% of the raw stalling efficiency of Col-0 ACE, while that of uL4D(WT):FLAG ACE and uL4D(*R77A*):FLAG ACE was not appreciably different from Col-0 ACE (Figure 3.7B). The effects of uL4D mutations on CGS1 and hCMV systems were similar in that uL4D(ΔTV) but not uL4D(*R77A*) affected stalling; however, the reduction in the uL4D(ΔTV) mutant was stronger in hCMV than in CGS1.

To further validate corrected stalling efficiencies, the cell-free extracts from Col-0 and uL4D:FLAG ACE were mixed at different proportions and used for *in vitro* translation reactions (Figure 3.12). When *TagI:DP75:hCMV(WT)* RNA was translated in combined ACE, the raw stalling efficiency was gradually reduced depending on the levels of uL4D(ΔTV):FLAG-containing ribosomes in the reaction mixture (Figure 3.12A and C), whereas uL4D(WT):FLAG ACE did not show the corresponding effect on the raw stalling efficiency from Col-0 ACE (Figure 3.12A and B). These results support the validity of the corrected stalling efficiency calculations used in the present study.

Both uL4D(*R77A*) and uL4D(ΔTV) mutations reduce arginine-induced ribosome stalling of the AAP system

The 24-amino-acid AAP nascent peptide, encoded by *N. crassa arg-2* uORF, causes NPmRS in response to L-arginine (Wang and Sachs 1997, Wei *et al.* 2012). In Col-0 ACE, peptidyl-tRNA accumulated in a L-arginine-dependent manner, whereas substitution of Asp-12 to asparagine (*D12N*) of AAP, which has been shown to abolish the response to L-arginine (Wei *et al.* 2012), also abolished the peptidyl-tRNA accumulation in Col-0 ACE.

Translation analyses in uL4D mutant ACE showed that stalling was significantly reduced in both uL4D(*R77A*):FLAG and uL4D(ΔTV):FLAG ACE. The corrected stalling efficiencies were 57–61% and 37–42%, respectively, of the raw stalling efficiency of Col-0 ACE (Figure 3.7C).

Compared with the CGS1 and hCMV systems, AAP exhibited a qualitative difference in that a single-amino-acid substitution of uL4D(R77A) affected stalling.

Both uL4D(R77A) and uL4D(Δ TV) mutations strongly reduce polyamine-induced ribosome stalling in AtAMD1 system

The 52-amino-acid uORF2 of *AtAMD1* S-uORF directs the ribosome to stall at the translation termination in response to high polyamine concentrations. In the present study, spermidine was used as an effector (Uchiyama-Kadokura *et al.* 2014). In Col-0 ACE, peptidyl-tRNA accumulation was dependent on spermidine concentration (Uchiyama-Kadokura *et al.* 2014), which was abolished by introducing a frame-shift mutation in S-uORF.

The corrected stalling efficiency in uL4D(R77A):FLAG and uL4D(Δ TV):FLAG ACE at a high spermidine concentration (0.7 mM) was reduced to ~23% and ~15%, respectively, of the raw stalling efficiency of Col-0 ACE, while uL4D(WT):FLAG ACE showed similar levels of stalling efficiencies to Col-0 ACE (Figure 3.7D). As was the case in AAP, both uL4D(R77A) and uL4D(Δ TV) mutations reduced the stalling in AtAMD1; however, the effects of the mutations were stronger than in AAP.

Neither uL4D(R77A) nor uL4D(Δ TV) mutation affects polyamine-induced ribosome stalling on the six-amino-acid uORF of MAGDIS

In *mAMD1*, a uORF encoding six amino acids, MAGDIS, directs the ribosome to stall in response to polyamines. Translation in Col-0 ACE showed peptidyl-tRNA accumulation in a spermidine-dependent manner, while Ile-5 to leucine (*l5L*) substitution (Law *et al.* 2001, Raney *et al.* 2002) of MAGDIS abolished peptidyl-tRNA accumulation.

The stalling efficiencies in uL4D:FLAG ACEs were all essentially the same as the raw stalling efficiency of Col-0 ACE (Figure 3.7E). These results show that neither uL4D(R77A) nor uL4D(Δ TV) mutation affects the spermidine-dependent ribosome stalling directed by the six-amino-acid uORF of MAGDIS.

5'-UTRs carrying the uORFs also depict the differential effects of uL4D mutations

Translation of a uORF generally down-regulates translation of the main ORF, and if ribosomes stall on the uORF, translation of the main ORF is strongly down-regulated (Figure 1.4) (Hinnebush *et al.* 2016). For the stalling analyses, I joined artificial sequences of the tags and linker to the

uORF. In the case of MAGDIS, the constriction region is vacant when stalled on the natural uORF, whereas in the present stalling analysis a 75-amino-acid DP75 linker (Matheisl *et al.* 2015, Yamashita *et al.* 2017) resides in the constriction region. To test the effects of uL4D mutations on the natural uORF sequence, the 5'-UTR sequences of the hCMV, AtAMD1, and MAGDIS systems were joined to a luciferase (LUC) reporter, and the effects of uL4D mutations were analyzed by reporter assays (Figure 1.4).

The 5'-UTR of hCMV *gp48* (Degnin *et al.* 1993, Cao and Geballe 1996) was joined to a LUC reporter (Figure 3.13A) and was translated in ACE. When the RNA was translated in uL4D(Δ TV):FLAG ACE the LUC activity was ~3 times higher than in Col-0 ACE (Figure 3.14A). The LUC activity was corrected for the constitution fraction of FLAG-tagged ribosomes, as for the stalling efficiency correction (Figure 3.9B). The corrected relative reporter activity in uL4D(Δ TV):FLAG ACE was ~6 times that in Col-0 ACE, while those in uL4D(WT):FLAG and uL4D(R77A):FLAG ACE were essentially the same as in Col-0 ACE (Figure 3.13A). When the 5'-UTR of *AtAMD1* containing the S-uORF (Figure 3.13B) (Uchiyama-Kadokura *et al.* 2014) was analyzed, corrected reporter activities in uL4D(R77A):FLAG and uL4D(Δ TV):FLAG ACE were 7–9 times higher than in Col-0 ACE (Figure 3.13B).

The 5'-UTR of *mAMD1* was joined to the LUC reporter (Figure 3.13C) and translated in ACE. Relative reporter activities in uL4D:FLAG mutant ACEs were essentially the same as in Col-0 ACE (Figure 3.13C). These results are consistent with those of the stalling efficiency analyses (Figure 3.7B, D and E) and confirmed the effects of uL4D mutations on ribosome stalling.

Neither uL4D(R77A) nor uL4D(Δ TV) mutation affects boric acid-induced ribosome stalling on AUG-stop

The 5'-UTR of *AtNIP5;1*, encoding a boric acid transporter, has the shortest possible uORF, AUG-stop. Boric acid induces prolonged ribosome stalling at AUG-stop (Tanaka *et al.* 2016). Since insertion of even a single codon between the AUG and stop codons is detrimental to the response (Tanaka *et al.* 2016), joining a tag or linker sequence is impossible. Therefore, effects of the *uL4D* mutations were evaluated by a reporter assay. As in the case of MAGDIS, neither uL4D(R77A) nor uL4D(Δ TV) mutation affected reporter activities (Figure 3.13D).

3.4. DISCUSSION

In this study, I presented reverse genetics-based biochemical evidence showing that uL4 is involved in four of the NPmRS in eukaryotes, namely the CGS1, hCMV, AAP, and AtAMD1 systems. In contrast, the six-amino-acid uORF of MAGDIS was unaffected. The results show that the constriction region is crucial for inducing NPmRS, when the nascent peptide is long enough to cross over the constriction region, and that MAGDIS adopts a distinct mechanism for NPmRS induction

Analyses of transgenic lines carrying uL4D mutations

Regarding the uL4D(ΔTV):FLAG and uL4D($\Delta loop$):FLAG lines, accumulation of FLAG-tagged uL4D proteins was less than that in uL4D(WT):FLAG and uL4D(R77A):FLAG plants (Figure 3.5A). It is possible that high-level expressors were not isolated owing to growth retardation, because NPmRS is involved in a range of regulatory systems, including metabolism (Onouchi *et al.* 2005, Uchiyama-Kadokura *et al.* 2014) and transcription factor expression (Hayashi *et al.* 2017, Yamashita *et al.* 2017). In the uL4D(ΔTV):FLAG and uL4D($\Delta loop$):FLAG mutant plants, the effects of a defect in ribosome biogenesis could be a problem because the alterations in Loop 1 might retard the integrity of the internal extension loop (Figure 3.1A), which has been shown to be essential for the large-subunit assembly in bacteria and yeast (Pillet *et al.* 2015, Stelter *et al.* 2015, Lawrence *et al.* 2016). This might occur in uL4D($\Delta loop$):FLAG lines. A plausible scenario is that uL4D($\Delta loop$):FLAG protein was only poorly incorporated into ribosome particles and the surplus protein was rapidly degraded (Sung *et al.* 2016).

Differential effects of uL4D(R77A) and uL4D(ΔTV) mutations explain the structural data

The degree of reduction of stalling by uL4D(ΔTV) and uL4D(R77A) mutations showed qualitative differences among the stalling systems. Structures of stalled ribosomes in WGE have been solved in hCMV and AAP systems, and physical contacts between the nascent peptide and constriction region have been identified (Bhushan *et al.* 2010).

Cryo-EM studies of AAP-stalled ribosomes (Bhushan *et al.* 2010) showed that Asp-12 contacts uL4 between Gly-76 and Val-79 (*Arabidopsis* uL4D residue number) in Loop 1 (Figure 3.2B, magenta underline). This is consistent with the finding that uL4D(R77A) mutation strongly reduced the L-arginine-dependent stalling of AAP (Figure 3.7C). In the hCMV system, nascent

peptide physically contacts Loop 2, but not Loop 1 (Bhushan *et al.* 2010). This also is consistent with the finding that uL4D(R77A) mutation did not affect hCMV stalling (Figures 3.7B and 3.13A). Asp-12 of AAP is important for stalling (Wang and Sachs 1997, Spevak *et al.* 2010). Thus, the present data interconnect structural data and functional residues in the nascent peptide. The present data also suggest that the physical contacts of the nascent peptide with the constriction region observed by cryo-EM are the cause, not the result, of ribosome stalling.

The effects of uL4D mutations were strongest in AtAMD1 and weakest in CGS1. It is previously reported that, upon AdoMet-induced stalling of CGS1, 28S rRNA residues undergo conformational changes (Onoue *et al.* 2011). Among these, EcU744 and EcA750 (in *E. coli* rRNA numbering) mapped near the constriction region. Intriguingly, these residues are located close to uL22. Corroborating the weak effect of uL4D mutations in CGS1, the CGS1 nascent peptide might interact with uL22, rather than uL4, although other possibilities remain. In contrast, regarding the AtAMD1 system, in which uL4D mutations had strong effects on stalling, its nascent peptide might strongly interact with Loop 1 to induce polyamine-dependent ribosome stalling.

uL4D(Δ TV) mutation down-regulated four NPmRS systems, while uL4D(R77A) mutation affected only two of them. uL4D(Δ TV) mutation probably exhibited a general effect on interaction of nascent peptide and the constriction by altering the geometry of the constriction region. The two stalling systems affected by uL4D(R77A) mutation would specifically interact with the Arg-77 that was mutated in this study, which was supported by cryo-EM study of AAP-stalled ribosomes. The present data suggest that specific interaction of nascent peptide and the amino acid residue(s) within the β -loop(s) is superimposed over the general interaction with the constriction region.

3.5. TABLES

Table 3.1. Plasmids used in this study and primers used to construct plasmids.

Name	Construct ^a	Source	Primer ^b	
			Forward	Reverse
<i>Plasmids used for stalling assay</i>				
pST55	SP6::M8:His:HA:DP75:AAP(WT)	this study	AAPf	AAPr
pST56	SP6::M8:His:HA:DP75:AAP(D12N)	this study	D12Nf	AAPr
pST57	SP6::M8:His:HA:DP75:hCMV(WT)	this study	hCMVf	hCMVr
pST58	SP6::M8:His:HA:DP75:hCMV(P21A)	this study	hCMVf	P21Ar
pST76	SP6::M8:His:HA:DP75:S-uORF(WT)	this study	SAMDC1f	SAMDC1r
pST77	SP6::M8:His:HA:DP75:S-uORF(fs)	this study	SAMDC1fsf	SAMDC1fsr
pST116	SP6::M8:His:HA:DP75:MAGDIS(WT)	this study	DP75f	MAGDISr
pST117	SP6::M8:His:HA:DP75:MAGDIS(I5L)	this study	DP75f	I5Lr
pTI5	SP6::M8:His:HA:3xFLAG:Myc:DP75:AAP(WT)	this study	3xFLAGf	3xFLAGr
pTI6	SP6::M8:His:HA:3xFLAG:Myc:DP75:AAP(D12N)	this study	3xFLAGf	3xFLAGr
pYF2	SP6::GST:CGS1(WT)	Haraguchi <i>et al.</i> 2008		
pYF3	SP6::GST:CGS1(mto1-1)	Haraguchi <i>et al.</i> 2008		
<i>Plasmids used for reporter assay</i>				
pST118	SP6::mAMD1 5'-UTR(WT):LUC	this study	MAGDIS(WT)f	MAGDIS(WT)r
pST119	SP6::mAMD1 5'-UTR(I5L):LUC	this study	MAGDIS(I5L)f	MAGDIS(WT)r
pST120	SP6::AtAMD1 5'-UTR(WT):LUC	this study	SAMDC1f2	SAMDC1r2
pST121	SP6::AtAMD1 5'-UTR(fs):LUC	this study	SAMDC1f2	SAMDC1r2
pST122	SP6::gp48 5'-UTR(WT):LUC	this study	hCMVf2	hCMVr2
pST123	SP6::gp48 5'-UTR(P21A):LUC	this study	hCMVf2	P21Ar2
pMI27	SP6::RLUC	Chiba <i>et al.</i> 2003		
pMT131	SP6::AtNIP5;1 5'-UTR(WT):LUC	Tanaka <i>et al.</i> 2016		
pMT132	SP6::AtNIP5;1 5'-UTR(ATCTAA):LUC	Tanaka <i>et al.</i> 2016		

^a Double colons indicate fusion of promoter sequence and an ORF, and single colons indicate an in-frame translational fusion (*i.e.*, *Promoter::ORF:ORF: ...*).

^b Primers used for construction. Sequences of the primers are listed in Table 2.2 (see Chapter 2).

Table 3.2. Primers used in this study.

Name	Sequence (5' to 3')	Source
<i>Generating DNA templates for in vitro transcription</i>		
SP65'fp	CATCAGAGCAGATTGACTG	Onoue <i>et al.</i> 2011
G183r	ACCGGCATGAACAGT	this study
poly(A)r	ACGAGCCGGAAGCATAAAG	this study

3.6. FIGURES

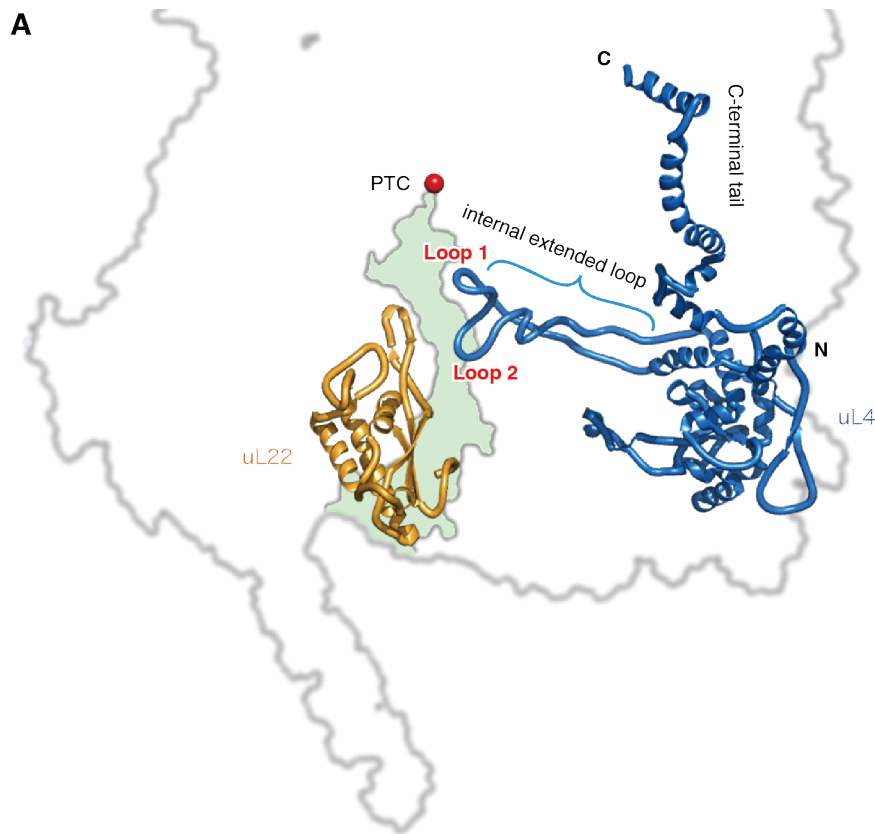


Figure 3.1. Structure and amino acid sequence alignment of uL4.

(A) Structure of wheat uL4 deduced by cryo-EM (PDB 4V7E) (Armache *et al.* 2010). The internal extended loop, Loops 1 and 2, C-terminal tail, and N- and C-termini of uL4 are marked. uL22, the exit tunnel (light green), and PTC are also shown. (B) Alignment of amino acid sequences of Arabidopsis uL4 paralogs, uL4A (At_uL4A; GenBank accession no. NP_187574) and uL4D (At_uL4D; accession no. NP_195907), wheat (*Triticum aestivum*) uL4 (Ta_uL4; Ensembl Plants id TraesCS4A02G091100), and yeast paralogs uL4A (Sc_uL4A; accession no. NP_009587) and uL4B (Sc_uL4B; accession no. NP_010295) were aligned using ClustalW (<http://www.ebi.ac.uk/Tools/msa/clustalw2/>). Alignments of Arabidopsis paralogs alone (At), and Arabidopsis and wheat alone (At/Ta) are also shown. Identical (asterisks) and similar (dots and colons) amino acid residues are marked. Regions of the internal extended loop (blue line) and β -loops (Loops 1 and 2; red lines) are marked above the Ta_uL4 sequence. Substituted amino acid in R77A, deleted amino acids in ΔTV , and $\Delta loop$ mutations in At_uL4D are reversed in violet, reversed in magenta, and underlined in brown, respectively. Wheat is hexaploid and has several copies of uL4 in its genome. One of the uL4 paralogs on chromosome 4A is shown here (International Wheat Genome Sequencing Consortium 2018).

CHAPTER 3. Exit tunnel constriction and ribosome stalling

B

At_uL4A	-MAAAAARPLVTIQTLGDGMSTDQSSTVVLPDVMTAPVRPDI VNFVHAQISNNSRQPYAV	59
At_uL4D	MVASAAAARPLVTVQGLDGMSTDQSTTVTLPDVMTAPVRPDI VNFVHAQISNNSRQPYAV	60
At	:. *****. * *****. * *****	
Ta_uL4	--MATTARPLVSVKALDGDMPDAAAG-VPMPHVMPKAPIRDPDITFVHRLVSCNSRQPYAV	57
At/Ta	::*****:: *****. * * : * : * : * : * : * : * : * : * : * : * : * : *	
Sc_uL4A	-----MSRPQVTVHSLTGEAT---ANALPLPAVFSAPIRDPDI VHTVFTSVNKNKRQAYAV	52
Sc_uL4B	-----MSRPQVTVHSLTGEAT---ANALPLPAVFSAPIRDPDI VHTVFTSVNKNKRQAYAV	52
All	: * * : : * * : : : * : : * : * : * : * : * : * : * : * : *	
At_uL4A	SKKAGHQTSAESWGTGRAVSRIPRVPGGGTHRAGQAAFNMCRGGRMFAPTKIWRRWHR	119
At_uL4D	SKKAGHQTSAESWGTGRAVSRIPRVPGGGTHRAGQAAFNMCRGGRMFAPTKIWRRWHR	120
At	*****	
	<u>Loop 1</u> <u>Loop 2</u> <u>Internal extended loop</u>	
Ta_uL4	SRKAGHQTSAESWGTGRAVSRIPRVPGGGTHRSQQGAFNMCRGGRMFAPTRIWRKWHR	117
At/Ta	* : * : * : * : * : * : * : * : * : * : * : * : * : * : * : * : * : * : * : *	
Sc_uL4A	SEKAGHQTSAESWGTGRAVARIPRVPGGGGRSQQGAFNMCRGGRMFAPTKTWRKWNVK	112
Sc_uL4B	SEKAGHQTSAESWGTGRAVARIPRVPGGGGRSQQGAFNMCRGGRMFAPTKTWRKWNVK	112
All	* : * : * : * : * : * : * : * : * : * : * : * : * : * : * : * : * : * : *	
At_uL4A	VNVNMRHAI VSAIAATAVPALVMARGHKIENVPEMPLVVS DSAEAVEKTSAAIKVLKQI	179
At_uL4D	VNVNMRHAI VSAIAATAVPALVMARGHKIENVPEMPLVVS DSAEAVEKTSAAIKVLKQI	180
At	*****	
Ta_uL4	VNIRLRVAVASALAATAVPAIVTARGHRIESVPEFPLVVS DSAEGIEKTSQAVKVLKQL	177
At/Ta	** : : * * : * : * : * : * : * : * : * : * : * : * : * : * : * : * : * : *	
Sc_uL4A	VNHNEKRYATASAI AATAVASLVLARGHRVEKIPEIPLV VSTDLESIQKTKEAVAALKAV	172
Sc_uL4B	VNHNEKRYATASAI AATAVASLVLARGHRVEKIPEIPLV VSTDLESIQKTKEAVAALKAV	172
All	** : : * * : * : * : * : * : * : * : * : * : * : * : * : * : * : * : * : *	
At_uL4A	GAYDDAEKAKNSIGIRPGKGMNRNRRYISRKGPLVVYGT EGSKIVKAFRNLPVELCHVE	239
At_uL4D	GAYDDAEKAKNSIGIRPGKGMNRNRRYISRKGPLVVYGT EGAIVKAFRNLPVELCHVE	240
At	*****	
Ta_uL4	GAYADADKAKDSVIRPGKGMNRNRRYINRKGPLIVYATE GSKIVKAFRNLPGV DVANVE	237
At/Ta	** * : * : * : * : * : * : * : * : * : * : * : * : * : * : * : * : * : * : *	
Sc_uL4A	GAHSDLKVLKSKKL RAGKGYRNRRTQRRGPLV VYAED-NGIVKALRNVP G VETANVA	231
Sc_uL4B	GAHSDLKVLKSKKL RAGKGYRNRRTQRRGPLV VYAED-NGIVKALRNVP G VETANVA	231
All	** : * * : * : * : * : * : * : * : * : * : * : * : * : * : * : * : * : * : *	
At_uL4A	RLNLLKLAPGGHLGRFVIWTKSAFEKLESIYGSFEK PSEKKG YVLPRAKMNADLARI	299
At_uL4D	RLNLLKLAPGGHLGRFVIWTKSAFEKLESIYGSFEK PSEKKG YVLPRAKMNADLARI	300
At	*****	
Ta_uL4	RLNLLDLAPGGHLGRFVIWTESAFKKLDEVYGSFEASS KKKGFVLPRPKMTNADLR LI	297
At/Ta	****. *****. * : * : * : * : * : * : * : * : * : * : * : * : * : * : *	
Sc_uL4A	SLNLLQLAPGAHLGRFVIWTEAAFTKLDQVWGSETV- ASSKVG YTLPSHIIISTD VTRII	290
Sc_uL4B	SLNLLQLAPGAHLGRFVIWTEAAFTKLDQVWGSETV- ASSKVG YTLPSHIIISTD VTRII	290
All	****. ****. *****. : * * : : * * * : * : * : * : * : * : * : * : * : *	
At_uL4A	NSDEIQSVVNP IKKDAKRA--VLKKNPLKLNVM LKLN PYAKTAKRMSLLAE AQRVKAKK	357
At_uL4D	NSDEVQSVVNP IKDGSKRA--VLKKNPLKLNVM FKL NPYAKTAKRMSLLAE ASRVKAKK	358
At	****. *****. : * * *****. *****. *****. *****. *****	
Ta_uL4	NSDEVQSVVKPINKEVKRR--EARKNPLKNA AAVLKLNPYFGTARRMAVLA EAARVKARK	355
At/Ta	****. ****. * : * : * : * : * : * : * : * : * : * : * : * : * : * : * : *	
Sc_uL4A	NSSEIQSAIRPAGQATQKRTHVLKKNPLKKNQVLLRLN PYAKVFA-----A	336
Sc_uL4B	NSSEIQSAIRPAGQATQKRTHVLKKNPLKKNQVLLRLN PYAKVFA-----A	336
All	** : * : * : * : * : * : * : * : * : * : * : * : * : * : * : * : * : * : *	
At_uL4A	EKLAKRRTVTKEEALAIKAAGKSWYKTMISDS DYTEFDNFTKWL GASQ	406
At_uL4D	EKLEKRRVVTKEEAQA IKAAGKAWYQTMISDS DYTEFDNFTKWL GASQ	407
At	** * * * * . * * * * * . * * * * * . * : * : * : * : * : * : * : * : * : *	
Ta_uL4	DKINSKRKLSVEEASKIKAAGKAWYQTMISDS DYMFDVFSKWL GVSQ	404
At/Ta	: * : * * : * : * : * * * * * : * : * : * : * : * : * : * : * : * : *	
Sc_uL4A	EKLGSK-----AEKTGKPA-AVFTETL KHD-----	362
Sc_uL4B	EKLGSK-----AEKTGKPA-AVFAETL KHD-----	362
All	: * : * : * : * : * : * : * : * : * : * : * : * : * : * : * : * : * : *	

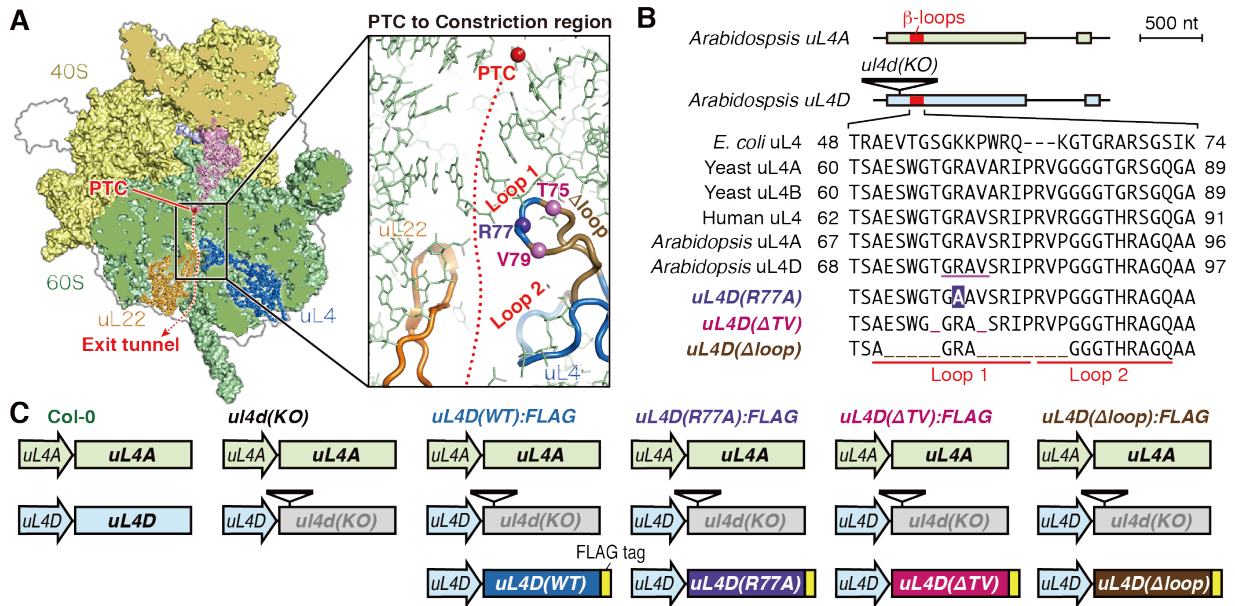


Figure 3.2. *uL4D* mutations and transgenic Arabidopsis lines carrying the *uL4D* mutations.

(A) Structure of wheat 80S ribosome (PDB 4V7E) (Armache *et al.* 2010) (Left panel) and expansion of the constriction region (Right panel). The α -carbon atoms of uL4 residues substituted in *R77A* (Arg-77) and deleted in ΔTV (Thr-75 and Val-79) mutations are marked in violet and magenta balls, respectively, while those deleted in $\Delta loop$ (Glu-71 to Thr-75 and Val-79 to Pro-86) mutation is marked with light brown main chain. (B) (Upper panel) Schematic representation of gene structures of *uL4A* and *uL4D*, and T-DNA insertion in *ul4d(KO)* (SALK_029203). Exons and introns are indicated as boxes and lines, respectively, with the β -loop region marked in red. (Lower panel) Alignment of amino acid sequences of Loop 1 and 2 regions. Substitutions and deletions in *uL4D* mutants are shown in reversed letters and underscores, respectively. The residues of uL4 in physical contact with AAP nascent peptide as deduced by cryo-EM in WGE (Bhushan *et al.* 2010) are underlined in magenta in Arabidopsis uL4D. (C) Schematic representation of *uL4* gene sets carried by Arabidopsis wild-type Col-0, *ul4d(KO)*, and FLAG-tagged *uL4D* mutant lines.

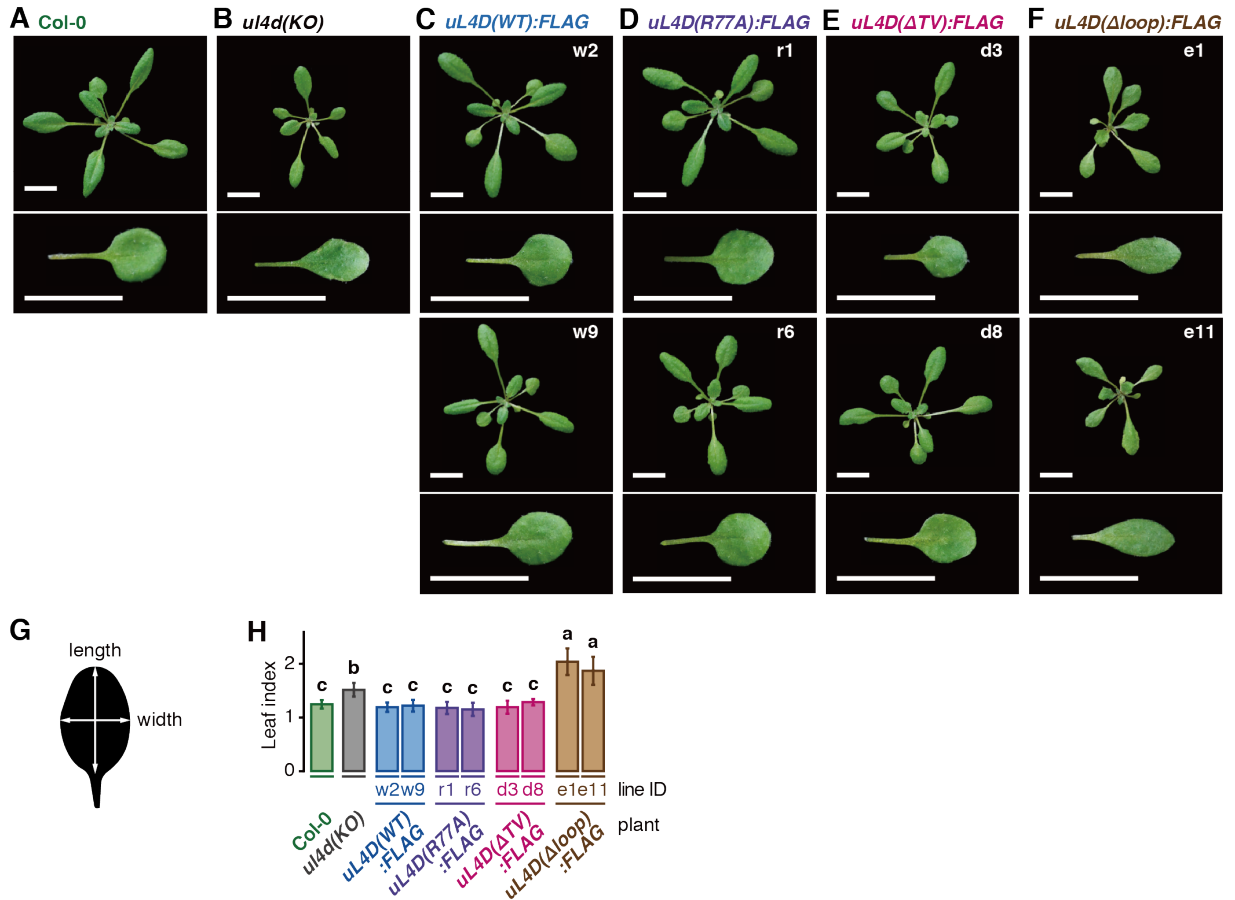


Figure 3.3. FLAG-tagged uL4Ds complement the *pointed leaf* phenotype of *ul4d(KO)* plants.

(A–F) Rosettes and one of the first pair of true leaves of wild-type Col-0, *ul4d(KO)*, and FLAG-tagged uL4D mutant transgenic plants (indicated by labels) grown for 21 days. Independent transgenic line IDs used in this study are indicated. Bars = 10 mm. (G) Schematic representation of length-to-width ratio (leaf index). (H) Leaf index of Col-0 and *uL4D* mutant plants. Different letters indicate significant differences ($p < 0.05$, Tukey-Kramer test).

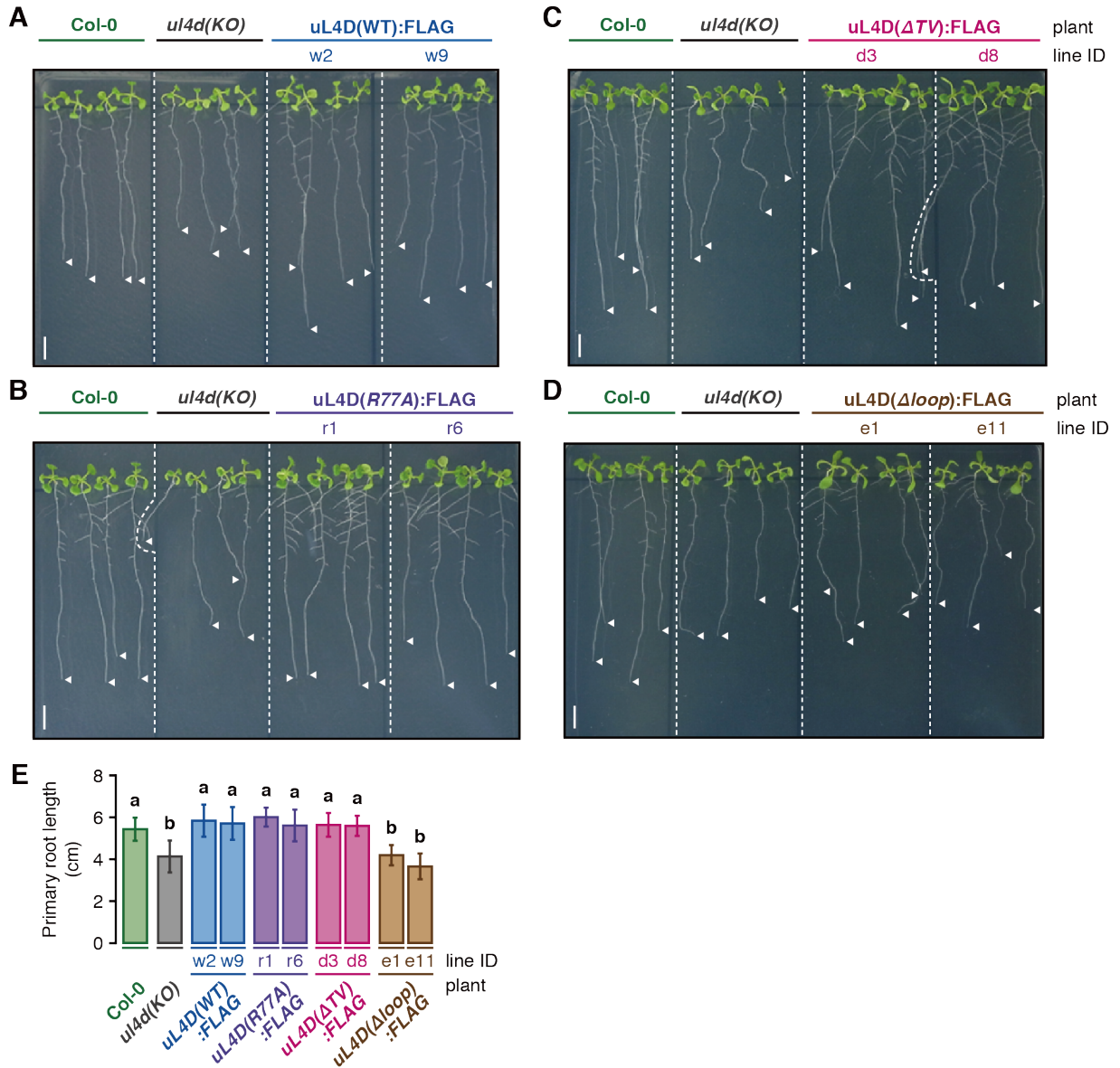


Figure 3.4. FLAG-tagged uL4Ds complement the short-root phenotype of *ul4d(KO)* plants.

Wild-type Col-0 plants, *ul4d(KO)*, and transgenic plants expressing FLAG-tagged uL4D(WT) (A), uL4D(R77A) (B), uL4D(Δ TV) (C), or uL4D(Δ loop) (D) were grown for 10 days on half-strength MS medium plates under long-day conditions. Arrowheads indicate the tip of the primary roots. Bars = 10 mm. (E) Primary root lengths in (A–D) were measured and means \pm SD ($n > 7$) are shown. Different letters indicate significant differences ($p < 0.05$, Tukey-Kramer test).

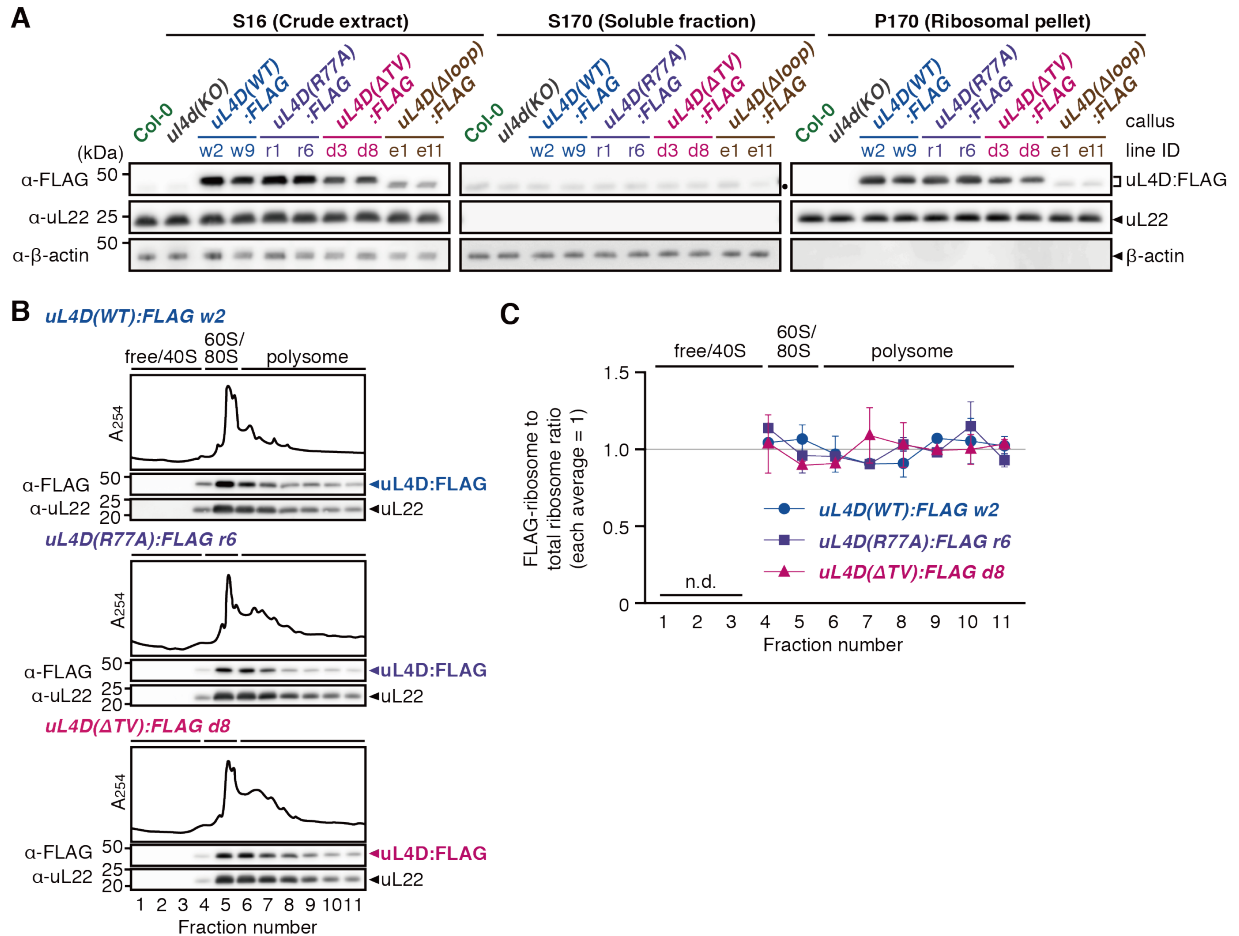


Figure 3.5. Functionality of FLAG-tagged mutant uL4D-containing ribosomes.

(A) Crude extracts (S16), post-ribosomal supernatants (S170), and ribosomal pellets (P170) prepared from callus cultures derived from wild-type Col-0 plants, *ul4d(KO)*, and FLAG-tagged mutant uL4D transgenic lines are shown. Total proteins (10 μ g in S16/S170; 1 μ g in P170) were separated by SDS-PAGE and analyzed by immunoblotting using anti-FLAG antibody, anti-uL22 antiserum, and anti- β -actin antiserum. Positions of FLAG-tagged uL4D mutant proteins (uL4D:FLAG), 19-kDa uL22, and 43-kDa β -actin bands are marked. β -actin was used as a soluble protein marker. Note that uL4D(Δ loop):FLAG protein is smaller than uL4D(WT):FLAG by ~1 kDa due to a 13-amino acid-deletion. A black dot in S170 marks the cross-reaction band. Representative results of two biological replicates are shown. (B) P-170 fractions from *uL4D(WT):FLAG w2* line, *uL4D(R77A):FLAG r6* line, and *uL4D(Δ TV):FLAG d8* line were fractionated by ultracentrifugation through a 15–60% (w/v) sucrose density gradient. UV absorbance profile at 254 nm and immunoblot analysis using anti-FLAG antibody and anti-uL22 antiserum are shown. Positions of free proteins and 40S subunit, 60S subunit, 80S ribosome, and polysome fractions are indicated. Representative results of two biological replicates are shown. (C) The immunoblot signals in (B) were quantified and the distributions of FLAG-tagged

mutant uL4D-containing ribosomes (detected by using anti-FLAG antibody) among total ribosome (detected by using anti-uL22 antiserum) were calculated. The positions of free proteins and 40S subunit, 60S subunit, 80S ribosome, and polysome fractions are indicated. The y-axis was set so that the means of uL4D(WT):FLAG w2 line, uL4D(R77A):FLAG r6 line, and uL4D(Δ TV):FLAG d8 line are 1. Means \pm SD of two biological repeats are shown.

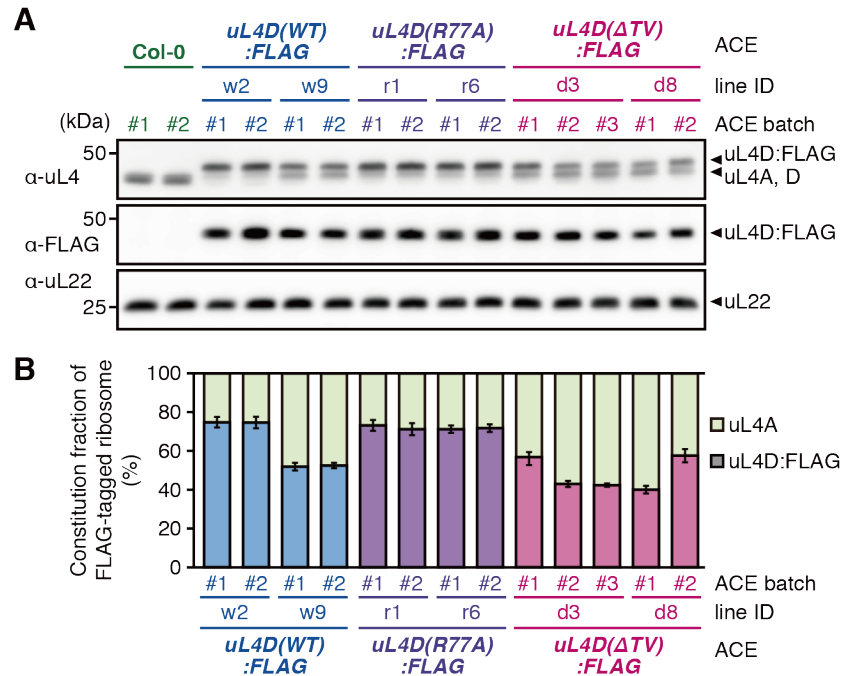


Figure 3.6. Constitution fraction of FLAG-tagged mutant uL4D-containing ribosomes.

(A) Immunoblot analysis of ACE batches using anti-uL4 antiserum, anti-FLAG antibody, and anti-uL22 antiserum. Representative results of three technical repeats are shown. Anti-uL4 detects both FLAG-tagged mutant uL4D and endogenous uL4A. (B) Immunoblot signals obtained using anti-uL4 antiserum in (A) were quantified, and the constitution fractions of FLAG-tagged uL4D-containing ribosomes among total ribosomes were calculated. Means \pm SD of three technical repeats are shown.

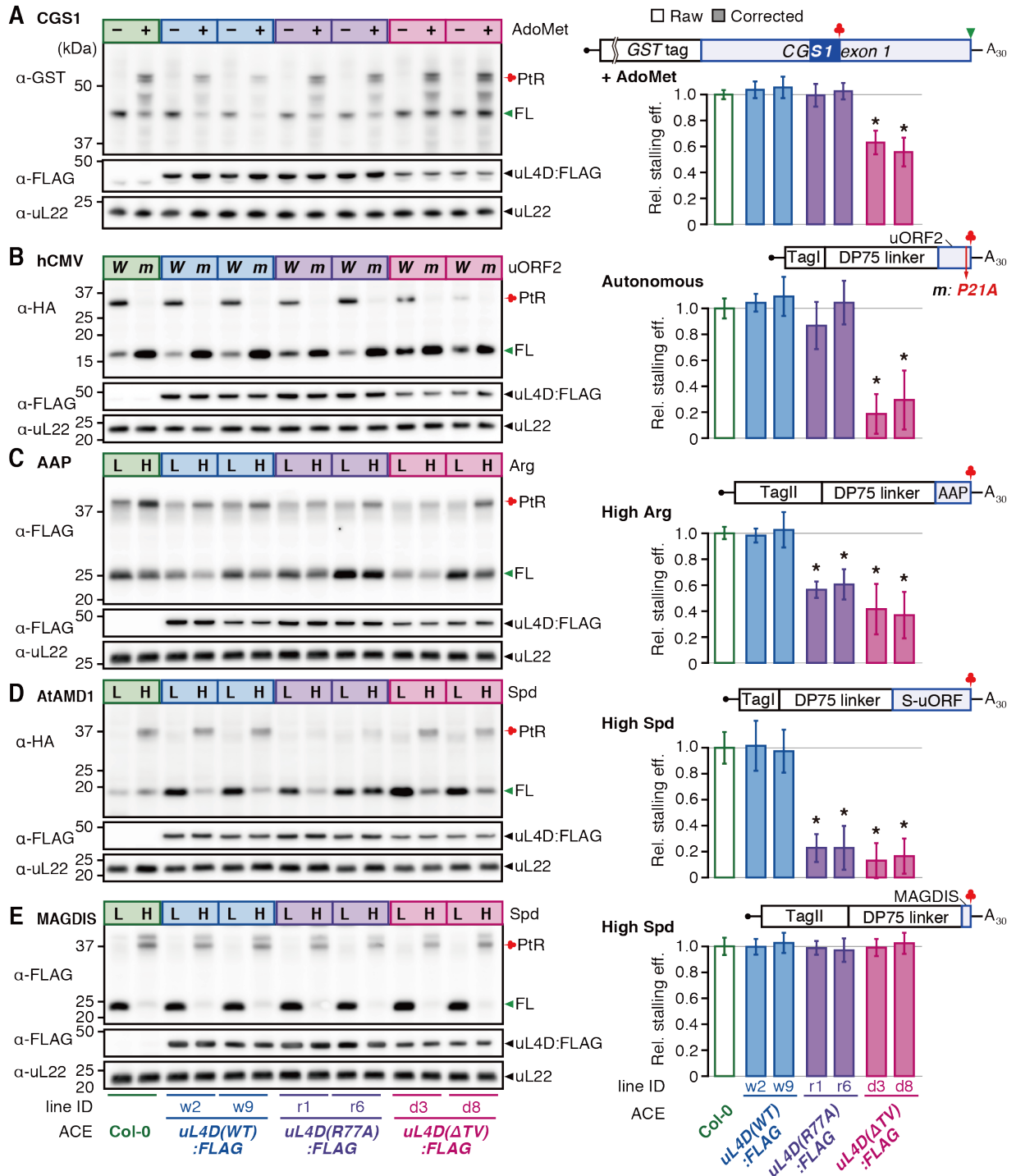


Figure 3.7. Differential effects of uL4D mutant ribosomes on stalling.

RNA construct shown above the bar graphs was translated in ACE prepared from wild-type Col-0, or from two independent lines of FLAG-tagged uL4D mutants as indicated. (*Left panels*) Translation products were separated by SDS-PAGE and analyzed by immunoblotting. The antibodies used to detect translation products are indicated. Immunoblots with anti-FLAG

antibody and anti-uL22 antiserum are also shown. Positions of the full-length product (FL), peptidyl-tRNA (PtR), 48-kDa FLAG-tagged uL4Ds (uL4D:FLAG), and 19-kDa uL22 are marked. The experiments were carried out with two batches of ACE preparations for each of the Col-0 and mutant lines, and a representative result of triplicate experiments in one of the batches is shown. (*Right panels*) The corrected stalling efficiencies (shaded box) relative to the raw stalling efficiency in Col-0 ACE (open box) were calculated and means \pm SD of six experiments performed with two ACE batches in triplicate are shown. Asterisks indicate significant differences compared with Col-0 ACE ($q < 0.05$ by Welch's t -test with false discovery rate (FDR) correction).

(A) CGS1 system. *GST:CGS1(WT)* RNA was translated for 30 min in ACE in the absence (-) or presence (+) of 1 mM AdoMet. The immunoblot signals of the "+" lanes in the left panel were quantified and stalling efficiencies were calculated. The MTO1 region (Ominato *et al.* 2002) is indicated by a filled blue box. **(B)** hCMV system. *Tagl:DP75:hCMV(WT)* RNA (W) and *Tagl:DP75:hCMV(P21A)* RNA (m) were translated for 30 min. The immunoblot signals of the "W" lanes were quantified. **(C)** AAP system. *TagII:DP75:AAP(WT)* RNA was translated for 10 min in the presence of a low (L, 0.08 mM) or high (H, 2.08 mM) L-arginine concentration as indicated. The immunoblot signals of the "H" lanes were quantified. **(D)** AtAMD1 system. *Tagl:DP75:S-ORF(WT)* RNA was translated for 30 min in the presence of a low (L, 0.2 mM) or high (H, 0.7 mM) spermidine (Spd) concentration as indicated. The immunoblot signals of the "H" lanes were quantified. **(E)** MAGDIS system. *TagII:DP75:MAGDIS(WT)* RNA was translated for 10 min in the presence of a low (L, 0.2 mM) or high (H, 0.7 mM) Spd concentration as indicated. The immunoblot signals of the "H" lanes were quantified. *Tagl* and *TagII* carry *M8:His:HA* and *M8:His:HA:3xFLAG:Myc* tags, respectively.

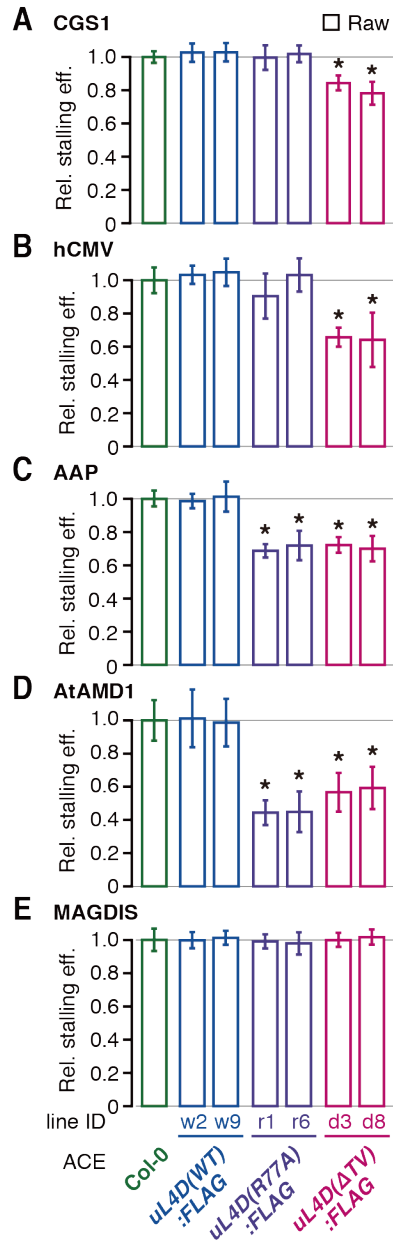


Figure 3.8. Differential effects of uL4D mutant ribosomes on stalling.

(A–E) The raw stalling efficiencies corresponding to the right panels of Figure 3.7, respectively, are shown. Asterisks indicate significant differences compared with Col-0 ACE ($q < 0.05$ by Welch’s t -test with FDR correction).

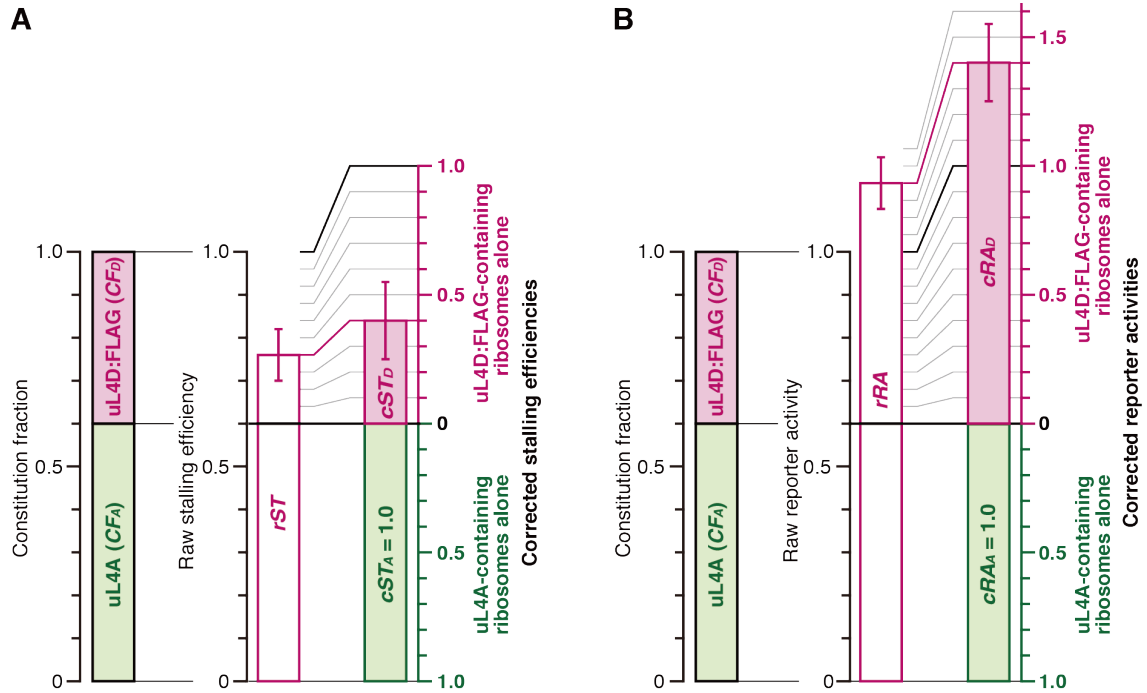


Figure 3.9. Correction of raw values of stalling efficiencies and reporter activities for the constitution fraction of uL4D mutant ribosome

(A) Correction of the stalling efficiency. The raw stalling efficiency relative to Col-0 ACE (rST) contains contributions from both FLAG-tagged mutant uL4D- and endogenous uL4A-containing ribosomes. To evaluate the stalling efficiencies of the mutant uL4D-containing ribosomes alone, the corrected stalling efficiencies (cST_D) were calculated by taking the constitution fraction of mutant uL4D-containing ribosomes (CF_D):

$$rST = CF_A + CF_D \times cST_D, \text{ where } CF_A = 1 - CF_D.$$

Therefore,

$$cST_D = 1 - (1 - rST) / CF_D.$$

SD values before (rSD) and after correction (cSD_D) are,

$$cSD_D = rSD / CF_D.$$

This calculation assumes that the stalling efficiency of endogenous uL4A-containing ribosomes alone (cST_A) is the same as that in Col-0 ACE (*i.e.*, $cST_A = 1$), which should be reasonable. The rSD value is ascribed all to cSD_D in this calculation.

(B) Correction of the reporter activity. Likewise, the raw reporter activity relative to Col-0 ACE (rRA) and its SD values (rSD) were corrected for the constitution fraction of mutant uL4D-containing ribosomes (CF_D):

$$cRA_D = 1 - (1 - rRA) / CF_D$$

$$cSD_D = rSD / CF_D.$$

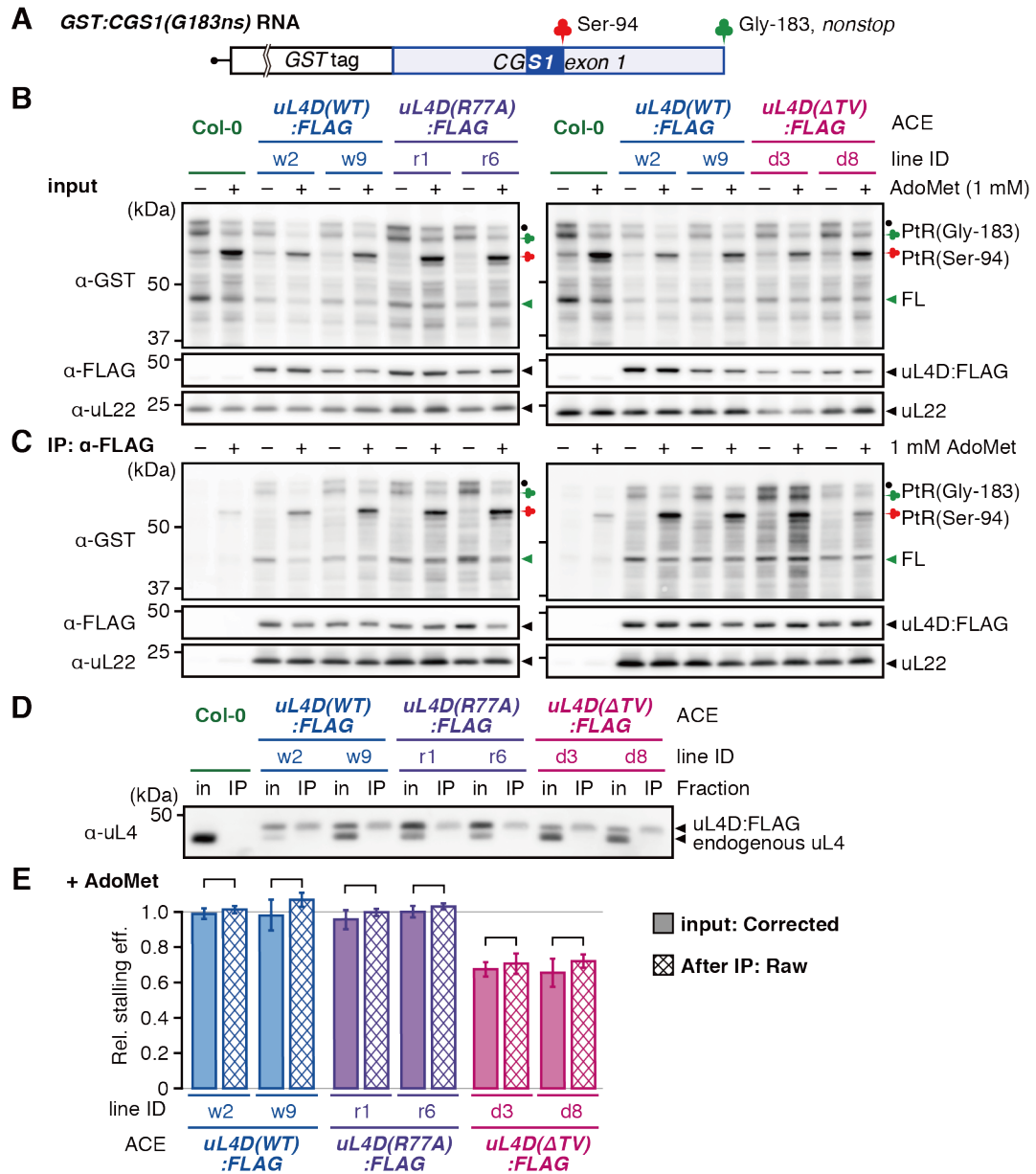


Figure 3.10. Affinity purification of stalled ribosomes.

(A) Schematic representation of *GST:CGS1(G183-ns)* RNA, which is a *nonstop* RNA that is truncated at the Gly-183 codon located at the end of *CGS1* exon 1 and does not carry a stop codon. The MTO1 region (Ominato *et al.* 2002) is indicated by a filled blue box. (B and C) *GST:CGS1(G183-ns)* RNA ($500 \text{ fmol } \mu\text{l}^{-1}$) was translated in ACE prepared from wild-type Col-0 and mutant lines expressing *uL4D:FLAG* in the absence (-) or presence (+) of 1 mM AdoMet, as indicated. After 30 min of translation, stalled ribosomes were affinity-purified by IP using anti-FLAG antibody. Translation products of input controls (B) and IP fractions (IP: α -FLAG) (C) were analyzed by immunoblotting using anti-GST antibody. Positions of 65-kDa peptidyl-tRNA

[PtR(Gly-183)] produced at the nonstop RNA end of Gly-183 and the 55-kDa peptidyl-tRNA [PtR(Ser-94)] produced by AdoMet-induced NPmRS at Ser-94, and the full-length peptide, which was dissociated from PtR(Gly-183) (FL), are marked. The band marked with a black dot is probably a peptidyl-tRNA that is produced by a ribosome stacked behind the one stalled at the nonstop RNA end. Immunoblots using anti-FLAG antibody and anti-uL22 antiserum are shown as loading controls. A representative result of triplicate experiments is shown. **(D)** Immunoblot analysis of the translation mixture before (in) and after IP (IP) using anti-uL4 antiserum to show the constitution fractions of FLAG-tagged ribosomes. Positions of the 48-kDa FLAG-tagged uL4D (uL4D:FLAG) and the 47-kDa endogenous uL4 are marked. The band marked as endogenous uL4 in Col-0 ACE (lanes 1 and 2) includes both endogenous uL4A and endogenous uL4D, while that in uL4D:FLAG mutant ACE (lanes 3–14) is endogenous uL4A alone. A representative result of triplicate experiments is shown. **(E)** The immunoblot signals in (B) and (C) were quantified. The corrected stalling efficiency in the input sample (shaded box), and the raw stalling efficiency after IP (cross hatched box) were calculated and means \pm SD ($n = 3$) are shown. No significant difference was observed between the corrected stalling efficiency before IP and raw stalling efficiency after IP in each pair of the samples ($p > 0.05$ by Welch's t -test).

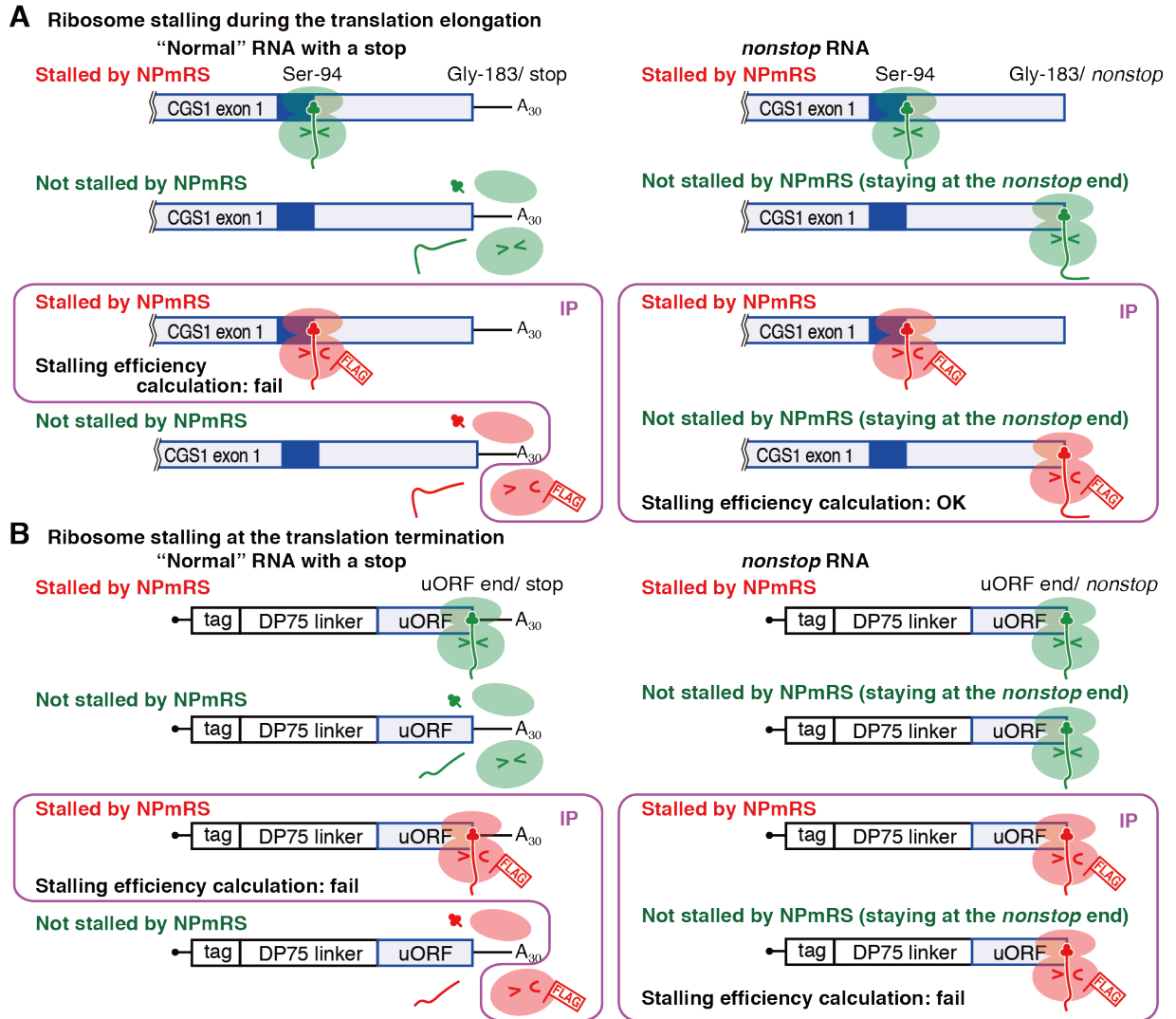


Figure 3.11. Affinity purification strategy of the stalled ribosomes.

The green ribosomes represent wild-type ribosomes, and the red ribosomes represent FLAG-tagged mutant ribosomes. tRNAs are represented by clovers. To calculate the stalling efficiency of FLAG-tagged mutant ribosomes alone, peptidyl-tRNAs from both stalled and non-stalled mutant ribosomes have to be purified. **(A)** Affinity purification of ribosomes stalled during the translation elongation by IP. The MTO1 region (Ominato *et al.* 2002) is indicated by a filled blue box. *(Left)* On a “normal” RNA with a stop codon, those ribosomes that did not stall by NPmRS will translate to the stop codon and dissociate into large and small subunits and peptidyl-tRNA are hydrolyzed to tRNA and peptides. Therefore, those ribosomes that did not stall by NPmRS cannot be affinity-purified. *(Right)* On a *nonstop* RNA, those ribosomes that did not stall by NPmRS will translate to the nonstop RNA end and will be staying there. Therefore, both of them can be affinity-purified and stalling efficiency can be calculated. **(B)** Affinity purification of ribosomes stalled at the translation termination by IP. *(Left)* On a “normal” RNA with a stop codon,

those ribosomes that did not stall by NPmRS will translate to the stop codon and dissociate into large and small subunits and peptidyl-tRNA are hydrolyzed to tRNA and peptides. Therefore, those ribosomes that did not stall by NPmRS cannot be affinity-purified. (*Right*) On a *nonstop* RNA, those ribosomes that did not stall by NPmRS will be staying at the *nonstop* RNA end. Therefore, both stalled and non-stalled ribosomes can be affinity-purified. However, stalling efficiency cannot be calculated, because these ribosomes bear the same peptidyl-tRNA species.

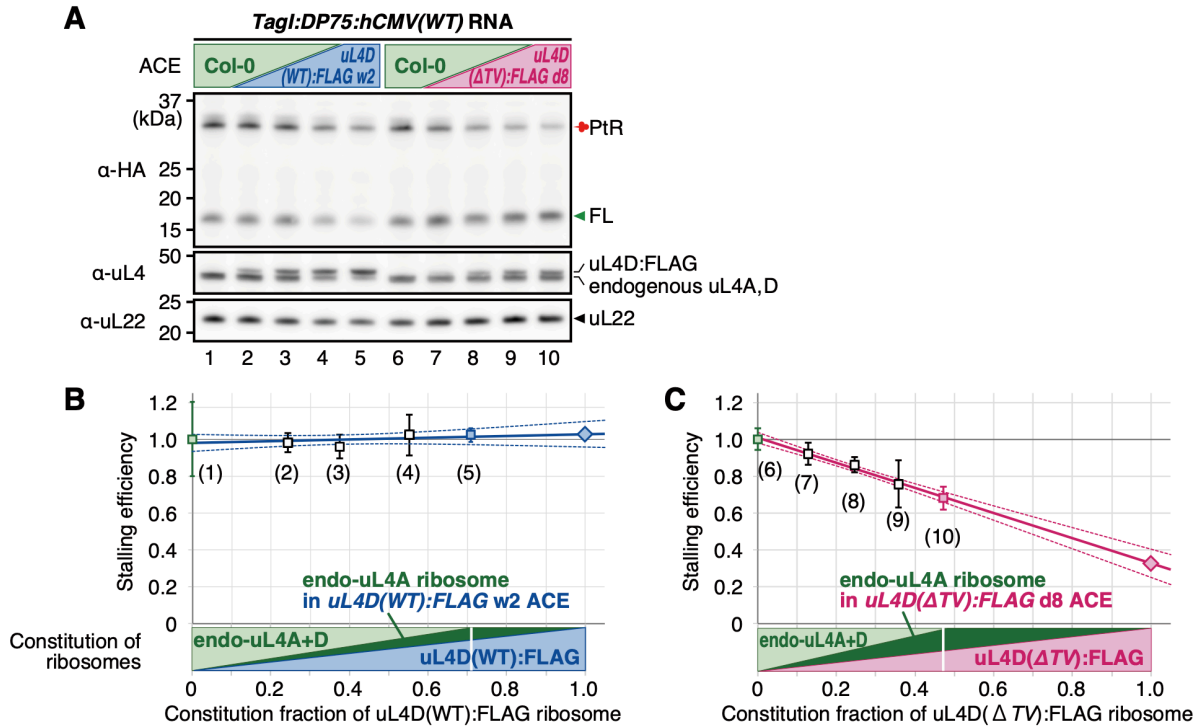


Figure 3.12. Deduction of the stalling efficiencies by the mutant ribosomes alone by linear regression.

(A) Col-0 ACE and $uL4D(WT):FLAG$ line w2 ACE were mixed at 1:0, 3:1, 1:1, 1:3, and 0:1 volume ratios (lanes 1 to 5, respectively), or Col-0 ACE and $uL4D(\Delta TV):FLAG$ line d8 ACE were mixed at 1:0, 3:1, 1:1, 1:3, and 0:1 volume ratios (lanes 6 to 10, respectively). These mixtures were used to translate *Tagl:DP75:hCMV(WT) RNA*. Translation products were separated by SDS-PAGE and analyzed by immunoblotting using anti-HA antibody. Immunoblots with anti-uL4 and anti-uL22 are also shown. Positions of the full-length product (FL), peptidyl-tRNA (PtR), 48-kDa FLAG-tagged uL4Ds ($uL4D:FLAG$), endogenous uL4A and uL4D ($uL4A, D$), and 19-kDa uL22 are marked. The experiments were carried out in one of the batches of ACE preparations for each of the Col-0 and mutant lines, and a representative result of triplicate experiments is shown. (B) Linear regression (solid blue line) of stalling efficiency vs construction fraction of $uL4D(WT):FLAG$ ribosome. Raw stalling efficiencies obtained from lanes 1–5 of (A) were plotted against the constitution fractions of the $uL4D(WT):FLAG$ ribosome of each of the ACE mixtures (means \pm SD, $n = 3$). The constitution fraction was determined based on the intensities of the upper and lower bands of the immunoblot with anti-uL4 antibody. The numbers in parentheses below the data refer to the lane numbers in (A). The blue diamond indicates the estimated stalling efficiency by the $uL4D(WT):FLAG$ ribosome alone. The dashed blue curves represent the upper and lower limits of the mean prediction 95% confidence interval. (C) Linear regression (solid magenta line) of stalling efficiency vs construction fraction of $uL4D(\Delta TV):FLAG$ ribosome. Raw stalling efficiencies

CHAPTER 3. Exit tunnel constriction and ribosome stalling

obtained from lanes 6–10 of (A) were plotted against the constitution fractions of the uL4D($\Delta 7V$):FLAG ribosome of each of the ACE mixtures (means \pm SD, $n = 3$). The constitution fraction was determined as in (B). The numbers in parentheses below the data refer to the lane numbers in (A). The magenta diamond indicates the estimated stalling efficiency by the uL4D($\Delta 7V$):FLAG ribosome alone. The dashed magenta curves represent the upper and lower limits of the mean prediction 95% confidence interval. In (B) and (C), calculated constitution fractions of endogenous uL4A- and D-containing ribosomes in Col-0 ACE (light green), endogenous uL4A-containing ribosomes in the mutant ACE (dark green), and FLAG-tagged mutant uL4D-containing ribosomes (light blue or light magenta) are shown below the graph. Note that to the right of the vertical white lines are extrapolated values. The linear regression and mean prediction 95% confidence interval were calculated using Mathematica software (Wolfram Research, Champaign, IL, USA).

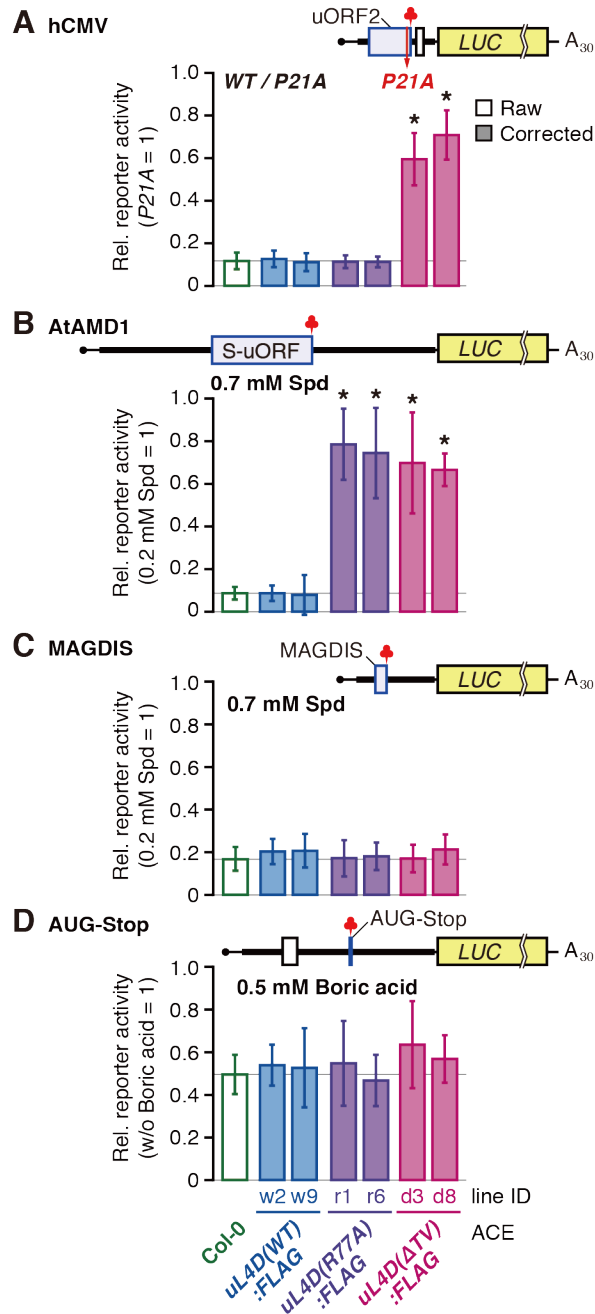


Figure 3.13. Differential effects of uL4D mutant ribosomes on LUC reporter expression.

RNA was translated in ACE prepared from wild-type Col-0 or from two independent lines of FLAG-tagged uL4D mutants. After translation of RNA for 120 min, LUC activities were measured and normalized with the *Renilla* luciferase (RLUC) activity of the co-translated control RNA. The corrected reporter activities (shaded box) relative to the raw reporter activity in Col-0 ACE (open box) were calculated and means \pm SD of six experiments performed with two ACE batches in triplicate are shown. Asterisks indicate significant difference from raw reporter activity in Col-0

ACE ($q < 0.05$ by Welch's t -test with FDR correction). **(A)** hCMV system. $5'$ -hCMV:LUC(WT) and $5'$ -hCMV:LUC(P21A) RNAs were translated. LUC activities in $5'$ -hCMV:LUC(WT) RNA relative to those of $5'$ -hCMV:LUC(P21A) RNA were calculated. **(B)** AtAMD1 system. $5'$ -AtAMD1:LUC RNA was translated in the presence of 0.2 or 0.7 mM spermidine (Spd). LUC activities in the presence of 0.7 mM Spd relative to those of 0.2 mM were calculated. **(C)** MAGDIS system. $5'$ -mAMD1:LUC RNA was translated in the presence of 0.2 or 0.7 mM Spd. LUC activities in the presence of 0.7 mM Spd relative to those at 0.2 mM were calculated. **(D)** AUG-Stop system. $5'$ -NIP5;1:LUC RNA was translated in the presence or absence of 0.5 mM boric acid. LUC activities in the presence of boric acid relative to those in its absence were calculated.

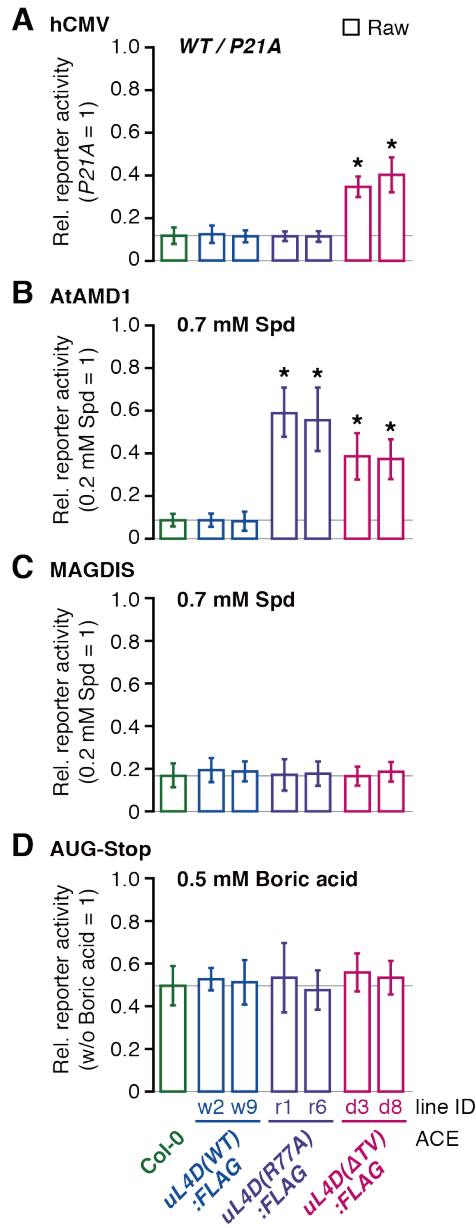


Figure 3.14. Raw reporter activities.

(A–D) The raw reporter activities corresponding to Figure 3.13, respectively, are shown. Asterisks indicate significant differences compared with Col-0 ACE ($p < 0.05$ by Welch's t -test with FDR correction).

CHAPTER 4.

General discussion

In the present study, I used transgenic *Arabidopsis* lines carrying mutant r-proteins, and analyzed their effects on several NPmRSs in eukaryotes by using *Arabidopsis in vitro* translation system derived from the mutant lines (Chapter 3). I analyzed two types of uL4 mutations: a point mutation (*R77A*) and a small deletion (ΔTV). The latter will alter the geometry of the constriction region, while the former may be able to detect specific interaction with the nascent peptide. For the NPmRS systems to be tested, I chose five well-characterized eukaryotic NPmRS systems including virus, fungi, plants, and mammals (Figure 2.1). I found that all regulatory peptides function in *Arabidopsis* ribosomes prepared from wild-type plants (Chapter 2). Among these, ribosome stalling of the four systems were reduced in uL4(ΔTV) mutant ribosomes, namely the CGS1, hCMV, AAP, and AtAMD1 systems, while two were also reduced in uL4D(*R77A*) mutant ribosomes. The qualitative differences in the effects of the mutant ribosomes explained the difference in spatial allocation of the nascent peptides in the constriction region that have been revealed by the structural analyses. In contrast, one NPmRS, the MAGDIS system, was not affected by the ribosome mutation. This uORF codes for six-amino-acid sequence of MAGDIS to cause stalling, which is too short to reach the constriction region. Therefore, my study clearly showed that the constriction region is crucial for most of the NPmRS systems that have their functional amino acids > 20 amino acids, whereas the MAGDIS uORF uses a distinct mechanism for the induction of stalling.

Direct effect of uL4D mutant ribosomes on stalling function

Two possibilities can be envisaged for the direct effect of the uL4D(*R77A*) and uL4D(ΔTV) mutations on stalling function: (i) specific amino acid residues substituted or deleted in these mutation, namely Arg-77, and Thr-75 and Val-79 of uL4, respectively, are necessary for stalling, or (ii) integrity of β -loop structure of uL4 is necessary for stalling. Concerning the possibility (i), the Arg-77 residue is at the tip of the β -loop structure, whereas the Thr-75 and Val-79 residues flank the tip, and these amino acid sequences are highly conserved in both bacterial and eukaryotic orthologs (Figures 3.1B and 3.2B). This region may be essential for establishing interactions with specific motifs of regulatory peptides when these peptides adopt a distinct conformation inside the exit tunnel, as reported in the *E. coli* SecM and fungal AAP (Yap and Bernstein 2009,

Bhushan *et al.* 2010, Wu *et al.* 2012), which may argue for the possibility (i). As for the possibility (ii), the high-resolution crystal structure of the ribosomal large subunit with a three amino acids insertion in the β -loop of uL22 has been determined in *Deinococcus radiodurans* (Wekselman *et al.* 2017). This structure has revealed that the insertion causes a shift of the β -loop structure of the mutated uL22 toward the interior of the exit tunnel, thereby alter the conformation of the surrounding 23S rRNA residues, which is consistent with previous biochemical and structural analyses (Gabashvili *et al.* 2001, Davydova *et al.* 2002, Berisio *et al.* 2003). This finding indicates that mutation of the constriction region may modulate the shape of overall structure of the constriction and thus affect ribosome stalling. The nascent peptide of MifM induces ribosome stalling in *B. subtilis* but not in *E. coli* (Chiba *et al.* 2011). This species specificity was dictated by the identity of a single amino acid within the β -loop of uL22 (Sohmen *et al.* 2015). This finding also suggests that even minor conformational changes in the constriction region can have a major influence on ribosome stalling. Based on these findings, the uL4D mutant ribosome may trigger structural rearrangements of ribosomal component(s) including uL4 and uL22 and/or rRNA nucleotides; however, it is not yet possible to obtain any structural information of the ribosome carrying these mutations since only a limited number of structural information related to plant 80S ribosomes is available at present.

Commonality and specificity of mechanisms involved in NPmRS

Known regulatory nascent peptides have divergent sequences (Table 1.1 and Figure 2.1), and even the relatively short ErmCL homologs (19 amino acids) exhibit considerable variation among different bacterial species (Ramu *et al.* 2009). Thus, it has been thought that each regulatory peptide acts with the translating ribosome in a distinct fashion (Bhushan *et al.* 2010, Ito and Chiba 2013). My biochemical data provide insights into the common features of underlying molecular mechanisms of NPmRS as well as its specificity. First, several aspects have been identified that all NPmRS systems have in common: (i) The critical regions of regulatory peptides appear to be concentrated on the upper half of the ribosomal exit tunnel, extending from the PTC to the constriction region (Figure 2.1) (Su *et al.* 2017, Mori *et al.* 2018, Shanmuganathan *et al.* 2019). (ii) In all cases, specific contacts of nascent peptides are established to the wall of the ribosomal exit tunnel if the length of functional amino acids is long enough to reach the constriction region (Chapter 3). (iii) Apart from my biochemical evidence-based aspects, the geometry of the PTC is perturbed in order to achieve ribosome stalling, as evidenced by cryo-EM studies of the AAP and hCMV systems (Bhushan *et al.* 2010, Wilson *et al.* 2016). In particular,

three nucleotides around the PTC, namely U2506, U2585, and A2602, are most strongly affected due to their critical contribution to peptide bond formation and/or termination, which could contribute to PTC inactivation. Second, there is no simple consensus for stalling, but rather a high degree of variety is present. (i) The length of the critical amino acid stretch is ranging from as short as six-amino-acid MAGDIS of mAMD1 to as long as >30 amino acids as observed in several stalling systems (Figure 2.1). Indeed, polyamine-induced stalling of mAMD1 was not affected by uL4D mutant ribosomes as well as boric acid-dependent stalling of NIP5;1. (ii) There is no consensus and no common contact pattern between the nascent peptide and the exit tunnel wall, with some functional amino acid sequences even adopting a distinct conformation in the tunnel (Yap and Bernstein 2009, Bhushan *et al.* 2010, Onoue *et al.* 2011, Wu *et al.* 2012, Matheisl *et al.* 2015). (iii) Effector-dependent stalling participates in composite binding pockets together with the exit tunnel, while autonomous stalling induces a perturbed geometry at the PTC without any assistance by an effector. Therefore, to obtain more comprehensive picture of the commonality and specificity of mechanisms involved in RPmRS, further biochemical insight into other stalling will be required.

Novel approaches for translating mRNAs in the whole genome

Novel technologies enable an investigation of the genome-wide translational landscape. Recently, ribosome profiling (Ingolia *et al.* 2009), which sequences ribosome-protected mRNA fragments, has been developed and applied for calculation of translation efficiency in the genomic scale. In plants, for example, Hsu *et al.* (2016) used this method to discover proteins missed in the annotation of the Arabidopsis genome, and confirmed unannotated small proteins that might have important functions in plants as well as a lot of stalling events. The availability of such translome data for both model and non-model plants would facilitate fundamental and applied research for protein-coding genes and transposable elements in the genome.

The affinity purification of epitope-tagged r-proteins has been extensively used as a valuable tool for biochemical and structural studies, including ribosome biogenesis and translational regulation in eukaryotes. For example, a tissue-specific translational abundance has been analyzed using ribosome profiling methods such as translating ribosome affinity purification followed by RNA sequencing in organisms ranging from *Drosophila melanogaster* to mice and human cultured cells (Heiman *et al.* 2014, Chen and Dickman 2018). In plants, FLAG-tagged Arabidopsis eL18 was expressed in wild-type plants under the control of the cauliflower mosaic virus 35S promoter (Zanetti *et al.* 2005), and used for analysis of ribosome-associated mRNAs

and lncRNAs (Juntawong *et al.* 2013, Bazin *et al.* 2017). More recently, transgenic rice with an epitope-tagged uL18 was generated and revealed the importance of transcript size and GC content in mRNA translation (Zhao *et al.* 2017). However, few attempts have been made to express mutant r-proteins, because ribosome mutants often suffer from sick phenotypes, such as growth defects and developmental alterations, making it difficult to establish “healthy” mutant plants (Byrne 2009, Horiguchi *et al.* 2012). In *Arabidopsis*, a plant-specific transcription factor ANAC082 plays a central role in the pathways connecting ribosomal perturbations, including genetic impairment of ribosome biogenesis factors or ribosomal components (Ohbayashi *et al.* 2017). The *uL4D* mutant *Arabidopsis* lines used in my study have one copy of endogenous *uL4A* intact, which allowed me to obtain clear biochemical data (Chapter 3).

Comprehensive identification of functional amino acids responsible for induction of ribosome stalling has been conducted using bioinformatics analysis in *Arabidopsis* and identified eight novel uORFs that repress main ORF expression in an amino acid sequence-dependent manner (Ebina *et al.* 2015, Hayashi *et al.* 2017), but has been limited to uORF. In these approaches, uORF sequences are compared between a certain range of species and any others with available transcript sequence databases (Hayden and Jorgensen 2008, Takahashi *et al.* 2012, Vaughn *et al.* 2012). In contrast to uORF, only two stalling events at main ORF have been reported in eukaryotes, namely CGS1 in *Arabidopsis* and XBP1u in human (Chiba *et al.* 2003, Onouchi *et al.* 2005, Yanagaitani *et al.* 2011). My study with transgenic *Arabidopsis* lines carrying mutant ribosomes provides a powerful tool for genome-wide searches to investigate novel stalling events at either uORF or main ORF and sheds light on the possible roles of the ribosomal exit tunnel in global translation processes.

References

- Aibara, I., Hirai, T., Kasai, K., Takano, J., Onouchi, H., Naito, S., Fujiwara, T. and Miwa, K. (2018) Boron-Dependent Translational Suppression of the Borate Exporter *BOR1* Contributes to the Avoidance of Boron Toxicity. *Plant Physiol.*, 177, 759–774.
- Alderete, J.P., Jarrahan, S. and Geballe, A.P. (1999) Translational effects of mutations and polymorphisms in a repressive upstream open reading frame of the human cytomegalovirus UL4 gene. *J. Virol.*, 73, 8330–8337.
- Alonso, J.M., Stepanova, A.N., Leisse, T.J., Kim, C.J., Chen, H., Shinn, P., Stevenson, D.K., Zimmerman, J., Barajas, P., Cheuk, R., Gadrinab, C., Heller, C., Jeske, A., Koesema, E., Meyers, C.C., Parker, H., Prednis, L., Ansari, Y., Choy, N., Deen, H., Geralt, M., Hazari, N., Hom, E., Karnes, M., Mulholland, C., Ndubaku, R., Schmidt, I., Guzman, P., Aguilar-Henonin, L., Schmid, M., Weigel, D., Carter, D.E., Marchand, T., Risseuw, E., Brogden, D., Zeko, A., Crosby, W.L., Berry, C.C. and Ecker, J.R. (2003) Genome-wide insertional mutagenesis of *Arabidopsis thaliana*. *Science*, 301, 653–657.
- Amrani, N., Sachs, M.S. and Jacobson, A. (2006) Early nonsense: mRNA decay solves a translational problem. *Nat. Rev. Mol. Cell Biol.*, 7, 415–425.
- Arenz, S., Meydan, S., Starosta, A.L., Berninghausen, O., Beckmann, R., Vázquez-Laslop, N. and Wilson, D.N. (2014) Drug sensing by the ribosome induces translational arrest via active site perturbation. *Mol. Cell*, 56, 446–452.
- Arenz, S., Bock, L.V., Graf, M., Innis, C.A., Beckmann, R., Grubmüller, H., Vaiana, A.C. and Wilson, D.N. (2016) A combined cryo-EM and molecular dynamics approach reveals the mechanism of ErmBL-mediated translation arrest. *Nat. Commun.*, 7, 12026.
- Armache, J., Jarasch, A., Anger, A.M., Villa, E., Becker, T., Bhushan, S., Jossinet, F., Habeck, M., Dindar, G., Franckenberg, S., Marquez, V., Mielke, T., Thomm, M., Berninghausen, O., Beatrix, B., Söding, J., Westhof, E., Wilson, D.N. and Beckmann, R. (2010) Cryo-EM structure and rRNA model of a translating eukaryotic 80S ribosome at 5.5-Å resolution. *Proc. Natl. Acad. Sci. USA*, 107, 19748–19753.
- von Arnim, A.G., Jia, Q. and Vaughn, J.N. (2014) Regulation of plant translation by upstream open reading frames. *Plant Sci.*, 214, 1–12.

- Balasubramanian, S., Zheng, D., Liu, Y.J., Fang, G., Frankish, A., Carriero, N., Robilotto, R., Cayting, P. and Gerstein, M. (2009) Comparative analysis of processed ribosomal protein pseudogenes in four mammalian genomes. *Genome Biol.*, 10, R2.
- Ban, N., Beckmann, R., Cate, J.H.D., Dinman, J.D., Dragon, F., Ellis, S.R., Lafontaine, D.L.J., Lindahl, L., Liljas, A., Lipton, J.M., McAlear, M.A., Moore, P.B., Noller, H.F., Ortega, J., Panse, V.G., Ramakrishnan, V., Spahn, C.M., Steitz, T.A., Tchorzewski, M., Tollervey, D., Warren, A.J., Williamson, J.R., Wilson, D., Yonath, A. and Yusupov, M.. (2014) A new system for naming ribosomal proteins. *Curr. Opin. Struct. Biol.*, 24,165–169.
- Barakat, A., Szick-Miranda, K., Chang, I.F., Guyot, R., Blanc, G., Cooke, R., Delseny, M. and Bailey-Serres, J. (2001) The organization of cytoplasmic ribosomal protein genes in the Arabidopsis genome. *Plant Physiol.*, 127, 398–415.
- Bazin, J., Baerenfaller, K., Gosai, S.J., Gregory, B.D., Crespi, M. and Bailey-Serres, J. (2017) Global analysis of ribosome-associated noncoding RNAs unveils new modes of translational regulation. *Proc. Natl. Acad. Sci. USA*, 114, E10018–E10027.
- Benjamini, Y. and Hochberg, Y. (1995) Controlling the false discovery rate: a practical and powerful approach to multiple testing. *J. R. Statist. Soc. B*, 57, 289–300.
- Berisio, R., Schluenzen, F., Harms, J., Bashan, A., Auerbach, T., Baram, D. and Yonath, A. (2003) Structural insight into the role of the ribosomal tunnel in cellular regulation. *Nat. Struct. Biol.*, 10, 366–370.
- Bhushan, S., Hoffmann, T., Seidelt, B., Frauenfeld, J., Mielke, T., Berninghausen, O., Wilson, D.N. and Beckmann, R. (2011) SecM-stalled ribosomes adopt an altered geometry at the peptidyl transferase center. *PLoS Biol.*, 9, e1000581.
- Bhushan, S., Meyer, H., Starosta, A.L., Becker, T., Mielke, T., Berninghausen, O., Sattler, M., Wilson, D.N. and Beckmann, R. (2010) Structural basis for translational stalling by human cytomegalovirus and fungal arginine attenuator peptide. *Mol. Cell*, 40, 138–146.
- Bingel-Erlenmeyer, R., Kohler, R., Kramer, G., Sandikci, A., Antolić, S., Maier, T., Schaffitzel, C., Wiedmann, B., Bukau, B. and Ban, N. (2008) A peptide deformylase-ribosome complex reveals mechanism of nascent chain processing. *Nature*, 452, 108–111.
- Bischoff, L., Berninghausen, O. and Beckmann, R. (2014) Molecular basis for the ribosome functioning as an L-tryptophan sensor. *Cell Rep.*, 9, 469–475.

- Blobel, G. and Sabatini, D.D. (1970) Controlled proteolysis of nascent polypeptides in rat liver cell fractions. I. Location of the polypeptides within ribosomes. *J. Cell. Biol.*, 45, 130–145.
- Byrne, M.E. (2009) A role for the ribosome in development. *Trends Plant Sci.*, 14, 512–519.
- Cao, J. and Geballe, A.P. (1995) Translational inhibition by a human cytomegalovirus upstream open reading frame despite inefficient utilization of its AUG codon. *J. Virol.*, 69, 1030–1036.
- Cao, J. and Geballe, A.P. (1996) Coding sequence-dependent ribosomal arrest at termination of translation. *Mol. Cell. Biol.*, 16, 603–608.
- Carrasco, L., Fernandez-Puentes, C. and Vazquez, D. (1976) Antibiotics and compounds affecting translation by eukaryotic ribosomes. *Mol. Cell. Biochem.*, 16, 97–122.
- Carroll, A.J., Heazlewood, J.L., Ito, J. and Millar, A.H. (2008) Analysis of the *Arabidopsis* Cytosolic Ribosome Proteome Provides Detailed Insights into Its Components and Their Post-translational Modification. *Mol. Cell. Proteomics.*, 7, 347–369.
- Chang, I.F., Szick-Miranda, K., Pan, S. and Bailey-Serres, J. (2005) Proteomic characterization of evolutionarily conserved and variable proteins of *Arabidopsis* cytosolic ribosomes. *Plant Physiol.*, 137, 848–862.
- Chen, X. and Dickman, D. (2018) Development of a tissue-specific ribosome profiling approach in *Drosophila* enables genome-wide evaluation of translational adaptations. *PLoS Genet.*, 13, e1007117.
- Chiba, S., Lamsa, A. and Pogliano, K. (2009) A ribosome-nascent chain sensor of membrane protein biogenesis in *Bacillus subtilis*. *EMBO J.*, 28, 3461–3475.
- Chiba, S., Kanamori, T., Ueda, T., Akiyama, Y., Pogliano, K. and Ito, K. (2011) Recruitment of a species-specific translational arrest module to monitor different cellular processes. *Proc. Natl. Acad. Sci. USA*, 108, 6073–6078.
- Chiba, S. and Ito, K. (2012) Multisite ribosomal stalling: a unique mode of regulatory nascent chain action revealed for MifM. *Mol. Cell*, 47, 863–872.
- Chiba, Y., Ishikawa, M., Kijima, F., Tyson, R.H., Kim, J., Yamamoto, A., Nambara, E., Leustek, T., Wallsgrove, R.M. and Naito, S. (1999) Evidence for autoregulation of cystathionine γ -synthase mRNA stability in *Arabidopsis*. *Science*, 286, 1371–1374.

- Chiba, Y., Sakurai, R., Yoshino, M., Ominato, K., Ishikawa, M., Onouchi, H. and Naito, S. (2003) S-Adenosyl-L-methionine is an effector in the posttranscriptional autoregulation of the cystathionine γ -synthase gene in *Arabidopsis*. *Proc. Natl. Acad. Sci. USA*, 100, 10225–10230.
- Clough, S.J. and Bent, A.F. (1998) Floral dip: a simplified method for *Agrobacterium*-mediated transformation of *Arabidopsis thaliana*. *Plant J.*, 16, 735–743.
- Creff, A., Sormani, R. and Desnos, T. (2010) The two *Arabidopsis RPS6* genes, encoding for cytoplasmic ribosomal proteins S6, are functionally equivalent. *Plant Mol. Biol.*, 73, 533–546.
- Crowe, M.L., Wang, X.Q. and Rothnagel, J.A. (2006) Evidence for conservation and selection of upstream open reading frames suggests probable encoding of bioactive peptides. *BMC Genomics*, 7, 16.
- Cruz-Vera, L.R., Rajagopal, S., Squires, C. and Yanofsky, C. (2005) Features of ribosome-peptidyl-tRNA interactions essential for tryptophan induction of *tna* operon expression. *Mol. Cell*, 19, 333–343.
- Cruz-Vera, L.R. and Yanofsky, C. (2008) Conserved residues Asp16 and Pro24 of TnaC-tRNA^{Pro} participate in tryptophan induction of *Tna* operon expression. *J. Bacteriol.*, 190, 4791–4797.
- Curtis, M.D. and Grossniklaus, U. (2003) A gateway cloning vector set for high-throughput functional analysis of genes in planta. *Plant Physiol.*, 133, 462–469.
- Cymer, F., Hedman, R., Ismail, N. and von Heijne, G. (2015) Exploration of the arrest peptide sequence space reveals arrest-enhanced variants. *J. Biol. Chem.*, 290, 10208–10215.
- Davydova, N., Streltsov, V., Wilce, M., Liljas, A. and Garber, M. (2002) L22 ribosomal protein and effect of its mutation on ribosome resistance to erythromycin. *J. Mol. Biol.*, 322, 635–644.
- Degenhardt, R.F. and Bonham-Smith, P.C. (2008) *Arabidopsis* ribosomal proteins RPL23aA and RPL23aB are differentially targeted to the nucleolus and are disparately required for normal development. *Plant Physiol.*, 147, 128–142.
- Degnin, C.R., Schleiss, M.R., Cao, J. and Geballe, A.P. (1993) Translational inhibition mediated by a short upstream open reading frame in the human cytomegalovirus gpUL4 (gp48) transcript. *J. Virol.*, 67, 5514–5521.
- Doma, M.K. and Parker, R. (2006) Endonucleolytic cleavage of eukaryotic mRNAs with stalls in translation elongation. *Nature*, 440, 561–564.

- Falcone Ferreyra, M.L., Pezza, A., Biarc, J., Burlingame, A.L. and Casati, P. (2010) Plant L10 ribosomal proteins have different roles during development and translation under ultraviolet-B stress. *Plant Physiol.*, 153, 1878–1894.
- Fang, P., Spevak, C.C., Wu, C. and Sachs, M.S. (2004) A nascent polypeptide domain that can regulate translation elongation. *Proc. Natl. Acad. Sci. USA*, 101, 4059–4064.
- Franceschetti, M., Hanfrey, C., Scaramagli, S., Torrigiani, P., Bagni, N., Burtin, D. and Michael, A.J. (2001) Characterization of monocot and dicot plant S-adenosyl-L-methionine decarboxylase gene families including identification in the mRNA of a highly conserved pair of upstream overlapping open reading frames. *Biochem. J.*, 353, 403–409.
- Fujiwara, K., Ito, K. and Chiba, S. (2018) MifM-instructed translation arrest involves nascent chain interactions with the exterior as well as the interior of the ribosome. *Sci. Rep.*, 8, 10311.
- Gaba, A., Jacobson, A. and Sachs, M.S. (2005) Ribosome occupancy of the yeast *CPA1* upstream open reading frame termination codon modulates nonsense-mediated mRNA decay. *Mol. Cell*, 20, 449–460.
- Gabashvili, I.S., Gregory, S.T., Valle, M., Grassucci, R., Worbs, M., Wahl, M.C., Dahlberg, A.E. and Frank, J. (2001) The polypeptide tunnel system in the ribosome and its gating in erythromycin resistance mutants of L4 and L22. *Mol. Cell*, 8, 181–188.
- Geballe, A.P., Spaete, R.R. and Mocarski, E.S. (1986) A *cis*-acting element within the 5' leader of a cytomegalovirus β transcript determines kinetic class. *Cell*, 46, 865–872.
- Gong, F., Ito, K., Nakamura, Y. and Yanofsky, C. (2001) The mechanism of tryptophan induction of tryptophanase operon expression: Tryptophan inhibits release factor-mediated cleavage of TnaC-peptidyl-tRNA^{Pro}. *Proc. Natl. Acad. Sci. USA*, 98, 8997–9001.
- Gong, F. and Yanofsky, C. (2002) Instruction of translating ribosome by nascent peptide. *Science*, 297, 1864–1867.
- Hanfrey, C., Elliott, K.A., Franceschetti, M., Mayer, M.J., Illingworth, C. and Michael, A.J. (2005) A dual upstream open reading frame-based autoregulatory circuit controlling polyamine-responsive translation. *J. Biol. Chem.*, 280, 39229–39237.
- Haraguchi, Y., Kadokura, Y., Nakamoto, M., Onouchi, H. and Naito, S. (2008) Ribosome stacking defines *CGS1* mRNA degradation sites during nascent peptide-mediated translation arrest. *Plant Cell Physiol.*, 49, 314–323.

- Hayashi, N., Sasaki, S., Takahashi, H., Yamashita, Y., Naito, S. and Onouchi, H. (2017) Identification of *Arabidopsis thaliana* upstream open reading frames encoding peptide sequences that cause ribosomal arrest. *Nucleic Acids Res.*, 45, 8844–8858.
- Hayden, C.A. and Jorgensen, R.A. (2007) Identification of novel conserved peptide uORF homology groups in *Arabidopsis* and rice reveals ancient eukaryotic origin of select groups and preferential association with transcription factor-encoding genes. *BMC Biol.*, 5, 32.
- Heiman, M., Kulicke, R., Fenster, R.J., Greengard, P. and Heintz, N. (2014) Cell type-specific mRNA purification by translating ribosome affinity purification (TRAP). *Nat Protoc.*, 9, 1282–1291.
- Hill, J.R. and Morris, D.R. (1992) Cell-specific translation of S-adenosylmethionine decarboxylase mRNA. Regulation by the 5' transcript leader. *J. Biol. Chem.*, 267, 21886–21893.
- Hinnebush, A.G., Ivanov, I.P. and Sonenberg, N. (2016) Translational control by 5'-untranslated regions of eukaryotic mRNAs. *Science*, 352, 1413–1416.
- Ho, S.N., Hunt, H.D., Horton, R.M., Pullen, J.K. and Pease, L.R. (1989) Site-directed mutagenesis by overlap extension using the polymerase chain reaction. *Gene*, 77, 51–59.
- Horiguchi, G., Mollá-Morales, A., Pérez-Pérez, J.M., Kojima, K., Robles, P., Ponce, M.R., Micol, J.L. and Tsukaya, H. (2011) Differential contributions of ribosomal protein genes to *Arabidopsis thaliana* leaf development. *Plant J.*, 65, 724–736.
- Horiguchi, G., van Lijsebettens, M., Candela, H., Micol, J.L. and Tsukaya, H. (2012) Ribosomes and translation in plant developmental control. *Plant Sci.*, 191–192, 24–34.
- Hou, C.Y., Lee, W.C., Chou, H.C., Chen, A.P., Chou, S.J. and Chen, H.M. (2016) Global Analysis of Truncated RNA Ends Reveals New Insights into Ribosome Stalling in Plants. *Plant Cell*, 28, 2398–2416.
- Hsu, P.Y., Calviello, L., Wu, H.Y.L., Li, F.W., Rothfels, C.J., Ohler, U. and Benfey, P.N. (2016) Super-resolution ribosome profiling reveals unannotated translation events in *Arabidopsis*. *Proc. Natl. Acad. Sci. USA*, 113, E7126–E7135.
- Hummel, M., Dobrenel, T., Cordewener, J.J.H.G., Davanture, M., Meyer, C., Smeekens, S.J.C.M., Bailey-Serres, J., America, T.A.H.P. and Hanson, J. (2015) Proteomic LC-MS analysis of *Arabidopsis* cytosolic ribosomes: Identification of ribosomal protein paralogs and re-annotation of the ribosomal protein genes. *J. Proteomics*, 128, 436–449.

- Inada, T., Winstall, E., Tarun, S.Z.J., Yates, J.R., Schieltz, D. and Sachs, A.B. (2002) One-step affinity purification of the yeast ribosome and its associated proteins and mRNAs. *RNA*, 8, 948–958.
- Ingolia, N.T., Ghaemmaghami, S., Newman, J.R. and Weissman, J.S. (2009) Genome-wide analysis in vivo of translation with nucleotide resolution using ribosome profiling. *Science*, 324, 218–223.
- International Wheat Genome Sequencing Consortium (2018) Shifting the limits in wheat research and breeding using a fully annotated reference genome. *Science*, 361, eaar7191.
- Ishii, E., Chiba, S., Hashimoto, N., Kojima, S., Homma, M., Ito, K., Akiyama, Y. and Mori, H. (2015) Nascent chain-monitored remodeling of the Sec machinery for salinity adaptation of marine bacteria. *Proc. Natl. Acad. Sci. USA*, 112, E5513–22.
- Ito, T., Kim, G.T. and Shinozaki, K. (2000) Disruption of an *Arabidopsis* cytoplasmic ribosomal protein S13-homologous gene by transposon-mediated mutagenesis causes aberrant growth and development. *Plant J.*, 22, 257–264.
- Ito, K. and Chiba, S. (2013) Arrest peptides: *cis*-acting modulators of translation. *Annu. Rev. Biochem.*, 82, 171–202.
- Janzen, D.M., Frolova, L. and Geballe, A.P. (2002) Inhibition of translation termination mediated by an interaction of eukaryotic release factor 1 with a nascent peptidyl-tRNA. *Mol. Cell. Biol.*, 22, 8562–8570.
- Jin, H., Kelley, A.C., Loakes, D. and Ramakrishnan, V. (2010) Structure of the 70S ribosome bound to release factor 2 and a substrate analog provides insights into catalysis of peptide release. *Proc. Natl. Acad. Sci. USA*, 107, 8593–8598.
- Joshi, C.O., Zhou, H., Huang, X. and Chiang, V.L. (1997) Context sequences of translation initiation codon in plants. *Plant Mol. Biol.*, 35, 993–1001.
- Juntawong, P., Girke, T., Bazin, J. and Bailey-Serrers, J. (2013) Translational dynamics revealed by genome-wide profiling of ribosome footprints in *Arabidopsis*. *Proc. Natl. Acad. Sci. USA*, 111, E203–E212.
- Kanda, S., Yanagitani, K., Yokota, Y., Esaki, Y. and Kohno, K. (2016) Autonomous translational pausing is required for *XBP1u* mRNA recruitment to the ER via the SRP pathway. *Proc. Natl. Acad. Sci. USA*, 113, E5886–E5895.

- Komili, S., Farny, N.G., Roth, F.P. and Silver, P.A. (2007) Functional specificity among ribosomal proteins regulates gene expression. *Cell*, 131, 557–571.
- Kosolapov, A. and Deutsch, C. (2009) Tertiary interactions within the ribosomal exit tunnel. *Nat. Struct. Mol. Biol.*, 16, 405–411.
- Kozak, M. (1986) Point mutations define a sequence flanking the AUG initiator codon that modulates translation by eukaryotic ribosomes. *Cell*, 44, 283–292.
- Kozak, M. (1987) Effects of intercistronic length on the efficiency of reinitiation by eukaryotic ribosomes. *Mol. Cell. Biol.*, 7, 3438–3445.
- Kozak, M. (1999) Initiation of translation in prokaryotes and eukaryotes. *Gene*, 234, 187–208.
- Kozak, M. (2002) Pushing the limits of the scanning mechanism of initiation of translation. *Gene*, 299, 1–34.
- Kurian, L., Palanimurugan, R., Gödderz, D. and Dohmen, R.J. (2011) Polyamine sensing by nascent ornithine decarboxylase antizyme stimulates decoding of its mRNA. *Nature*, 477, 490–494.
- Law, G.L., Raney, A., Heusner, C. and Morris, D.R. (2001) Polyamine regulation of ribosome pausing at the upstream open reading frame of S-adenosylmethionine decarboxylase. *J. Biol. Chem.* 276, 38036–38043.
- Lawrence, M.G., Lindahl, L. and Zengel, J.M. (2008) Effects on translation pausing of alterations in protein and RNA components of the ribosome exit tunnel. *J. Bacteriol.*, 190, 5862–5869.
- Lawrence, M.G., Shamsuzzaman, M., Kondopaka, M., Pascual, C., Zengel, J.M. and Lindahl, L. (2016) The extended loops of ribosomal proteins uL4 and uL22 of *Escherichia coli* contribute to ribosome assembly and protein translation. *Nucleic Acids Res.*, 44, 5798–5810.
- Li, G.W., Oh, E. and Weissman, J.S. (2012) The anti-Shine-Dalgarno sequence drives translational pausing and codon choice in bacteria. *Nature*, 484, 538–541.
- van Lijsebettens, M., Vanderhaeghen, R., De Block, M., Bauw, G., Villarroel, R. and van Montagu, M. (1994) An S18 ribosomal protein gene copy at the Arabidopsis *PFL* locus affects plant development by its specific expression in meristems. *EMBO J.*, 13, 3378–3388.
- Lu, J. and Deutsch, C. (2008) Electrostatics in the ribosomal tunnel modulate chain elongation rates. *J. Mol. Biol.*, 384, 73–86.
- Malkin, L.I. and Rich, A. (1967) Partial resistance of nascent polypeptide chains to proteolytic digestion due to ribosomal shielding. *J. Mol. Biol.*, 26, 329–346.

- Matheisl, S., Berninghausen, O., Becker, T. and Beckmann, R. (2015) Structure of a human translation termination complex. *Nucleic Acids Res.*, 43, 8615–8626.
- McIntosh, K.B. and Warner, J.R. (2007) Yeast ribosomes: variety is the spice of life. *Cell*, 131, 450–451.
- Melnikov, S., Ben-Shem, A., Garreau de Loubresse, N., Jenner, L., Yusupova, G. and Yusupov, M. (2012) One core, two shells: bacterial and eukaryotic ribosomes. *Nat. Struct. Mol. Biol.*, 19, 560–567.
- van Minnebruggen, A., Neyt, P., De Groeve, S., Coussens, G., Ponce, M.R., Micol, J.L. and van Lijsebettens, M. (2010) The *ang3* mutation identified the ribosomal protein gene *RPL5B* with a role in cell expansion during organ growth. *Physiol. Plant.*, 138, 91–101.
- Mora, L., Zavialov, A., Ehrenberg, M. and Buckingham, R.H. (2003) Stop codon recognition and interactions with peptide release factor RF3 of truncated and chimeric RF1 and RF2 from *Escherichia coli*. *Mol. Microbiol.*, 50, 1467–76.
- Morgan, D.G., Ménétret, J.F., Radermacher, M., Neuhof, A., Akey, I.V., Rapoport, T.A. and Akey, C.W. (2000) A comparison of the yeast and rabbit 80 S ribosome reveals the topology of the nascent chain exit tunnel, inter-subunit bridges and mammalian rRNA expansion segments. *J. Mol. Biol.*, 301, 301–321.
- Mori, H., Sakashita, S., Itom J., Ishii, E. and Akiyama, Y. (2018) Identification and characterization of a translation arrest motif in VemP by systematic mutational analysis. *J. Biol. Chem.*, 293, 2915–2926.
- Murota, K., Hagiwara-Komoda, Y., Komoda, K., Onouchi, H., Ishikawa, M. and Naito, S. (2011) Arabidopsis cell-free extract, ACE, a new in vitro translation system derived from Arabidopsis callus cultures. *Plant Cell Physiol.*, 52, 1443–1453.
- Murota, K., Hagiwara-Komoda, Y., Komoda, K., Onouchi, H., Ishikawa, M. and Naito, S. (2012) Corrigendum: Arabidopsis cell-free extract, ACE, a new in vitro translation system derived from Arabidopsis callus cultures. *Plant Cell Physiol.*, 53, 602.
- Muto, H., Nakatogawa, H. and Ito, K. (2006) Genetically encoded but nonpolypeptide proyl-tRNA functions in the A site for SecM-mediated ribosomal stall. *Mol. Cell*, 22, 545–552.

- Nakagawa, T., Kurose, T., Hino, T., Tanaka, K., Kawamukai, M., Niwa, Y., Toyooka, K., Matsuoka, K., Jinbo, T. and Kimura, T. (2007) Development of series of gateway binary vectors, pGWBs, for realizing efficient construction of fusion genes for plant transformation. *J. Biosci. Bioeng.*, 104, 34–41.
- Nakatogawa, H and Ito, K. (2001) Secretion monitor, SecM, undergoes self-translation arrest in the cytosol. *Mol. Cell*, 7, 185–192.
- Nakatogawa, H. and Ito, K. (2002) The ribosomal exit tunnel functions as a discriminating gate. *Cell*, 108, 629–636.
- Nilsson, O.B., Hedman, R., Marino, J., Wickles, S., Bischoff, L., Johansson, M., Müller-Lucks, A., Trovato, F., Puglisi, J.D., O'Brien, E.P., Beckmann, R. and von Heijne, G. (2015) Cotranslational Protein Folding inside the Ribosome Exit Tunnel. *Cell Rep.*, 12, 1533–1540.
- Nishimura, T., Wada, T., Yamamoto, K.T. and Okada, K. (2005) The *Arabidopsis* STV1 protein, responsible for translation reinitiation, is required for auxin-mediated gynoecium patterning. *Plant Cell*, 17, 2940–2953.
- Nissen, P., Hansen, J., Ban, N., Moore, P.B. and Steitz, T.A. (2000) The structural basis of ribosome activity in peptide bond synthesis. *Science*, 289, 920–930.
- Nyikó, T., Sonkoly, B., Mérai, Z., Benkovics, A.H. and Silhavy, D. (2009) Plant upstream ORFs can trigger nonsense-mediated mRNA decay in a size-dependent manner. *Plant Mol. Biol.*, 71, 367–378.
- Ohbayashi, I., Lin, C.Y., Shinohara, N., Matsumura, Y., Machida, Y., Horiguchi, G., Tsukaya, H. and Sugiyama, M. (2017) Evidence for a Role of ANAC082 as a Ribosomal Stress Response Mediator Leading to Growth Defects and Developmental Alterations in *Arabidopsis*. *Plant Cell*, 29, 2644–2660.
- Oliver, E.R., Saunders, T.L., Tarlé, S.A. and Glaser, T. (2004) Ribosomal protein L24 defect in Belly spot and tail (*Bst*), a mouse *Minute*. *Development*, 131, 3907–3920.
- Ominato, K., Akita, H., Suzuki, A., Kijima, F., Yoshino, T., Yoshino, M., Chiba, Y., Onouchi, H. and Naito, S. (2002) Identification of a short highly conserved amino acid sequence as the functional region required for posttranscriptional autoregulation of the cystathionine γ -synthase gene in *Arabidopsis*. *J. Biol. Chem.*, 277, 36380–36386.

- Onouchi, H., Nagami, Y., Haraguchi, Y., Nakamoto, M., Nishimura, Y., Sakurai, R., Nagao, N., Kawasaki, D., Kadokura, Y. and Naito, S. (2005) Nascent peptide-mediated translation elongation arrest coupled with mRNA degradation in the *CGS1* gene of *Arabidopsis*. *Genes Dev.*, 19, 1799–1810.
- Onoue, N., Yamashita, Y., Nagao, N., Goto, D.B., Onouchi, H. and Naito, S. (2011) S-Adenosyl-L-methionine induces compaction of nascent peptide chain inside the ribosomal exit tunnel upon translation arrest in the *Arabidopsis CGS1* gene. *J. Biol. Chem.*, 286, 14903–14912.
- Peisker, K., Braun, D., Wöflle, T., Hentschel, J., Fünfschilling, U., Fischer, G., Sickmann, A. and Rospert, S. (2008) Ribosome-associated complex binds to ribosomes in close proximity of Rpl31 at the exit of the polypeptide tunnel in yeast. *Mol. Biol. Cell*, 19, 5279–5288.
- Pillet, B., García-Gómez, J.J., Pausch, P., Falquet, L., Bange, G., de la Cruz, J. and Kressler, D. (2015) The dedicated chaperone Acl4 escorts ribosomal protein Rpl4 to its nuclear Pre-60S assembly site. *PLoS Genet.*, 11, e1005565.
- Pinon, V., Etchells, J.P., Rossignol, P., Collier, S.A., Arroyo, J.M., Martienssen, R.A. and Byrne, M.E. (2008) Three *PIGGYBACK* genes that specifically influence leaf patterning encode ribosomal proteins. *Development*, 135, 1315–1324.
- Plotkin, J.B. and Kudla, G. (2011) Synonymous but not the same: the causes and consequences of codon bias. *Nat. Rev. Genet.*, 12, 32–42.
- Pogulis, R.J., Vallejo, A.N. and Pease, L.R. (1996) *In vitro* recombination and mutagenesis by overlap extension PCR. *Methods Mol. Biol.*, 57, 167–176.
- Pound, M.P., French, A.P., Atkinson, J.A., Wells, D.M., Bennett, M.J. and Pridmore, T. (2013) RootNav: navigating images of complex root architectures. *Plant Physiol.*, 162, 1802–1814.
- Ramu, H., Mankin, A. and Vázquez-Laslop, N. (2009) Programmed drug-dependent ribosome stalling. *Mol. Microbiol.*, 71, 811–824.
- Ramu, H., Vázquez-Laslop, N., Klepacki, D., Dai, Q., Piccirilli, J., Micura, R. and Mankin, A.S. (2011) Nascent peptide in the ribosome exit tunnel affects functional properties of the A-site of the peptidyl transferase center. *Mol. Cell*, 41, 321–330.
- Raney, A., Law, G.L., Mize, G.J. and Morris, D.R. (2002) Regulated translation termination at the upstream open reading frame in S-adenosylmethionine decarboxylase mRNA. *J. Biol. Chem.*, 277, 5988–5994.

- Revenkova, E., Masson, J., Koncz, C., Afsar, K., Jakovleva, L. and Paszkowski, J. (1999) Involvement of *Arabidopsis thaliana* ribosomal protein S27 in mRNA degradation triggered by genotoxic stress. *EMBO J.*, 18, 490–499.
- Rosado, A., Li, R., van de Ven, W., Hsu, E. and Raikhel, N.V. (2012) *Arabidopsis* ribosomal proteins control developmental programs through translational regulation of auxin response factors. *Proc. Natl. Acad. Sci. USA*, 109, 19537–19544.
- Rosado, A., Sohn, E.J., Drakakaki, G., Pan, S., Swidergal, A., Xiong, Y., Kang, B.H., Bressan, R.A. and Raikhel, N.V. (2010) Auxin-mediated ribosomal biogenesis regulates vacuolar trafficking in *Arabidopsis*. *Plant Cell*, 22, 143–158.
- Ruan, H., Shantz, L.M., Pegg, A.E. and Morris, D.R. (1996) The upstream open reading frame of the mRNA encoding *S*-adenosylmethionine decarboxylase is a polyamine-responsive translational control element. *J. Biol. Chem.*, 47, 29576–29582.
- Sato, N.S., Hirabayashi, N., Agmon, I., Yonath, A. and Suzuki, T. (2006) Comprehensive genetic selection revealed essential bases in the peptidyl-transferase center. *Proc. Natl. Acad. Sci. USA*, 103, 15386–15391.
- Schleiss, M.R., Degnin, C.R. and Geballe, A.P. (1991) Translational control of human cytomegalovirus gp48 expression. *J. Virol.*, 65, 6782–6789.
- Schmeing, T.M., Huang, K.S., Kitchen, D.E., Strobel, S.A. and Steitz, T.A. (2005a) Structural insights into the roles of water and the 2' hydroxyl of the P site tRNA in the peptidyl transferase reaction. *Mol. Cell*, 20, 437–448.
- Schmeing, T.M., Huang, K.S., Strobel, S.A. and Steitz, T.A. (2005b) An induced-fit mechanism to promote peptide bond formation and exclude hydrolysis of peptidyl-tRNA. *Nature*, 438, 520–524.
- Shanmuganathan, V., Schiller, N., Magoulopoulou, A., Cheng, J., Braunger, K., Cymer, F., Berninghausen, O., Beatrix, B., Kohno, K., von Heijne, G. and Beckmann, R. (2019) Structural and mutational analysis of the ribosome-arresting human XBP1u. *eLife*, 8, e46267.
- Sievers, A., Beringer, M., Rodnina, M.V. and Wolfenden, R. (2004) The ribosome as an entropy trap. *Proc. Natl. Acad. Sci. USA*, 101, 7897–7901.
- Simonović, M. and Steitz, T.A. (2009) A structural view on the mechanism of the ribosome-catalyzed peptide bond formation. *Biochim Biophys Acta.*, 1789, 612–623.

- Skinner, R., Cundliffe, E. and Schmidt, F.J. (1983) Site of action of a ribosomal RNA methylase responsible for resistance to erythromycin and other antibiotics. *J. Biol. Chem.*, 258, 12702–12706.
- Slavov, N., Semrau, S., Airoidi, E., Budnik, B. and van Oudenaarden, A. (2015) Differential Stoichiometry among Core Ribosomal Proteins. *Cell Rep.*, 13, 865–873.
- Sohmen, D., Chiba, S., Shimokawa-Chiba, N., Innis, C.A., Berninghausen, O., Beckmann, R., Ito, K. and Wilson, D.N. (2015) Structure of the *Bacillus subtilis* 70S ribosome reveals the basis for species-specific stalling. *Nat. Commun.*, 6, 6941.
- Sørensen, M.A., Kurland, C.G. and Pedersen, S. (1989) Codon usage determines translation rate in *Escherichia coli*. *J. Mol. Biol.*, 207, 365–377.
- Souret, F.F., Kastenmayer, J.P. and Green, P.J. (2004) AtXRN4 Degrades mRNA in *Arabidopsis* and Its Substrates Include Selected miRNA Targets. *Mol. Cell*, 15, 173–183.
- Su, T., Cheng, J., Sohmen, D., Hedman, R., Berninghausen, O., von Heijne, G., Wilson, D.N. and Beckmann, R. (2017) The force-sensing peptide VemP employs extreme compaction and secondary structure formation to induce ribosomal stalling. *eLife*, 6, e25642.
- Spevak, C.C., Ivanov, I.P. and Sachs, M.S. (2010) Sequence requirements for ribosome stalling by the arginine attenuator peptide. *J. Biol. Chem.*, 285, 40933–40942.
- Stelter, P., Huber, F.M., Kunze, R., Flemming, D., Hoelz, A. and Hurt, E. (2015) Coordinated ribosomal L4 protein assembly into the pre-ribosome is regulated by its eukaryote-specific extension. *Mol. Cell*, 58, 854–862.
- Sugihara, Y., Honda, H., Iida, T., Morinaga, T., Hino, S., Okajima, T., Matsuda, T. and Nadano, D. (2010) Proteomic analysis of rodent ribosomes revealed heterogeneity including ribosomal proteins L10-like, L22-like 1, and L39-like. *J. Proteome Res.*, 9, 1351–1366.
- Sung, M.K., Porras-Yakushi, T.R., Reitsma, J.M., Huber, F.M., Sweredoski, M.J., Hoelz, A., Hess, S. and Deshaies, R.J. (2016) A conserved quality-control pathway that mediates degradation of unassembled ribosomal proteins. *eLife*, 5, e19105.
- Suzuki, A., Shirata, Y., Ishida, H., Chiba, Y., Onouchi, H. and Naito, S. (2001) The first exon coding region of cystathionine γ -synthase gene is necessary and sufficient for downregulation of its own mRNA accumulation in transgenic *Arabidopsis thaliana*. *Plant Cell Physiol.*, 42, 1174–1180.

- Szakonyi, D., Byrne, M.E. (2011) Ribosomal protein L27a is required for growth and patterning in *Arabidopsis thaliana*. *Plant J*, 65, 269–281.
- Takahashi, H., Takahashi, A., Naito, S. and Onouchi, H. (2012) BAIUCAS: a novel BLAST-based algorithm for the identification of upstream open reading frames with conserved amino acid sequences and its application to the *Arabidopsis thaliana* genome. *Bioinformatics*, 28, 2231–2241.
- Takamatsu, S., Ohashi, Y., Onoue, N., Tajima, Y., Imamichi, T., Yonezawa, S., Morimoto, K., Onouchi, H., Yamashita, Y. and Naito, S. (2019) Reverse genetics-based biochemical studies of the ribosomal exit tunnel constriction region in eukaryotic ribosome stalling: spatial allocation of the regulatory nascent peptide at the constriction. *Nucleic Acids Res.*, *in press* (Doi: 10.1093/nar/gkz1190).
- Takano, J., Wada, M., Ludewig, U., Schaaf, G., von Wirén, N. and Fujiwara, T. (2006) The *Arabidopsis* major intrinsic protein NIP5;1 is essential for efficient boron uptake and plant development under boron limitation. *Plant Cell*, 18, 1498–1509.
- Tanaka, M., Sotta, N., Yamazumi, Y., Yamashita, Y., Miwa, K., Murota, K., Chiba, Y., Hirai, M.Y., Akiyama, T., Onouchi, H., Naito, S. and Fujiwara, T. (2016) The minimum open reading frame, AUG-stop, induces boron-dependent ribosome stalling and mRNA degradation. *Plant Cell*, 28, 2830–2849.
- Tholstrup, J., Oddershede, L.B. and Sørensen, M.A. (2012) mRNA pseudoknot structures can act as ribosomal roadblocks. *Nucleic Acids Res.*, 40, 303–313.
- Thompson, J., Kim, D.F., O'Connor, M., Lieberman, K.R., Bayfield, M.A., Gregory, S.T., Green, R., Noller, H.F. and Dahlberg, A.E. (2001) Analysis of mutations at residues A2451 and G2447 of 23S rRNA in the peptidyltransferase active site of the 50S ribosomal subunit. *Proc. Natl. Acad. Sci. USA*, 98, 9002–9007.
- Tu, D., Blaha, G., Moore, P.B. and Steitz, T.A. (2005) Structures of MLSBK antibiotics bound to mutated large ribosomal subunits provide a structural explanation for resistance. *Cell*, 121, 257–270.
- Tzafrir, I., Pena-Muralla, R., Dickerman, A., Berg, M., Rogers, R., Hutchens, S., Sweeney, T.C., McElver, J., Aux, G., Pattonm D. and Meinke, D. (2004) Identification of genes required for embryo development in *Arabidopsis*. *Plant Physiol.*, 135, 1206–1220.

- Uchiyama-Kadokura, N., Murakami, K., Takemoto, M., Koyanagi, N., Murota, K., Naito, S. and Onouchi, H. (2014) Polyamine-responsive ribosomal arrest at the stop codon of an upstream open reading frame of the *AdoMetDC1* gene triggers nonsense-mediated mRNA decay in *Arabidopsis thaliana*. *Plant Cell Physiol.*, 55, 1556–1567.
- Vaughn, J.N., Ellingson, S.R., Mignone, F. and Arim, A. (2012) Known and novel post-transcriptional regulatory sequences are conserved across plant families. *RNA*, 18, 368–384.
- Vázquez-Laslop, N., Thum, C. and Mankin, A.S. (2008) Molecular mechanism of drug-dependent ribosome stalling. *Mol. Cell*, 30, 190–202.
- Vázquez-Laslop, N., Ramu, H., Klepacki, D., Kannan, K. and Mankin, A.S. (2010) The key function of a conserved and modified rRNA residue in the ribosomal response to the nascent peptide. *EMBO J.*, 29, 3108–3117.
- Wallsgrave, R.M., Lea, P.J. and Mifflin, B.J. (1983) Intracellular localization of aspartate kinase and the enzymes of threonine and methionine biosynthesis in green leaves. *Plant Physiol.*, 71, 780–784.
- Walter, P. and Ron, D. (2011) The unfolded protein response: from stress pathway to homeostatic regulation. *Science*, 334, 1081–1086.
- Wang, Z. and Sachs, M.S. (1997) Ribosome stalling is responsible for arginine-specific translational attenuation in *Neurospora crassa*. *Mol. Cell. Biol.*, 17, 4904–4913.
- Wei, J., Wu, C. and Sachs, M.S. (2012) The arginine attenuator peptide interferes with the ribosome peptidyl transferase center. *Mol. Cell. Biol.*, 32, 2396–2406.
- Weijers, D., Franke-van Dijk, M., Vencken, R.J., Quint, A., Hooykaas, P. and Offringa, R. (2001) An *Arabidopsis* Minute-like phenotype caused by a semi-dominant mutation in a *RIBOSOMAL PROTEIN S5* gene. *Development*, 128, 4289–4299.
- Wekselman, I., Zimmerman, E., Davidovich, C., Belousoff, M., Matzov, D., Krupkin, M., Rozenberg, H., Bashan, A., Friedlander, G., Kjeldgaard, J., Ingmer, H., Lindahl, L., Zengel, J.M. and Yonath, A. (2017) The Ribosomal Protein uL22 Modulates the Shape of the Protein Exit Tunnel. *Structure*, 25, 1233–1241.
- Wethmar, K. (2014) The regulatory potential of upstream open reading frames in eukaryotic gene expression. *Wiley Interdiscip. Rev. RNA*, 5, 765–778.

- Williams, M.E. and Sussex, I.M. (1995) Developmental regulation of ribosomal protein L16 genes in *Arabidopsis thaliana*. *Plant J.*, 8, 65–76.
- Wilson, D.N. and Cate, J.H.D. (2012) The structure and function of the eukaryotic ribosome. *Cold Spring Harb. Perspect. Biol.*, 4, a011536.
- Wilson, D.N., Arenz, S. and Beckmann, R. (2016) Translation regulation via nascent polypeptide-mediated ribosome stalling. *Curr. Opin. Struct. Biol.*, 37, 123–133.
- Wolin, S.L. and Walter, P. (1988) Ribosome pausing and stacking during translation of a eukaryotic mRNA. *EMBO J.*, 7, 3559–69.
- Wool, I.G., Chan, Y.L. and Glück, A. (1995) Structure and evolution of mammalian ribosomal proteins. *Biochem. Cell Biol.*, 73, 933–947.
- Wu, C., Wei, J., Lin, P.J., Tu, L., Deutsch, C., Johnson, A.E. and Sachs, M.S. (2012) Arginine changes the conformation of the arginine attenuator peptide relative to the ribosome tunnel. *J. Mol. Biol.*, 416, 518–533.
- Xue, S. and Barna, M. (2012) Specialized ribosomes: a new frontier in gene regulation and organismal biology. *Nat. Rev. Mol. Cell Biol.*, 13, 355–369.
- Xue, S. and Barna, M. (2015) *Cis*-regulatory RNA elements that regulate specialized ribosome activity. *RNA Biol.*, 12, 1083–1087.
- Yamashita, Y., Kadokura, Y., Sotta, N., Fujiwara, T., Takigawa, I., Satake, A., Onouchi, H. and Naito, S. (2014) Ribosomes in a stacked array: elucidation of the step in translation elongation at which they are stalled during *S*-adenosyl-L-methionine-induced translation arrest of *CGS1* mRNA. *J. Biol. Chem.*, 289, 12693–12704.
- Yamashita, Y., Takamatsu, S., Glasbrenner, M., Becker, T., Naito, S. and Beckmann, R. (2017) Sucrose sensing through nascent peptide-mediated ribosome stalling at the stop codon of *Arabidopsis bZIP11* uORF2. *FEBS Lett.*, 591, 1266–1277.
- Yanagitani, K., Kimata, Y., Kadokura, H. and Kohno, K. (2011) Translational pausing ensures membrane targeting and cytoplasmic splicing of *XBP1u* mRNA. *Science*, 331, 586–589.
- Yang, Z., Iizuka, R. and Funatsu, T. (2015) Nascent SecM chain outside the ribosome reinforces translation arrest. *PLoS One*, 10, e0122017.
- Yao, Y., Ling, Q., Wang, H. and Huang, H. (2008) Ribosomal proteins promote leaf adaxial identity. *Development*, 135, 1325–1334.

- Yap, M.N. and Bernstein, H.D. (2009) The plasticity of a translation arrest motif yields insights into nascent polypeptide recognition inside the ribosome tunnel. *Mol. Cell*, 34, 201–211.
- Zaman, S., Fitzpatrick, M., Lindahl, L. and Zengel, J. (2007) Novel mutations in ribosomal proteins L4 and L22 that confer erythromycin resistance in *Escherichia coli*. *Mol. Microbiol.*, 66, 1039–1050.
- Zanetti, M.E., Chang, I.F., Gong, F., Galbraith, D.W. and Bailey-Serres, J. (2005) Immunopurification of polyribosomal complexes of Arabidopsis for global analysis of gene expression. *Plant Physiol.*, 138, 624–635.
- Zavialov, A.V., Mora, L., Buckingham, R.H. and Ehrenberg, M. (2002) Release of peptide promoted by the GGQ motif of class 1 release factors regulates the GTPase activity of RF3. *Mol. Cell*, 10, 789–798.
- Zhang, J., Pan, X., Yan, K., Sun, S., Gao, N. and Sui, S.F. (2015) Mechanisms of ribosome stalling by SecM at multiple elongation steps. *eLife*, 4, e09684.
- Zhang, Y., Werling, U. and Edlmann, W. (2012) SLiCE: a novel bacterial cell extract-based DNA cloning method. *Nucleic Acids Res.*, 40, e55.
- Zhang, Z., Carriero, N. and Gerstein, M. (2004) Comparative analysis of processed pseudogenes in the mouse and human genomes. *Trends Genet.*, 20, 62–67.
- Zhao, D., Hamilton, J.P., Hardigan, M., Yin, D., He, T., Vaillancourt, B., Reynoso, M., Pauluzzi, G., Funkhouser, S., Cui, Y., Bailey-Serres, J., Jiang, J., Buell, C.R. and Jiang, N. (2017) Analysis of Ribosome-Associated mRNAs in Rice Reveals the Importance of Transcript Size and GC Content in Translation. *G3*, 7, 203–219.

Acknowledgements

I would firstly like to express my sincere gratitude to my supervisor Prof. Satoshi Naito for long-term encouragements and guidance throughout this project. His guidance helped me in all the time of research and writing of this thesis. I could not have imagined having a better advisor and mentor for my Ph.D. study.

I would also like to thank my thesis committee: Profs. Atsushi Kato, Yukako Chiba, and Yui Yamashita for critical reading of this thesis and insightful comments. I would also like to thank Prof. Hitoshi Onouchi for valuable advice during this project.

I am grateful to Dr. Tsuyoshi Nakagawa (Shimane University) for the pGWB10 vector and to Arabidopsis Biological Resource Center for Arabidopsis SALK_029203 seeds.

I would like to thank Ms. Saeko Yasokawa for technical assistance, and Ms. Maki Mori and Ms. Kazuko Harada for general assistance, and all the members of Naito laboratory, including members who have already graduated, for support and all the good times. In particular, I am grateful to Mr. Yubun Ohashi for initial contribution to this project, and to Drs. Noriyuki Onoue, Kyoko Morimoto, and Yoko Tajima for generation of transgenic Arabidopsis lines that I used.

I was a recipient of a Japan Society of the Promotion of Science (JSPS) Research Fellowship. This work was supported by Grant-in-Aid for JSPS Fellows to me (No. JP17J00982). I used the DNA Sequencing Facility of the Graduate School of Agriculture, Hokkaido University.

Last but not the least, I would like to thank my family, Mariko and Ami, for encouragements and support throughout my Ph.D. study and my life in general. Without them, this Ph.D. would not have been achievable.

List of publications

- [1] Yamashita, Y., Takamatsu, S., Glasbrenner, M., Becker, T., Naito, S. and Beckmann, R. (2017) Sucrose sensing through nascent peptide-mediated ribosome stalling at the stop codon of *Arabidopsis bZIP11* uORF2. *FEBS Lett.*, 591, 1266–1277.
- [2] Takamatsu, S., Ohashi, Y., Onoue, N., Tajima, Y., Imamichi, T., Yonezawa, S., Morimoto, K., Onouchi, H., Yamashita, Y. and Naito, S. (2019) Reverse genetics-based biochemical studies of the ribosomal exit tunnel constriction region in eukaryotic ribosome stalling: spatial allocation of the regulatory nascent peptide at the constriction. *Nucleic Acids Res.*, *in press* (Doi: 10.1093/nar/gkz1190).

Appendix to Doctoral Dissertation (学位論文別冊)

Publication on:

**Studies on the Eukaryotic Ribosomal Exit Tunnel Function
in Nascent Peptide-Mediated Ribosome Stalling**

新生ペプチド鎖が司るリボソーム停滞における
真核生物リボソーム出口トンネル機能の研究

Takamatsu *et al.*,

Reverse genetics-based biochemical studies of the
ribosomal exit tunnel constriction region in eukaryotic
ribosome stalling: spatial allocation of the regulatory
nascent peptide at the constriction.

Nucleic Acids Research, in press.

Doi: 10.1093/nar/gkz1190

Seidai Takamatsu

高松 世大

Graduate School of Life Science

Hokkaido University

March, 2020

Reverse genetics-based biochemical studies of the ribosomal exit tunnel constriction region in eukaryotic ribosome stalling: spatial allocation of the regulatory nascent peptide at the constriction

Seidai Takamatsu¹, Yubun Ohashi², Noriyuki Onoue¹, Yoko Tajima³, Tomoya Imamichi¹, Shinya Yonezawa¹, Kyoko Morimoto³, Hitoshi Onouchi^{2,3,4}, Yui Yamashita^{2,3,4,*} and Satoshi Naito^{1,3,4,*}

¹Division of Life Science, Graduate School of Life Science, Hokkaido University, Sapporo 060-0810, Japan, ²Frontiers in Biosciences, Graduate School of Agriculture, Hokkaido University, Sapporo 060-8589, Japan, ³Department of Applied Bioscience, Faculty of Agriculture, Hokkaido University, Sapporo 060-8589, Japan and ⁴Research Group of Applied Bioscience, Research Faculty of Agriculture, Hokkaido University, Sapporo 060-8589, Japan

Received October 14, 2019; Revised December 09, 2019; Editorial Decision December 11, 2019; Accepted December 12, 2019

ABSTRACT

A number of regulatory nascent peptides have been shown to regulate gene expression by causing programmed ribosome stalling during translation. Nascent peptide emerges from the ribosome through the exit tunnel, and one-third of the way along which β -loop structures of ribosomal proteins uL4 and uL22 protrude into the tunnel to form the constriction region. Structural studies have shown interactions between nascent peptides and the exit tunnel components including the constriction region. In eukaryotes, however, there is a lack of genetic studies for the involvement of the constriction region in ribosome stalling. Here, we established transgenic *Arabidopsis* lines that carry mutations in the β -loop structure of uL4. Translation analyses using a cell-free translation system derived from the transgenic *Arabidopsis* carrying the mutant ribosome showed that the uL4 mutations reduced the ribosome stalling of four eukaryotic stalling systems, including those for which stalled structures have been solved. Our data, which showed differential effects of the uL4 mutations depending on the stalling systems, explained the spatial allocations of the nascent peptides at the

constriction that were deduced by structural studies. Conversely, our data may predict allocation of the nascent peptide at the constriction of stalling systems for which structural studies are not done.

INTRODUCTION

During translation, new peptide bonds are formed at the peptidyltransferase center (PTC) in the ribosomal large subunit, and the growing peptide passes through the exit tunnel that penetrates the large subunit before emerging from the ribosome. However, some of the nascent peptides, or the regulatory nascent peptides, direct the ribosome to stall during translation. This nascent peptide-mediated ribosome stalling (NPMRS) occurs either autonomously or is facilitated by an effector molecule, at either elongation or termination of translation, and on either the main open reading frame (ORF) or an upstream ORF (uORF) (1), which is a small ORF present upstream of the main ORF of eukaryotic mRNAs.

The exit tunnel is ~ 100 Å long and holds 30–40 amino acid residues of the nascent peptide (2,3). Regulatory nascent peptides are usually 20–30 amino acids long and function while inside the exit tunnel. In both bacteria and eukaryotes, β -loop structures of two ribosomal proteins, uL4 and uL22 (4), which protrude into the exit tunnel, form a constriction region located 30–40 Å from the PTC (2,3).

*To whom correspondence should be addressed. Tel: +81 11 706 2800; Fax: +81 11 706 4932; Email: naito@abs.agr.hokudai.ac.jp
Correspondence may also be addressed to Yui Yamashita. Email: yuiyama@abs.agr.hokudai.ac.jp
Present addresses:

Yubun Ohashi, NOF Corp., Kawasaki 210-0865, Japan.

Noriyuki Onoue, NARO Institute of Fruit Tree and Tea Science, Higashi-Hiroshima 739-2494, Japan.

Yoko Tajima, Laboratory of Molecular Neuro-Oncology, The Rockefeller University, York Avenue, New York, NY 10065, USA.

Shinya Yonezawa, Department of Medical Innovations, Otsuka Pharmaceutical Co. Ltd., Tokushima 771-0192, Japan.

Kyoko Morimoto, Department of Plant Sciences, University of Oxford, South Parks Road, Oxford OX1 3RB, UK.

This region has been suggested to function as a discriminating gate by interacting with the nascent peptides (5).

In bacteria, forward and reverse genetics studies have revealed the importance of interactions between the nascent peptide and the constriction region in mediating NPmRS (5–9). This is supported by structural analyses of stalled ribosomes using cryo-electron microscopy (cryo-EM), which identified physical contacts of the nascent peptides with exit tunnel components, including the constriction region (10–13).

In eukaryotes, cryo-EM studies revealed physical contacts of the nascent peptides with the constriction region in stalled ribosomes of *Neurospora crassa arg-2* uORF, termed the arginine attenuator peptide (AAP) (the AAP system), and human cytomegalovirus (hCMV) *gp48* uORF (the hCMV system) (14–16). However, there is no genetic evidence showing the contribution of the constriction region to ribosome stalling.

In *Arabidopsis CGS1*, encoding cystathionine γ -synthase, the first committed enzyme of methionine biosynthesis, *S*-adenosyl-L-methionine (AdoMet), a direct metabolite of methionine, induces NPmRS during translation elongation at Ser-94 (the CGS1 system) (17–19). The functional amino acid sequence for the response to AdoMet is termed as MTO1 region (20–22). Studies using the wheat germ extract (WGE) *in vitro* translation system revealed that the nascent peptide adopts a compact conformation and 28S rRNA residues, including those near the constriction region, undergo conformation changes upon stalling (18). Notably, these rRNA residues are located at or near the rRNA residues for which structural studies have identified physical contacts with the nascent peptides in other stalling systems (14). This suggests involvement of the constriction region in the CGS1 system, but whether the conformation changes are the cause or result of stalling remains unknown.

Here, we conducted reverse genetics-based biochemical studies to determine the involvement of the constriction region in eukaryotic NPmRS. To this end, we constructed transgenic *Arabidopsis* lines carrying mutant uL4-containing ribosomes. We examined effects of the mutations on ribosome stalling using an *Arabidopsis* cell-free extract (ACE) *in vitro* translation system (23) prepared from transgenic lines carrying FLAG-tagged mutant uL4.

For the NPmRS systems to be tested, we selected five from divergent eukaryotes (Figure 1), of which four have their relevant amino acid residues >20 from the stalled residue, as in most NPmRS systems, and should cross over the constriction region. These include the CGS1, hCMV (27–29) and AAP (24–26) systems mentioned above, and *Arabidopsis AdoMet decarboxylase 1 (AtAMD1)* S-uORF (the AtAMD1 system) (30,31). We also tested another NPmRS system, mammalian *AdoMet decarboxylase 1 (mAMD1)* uORF. This uORF, encoding six amino acids, MAGDIS (the MAGDIS system) (32,33), is the shortest among the NPmRS systems thus far identified and its nascent peptide is too short to reach the constriction region (Figure 1). Lastly, we tested the shortest possible uORF, AUG-stop, of *AtNIP5;1*. AUG-stop causes prolonged ribosome stalling in response to boric acid (the AUG-Stop system) (34). This minimum uORF codes for only one amino

acid, methionine, and is not actually an NPmRS, but was included as a negative control.

We present here biochemical evidence that the constriction region plays a crucial role in inducing NPmRS, in which nascent peptides cross over the constriction. The differential effects of the uL4 mutations explained the structural data for stalled ribosomes of the AAP and hCMV systems.

MATERIALS AND METHODS

Plant materials, transformation and growth conditions

Arabidopsis thaliana (L.) Heynh. ecotype Columbia (Col-0) was used as the wild-type plant line. A T-DNA insertion knockout mutant of *uL4D* (SALK_029203) (35) was obtained from the *Arabidopsis* Biological Resource Center (Ohio State University, Columbus, OH, USA) and is referred to as *uL4d(KO)* in this paper. Transformation of *Arabidopsis* plants was performed using the floral dip method (36) with *Agrobacterium tumefaciens* strain GV3101. Plant growth conditions were as described previously (37). T₁ transgenic plants were selected on Murashige and Skoog (MS) medium supplemented with 15 $\mu\text{g ml}^{-1}$ hygromycin. T₃ homozygous lines with single insertions of *uL4D promoter::uL4D(WT):FLAG* and its variants were established based on the segregation of hygromycin resistance.

For root observations, plants were grown on vertically placed half-strength MS medium containing 1% (w/v) sucrose, 0.5% (w/v) MES (pH 5.7) and 1.5% (w/v) gellan gum for 10 days in a growth chamber at 22°C under fluorescent light with a 16 h-light/8 h-dark cycle. Root length was measured using RootNav software (38). For leaf morphology analysis, plants were grown for 21 days as described previously (37) and one of the first pair of the true leaves was dissected. Leaf index (ratio of length to width of the leaf blade) was calculated using ImageJ software (National Institutes of Health, Bethesda, MD, USA).

Chemicals

AdoMet and spermidine were purchased from Sigma-Aldrich (St. Louis, MO, USA), and L-arginine was purchased from Wako Pure Chemicals (Osaka, Japan). Other chemicals were obtained as described previously (18, 23).

Construction of plasmids used for plant transformation

Plasmids pYTJ10, pYTJ1, pYTJ7 and pYTJ4 (Supplementary Table S1) carry *uL4D promoter::uL4D(WT):FLAG*, *uL4D promoter::uL4D(R77A):FLAG*, *uL4D promoter::uL4D(Δ TV):FLAG* and *uL4D promoter::uL4D(Δ loop):FLAG* DNA, respectively, in the pGWB10 T-DNA binary vector (39). To construct pYTJ10, the –1020 to –1 nt region (relative to the translation start site) of wild-type *uL4D* and the coding region were amplified by PCR from genomic DNA of Col-0 using the primers uL4Df and uL4Dr (Supplementary Table S2). The amplified fragment was subcloned into the pENTR/D-TOPO vector (Invitrogen, Carlsbad, CA, USA) using the TOPO cloning reaction. The cloned full-length *uL4D(WT)* DNA was subsequently recombined into the pGWB10 T-DNA

Amino acid residues from PTC when stalled	Constriction region		Stall system	Organism	Gene / ORF	Effector	Step
-50	-40	-30	-20	-10	-1		
...AGISSFTGDAGLSSRILRFPPNFVRQLSIKARRNCSNIGVAQIVAAKWS...	<u>MEPLVLSAKKLSLLTCKYIPP*</u>		CGS1	plant	<i>AtCGS1</i> / main	AdoMet	elongation
	<u>MNGRPSVFTSQDYLSDHLWRALNA*</u>		hCMV	virus	<i>gp48</i> / uORF	autonomous	termination
	<u>MAGDIS*</u>		AAP	fungi	<i>Nc arg-2</i> / uORF	L-arginine	termination
	<u>MAGDIS*</u>		AtAMD	plant	<i>AtAMD1</i> / uORF	polyamines	termination
	<u>MAGDIS*</u>		MAGDIS	mammal	<i>mAMD1</i> / uORF	polyamines	termination
	<u>M*</u>		AUG-Stop	plant	<i>AtNIP5;1</i> / uORF	boric acid	termination

Figure 1. The stalling systems analyzed in this study. For each system, the gene and ORF (main ORF or uORF) in which stalling occurs, effector molecule, and translation step at which stalling occurs (elongation or termination) are shown. Amino acid sequences relevant for stalling in CGS1 or those encoded by the uORFs are shown. Amino acid residues important for NPmRS (17,21, 24,26,28,29,32–34) are marked in red. For AtAMD1, functional amino acids are not reported, while importance of the amino acid sequence was shown by frame-shift mutation (31). The MTO1 (21) region of CGS1 is underlined with ambiguous amino acids in dotted underline. Amino acid residues are numbered from the stalled residue (–1, marked with a clover). Approximate position of the constriction region is shaded. Since the nascent peptide may form α -helix in the PTC-proximal region as reported in AAP and hCMV (14,16), residues that cross over the constriction region may be shifted to the left.

binary vector using the Gateway system (40). For the construction of *uL4D(R77A)*, *uL4D(Δ TV)* and *uL4D(Δ loop)* mutations, the overlap extension PCR method (41,42) was employed. The flanking primers, R77Af and R77Ar for the *uL4D(R77A)* mutation, dTVf and dTVr for the *uL4D(Δ TV)* mutation, and dLoopf and dLoopr for the *uL4D(Δ loop)* mutation, and the flanking primers uL4Fflankf and uL4Fflankr (Supplementary Table S2) were used. The mutated DNA fragment was introduced into the *uL4D(WT)* coding region of pYTJ10 to generate pYTJ1, pYTJ7 and pYTJ4 plasmids. For all constructs, the integrity of PCR-amplified regions was confirmed by sequence analysis.

Construction of plasmids used for stalling assay

Plasmid pST00 (Supplementary Table S1) carries the *M8:His:HA:DP75* sequence between the SP6 promoter and the 30-nt poly(A) in the pSP64 poly(A) vector (Promega, Madison, WI, USA). The DP75 linker was derived from the dipeptidyl-aminopeptidase B coding sequence (15,43). To construct pST00, the *His:HA:DP75* coding region was amplified by PCR from pYY105, which carries *T7::His:HA:DP75:uORF2(WT)* DNA in the pEX-A2 vector (43), using the primers DP75f and DP75r (Supplementary Table S2). The amplified fragment was digested with XbaI and BamHI and inserted between the XbaI and BamHI sites of pYK00, which harbors *M8:CGS1(WT)* DNA in the pSP64 poly(A) vector (18).

Plasmids pST55 and pST56 (Supplementary Table S1) carry *M8:His:HA:DP75:AAP(WT)* and *M8:His:HA:DP75:AAP(D12N)*, respectively, in the pSP64 poly(A) vector. To construct these plasmids, complementary oligonucleotides AAPf/AAPr or D12Nf/AAPr (Supplementary Table S2), encoding wild-type or mutated *N. crassa arg-2* (24), respectively, were annealed and filled-in using KOD-Plus-Neo DNA polymerase (Toyobo, Osaka, Japan). The amplified fragments were digested with EcoRV and BamHI and inserted between the EcoRV and BamHI sites of pST00.

Plasmids pTI5 and pTI6 (Supplementary Table S1) carry *M8:His:HA:3xFLAG:Myc:DP75:AAP(WT)* and

M8:His:HA:3xFLAG:Myc:DP75:AAP(D12N), respectively, in the pSP64 poly(A) vector. To introduce the *Myc* tag sequence between the *HA* tag and the DP75 linker in pST55 and pST56, *in vitro* mutagenesis was carried out by inverse PCR using the primers MycDP75f and HAMycr (Supplementary Table S2), followed by digestion of the plasmid DNA by DpnI (Toyobo). The amplified fragments were self-ligated using T4 DNA ligase (Wako Pure Chemicals) and T4 polynucleotide kinase (Toyobo). To construct pTI5 and pTI6, complementary oligonucleotides 3xFLAGf and 3xFLAGr (Supplementary Table S2) were annealed and filled-in by PCR, and the amplified fragments were ligated with the PCR-amplified fragment from the *Myc* tag-fused pST55 or pST56 using Mycf and HAR primers (Supplementary Table S2) by the SLiCE reaction (44).

Plasmids pST57 and pST58 (Supplementary Table S1) carry *M8:His:HA:DP75:hCMV(WT)* and *M8:His:HA:DP75:hCMV(P21A)*, respectively, in the pSP64 poly(A) vector. To construct these plasmids, complementary oligonucleotides hCMVf/hCMVr or hCMVf/P21Ar (Supplementary Table S2), encoding wild-type or mutated uORF2 of hCMV *gp48* (15,45), respectively, were annealed and filled-in by PCR. The amplified fragments were inserted into pST00 in the same way as for the construction of pST55.

Plasmids pST76 and pST77 (Supplementary Table S1) carry *M8:His:HA:DP75:S-uORF(WT)* and *M8:His:HA:DP75:S-uORF(fs)*, respectively, in the pSP64 poly(A) vector. To construct these plasmids, the coding region of the *AtAMD1* S-uORF was amplified from pNU14 or pNU15, which carries *GST:S-uORF(WT):RLUC* or *GST:S-uORF(fs):RLUC*, respectively, in the pSP64 poly(A) vector (31), using the primer sets SAMDC1f/SAMDC1r or SAMDC1fsf/SAMDC1fsr (Supplementary Table S2), respectively. The amplified fragments were inserted into pST00 in the same way as for the construction of pST55.

Plasmids pST116 and pST117 (Supplementary Table S1) carry *M8:His:HA:DP75:MAGDIS(WT)* and *M8:His:HA:DP75:MAGDIS(I5L)*, respectively, in the pSP64 poly(A) vector. To construct these plasmids, the *His:HA:DP75* tag sequence was amplified from pST00 using the primer sets DP75f/MAGDISr or DP75f/I5Lr

(Supplementary Table S2), respectively, and the amplified fragments were digested with XbaI and BamHI and inserted between the XbaI and BamHI sites of pST00.

Plasmids pST124 and pST125 (Supplementary Table S1) carry *M8:His:HA:3xFLAG:Myc:DP75:MAGDIS(WT)* and *M8:His:HA:3xFLAG:Myc:DP75:MAGDIS(I5L)*, respectively, in the pSP64 poly(A) vector. To construct these plasmids, the *His:HA:3xFLAG:Myc:DP75* tag sequence was amplified from pT15 using the primer sets DP75f/MAGDISr or DP75f/I5Lr (Supplementary Table S2), respectively, and the amplified fragments were inserted into pST00 in the same way as for the construction of pST55. For all constructs, the integrity of PCR-amplified regions was confirmed by sequence analysis.

In the Results section, *M8:His:HA* and *M8:His:HA:3xFLAG:Myc* sequences are referred to as *TagI* and *TagII*, respectively.

Construction of plasmids used for reporter assay

Plasmids pST122 and pST123 (Supplementary Table S1) carry *gp48 5'-UTR(WT):LUC* and *gp48 5'-UTR(P21A):LUC*, respectively, in the pSP64 poly(A) vector. To construct these plasmids, complementary oligonucleotides hCMVf2/hCMVr2 or hCMVf2/P21Ar2 (Supplementary Table S2), which correspond to the wild-type or mutated 5'-UTR of the hCMV *gp48* sequence (45,46), respectively, were annealed and filled-in by PCR. The amplified fragments were digested with HindIII and inserted at the HindIII site of pMI21, which carries *CGS1(WT):LUC* in the pSP64 poly(A) vector (22).

Plasmids pST120 and pST121 (Supplementary Table S1) carry *AtAMD1 5'-UTR(WT):LUC* and *AtAMD1 5'-UTR(fs):LUC*, respectively, in the pSP64 poly(A) vector. To construct these plasmids, the 5'-UTR of *AtAMD1* was amplified from pSY209 or pSY214, which carry *S-uORF(WT):RLUC* or *S-uORF(fs):RLUC*, respectively, in the pSP64 poly(A) vector (31) using the primers SAMDC1f2 and SAMDC1r2 (Supplementary Table S2). The amplified fragments were digested with XbaI and NcoI and inserted between the XbaI and NcoI sites of pMI21.

Plasmids pST118 and pST119 (Supplementary Table S1) carry *mAMD1 5'-UTR(WT):LUC* and *mAMD1 5'-UTR(I5L):LUC*, respectively, in the pSP64 poly(A) vector. To construct these plasmids, complementary oligonucleotides MAGDIS(WT)f/MAGDIS(WT)r or MAGDIS(WT)f/MAGDIS(I5L)r (Supplementary Table S2), which correspond to the wild-type or I5L mutant 5'-UTR (47), respectively, were annealed and filled-in by PCR. pSR327 carries a chimeric 5'-UTR: -327 to -311 nt of the human *AMD1* and -310 to -1 nt of the bovine *AMD1* (47). The amplified fragments were inserted into pMI21 in the same way as for the construction of pST120. For all constructs, the integrity of PCR-amplified regions was confirmed by sequence analysis.

Plasmid pMI27 carries the *RLUC* gene in the pSP64 poly(A) vector (22). Plasmids pMT131 and pMT132 carry the wild-type or mutated 5'-UTR of *AtNIP5;1*, respectively, joined to the *LUC* gene in the pSP64 poly(A) vector (34).

Quantitative RT-PCR

Total RNA was extracted from plants grown for 14 days using the RNeasy Plant Mini Kit (Qiagen, Hilden, Germany) and treated with DNase I. Total RNA was reverse-transcribed to cDNA using the SuperScript III First-Strand Synthesis System (Invitrogen) with oligo-d(T)₁₂₋₁₈ primers. Real-time PCR was performed using a LightCycler 480 Real-time System (Roche, Basel, Switzerland) and the LightCycler 480 SYBR Green I Master kit. The Arabidopsis *UBQ5* gene was used as an internal control. The primers used are listed in Supplementary Table S2.

In vitro transcription

DNA templates in the pSP64 poly(A) vector were linearized with EcoRI and purified using the QIAquick Nucleotide Removal Kit (Qiagen), with the exception of the *M8:His:HA:DP75* and *M8:His:HA:3xFLAG:Myc:DP75* fusion constructs. DNA templates for these plasmids and *nonstop* RNAs were prepared by amplifying the corresponding region by PCR using KOD-Plus-Neo DNA polymerase. For PCR amplification, SP65'fP (18) was used as a forward primer and the reverse primers as listed in Supplementary Table S2 were used. *In vitro* transcription in the presence of a cap analog, m⁷G[5']ppp[5']GTP, was carried out as described previously (22).

In vitro translation

Preparation of ACE and *in vitro* translation reactions using ACE were carried out at 25°C as described previously (23). Unless otherwise stated, the template RNA was used at 50 fmol μl⁻¹. For RNase A treatment, RNase A was added at a final concentration of 0.5 mg ml⁻¹ and reaction mixtures were incubated for 15 min at 37°C. For immunoblot analysis, reaction mixtures were diluted with the 1× SDS-PAGE gel sample buffer (50 mM Tris-HCl pH 6.8, 50 mM DTT, 10% (v/v) glycerol and 1% (w/v) SDS).

Immunoblot analysis

For immunoblot analysis of *in vitro* translation products, samples were separated on a NuPAGE 4–12% or 12% Bis-Tris Gel (Invitrogen), transferred to an Immobilon-P membrane (Millipore, Billerica, MA, USA), and immunoreacted with either a polyclonal anti-GST antibody (Santa Cruz Biotechnology, Santa Cruz, CA, USA), a monoclonal anti-HA antibody (Santa Cruz Biotechnology), or a monoclonal anti-FLAG M2 antibody (Sigma-Aldrich). MOPS running buffer (Life Technologies, Carlsbad, CA, USA) was used for the *GST* tag-fusion construct. MES running buffer (Life Technologies) was used for the *M8:His:HA:DP75* or *M8:His:HA:3xFLAG:Myc:DP75* fusion constructs. The signals were detected using an Immobilon Forte Western HRP substrate (Millipore) and visualized using a LAS-3000 mini imaging system (GE Healthcare, Little Chalfont, UK). The band intensities were quantified using MultiGauge software (Fuji Photo Film, Tokyo, Japan).

Total proteins from Arabidopsis callus cultures were separated by SDS-PAGE with MOPS running buffer and

subjected to immunoblot analyses using a monoclonal anti-FLAG M2 antibody (Sigma-Aldrich), anti-uL22 antiserum, anti-uL4 antiserum (Proteintech, Rosemont, IL, USA), or anti- β -actin antiserum (Gene Tex, Irvine, CA, USA). The polyclonal antibody against human uL4 (accession no. BC009888) recognizes both endogenous Arabidopsis uL4A and uL4D as epitopes (48). The polyclonal antiserum raised against Arabidopsis uL22 was generated by immunizing rabbit with a synthetic peptide corresponding to amino acids 4–20 of Arabidopsis uL22B (YSQEPDNQTKSCKARGS; At1g67430).

Isolation of Arabidopsis ribosomes

For ribosome isolation, liquid callus cultures were prepared from Arabidopsis seedlings as described previously (23) and harvested on the 21st day after callus induction. Frozen tissues were homogenized in buffer D (49). After clarification by centrifugation at $16\,000 \times g$ for 30 min, crude extract (S16) was loaded on the 1.75 M sucrose cushion (100 mM Tris-HCl pH 8.0, 40 mM KCl, 20 mM MgCl₂, 1 mM DTT and 100 $\mu\text{g ml}^{-1}$ cycloheximide) and centrifuged at $170\,000 \times g$ for 4 h at 4°C in a TLA100.3 rotor (Beckman Coulter, Brea, CA, USA) to obtain the S170 soluble protein fraction and the P170 ribosomal pellet. The P170 fraction was suspended in the resuspension buffer (100 mM Tris-HCl pH 8.0, 40 mM KCl, 20 mM MgCl₂, 1 mM DTT and 100 $\mu\text{g ml}^{-1}$ cycloheximide). For immunoblot analysis, the protein concentration was measured using a Pierce 660 nm Protein Assay Reagent (Invitrogen), in accordance with the manufacturer's instructions.

Polysome profiling analysis

For the fractionation of total polysomes, ribosomes (P170) were isolated as described above. Ribosome suspension was loaded on a 15–60% (w/v) sucrose density gradient (40 mM Tris-HCl pH 8.4, 20 mM KCl, 10 mM MgCl₂ and 5 $\mu\text{g ml}^{-1}$ cycloheximide) and centrifuged at $275\,000 \times g$ for 1.5 h at 4°C in an SW55 Ti rotor (Beckman Coulter). The UV absorbance profile at 254 nm was recorded using an ISCO 520 gradient system (ISCO, Lincoln, NE, USA). For immunoblot analysis, fractions were analyzed as described above.

Affinity purification of FLAG-tagged ribosomes

Immunoprecipitation of FLAG-tagged ribosomes using an anti-FLAG M2 affinity resin (Sigma-Aldrich) was performed as described previously (50) with some modifications. All procedures were carried out at 4°C. After *in vitro* translation of 25 pmol *GST:CGS1(G183-ns)* RNA in a 50- μl reaction mixture, translation products were diluted with 50 μl of ice-cold 2 \times binding buffer (100 mM Tris-HCl pH 7.5, 24 mM Mg(OAc)₂, 1 mM DTT, 1 mM PMSF, 20 $\mu\text{g ml}^{-1}$ cycloheximide and 0.05 U μl^{-1} RNase inhibitor (Promega)) and 40 μl (bed volume) of anti-FLAG M2 affinity resin. After incubation with gentle shaking for 1 h, the resin was washed with ice-cold IXA-100 buffer (50 mM Tris-HCl pH 7.5, 100 mM KCl, 12 mM Mg(OAc)₂, 1 mM DTT, 1 mM PMSF and 20 $\mu\text{g ml}^{-1}$ cycloheximide). Bound

proteins were eluted by the addition of 15 μl of the IXA-100 buffer containing 200 $\mu\text{g ml}^{-1}$ FLAG peptides (Sigma-Aldrich). For immunoblot analysis, eluate was diluted with 2 \times SDS-PAGE gel sample buffer (100 mM Tris-HCl pH 6.8, 100 mM DTT, 20% glycerol and 2% SDS).

Reporter assay

Tester RNA at 2 fmol μl^{-1} carrying firefly luciferase (LUC) reporter gene and 1 fmol μl^{-1} *Renilla reniformis* luciferase (RLUC) control RNA were co-translated for 120 min. LUC and RLUC activities were measured as described previously (22), and the LUC activity was normalized with the control RLUC activity to obtain reporter activity.

Statistical treatments

For comparisons of stalling efficiencies, Welch's *t*-test followed by false discovery rate (FDR) correction of Benjamini and Hochberg (51) was applied. The same FDR correction was also applied to comparisons of mRNA levels among the transgenic lines. For multiple comparisons of plant phenotypes, the Tukey–Kramer test was applied. For other comparisons, Welch's *t*-test was applied.

RESULTS

Construction of transgenic Arabidopsis carrying mutations in uL4

The uL4 protein contains a large loop structure termed the internal extended loop, at the tip of which are two smaller β -loop structures, designated here as Loops 1 and 2 (Supplementary Figure S1A). Loops 1 and 2 protrude into the exit tunnel to constitute the constriction region (Figure 2A).

In Arabidopsis, uL4 is encoded by two paralogous genes, *uL4A* and *uL4D* (52,53), sharing 95% amino acid identity. The amino acid sequences of Loops 1 and 2 are highly conserved among eukaryotes (Figure 2B and Supplementary Figure S1B). Since double-*knockout* mutant of *uL4A* and *uL4D* is lethal (48), we introduced a modified *uL4D* gene into the T-DNA insertion *knockout* mutant of *uL4D*, referred to here as the *uL4d(KO)* line, while keeping endogenous *uL4A* intact (Figure 2C).

We constructed three mutant *uL4Ds*, namely *uL4D(R77A)*, *uL4D(Δ TV)* and *uL4D(Δ loop)* (Figure 2A–C). *uL4D(R77A)* carries an Arg-77 to alanine substitution, located near the tip of Loop 1. *uL4D(Δ TV)* carries deletions of Thr-75 and Val-79 flanking the tip, while *uL4D(Δ loop)* carries larger deletions flanking the tip (deletions of Glu-71 to Thr-75 and Val-79 to Pro-86). These mutant *uL4Ds* and the control gene, *uL4D(WT)*, were FLAG-tagged at their C-termini and placed under the control of their native promoter (Figure 2C). The C-terminus of uL4 is exposed to the ribosomal surface (54). A large complex of the ribosome on mRNA can be affinity-purified using a FLAG tag (50,55).

In Arabidopsis ecotype Col-0 wild-type plants (hereafter Col-0), *uL4A* and *uL4D* mRNAs accumulate to comparable levels (Supplementary Figure S2). *uL4* mRNA accumulation levels in the *uL4D* mutant plants that we constructed were quantified (Figure 3). In all the transgenic plants, en-

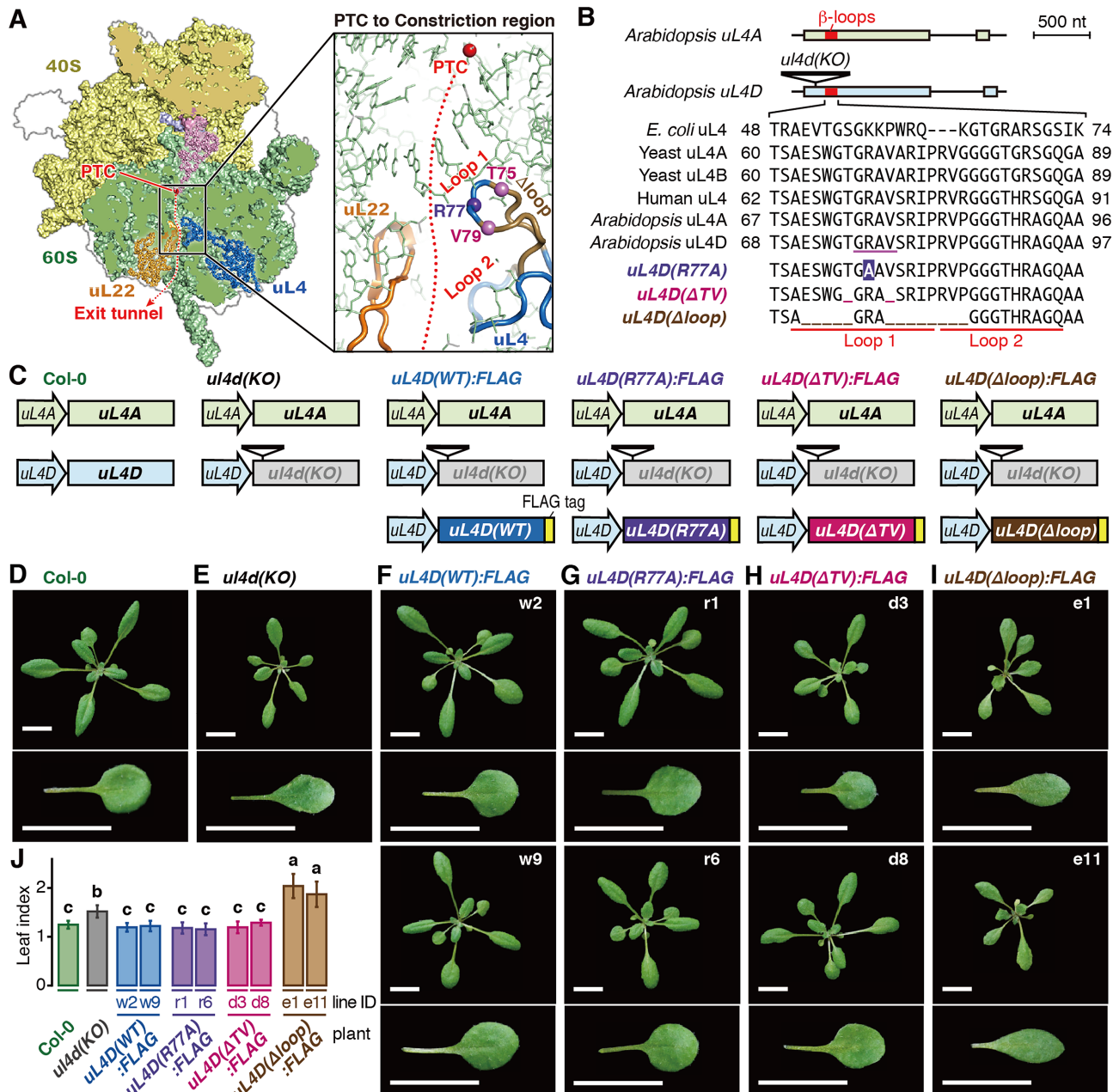


Figure 2. Construction of transgenic Arabidopsis carrying *uL4D* mutations and their phenotypes. (A) Structure of wheat 80S ribosome (PDB 4V7E) (54) (Left panel) and expansion of the constriction region (Right panel). The α -carbon atoms of *uL4* residues substituted in *R77A* (Arg-77) and deleted in ΔTV (Thr-75 and Val-79) mutations are marked in violet and magenta balls, respectively, while those deleted in $\Delta loop$ (Glu-71 to Thr-75 and Val-79 to Pro-86) mutation is marked with light brown main chain. (B) (Upper panel) Schematic representation of gene structures of *uL4A* and *uL4D*, and T-DNA insertion in *uL4d(KO)* (SALK_029203). Exons and introns are indicated as boxes and lines, respectively, with the β -loop region marked in red. (Lower panel) Alignment of amino acid sequences of Loop 1 and 2 regions. Substitutions and deletions in *uL4D* mutants are shown in reversed letters and underscores, respectively. The residues of *uL4* in physical contact with AAP nascent peptide as deduced by cryo-EM in WGE (14) are underlined in magenta in Arabidopsis *uL4D*. (C) Schematic representation of *uL4* gene sets carried by Arabidopsis wild-type Col-0, *uL4d(KO)*, and FLAG-tagged *uL4D* mutant lines. (D–I) Rosettes and one of the first pair of true leaves of wild-type Col-0, *uL4d(KO)*, and FLAG-tagged *uL4D* mutant transgenic plants (indicated by labels) grown for 21 days. Independent transgenic line IDs used in this study are indicated. Bars = 10 mm. (J) Length-to-width ratio (leaf index) of Col-0 and *uL4D* mutant plants. Different letters indicate significant differences ($P < 0.05$, Tukey–Kramer test).

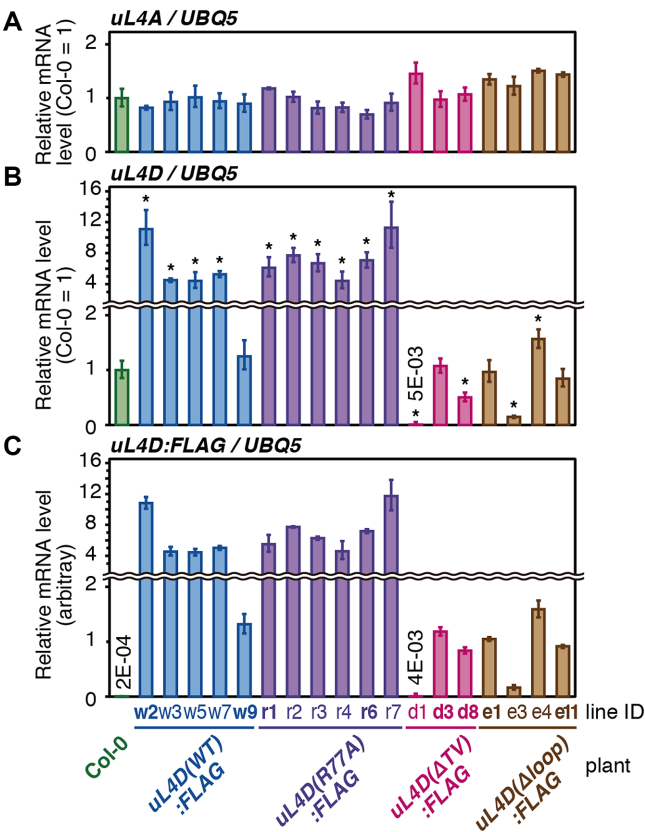


Figure 3. Accumulation levels of endogenous *uL4A* and FLAG-tagged mutant *uL4D* mRNAs in transgenic lines. Total RNA was extracted from seedlings of wild-type Col-0 and transgenic plants 14 days after imbibition. *uL4A* (A), *uL4D* (B), and *uL4D:FLAG* (C) mRNAs were quantified by qRT-PCR using *UBQ5* mRNA as a control. Means \pm SD of triplicated experiments are shown. The y-axis in (C) was set so that the means, excluding Col-0, of *uL4D:FLAG* mRNA in (C) and *uL4D* mRNA in (B) are the same. In (A) and (B), asterisks indicate significant differences from wild-type Col-0 plants ($q < 0.05$, Welch's *t*-test with FDR correction). In (A), no significant difference was detected. The line IDs of transgenic lines that were used for further experiments are shown in bold letters.

ogenous *uL4A* mRNA levels were similar to those in wild-type Col-0 plants, whereas *uL4D* mRNA levels varied depending on the mutant construct. In *uL4D(WT):FLAG* and *uL4D(R77A):FLAG* plants, *uL4D* mRNA levels were generally higher than in Col-0, while in *uL4D(ΔTV):FLAG* and *uL4D($\Delta loop$):FLAG* plants, they were about the same or lower than in Col-0. In subsequent experiments, we used two independent transgenic lines for each mutant construct (Figure 3, line IDs in bold letters).

Mutant uL4Ds complement the ribosome-deficient phenotypes *in vivo*, except in *uL4D($\Delta loop$):FLAG* plants

In *Arabidopsis*, mutations of ribosomal proteins often have multiple effects on growth and development, including narrower leaf morphology, termed the *pointed leaf*, and a short-root phenotype (56). *uL4d(KO)* plants also exhibited these phenotypes (Figure 2E and Supplementary Figure S3) (48,57,58). Both phenotypes were complemented not only in the *uL4D(WT):FLAG* plants but also in the *uL4D(R77A):FLAG* and *uL4D(ΔTV):FLAG*

plants (Figure 2F–H and J, and Supplementary Figure S3), indicating the functionality of mutant ribosomes *in vivo*. In contrast, neither phenotype was complemented in *uL4D($\Delta loop$):FLAG* plants. Notably, the plants exhibited even narrower leaves (Figure 2I and J).

Mutant uL4D proteins are efficiently incorporated into translating ribosomes, except in the *uL4D($\Delta loop$):FLAG* line

To determine whether the *uL4D* mutant proteins are incorporated into ribosome particles, we tested the association of FLAG-tagged *uL4D* proteins with 80S ribosomes (Figure 4A). Since the ACE *in vitro* translation system is prepared from callus cultures raised from the mutant *Arabidopsis* seedlings (Supplementary Figure S4) (23), we used the same culture system here. Crude extracts (S16) were subjected to ultracentrifugation through a sucrose cushion to obtain ribosomal pellet (P170) and post-ribosomal supernatant (S170) fractions. Immunoblot analysis of the fractions using an anti-FLAG antibody identified the \sim 48-kDa *uL4D:FLAG* proteins in the S16 and P170 fractions, but not in S170, in all mutant lines (Figure 4A). This indicates that the FLAG-tagged *uL4D(WT)*, *uL4D(R77A)* and *uL4D(ΔTV)* proteins are efficiently incorporated into ribosome particles. *uL4D($\Delta loop$):FLAG* protein is also incorporated into ribosome particles; however, the antibody detected only a faint band, indicating that the mutant ribosome constitutes a very minor fraction of the total ribosomes. Since the *uL4D($\Delta loop$):FLAG* line did not seem promising for use in the present study, we excluded this line from further analyses.

To determine whether the mutant ribosomes are actively translating, we performed polysome profiling of the P170 fractions using sucrose density gradient centrifugation. Immunoblot analysis detected mutant *uL4Ds* in the polysome, monosome, and 60S subunit fractions, but not in the 40S subunit and free-protein fractions (Figure 4B). Distributions of the mutant *uL4Ds* in polysome fractions appeared similar to those of the total ribosome (Supplementary Figure S5), suggesting that the mutant *uL4D*-containing ribosomes can all achieve active translation *in vivo*.

Mutant ribosomes constitute substantial proportions of total ribosomes in ACE

Since the *uL4D:FLAG* mutant lines carry an endogenous *uL4A*, we investigated what proportion of ribosomes consisted of mutant *uL4Ds* in ACE (hereafter, the constitution fraction). To determine this, we subjected ACE preparations to immunoblot analysis using anti-*uL4* antiserum, to distinguish FLAG-tagged mutant *uL4D* from endogenous *uL4A* by \sim 1-kDa gel mobility shift (Figure 4C). The constitution fractions ranged from 40% to 80% (Figure 4D), indicating that substantial proportions of the ribosomes carry mutant *uL4D* in ACE.

AdoMet-induced ribosome stalling of CGS1 is reduced in *uL4D(ΔTV):FLAG* ribosomes

When a ribosome stalls during translation, a peptidyl-tRNA species accumulates as an intermediate of transla-

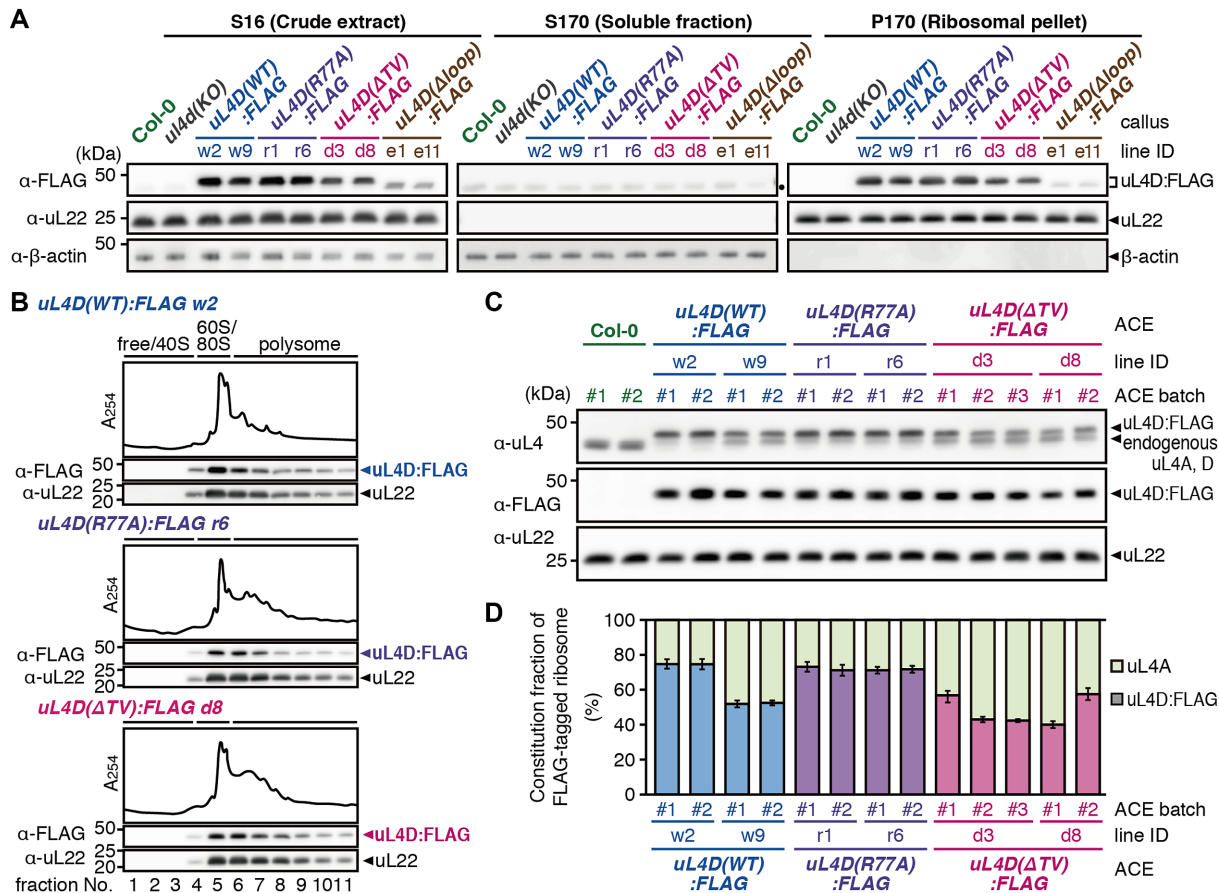


Figure 4. Functionality and constitution fraction of FLAG-tagged mutant uL4D-containing ribosomes. (A) Crude extracts (S16), post-ribosomal supernatants (S170), and ribosomal pellets (P170) prepared from callus cultures derived from wild-type Col-0 plants, *uL4d*(KO), and FLAG-tagged mutant uL4D transgenic lines are shown. Total proteins (10 μ g in S16/S170; 1 μ g in P170) were separated by SDS-PAGE and analyzed by immunoblotting using anti-FLAG antibody, anti-uL22 antiserum, and anti- β -actin antiserum. Positions of FLAG-tagged uL4D mutant proteins (uL4D:FLAG), 19-kDa uL22, and 43-kDa β -actin bands are marked. β -Actin was used as a soluble protein marker. A black dot in S170 marks the cross-reaction band. Representative results of two biological replicates are shown. (B) P-170 fractions from uL4D(WT):FLAG w2 line, uL4D(R77A):FLAG r6 line, and uL4D(Δ TV):FLAG d8 line were fractionated by ultracentrifugation through a 15–60% (w/v) sucrose density gradient. UV absorbance profile at 254 nm and immunoblot analysis using anti-FLAG antibody and anti-uL22 antiserum are shown. Positions of free proteins and 40S subunit, 60S subunit, 80S ribosome and polysome fractions are indicated. Representative results of two biological replicates are shown. (C) Immunoblot analysis of ACE batches using anti-uL4 antiserum, anti-FLAG antibody, and anti-uL22 antiserum. Representative results of three technical repeats are shown. Anti-uL4 detects both FLAG-tagged mutant uL4D and endogenous uL4A. (D) Immunoblot signals obtained using anti-uL4 antiserum in (C) were quantified, and the constitution fractions of FLAG-tagged uL4D-containing ribosomes among total ribosomes were calculated. Means \pm SD of three technical repeats are shown.

tion. A tRNA moiety confers a 10- to 20-kDa gel mobility shift on the peptide, depending on the tRNA species and gel conditions. Peptidyl-tRNA can be identified as an RNase-sensitive band.

In response to AdoMet, CGS1 nascent peptide induces ribosome stalling at the Ser-94 codon, leading to peptidyl-tRNA accumulation (17). This response was recapitulated in Col-0 ACE (Supplementary Results 1.1 and Figure S6) (23). To determine the effects of mutant uL4D-containing ribosomes, *GST:CGS1(WT)* RNA (Figure 5A and Supplementary Figure S6A) (17) was translated in ACE in the presence of AdoMet. Immunoblot analysis using an anti-GST antibody detected a 55-kDa peptidyl-tRNA in addition to a 45-kDa full-length product, whereas in the absence of AdoMet the peptidyl-tRNA was barely detectable (Figure 5A).

To evaluate the effect of *uL4D* mutations, we calculated the stalling efficiency, which is defined as the peptidyl-tRNA signal intensity divided by the sum of peptidyl-tRNA and full-length product signal intensities (Supplementary Figure S7A) (31,43). Since the ACE preparations contain both mutant uL4D- and endogenous uL4A-containing ribosomes, the stalling efficiency of the mutant ribosome alone has to be evaluated. To achieve this, we corrected the raw stalling efficiency for the constitution fraction of the mutant ribosomes, referred to as the corrected stalling efficiency. This calculation assumes that the stalling efficiency of endogenous uL4A-containing ribosomes alone is the same as that in Col-0 ACE, which we believe is reasonable (Supplementary Figure S8A). The corrected stalling efficiency of uL4D(Δ TV):FLAG lines d3 and d8 ACE was 63% and 56%, respectively (Figure 5A, shaded

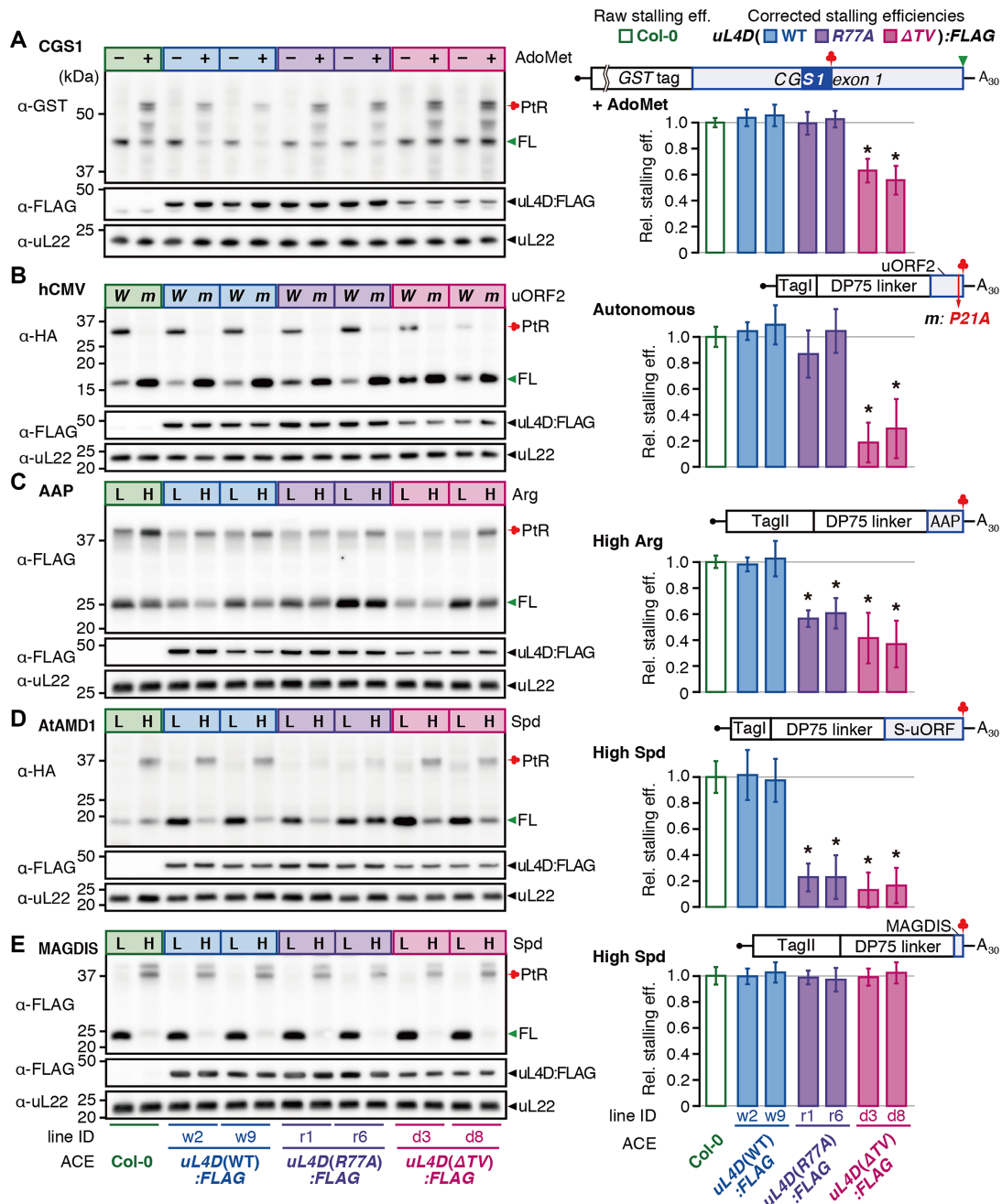


Figure 5. Differential effects of uL4D mutant ribosomes on stalling. RNA construct shown above the bar graphs was translated in ACE prepared from wild-type Col-0, or from two independent lines of FLAG-tagged uL4D mutants as indicated. (Left panels) Translation products were separated by SDS-PAGE and analyzed by immunoblotting. The antibodies used to detect translation products are indicated. (Left panels) Immunoblots with anti-FLAG antibody and anti-uL22 antiserum are also shown. Positions of the full-length product (FL), peptidyl-tRNA (PtR), 48-kDa FLAG-tagged uL4Ds (uL4D:FLAG), and 19-kDa uL22 are marked. The experiments were carried out with two batches of ACE preparations for each of the Col-0 and mutant lines, and a representative result of triplicate experiments in one of the batches is shown. (Right panels) The corrected stalling efficiencies (shaded box) relative to the raw stalling efficiency in Col-0 ACE (open box) were calculated and means \pm SD of six experiments performed with two ACE batches in triplicate are shown. Asterisks indicate significant differences compared with Col-0 ACE ($q < 0.05$ by Welch's t -test with false discovery rate (FDR) correction). (A) CGS1 system. *GST:CGS1(WT)* RNA (Supplementary Figure S6A) was translated for 30 min in ACE in the absence (-) or presence (+) of 1 mM AdoMet. The immunoblot signals of the '+' lanes in the left panel were quantified and stalling efficiencies were calculated. The MTO1 region (21) is indicated by a filled blue box. (B) hCMV system. *TagI:DP75:hCMV(WT)* RNA (W) and *TagI:DP75:hCMV(P21A)* RNA (m) (Supplementary Figure S10B) were translated for 30 min. The immunoblot signals of the 'W' lanes were quantified. (C) AAP system. *TagII:DP75:AAP(WT)* RNA (Supplementary Figure S12B) was translated for 10 min in the presence of a low (L, 0.08 mM) or high (H, 2.08 mM) L-arginine concentration as indicated. The immunoblot signals of the 'H' lanes were quantified. (D) AtAMD1 system. *TagI:DP75:S-ORF(WT)* RNA (Supplementary Figure S13B) was translated for 30 min in the presence of a low (L, 0.2 mM) or high (H, 0.7 mM) spermidine (Spd) concentration as indicated. The immunoblot signals of the 'H' lanes were quantified. (E) MAGDIS system. *TagII:DP75:MAGDIS(WT)* RNA (Supplementary Figure S14B) was translated for 10 min in the presence of a low (L, 0.2 mM) or high (H, 0.7 mM) Spd concentration as indicated. The immunoblot signals of the 'H' lanes were quantified. *TagI* and *TagII* carry M8:His:HA and M8:His:HA:3xFLAG:Myc tags, respectively.

bar), of the raw stalling efficiency of Col-0 ACE (Figure 5A, open bar), while the corrected stalling efficiencies of uL4D(WT):FLAG and uL4D(R77A):FLAG ACE were not appreciably different from the raw stalling efficiency of Col-0 ACE. These results show that uL4D(ΔTV) mutation weakens AdoMet-induced ribosome stalling, while uL4D(R77A) mutation does not.

Affinity purification of stalled ribosome confirms the calculation of corrected stalling efficiency

To validate the calculation of corrected stalling efficiencies, *GST:CGS1(G183-ns)* RNA (Figure 6A) was used to affinity-purify the FLAG-tagged mutant ribosomes by immunoprecipitation (IP) using an anti-FLAG antibody following translation in ACE. *GST:CGS1(G183-ns)* RNA is a *nonstop* RNA that is truncated at the Gly-183 codon and does not carry a stop codon. The use of this *nonstop* RNA is necessary to affinity-purify the stalled ribosomes because a ribosome that reached the termination codon will split into large and small subunits and the peptidyl-tRNA will be hydrolyzed into a peptide and tRNA (Supplementary Figure S9A), while on the *nonstop* RNA, the 80S ribosome will remain at the truncated RNA end with the peptidyl-tRNA on it (Supplementary Figure S9A). For this experiment, the RNA concentration was increased to reduce ribosome stacking behind the initially stalled ribosome at Ser-94 (Supplementary Figure S6C and D) (19).

When *GST:CGS1(G183-ns)* RNA was translated in Col-0 ACE in the presence of 1 mM AdoMet (Figure 6B and C), ~65-kDa peptidyl-tRNA [PtR(Gly-183), green clover] that had translated to the truncated end of the *nonstop* RNA, 55-kDa peptidyl-tRNA [PtR(Ser-94), red clover] formed on the stalled ribosome at Ser-94, and 45-kDa full-length peptide (FL, green arrowhead) were identified. The stalling efficiency in this experiment is defined as the signal intensity of PtR(Ser-94) divided by the sum of PtR(Ser-94) and PtR(Gly-183) signal intensities. The 45-kDa full-length peptide was probably produced by spontaneous hydrolysis of PtR(Gly-183). We previously observed spontaneous hydrolysis of peptidyl-tRNA at the *nonstop* RNA end (19). Since spontaneous hydrolysis of PtR(Gly-183) could occur at any step during this experiment, the signal intensity of this full-length product was not taken into account for the calculation of stalling efficiency.

After IP with the anti-FLAG antibody, anti-uL4 antiserum detected only FLAG-tagged uL4D (Figure 6D), indicating that IP efficiently purified FLAG-tagged mutant ribosomes. The corrected stalling efficiencies of uL4D(ΔTV):FLAG lines d3 and d8 ACE before IP were $68 \pm 4\%$ and $66 \pm 8\%$, respectively, while raw stalling efficiencies after IP were $71 \pm 6\%$ and $72 \pm 4\%$, respectively, of that of Col-0 ACE before IP (Figure 6E). For all pairwise comparisons of the corrected stalling efficiency before IP and the raw stalling efficiency after IP, similar values were obtained. These results support the validity of the corrected stalling efficiency calculations.

Affinity purification of stalled ribosomes, however, cannot be applied to NPmRS that occurs at the termination codon (Supplementary Figure S9B). Therefore, in the present study, we used the corrected stalling efficiency that

was calculated and compared it with the raw stalling efficiency of Col-0 ACE.

uL4D(ΔTV) mutation reduces autonomous ribosome stalling of the hCMV system

To further characterize the contribution of the constriction region to NPmRS, we tested other stalling systems from different eukaryotes. The 22-amino-acid uORF2 of hCMV *gp48* directs ribosomes to stall autonomously at the translation termination to downregulate *gp48* expression (27,28). The *gp48* uORF2-mediated stalling occurred in Col-0 ACE, and abrogation of stalling by Pro-21-to-alanine substitution (P21A) of uORF2 (28) was reproduced in Col-0 ACE (Supplementary Results 1.2 and Supplementary Figure S10), thus showing recapitulation of the *gp48* uORF2-mediated autonomous stalling in Col-0 ACE.

We tested the effects of uL4D(ΔTV) and uL4D(R77A) mutations. The corrected stalling efficiency in uL4D(ΔTV):FLAG ACE was estimated to be 19–30% of the raw stalling efficiency of Col-0 ACE, while that of uL4D(WT):FLAG ACE and uL4D(R77A):FLAG ACE was not appreciably different from Col-0 ACE (Figure 5B). The effects of uL4D mutations on CGS1 and hCMV systems were similar in that uL4D(ΔTV) but not uL4D(R77A) affected stalling; however, the reduction in the uL4D(ΔTV) mutant was stronger in hCMV than in CGS1.

To further confirm the accuracy of our calculation of the corrected stalling efficiency, we mixed uL4D(WT):FLAG w2 line ACE or uL4D(ΔTV):FLAG d8 line ACE with Col-0 ACE at different proportions, and analyzed the resulting stalling efficiencies. Extrapolation of the regression lines of the raw stalling efficiencies revealed stalling efficiency values for the mutant ribosomes alone that are similar to those in Figure 5B, again supporting the validity of our corrected stalling efficiency calculations (Supplementary Figure S11).

Both uL4D(R77A) and uL4D(ΔTV) mutations reduce arginine-induced ribosome stalling of the AAP system

The 24-amino-acid AAP nascent peptide, encoded by *N. crassa arg-2* uORF, causes NPmRS in response to L-arginine (24,25). In Col-0 ACE, peptidyl-tRNA accumulated in a L-arginine-dependent manner, whereas substitution of Asp-12 to asparagine (D12N) of AAP, which has been shown to abolish the response to L-arginine (25), also abolished the peptidyl-tRNA accumulation in Col-0 ACE (Supplementary Results 1.3 and Supplementary Figure S12). Thus, L-arginine-dependent NPmRS of AAP was recapitulated in Col-0 ACE.

Translation analyses in uL4D mutant ACE showed that stalling at a high L-arginine concentration (2.08 mM) was significantly reduced in both uL4D(R77A):FLAG and uL4D(ΔTV):FLAG ACE. The corrected stalling efficiencies were 57–61% and 37–42%, respectively, of the raw stalling efficiency of Col-0 ACE (Figure 5C). Compared with the CGS1 and hCMV systems, AAP exhibited a qualitative difference in that a single-amino-acid substitution of uL4D(R77A) affected stalling.

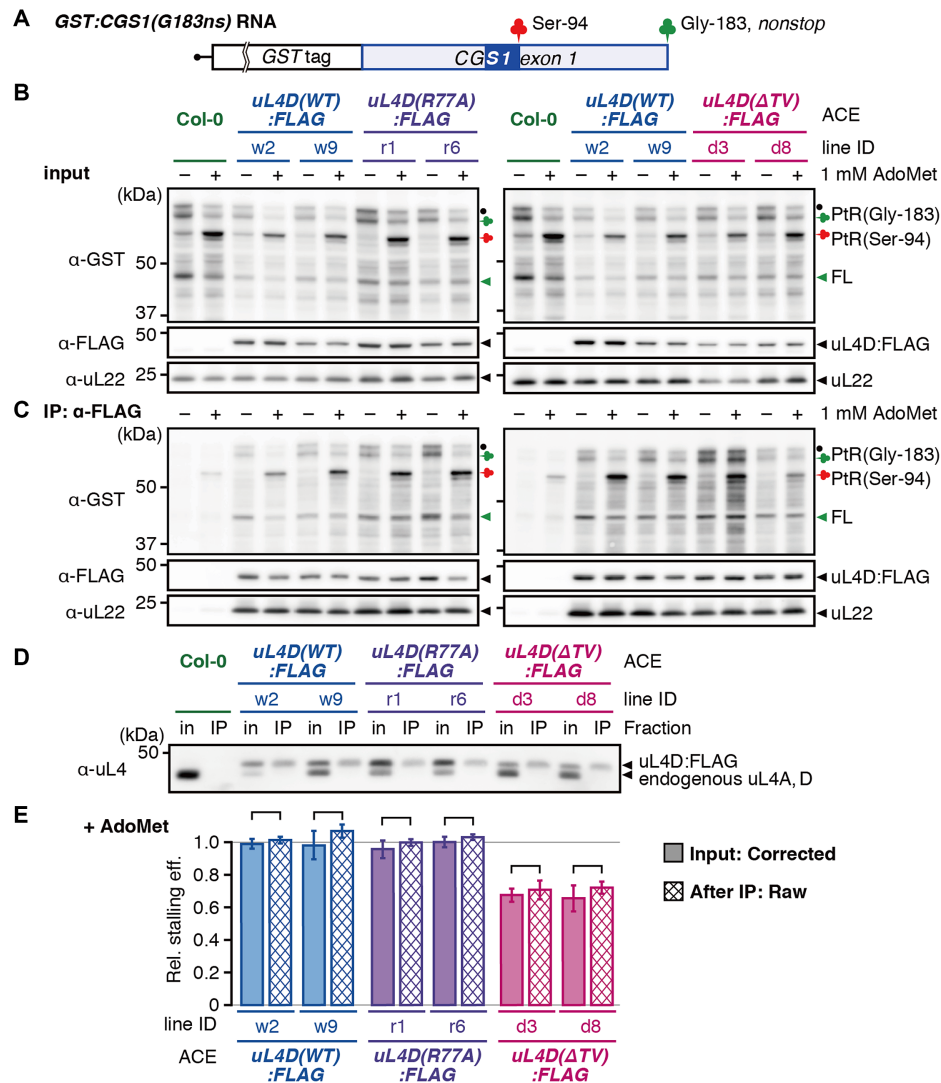


Figure 6. Affinity purification of stalled ribosomes. (A) Schematic representation of *GST:CGS1(G183-ns)* RNA, which is a *nonstop* RNA that is truncated at the Gly-183 codon located at the end of *CGS1* exon 1 and does not carry a stop codon. The MTO1 region (21) is indicated by a filled blue box. (B and C) *GST:CGS1(G183-ns)* RNA (500 fmol μl^{-1}) was translated in ACE prepared from wild-type Col-0 and mutant lines expressing *uL4D:FLAG* in the absence (-) or presence (+) of 1 mM AdoMet, as indicated. After 30 min of translation, stalled ribosomes were affinity-purified by IP using anti-FLAG antibody. Translation products of input controls (B) and IP fractions (IP: α -FLAG) (C) were analyzed by immunoblotting using anti-GST antibody. Positions of 65-kDa peptidyl-tRNA [PtR(Gly-183)] produced at the *nonstop* RNA end of Gly-183 and the 55-kDa peptidyl-tRNA [PtR(Ser-94)] produced by AdoMet-induced NPMRS at Ser-94, and the full-length peptide, which was dissociated from PtR(Gly-183) (FL), are marked. The band marked with a black dot is probably a peptidyl-tRNA that is produced by a ribosome stacked behind the one stalled at the *nonstop* RNA end. Immunoblots using anti-FLAG antibody and anti-uL22 antiserum are shown as loading controls. A representative result of triplicate experiments is shown. (D) Immunoblot analysis of the translation mixture before (in) and after IP (IP) using anti-uL4 antiserum to show the constitution fractions of FLAG-tagged ribosomes. Positions of the 48-kDa FLAG-tagged uL4D (uL4D:FLAG) and the 47-kDa endogenous uL4 are marked. The band marked as endogenous uL4 in Col-0 ACE (lanes 1 and 2) includes both endogenous uL4A and endogenous uL4D, while that in uL4D:FLAG mutant ACE (lanes 3–14) is endogenous uL4A alone. A representative result of triplicate experiments is shown. (E) The immunoblot signals in (B) and (C) were quantified. The corrected stalling efficiency in the input sample (shaded box), and the raw stalling efficiency after IP (cross hatched box) were calculated and means \pm SD ($n = 3$) are shown. No significant difference was observed between the corrected stalling efficiency before IP and raw stalling efficiency after IP in each pair of the samples ($P > 0.05$ by Welch's *t*-test).

Both *uL4D(R77A)* and *uL4D(ΔTV)* mutations strongly reduce polyamine-induced ribosome stalling in AtAMD1 system

The 52-amino-acid uORF2 of *AtAMD1* S-uORF directs the ribosome to stall at the translation termination in response to high polyamine concentrations. In the present study, spermidine was used as an effector (31). In Col-0 ACE, peptidyl-tRNA accumulation was dependent on sper-

midine concentration (31), which was abolished by introducing a frame-shift mutation in S-uORF (Supplementary Results 1.4 and Figure S13), indicating that Col-0 ACE recapitulates spermidine-dependent ribosome stalling.

The corrected stalling efficiency in *uL4D(R77A):FLAG* and *uL4D(ΔTV):FLAG* ACE at a high spermidine concentration (0.7 mM) was reduced to \sim 23% and \sim 15%, respectively, of the raw stalling efficiency of Col-0 ACE, while

uL4D(WT):FLAG ACE showed similar levels of stalling efficiencies to Col-0 ACE (Figure 5D). As was the case in AAP, both uL4D(R77A) and uL4D(ΔTV) mutations reduced the stalling in AtAMD1; however, the effects of the mutations were stronger than in AAP.

Neither uL4D(R77A) nor uL4D(ΔTV) mutation affects polyamine-induced ribosome stalling on the six-amino-acid uORF of MAGDIS

In *mAMD1*, a uORF encoding six amino acids, MAGDIS, directs the ribosome to stall in response to polyamines. Translation in Col-0 ACE showed peptidyl-tRNA accumulation in a spermidine-dependent manner, while Ile-5 to leucine (I5L) substitution (32,33) of MAGDIS abolished peptidyl-tRNA accumulation, indicating that the spermidine-induced NPmRS is recapitulated in Col-0 ACE (Supplementary Results 1.5 and Figure S14).

The corrected stalling efficiencies in uL4D:FLAG mutant ACEs were all essentially the same as the raw stalling efficiency of Col-0 ACE (Figure 5E). These results show that neither uL4D(R77A) nor uL4D(ΔTV) mutation affects the spermidine-dependent ribosome stalling directed by the six-amino-acid uORF of MAGDIS.

5'-UTRs carrying the uORFs also depict the differential effects of uL4D mutations

Translation of a uORF generally downregulates translation of the main ORF, and if ribosomes stall on the uORF, translation of the main ORF is strongly downregulated (Supplementary Figure S15) (59). For the stalling analyses, we joined artificial sequences of the tags and linker to the uORF. In the case of MAGDIS, the constriction region is vacant when stalled on the natural uORF, whereas in the present stalling analysis a 75-amino-acid DP75 linker (15,43) resides in the constriction region. To test the effects of uL4D mutations on the natural uORF sequence, the 5'-UTR sequences of the hCMV, AtAMD1, and MAGDIS systems were joined to a luciferase (LUC) reporter, and the effects of uL4D mutations were analyzed by reporter assays (Figure 7).

The 5'-UTR of hCMV *gp48* (27,28) was joined to a LUC reporter (Figure 7A, and Supplementary Figure S10A and D) and was translated in ACE. When the RNA was translated in uL4D(ΔTV):FLAG ACE the relative reporter activity was ~3 times higher than in Col-0 ACE (Supplementary Figure S16). The relative reporter activity was corrected for the constitution fraction of FLAG-tagged ribosomes, as for the stalling efficiency correction (Supplementary Figure S8B). The corrected relative reporter activity in uL4D(ΔTV):FLAG ACE was ~6 times the raw reporter activity of Col-0 ACE, while those in uL4D(WT):FLAG and uL4D(R77A):FLAG ACE were essentially the same as in Col-0 ACE (Figure 7A). When the 5'-UTR of *AtAMD1* containing the S-uORF (Figure 7B, and Supplementary Figure S13A, F, and G) (31) was analyzed, corrected reporter activities in uL4D(R77A):FLAG and uL4D(ΔTV):FLAG ACE were 7–9 times higher than in Col-0 ACE (Figure 7B).

The 5'-UTR of *mAMD1* was joined to the LUC reporter (Figure 7C, and Supplementary Figure S14A and

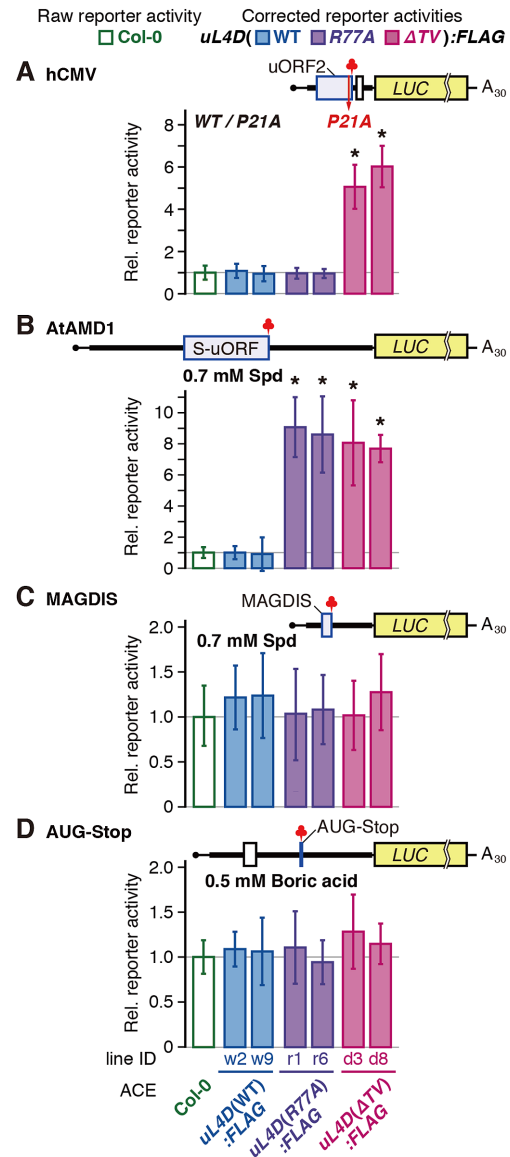


Figure 7. Differential effects of uL4D mutant ribosomes on LUC reporter expression. RNA was translated in ACE prepared from wild-type Col-0 or from two independent lines of FLAG-tagged uL4D mutants. After translation of RNA for 120 min, LUC activities were measured and normalized with the *Renilla* luciferase (RLUC) activity of the co-translated control RNA. The corrected reporter activities (shaded box) relative to the raw reporter activity in Col-0 ACE (open box) were calculated and means \pm SD of six experiments performed with two ACE batches in triplicate are shown. Asterisks indicate significant difference from raw reporter activity in Col-0 ACE ($q < 0.05$ by Welch's *t*-test with FDR correction). (A) hCMV system. 5'-hCMV:LUC(WT) and 5'-hCMV:LUC(P21A) RNAs (Supplementary Figure S10A and D) were translated. LUC activities in 5'-hCMV:LUC(WT) RNA relative to those of 5'-hCMV:LUC(P21A) RNA were calculated. (B) AtAMD1 system. 5'-AtAMD1:LUC RNA (Supplementary Figure S13A and F) was translated in the presence of 0.2 or 0.7 mM spermidine (Spd). LUC activities in the presence of 0.7 mM Spd relative to those of 0.2 mM were calculated. (C) MAGDIS system. 5'-mAMD1:LUC RNA (Supplementary Figure S14A and G) was translated in the presence of 0.2 or 0.7 mM Spd. LUC activities in the presence of 0.7 mM Spd relative to those at 0.2 mM were calculated. (D) AUG-Stop system. 5'-NIP5;1:LUC RNA (Supplementary Figure S17A and B) was translated in the presence or absence of 0.5 mM boric acid. LUC activities in the presence of boric acid relative to those in its absence were calculated.

G) and translated in ACE. Relative reporter activities in uL4D:FLAG mutant ACEs were essentially the same as in Col-0 ACE (Figure 7C). These results are consistent with those of the stalling efficiency analyses (Figure 5B, D and E) and confirmed the effects of uL4D mutations on ribosome stalling.

Neither uL4D(R77A) nor uL4D(ΔTV) mutation affects boric acid-induced ribosome stalling on AUG-stop

The 5'-UTR of *AtNIP5;1*, encoding a boric acid transporter, has the shortest possible uORF, AUG-stop (Supplementary Figure S17). Boric acid induces prolonged ribosome stalling at AUG-stop (34). Since insertion of even a single codon between the AUG and stop codons is detrimental to the response (34), joining a tag or linker sequence is impossible. Therefore, effects of the uL4D mutations were evaluated by a reporter assay. As in the case of MAGDIS, neither uL4D(R77A) nor uL4D(ΔTV) mutation affected reporter activities (Figure 7D).

DISCUSSION

In this study, we presented reverse genetics-based biochemical evidence showing that uL4 is involved in four of the NPmRS in eukaryotes, namely the CGS1, hCMV, AAP, and AtAMD1 systems. In contrast, the six-amino-acid uORF of MAGDIS was unaffected. The results show that the constriction region is crucial for inducing NPmRS, when the nascent peptide is long enough to cross over the constriction region, and that MAGDIS adopts a distinct mechanism for NPmRS induction.

Construction of transgenic lines carrying uL4D mutations

In transgenic plants uL4D(WT):FLAG line w2 and uL4D(R77A):FLAG lines r1 and r6, mutant *uL4D* mRNAs accumulated to 4- to 12-fold higher levels than in wild-type Col-0 plants (Figure 3). Nevertheless, free FLAG-tagged uL4D proteins were undetectable in S170 fractions (Figure 4A), suggesting the existence of unknown regulatory mechanism(s) at the mRNA and protein accumulation levels (48).

Regarding the uL4D(ΔTV):FLAG and uL4D($\Delta loop$):FLAG lines, mRNA accumulation was similar to or less than that in Col-0 plants (Figure 3). It is possible that high-level expressors were not isolated owing to growth retardation, because NPmRS is involved in a range of regulatory systems, including metabolism (17,20,21,31) and transcription factor expression (43,60). In the construction of uL4D(ΔTV):FLAG and uL4D($\Delta loop$):FLAG mutant plants, we also feared the effects of a defect in ribosome biogenesis because the alterations in Loop 1 might retard the integrity of the internal extension loop (Supplementary Figure S1), which has been shown to be essential for the large-subunit assembly in bacteria and yeast (61–63). This might occur in uL4D($\Delta loop$):FLAG lines. A plausible scenario is that uL4D($\Delta loop$):FLAG protein was only poorly incorporated into ribosome particles and the surplus protein was rapidly degraded. Degradation of surplus ribosomal proteins has been observed in yeast (64).

Differential effects of uL4D(R77A) and uL4D(ΔTV) mutations explain the structural data

The degree of reduction of stalling by uL4D(ΔTV) and uL4D(R77A) mutations showed qualitative differences among the stalling systems. Structures of stalled ribosomes in WGE have been solved in hCMV and AAP systems, and physical contacts between the nascent peptide and constriction region have been identified (14).

Cryo-EM studies of AAP-stalled ribosomes (14) showed that Asp-12 contacts uL4 between Gly-76 and Val-79 (Arabidopsis uL4D residue number) in Loop 1 (Figure 2B, magenta underline). This is consistent with our finding that uL4D(R77A) mutation strongly reduced the L-arginine-dependent stalling of AAP (Figure 5C). In the hCMV system, nascent peptide physically contacts Loop 2, but not Loop 1 (14). This also is consistent with our finding that uL4D(R77A) mutation did not affect hCMV stalling (Figures 5B and 7A). Asp-12 of AAP is important for stalling (Figure 1) (24,26). Thus, our data interconnect structural data and functional residues in the nascent peptide. Our data also suggest that the physical contacts of the nascent peptide with the constriction region observed by cryo-EM are the cause, not the result, of ribosome stalling.

The effects of uL4D mutations were strongest in AtAMD1 and weakest in CGS1. We previously reported that, upon AdoMet-induced stalling of CGS1, 28S rRNA residues undergo conformational changes (18). Among these, EcU744 and EcA750 (in *E. coli* rRNA numbering) mapped near the constriction region. Intriguingly, these residues are located close to uL22. Corroborating the weak effect of uL4D mutations in CGS1, the CGS1 nascent peptide might interact with uL22, rather than uL4, although other possibilities remain. In contrast, regarding the AtAMD1 system, in which uL4D mutations had strong effects on stalling, its nascent peptide might strongly interact with Loop 1 to induce polyamine-dependent ribosome stalling.

uL4D(ΔTV) mutation downregulated four NPmRS systems, while uL4D(R77A) mutation affected only two of them. uL4D(ΔTV) mutation probably exhibited a general effect on interaction of nascent peptide and the constriction by altering the geometry of the constriction region. The two stalling systems affected by uL4D(R77A) mutation would specifically interact with the Arg-77 that we mutated, which was supported by cryo-EM study of AAP-stalled ribosomes. Our data suggest that specific interaction of nascent peptide and the amino acid residue(s) within the β -loop(s) is superimposed over the general interaction with the constriction region.

SUPPLEMENTARY DATA

Supplementary Data are available at NAR Online.

ACKNOWLEDGEMENTS

We thank Dr Tsuyoshi Nakagawa (Shimane University) for the pGWB10 vector, Saeko Yasokawa, for technical assistance and Naoe Konno, Maki Mori and Kazuko Harada for general assistance. Arabidopsis SALK_029203 seeds

were obtained from Arabidopsis Biological Resource Center, OH, USA. We used the DNA Sequencing Facility of the Graduate School of Agriculture, Hokkaido University. N.O. and S.T. acknowledge JSPS for support. Y.Y. is a recipient of the Program for Fostering Researchers for the Next Generation conducted by the Consortium Office for Fostering of Researchers in Future Generations, Hokkaido University. The English text of a draft of this manuscript was edited by Edanz (Fukuoka, Japan).

Author contributions: S.N., H.O., and Y.Y. designed research. N.O., Y.T., and K.M. generated transgenic plants. S.T., Y.O., S.Y., and T.I. performed the experiments. S.T., Y.O., H.O., Y.Y., and S.N. analyzed data. S.T., Y.Y., and S.N. wrote the manuscript.

FUNDING

Grants-in-Aid for Scientific Research from the Ministry of Education, Culture, Sports, Science and Technology of Japan [JP15H01525, JP17H05658, JP22119006 to S.N.]; Japan Society for the Promotion of Science (JSPS) [JP16H05063, JP20370016 to S.N., JP19K16159 to Y.Y., JP19H02917 to H.O.]; JSPS Fellows [JP08J03032 to N.O., JP17J00982 to S.T.]. Funding for open access charge: Research Faculty of Agriculture, Hokkaido University.

Conflict of interest statement. None declared.

REFERENCES

- Ito, K. and Chiba, S. (2013) Arrest peptides: *cis*-acting modulators of translation. *Annu. Rev. Biochem.*, **82**, 171–202.
- Morgan, D.G., Ménétret, J.F., Radermacher, M., Neuhof, A., Akey, I.V., Rapoport, T.A. and Akey, C.W. (2000) A comparison of the yeast and rabbit 80 S ribosome reveals the topology of the nascent chain exit tunnel, inter-subunit bridges and mammalian rRNA expansion segments. *J. Mol. Biol.*, **301**, 301–321.
- Nissen, P., Hansen, J., Ban, N., Moore, P.B. and Steitz, T.A. (2000) The structural basis of ribosome activity in peptide bond synthesis. *Science*, **289**, 920–930.
- Ban, N., Beckmann, R., Cate, J.H.D., Dinman, J.D., Dragon, F., Ellis, S.R., Lafontaine, D.L.J., Lindahl, L., Liljas, A., Lipton, J.M. *et al.* (2014) A new system for naming ribosomal proteins. *Curr. Opin. Struct. Biol.*, **24**, 165–169.
- Nakatogawa, H. and Ito, K. (2002) The ribosomal exit tunnel functions as a discriminating gate. *Cell*, **108**, 629–636.
- Cruz-Vera, L.R., Rajagopal, S., Squires, C. and Yanofsky, C. (2005) Features of ribosome-peptidyl-tRNA interactions essential for tryptophan induction of *tna* operon expression. *Mol. Cell*, **19**, 333–343.
- Chiba, S., Kanamori, T., Ueda, T., Akiyama, Y., Pogliano, K. and Ito, K. (2011) Recruitment of a species-specific translational arrest module to monitor different cellular processes. *Proc. Natl. Acad. Sci. U.S.A.*, **108**, 6073–6078.
- Ramu, H., Vázquez-Laslop, N., Klepacki, D., Dai, Q., Piccirilli, J., Micura, R. and Mankin, A.S. (2011) Nascent peptide in the ribosome exit tunnel affects functional properties of the A-site of the peptidyl transferase center. *Mol. Cell*, **41**, 321–330.
- Cymer, F., Hedman, R., Ismail, N. and von Heijne, G. (2015) Exploration of the arrest peptide sequence space reveals arrest-enhanced variants. *J. Biol. Chem.*, **290**, 10208–10215.
- Bhushan, S., Hoffmann, T., Seidelt, B., Frauenfeld, J., Mielke, T., Berninghausen, O., Wilson, D.N. and Beckmann, R. (2011) SecM-stalled ribosomes adopt an altered geometry at the peptidyl transferase center. *PLoS Biol.*, **9**, e1000581.
- Bischoff, L., Berninghausen, O. and Beckmann, R. (2014) Molecular basis for the ribosome functioning as an L-tryptophan sensor. *Cell Rep.*, **9**, 469–475.
- Sohmen, D., Chiba, S., Shimokawa-Chiba, N., Innis, C.A., Berninghausen, O., Beckmann, R., Ito, K. and Wilson, D.N. (2015) Structure of the *Bacillus subtilis* 70S ribosome reveals the basis for species-specific stalling. *Nat. Commun.*, **6**, 6941.
- Zhang, J., Pan, X., Yan, K., Sun, S., Gao, N. and Sui, S.F. (2015) Mechanisms of ribosome stalling by SecM at multiple elongation steps. *eLife*, **4**, e09684.
- Bhushan, S., Meyer, H., Starosta, A.L., Becker, T., Mielke, T., Berninghausen, O., Sattler, M., Wilson, D.N. and Beckmann, R. (2010) Structural basis for translational stalling by human cytomegalovirus and fungal arginine attenuator peptide. *Mol. Cell*, **40**, 138–146.
- Matheisl, S., Berninghausen, O., Becker, T. and Beckmann, R. (2015) Structure of a human translation termination complex. *Nucleic Acids Res.*, **43**, 8615–8626.
- Wilson, D.N., Arenz, S. and Beckmann, R. (2016) Translation regulation via nascent polypeptide-mediated ribosome stalling. *Curr. Opin. Struct. Biol.*, **37**, 123–133.
- Onouchi, H., Nagami, Y., Haraguchi, Y., Nakamoto, M., Nishimura, Y., Sakurai, R., Nagao, N., Kawasaki, D., Kadokura, Y. and Naito, S. (2005) Nascent peptide-mediated translation elongation arrest coupled with mRNA degradation in the *CGSI* gene of *Arabidopsis*. *Genes Dev.*, **19**, 1799–1810.
- Onoue, N., Yamashita, Y., Nagao, N., Goto, D.B., Onouchi, H. and Naito, S. (2011) *S*-Adenosyl-L-methionine induces compaction of nascent peptide chain inside the ribosomal exit tunnel upon translation arrest in the *Arabidopsis CGSI* gene. *J. Biol. Chem.*, **286**, 14903–14912.
- Yamashita, Y., Kadokura, Y., Sotta, N., Fujiwara, T., Takigawa, I., Satake, A., Onouchi, H. and Naito, S. (2014) Ribosomes in a stacked array: elucidation of the step in translation elongation at which they are stalled during *S*-adenosyl-L-methionine-induced translation arrest of *CGSI* mRNA. *J. Biol. Chem.*, **289**, 12693–12704.
- Chiba, Y., Ishikawa, M., Kijima, F., Tyson, R.H., Kim, J., Yamamoto, A., Nambara, E., Leustek, T., Wallsgrove, R.M. and Naito, S. (1999) Evidence for autoregulation of cystathionine γ -synthase mRNA stability in *Arabidopsis*. *Science*, **286**, 1371–1374.
- Ominato, K., Akita, H., Suzuki, A., Kijima, F., Yoshino, T., Yoshino, M., Chiba, Y., Onouchi, H. and Naito, S. (2002) Identification of a short highly conserved amino acid sequence as the functional region required for posttranscriptional autoregulation of the cystathionine γ -synthase gene in *Arabidopsis*. *J. Biol. Chem.*, **277**, 36380–36386.
- Chiba, Y., Sakurai, R., Yoshino, M., Ominato, K., Ishikawa, M., Onouchi, H. and Naito, S. (2003) *S*-Adenosyl-L-methionine is an effector in the posttranscriptional autoregulation of the cystathionine γ -synthase gene in *Arabidopsis*. *Proc. Natl. Acad. Sci. U.S.A.*, **100**, 10225–10230.
- Murota, K., Hagiwara-Komoda, Y., Komoda, K., Onouchi, H., Ishikawa, M. and Naito, S. (2011) Arabidopsis cell-free extract, ACE, a new in vitro translation system derived from Arabidopsis callus cultures. *Plant Cell Physiol.*, **52**, 1443–1453.
- Wang, Z. and Sachs, M.S. (1997) Ribosome stalling is responsible for arginine-specific translational attenuation in *Neurospora crassa*. *Mol. Cell Biol.*, **17**, 4904–4913.
- Wei, J., Wu, C. and Sachs, M.S. (2012) The arginine attenuator peptide interferes with the ribosome peptidyl transferase center. *Mol. Cell Biol.*, **32**, 2396–2406.
- Spevak, C.C., Ivanov, I.P. and Sachs, M.S. (2010) Sequence requirements for ribosome stalling by the arginine attenuator peptide. *J. Biol. Chem.*, **285**, 40933–40942.
- Cao, J. and Geballe, A.P. (1996) Coding sequence-dependent ribosomal arrest at termination of translation. *Mol. Cell Biol.*, **16**, 603–608.
- Degnin, C.R., Schleiss, M.R., Cao, J. and Geballe, A.P. (1993) Translational inhibition mediated by a short upstream open reading frame in the human cytomegalovirus gpUL4 (gp48) transcript. *J. Virol.*, **67**, 5514–5521.
- Alderete, J.P., Jarrarian, S. and Geballe, A.P. (1999) Translational effects of mutations and polymorphisms in a repressive upstream open reading frame of the human cytomegalovirus UL4 gene. *J. Virol.*, **73**, 8330–8337.
- Hanfrey, C., Elliott, K.A., Franceschetti, M., Mayer, M.J., Illingworth, C. and Michael, A.J. (2005) A dual upstream open reading

- frame-based autoregulatory circuit controlling polyamine-responsive translation. *J. Biol. Chem.*, **280**, 39229–39237.
31. Uchiyama-Kadokura, N., Murakami, K., Takemoto, M., Koyanagi, N., Murota, K., Naito, S. and Onouchi, H. (2014) Polyamine-responsive ribosomal arrest at the stop codon of an upstream open reading frame of the *AdoMetDC1* gene triggers nonsense-mediated mRNA decay in *Arabidopsis thaliana*. *Plant Cell Physiol.*, **55**, 1556–1567.
 32. Law, G.L., Raney, A., Heusner, C. and Morris, D.R. (2001) Polyamine regulation of ribosome pausing at the upstream open reading frame of *S*-adenosylmethionine decarboxylase. *J. Biol. Chem.*, **276**, 38036–38043.
 33. Raney, A., Law, G.L., Mize, G.J. and Morris, D.R. (2002) Regulated translation termination at the upstream open reading frame in *S*-adenosylmethionine decarboxylase mRNA. *J. Biol. Chem.*, **277**, 5988–5994.
 34. Tanaka, M., Sotta, N., Yamazumi, Y., Yamashita, Y., Miwa, K., Murota, K., Chiba, Y., Hirai, M.Y., Akiyama, T., Onouchi, H. *et al.* (2016) The minimum open reading frame, AUG-stop, induces boron-dependent ribosome stalling and mRNA degradation. *Plant Cell*, **28**, 2830–2849.
 35. Alonso, J.M., Stepanova, A.N., Leisse, T.J., Kim, C.J., Chen, H., Shinn, P., Stevenson, D.K., Zimmermann, J., Barajas, P., Cheuk, R. *et al.* (2003) Genome-wide insertional mutagenesis of *Arabidopsis thaliana*. *Science*, **301**, 653–657.
 36. Clough, S.J. and Bent, A.F. (1998) Floral dip: a simplified method for *Agrobacterium*-mediated transformation of *Arabidopsis thaliana*. *Plant J.*, **16**, 735–743.
 37. Suzuki, A., Shirata, Y., Ishida, H., Chiba, Y., Onouchi, H. and Naito, S. (2001) The first exon coding region of cystathionine γ -synthase gene is necessary and sufficient for downregulation of its own mRNA accumulation in transgenic *Arabidopsis thaliana*. *Plant Cell Physiol.*, **42**, 1174–1180.
 38. Pound, M.P., French, A.P., Atkinson, J.A., Wells, D.M., Bennett, M.J. and Pridmore, T. (2013) RootNav: navigating images of complex root architectures. *Plant Physiol.*, **162**, 1802–1814.
 39. Nakagawa, T., Kurose, T., Hino, T., Tanaka, K., Kawamukai, M., Niwa, Y., Toyooka, K., Matsuoka, K., Jinbo, T. and Kimura, T. (2007) Development of series of gateway binary vectors, pGWBs, for realizing efficient construction of fusion genes for plant transformation. *J. Biosci. Bioeng.*, **104**, 34–41.
 40. Curtis, M.D. and Grossniklaus, U. (2003) A gateway cloning vector set for high-throughput functional analysis of genes in plants. *Plant Physiol.*, **133**, 462–469.
 41. Ho, S.N., Hunt, H.D., Horton, R.M., Pullen, J.K. and Pease, L.R. (1989) Site-directed mutagenesis by overlap extension using the polymerase chain reaction. *Gene*, **77**, 51–59.
 42. Pogulis, R.J., Vallejo, A.N. and Pease, L.R. (1996) *In vitro* recombination and mutagenesis by overlap extension PCR. *Methods Mol. Biol.*, **57**, 167–176.
 43. Yamashita, Y., Takamatsu, S., Glasbrenner, M., Becker, T., Naito, S. and Beckmann, R. (2017) Sucrose sensing through nascent peptide-mediated ribosome stalling at the stop codon of *Arabidopsis bZIP11* uORF2. *FEBS Lett.*, **591**, 1266–1277.
 44. Zhang, Y., Werling, U. and Edelmann, W. (2012) SLICE: a novel bacterial cell extract-based DNA cloning method. *Nucleic Acids Res.*, **40**, e55.
 45. Schleiss, M.R., Degnin, C.R. and Geballe, A.P. (1991) Translational control of human cytomegalovirus gp48 expression. *J. Virol.*, **65**, 6782–6789.
 46. Cao, J. and Geballe, A.P. (1995) Translational inhibition by a human cytomegalovirus upstream open reading frame despite inefficient utilization of its AUG codon. *J. Virol.*, **69**, 1030–1036.
 47. Hill, J.R. and Morris, D.R. (1992) Cell-specific translation of *S*-adenosylmethionine decarboxylase mRNA. Regulation by the 5' transcript leader. *J. Biol. Chem.*, **267**, 21886–21893.
 48. Rosado, A., Sohn, E.J., Drakakaki, G., Pan, S., Swidergal, A., Xiong, Y., Kang, B.H., Bressan, R.A. and Raikhel, N.V. (2010) Auxin-mediated ribosomal biogenesis regulates vacuolar trafficking in *Arabidopsis*. *Plant Cell*, **22**, 143–158.
 49. Hsu, P.Y., Calviello, L., Wu, H.Y.L., Li, F.W., Rothfels, C.J., Ohler, U. and Benfey, P.N. (2016) Super-resolution ribosome profiling reveals unannotated translation events in *Arabidopsis*. *Proc. Natl. Acad. Sci. U.S.A.*, **113**, E7126–E7135.
 50. Inada, T., Winstall, E., Tarun, S.Z.J., Yates, J.R., Schieltz, D. and Sachs, A.B. (2002) One-step affinity purification of the yeast ribosome and its associated proteins and mRNAs. *RNA*, **8**, 948–958.
 51. Benjamini, Y. and Hochberg, Y. (1995) Controlling the false discovery rate: a practical and powerful approach to multiple testing. *J. R. Statist. Soc. B*, **57**, 289–300.
 52. Barakat, A., Szick-Miranda, K., Chang, I.F., Guyot, R., Blanc, G., Cooke, R., Delseny, M. and Bailey-Serres, J. (2001) The organization of cytoplasmic ribosomal protein genes in the *Arabidopsis* genome. *Plant Physiol.*, **127**, 398–415.
 53. Hummel, M., Dobrenel, T., Cordewener, J.J.H.G., Davanture, M., Meyer, C., Smeekens, S.J.C.M., Bailey-Serres, J., America, T.A.H.P. and Hanson, J. (2015) Proteomic LC-MS analysis of *Arabidopsis* cytosolic ribosomes: Identification of ribosomal protein paralogs and re-annotation of the ribosomal protein genes. *J. Proteomics*, **128**, 436–449.
 54. Armache, J., Jarasch, A., Anger, A.M., Villa, E., Becker, T., Bhushan, S., Jossinet, F., Habeck, M., Dindar, G., Franckenberg, S. *et al.* (2010) Cryo-EM structure and rRNA model of a translating eukaryotic 80S ribosome at 5.5-Å resolution. *Proc. Natl. Acad. Sci. U.S.A.*, **107**, 19748–19753.
 55. Juntawong, P., Girke, T., Bazin, J. and Bailey-Serres, J. (2013) Translational dynamics revealed by genome-wide profiling of ribosome footprints in *Arabidopsis*. *Proc. Natl. Acad. Sci. U.S.A.*, **111**, E203–E212.
 56. Byrne, M.E. (2009) A role for the ribosome in development. *Trends Plant Sci.*, **14**, 512–519.
 57. Horiguchi, G., Mollá-Morales, A., Pérez-Pérez, J.M., Kojima, K., Robles, P., Ponce, M.R., Micol, J.L. and Tsukaya, H. (2011) Differential contributions of ribosomal protein genes to *Arabidopsis thaliana* leaf development. *Plant J.*, **65**, 724–736.
 58. Rosado, A., Li, R., van de Ven, W., Hsu, E. and Raikhel, N.V. (2012) *Arabidopsis* ribosomal proteins control developmental programs through translational regulation of auxin response factors. *Proc. Natl. Acad. Sci. U.S.A.*, **109**, 19537–19544.
 59. Hinnebusch, A.G., Ivanov, I.P. and Sonenberg, N. (2016) Translational control by 5'-untranslated regions of eukaryotic mRNAs. *Science*, **352**, 1413–1416.
 60. Hayashi, N., Sasaki, S., Takahashi, H., Yamashita, Y., Naito, S. and Onouchi, H. (2017) Identification of *Arabidopsis thaliana* upstream open reading frames encoding peptide sequences that cause ribosomal arrest. *Nucleic Acids Res.*, **45**, 8844–8858.
 61. Stelter, P., Huber, F.M., Kunze, R., Flemming, D., Hoelz, A. and Hurt, E. (2015) Coordinated ribosomal L4 protein assembly into the pre-ribosome is regulated by its eukaryote-specific extension. *Mol. Cell*, **58**, 854–862.
 62. Lawrence, M.G., Shamsuzzaman, M., Kondopaka, M., Pascual, C., Zengel, J.M. and Lindahl, L. (2016) The extended loops of ribosomal proteins uL4 and uL22 of *Escherichia coli* contribute to ribosome assembly and protein translation. *Nucleic Acids Res.*, **44**, 5798–5810.
 63. Pillet, B., García-Gómez, J.J., Pausch, P., Falquet, L., Bange, G., de la Cruz, J. and Kressler, D. (2015) The dedicated chaperone Acl4 escorts ribosomal protein Rpl4 to its nuclear Pre-60S assembly site. *PLoS Genet.*, **11**, e1005565.
 64. Sung, M.K., Porras-Yakushi, T.R., Reitsma, J.M., Huber, F.M., Sweredoski, M.J., Hoelz, A., Hess, S. and Deshaies, R.J. (2016) A conserved quality-control pathway that mediates degradation of unassembled ribosomal proteins. *eLife*, **5**, e19105.

Supplementary Data

Reverse genetics-based biochemical studies of the ribosomal exit tunnel constriction region in eukaryotic ribosome stalling: Spatial allocation of the regulatory nascent peptide at the constriction

Seidai Takamatsu¹, Yubun Ohashi², Noriyuki Onoue¹, Yoko Tajima³, Tomoya Imamichi¹, Shinya Yonezawa¹, Kyoko Morimoto³, Hitoshi Onouchi^{2,3,4}, Yui Yamashita^{2,3,4,*} and Satoshi Naito^{1,3,4,*}

¹Division of Life Science, Graduate School of Life Science, Hokkaido University, Sapporo 060-0810, Japan

²Frontiers in Biosciences, Graduate School of Agriculture, Hokkaido University, Sapporo 060-8589, Japan

³Department of Applied Bioscience, Faculty of Agriculture, Hokkaido University, Sapporo 060-8589, Japan

⁴Research Group of Applied Bioscience, Research Faculty of Agriculture, Hokkaido University, Sapporo 060-8589, Japan

*To whom correspondence should be addressed: Satoshi Naito. Tel: +81-11-706-2800; Fax: +81-11-706-4932; Email: naito@abs.agr.hokudai.ac.jp

Correspondence may also be addressed to Yui Yamashita. Tel: +81-11-706-3888; Fax: +81-11-706-4932; Email: yuiyama@abs.agr.hokudai.ac.jp

Contents

Supplementary Results 1.1. – 1.6.	2
Supplementary Figures S1 – S17	5
Supplementary Tables S1 – S2	22
Supplementary References	25

Supplementary Results

1.1. The CGS1 System in Col-0 ACE.

To determine the effects of mutant uL4D-containing ribosomes on AdoMet-induced NPmRS, we used *GST:CGS1(WT)* RNA (Figure 5A and Supplementary Figure S6A). The 183-amino-acid sequence of the *CGS1* exon 1 coding sequence, which contains the MTO1 region, is necessary and sufficient for AdoMet-induced NPmRS (37). The MTO1 region is the *cis* element for the AdoMet-induced NPmRS that occurs at Ser-94 (21).

AdoMet-induced NPmRS of CGS1 has been extensively studied by using WGE (17–22), but is only partially characterized in ACE (23). At the standard RNA concentration used in ACE ($50 \text{ fmol } \mu\text{l}^{-1}$), a second ribosome is stacked behind the initially stalled ribosome (19), and two peptidyl-tRNA species, PtR-I and PtR-II, are produced in ACE *in vitro* translation (Supplementary Figure S6B). To determine which one of the peptidyl-tRNA bands corresponds to the initially stalled ribosome at Ser-94, increasing amounts of *GST:CGS1(WT)* RNA were translated in Col-0 ACE (Supplementary Figure S6C and D). By increasing the amount of RNA to be translated, the relative intensity of the peptidyl-tRNA that corresponds to the secondary stalled ribosome will be reduced (19), because the number of ribosomes on one mRNA is reduced. The result indicated that PtR-I is the initially stalled ribosome at Ser-94, while PtR-II is the secondarily stalled ribosome. To confirm this, we analyzed the puromycin sensitivity of the peptidyl-tRNA (Supplementary Figure S6E and F). We previously reported that the initially stalled ribosome at Ser-94 exhibits lower reactivity to puromycin than the secondarily stalled ribosome in WGE (19). The results also indicated that PtR-I corresponds to the initially stalled ribosome at Ser-94. Therefore, PtR-I band intensities were measured in Figure 5A.

mtol-1 mutation (G84S) abolishes AdoMet-induced NPmRS of CGS1 (17,21,22). Translation of *GST:CGS1(mtol-1)* RNA (Supplementary Figure S6A) in Col-0 ACE in the presence of AdoMet did not show peptidyl-tRNA accumulation (Supplementary Figure S6B). These results show that the AdoMet-induced NPmRS of CGS1 is recapitulated in Col-0 ACE (23).

1.2. The hCMV System in Col-0 ACE

The 22-amino-acid nascent peptide of hCMV *gp48* uORF2 causes ribosome stalling autonomously to downregulate *gp48* expression during the early stages of infection (28,65). This reaction occurs in WGE and the structure of stalled ribosome in WGE has been solved by cryo-EM (14,16), but has not been studied in ACE.

Autonomous ribosome stalling of the hCMV system was analyzed in Col-0 ACE (Supplementary Figure S10). *TagI:DP75:hCMV* RNA (Supplementary Figure S10B) carries *M8:His:HA* tags (*TagI*) and DP75 linker fused in-frame to the N-terminus of hCMV *gp48* uORF2. DP75 linker (15,43) was used to facilitate the detection of short polypeptide. After the translation of *TagI:DP75:hCMV(WT)* RNA in Col-0 ACE, translation products were analyzed by immunoblotting using anti-HA antibody, which detected 15-kDa full-length product and RNase-sensitive 37-kDa peptidyl-tRNA bands. In contrast, the translation of *TagI:DP75:hCMV(P21A)* RNA produced only 15-kDa full-length product (Supplementary Figure S10C). The *P21A* mutation has been reported to abolish the NPmRS (15,28). The results show that autonomous ribosome stalling of the hCMV system is recapitulated in Col-0 ACE.

For the reporter assay in Figure 7A, *5'-hCMV:LUC* RNA that carries the 5'-UTR of hCMV *gp48* fused to *LUC* reporter gene (Supplementary Figure S10D) was used.

1.3. The AAP System in Col-0 ACE

N. crassa arg-2 codes for an enzyme involved in L-arginine biosynthesis. The 24-amino-acid nascent peptide of AAP, the sequence encoded by *arg-2* uORF, directs the ribosome to stall in response to L-arginine during translation termination of AAP in WGE (24,25). This reaction occurs in WGE and the structure of the stalled ribosome in WGE has been solved by cryo-EM (14), but has not been analyzed in ACE.

L-Arginine-induced ribosome stalling of the AAP system was analyzed in Col-0 ACE (Supplementary Figure S12). Since anti-HA antibody only poorly detected the translation products, the

experiments were carried out using *TagII:DP75:AAP* RNA that carry *M8:His:HA:3xFLAG:Myc* tag sequences (Supplementary Figure S12B) and the translation products were detected using anti-FLAG antibody. Translation of *TagII:DP75:AAP(WT)* RNA in the presence of 2.08 mM L-arginine produced RNase-sensitive 40-kDa peptidyl-tRNA in addition to 25-kDa full-length product, and the peptidyl-tRNA accumulation was evidently detected at 10 min after the start of translation (Supplementary Figure S12C). The accumulation of 40-kDa peptidyl-tRNA was also detected with 0.08 mM L-arginine, which is the basal L-arginine concentration in ACE (23), although the level of accumulation was lower than at 2.08 mM. This is consistent with a previous report describing that L-arginine-induced stalling was observed even at 0.01 mM (24). The accumulation of peptidyl-tRNA was diminished when *TagII:DP75:AAP(D12N)* RNA was translated in the presence of 2.08 mM L-arginine (Supplementary Figure S12C and D). The *D12N* mutation has been reported to abolish L-arginine-induced NPmRS of AAP (24). The results show that L-arginine-induced NPmRS of AAP is recapitulated in Col-0 ACE.

1.4. The AtAMD1 System in Col-0 ACE

AtAMD1 codes for an enzyme involved in spermidine and spermine biosynthesis in Arabidopsis. The 52-amino-acid nascent peptide of S-uORF directs the ribosome to stall in response to high concentrations of polyamines during translation termination of S-uORF in WGE (31). This reaction is only partially characterized in ACE (31).

Polyamine-induced ribosome stalling of the AtAMD1 system was analyzed in Col-0 ACE (Supplementary Figure S13). As an effector, spermidine was used in the present study (31). Polyamines are necessary for *in vitro* translation, but are inhibitory at high concentrations. We previously determined spermidine concentrations for stalling assays of AtAMD1 in WGE (31). In the present study, we confirmed that the same concentrations of spermidine (0.2 mM and 0.7 mM as control and stalling conditions, respectively) can be used in ACE. The spermidine concentration for the standard translation reaction in ACE is 0.5 mM (23).

TagI:DP75:S-uORF(WT) RNA (Supplementary Figure S13B) was translated in Col-0 ACE in the presence of 0.2 or 0.7 mM spermidine and analyzed by immunoblotting using anti-HA antibody (Supplementary Figure S13C). In the presence of 0.7 mM spermidine, RNase-sensitive 37-kDa peptidyl-tRNA was detected in addition to 18-kDa full-length product, and the accumulation of peptidyl-tRNA was dependent on the spermidine concentration (Supplementary Figure S13D and E). Introduction of a frame-shift mutation in S-uORF abolished the peptidyl-tRNA accumulation (Supplementary Figure S13C), as previously reported (31). These results show that polyamine-induced NPmRS of AtAMD1 is recapitulated in Col-0 ACE.

For the reporter assay in Figure 7B, 5'-*AtAMD1:LUC* RNA that carries the 5'-UTR of *AtAMD1* (Supplementary Figure S13A) fused to *LUC* reporter gene (Supplementary Figure S13F) was used. When the RNA carrying the WT S-uORF sequence was translated in Col-0 ACE, the reporter activity was reduced as the concentration of spermidine was increased, whereas the reporter activity was significantly higher if the S-uORF sequence bears a frame-shift mutation (Supplementary Figure S13G).

1.5. The MAGDIS System in Col-0 ACE

mAMD1 codes for an enzyme involved in spermidine and spermine biosynthesis in mammals. The six-amino-acid uORF sequence, MAGDIS, of *mAMD1* directs the ribosome to stall in response to high concentrations of polyamines in WGE (32,33). The ribosome stalling occurs at the termination codon of the uORF (32,33). Both *mAMD1* and *AtAMD1* genes codes for AdoMet decarboxylase, and are regulated by a uORF in a polyamine-dependent manner. However, the lengths and amino acid sequences of the uORFs are quite different.

Polyamine-induced ribosome stalling of the MAGDIS system was analyzed in Col-0 ACE (Supplementary Figure S14). Since anti-HA antibody barely detected a peptidyl-tRNA band, *TagII:DP75:MAGDIS(WT)* RNA (Supplementary Figure S14B) was translated in Col-0 ACE in the presence of 0.2 or 0.7 mM spermidine. Immunoblot analysis using anti-FLAG antibody detected double bands of ~38-kDa peptidyl-tRNA when translated in the presence of 0.7 mM spermidine, while 20-kDa full-length product predominated when translated in 0.2 mM spermidine (Supplementary Figure S14C,

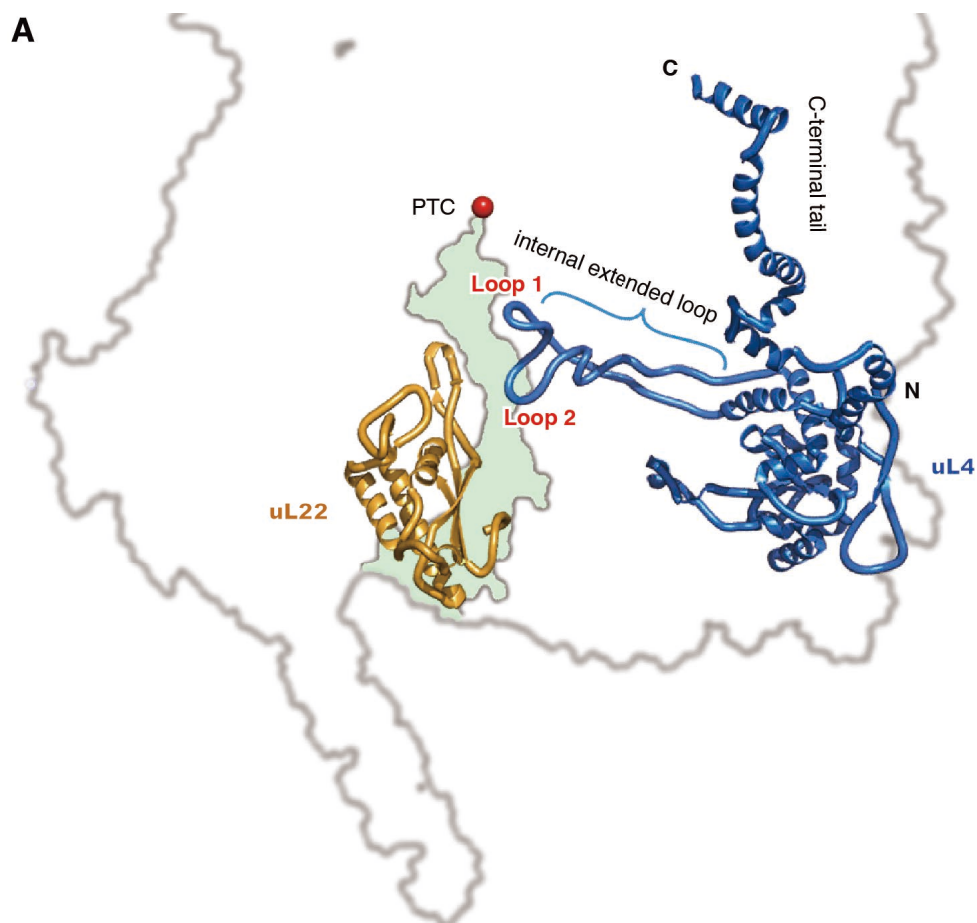
lanes 1 and 2). The accumulation of peptidyl-tRNA was evident at 10 min of translation (Supplementary Figure S14D) and was dependent on the spermidine concentration (Supplementary Figure S14E and F). When *TagII:DP75:MAGDIS(I5L)* RNA, which carries a mutation that abolishes the polyamine-dependent NPmRS of MAGDIS (32), was used, peptidyl-tRNA accumulation was diminished. These results show that polyamine-induced NPmRS of *mAMD1* is recapitulated in Col-0 ACE. Although the origin of the double bands for the peptidyl-tRNA is unknown, the intensities of the two bands paralleled in each of the experiments in Supplementary Figure S14. Therefore, we used both bands for calculation of stalling efficiencies in Supplementary Figure S14F and Figure 5E.

For the reporter assay in Figure 7C, *5'-mAMD1:LUC* RNA that carries the 5'-UTR of *mAMD1* (Supplementary Figure S14A) fused to *LUC* reporter gene (Supplementary Figure S14G) was used.

1.6. The AUG-Stop System in Col-0 ACE

The expression of Arabidopsis *NIP5;1*, encoding a boric acid transporter, is downregulated by ribosome stalling in response to high concentrations of boric acid at the minimum uORF, AUG-Stop, which is coupled with *NIP5;1* mRNA degradation in WGE. We used a 306-nt 5'-UTR containing uORF3 and uORF4 (Supplementary Figure S17A and B) (34), of which uORF4 is the AUG-Stop. In general, at both the start and the termination codons, decoding by the ribosome takes longer than at other codons, and boric acid induces prolonged ribosome stalling at AUG-Stop. For this response, the AUG codon has to be directly followed by one of the stop codons, and insertion of even a single codon is detrimental to the response (34). This reaction has been studied in WGE (34), but not in ACE.

When *5'-NIP5;1(WT):LUC* RNA (Supplementary Figure S17B) was translated in Col-0 ACE, relative reporter activity was reduced in a boric acid-dependent manner. In contrast, disruption of AUG abolished the response (Supplementary Figure S17C). These results show that the response of AUG-Stop to boric acid is recapitulated in Col-0 ACE.



Supplementary Figure S1. Structure and amino acid sequence alignment of uL4. **(A)** Structure of wheat uL4 deduced by cryo-EM (PDB 4V7E) (54). The internal extended loop, Loops 1 and 2, C-terminal tail, and N- and C-termini of uL4 are marked. uL22, the exit tunnel (light green), and PTC are also shown.

Next page: (B) Alignment of amino acid sequences of Arabidopsis uL4 paralogs, uL4A (At_uL4A; GenBank accession no. NP_187574) and uL4D (At_uL4D; accession no. NP_195907), wheat (*Triticum aestivum*) uL4 (Ta_uL4; Ensembl Plants id TraesCS4A02G091100), and yeast paralogs uL4A (Sc_uL4A; accession no. NP_009587) and uL4B (Sc_uL4B; accession no. NP_010295) were aligned using ClustalW (<http://www.ebi.ac.uk/Tools/msa/clustalw2/>). Alignments of Arabidopsis paralogs alone (At), and Arabidopsis and wheat alone (At/Ta) are also shown. Identical (asterisks) and similar (dots and colons) amino acid residues are marked. Regions of the internal extended loop (blue line) and β -loops (Loops 1 and 2; red lines) are marked above the Ta_uL4 sequence. Substituted amino acid in *R77A*, deleted amino acids in ΔTV , and $\Delta loop$ mutations in At_uL4D are reversed in violet, reversed in magenta, and underlined in brown, respectively. Wheat is hexaploid and has several copies of uL4 in its genome. One of the uL4 paralogs on chromosome 4A is shown here (66).

B

```

At_uL4A  -MAAAAARPLVTIQTL DGD MSTDQSSTVVL PDVMTAPVRP DIVNFVHAQISNNSRQPYAV 59
At_uL4D  MVASAAARPLVTVQGL DGD MSTDQSSTVTL PDVMTAPVRP DIVNFVHAQISNNSRQPYAV 60
    At    :*****.* *****.* *****.* *****.* *****.* *****.* *****.*
           Ta_uL4  --MATTARPLVSVKAL DGD MPTDAAG -VMPHVMKAPIRP DVITFVHRLVSCNSRQPYAV 57
           At/Ta  ::*****:: *****.* : * : * . * . * . * . * . * . * . * . * . * . * . *
Sc_uL4A  ----MSRPQVTVHSLT GEAT ----ANALPLPAVFSAPIR PDIVHTVFTSVNKNKRQAYAV 52
Sc_uL4B  ----MSRPQVTVHSLT GEAT ----ANALPLPAVFSAPIR PDIVHTVFTSVNKNKRQAYAV 52
           All   :** *::: * * : . : : * * . * . * . * . * . * . * . * . * . * . *

At_uL4A  SKKAGHQ TSAESWG TGRAV SRIPRV PGGG THRAGQA AFGNMCRGGRMFAPTKIWRRHRR 119
At_uL4D  SKKAGHQ TSAESWG TGRAV SRIPRV PGGG THRAGQA AFGNMCRGGRMFAPTKIWRRHRR 120
    At    *****.* *****.* *****.* *****.* *****.* *****.* *****.*
           Loop 1   Loop 2   Internal extended loop
           Ta_uL4  SRKAGHQ TSAESWG TGRAV SRIPRV GGGG THRSQGF AFGNMCRGGRMFAPT R IWRKHRR 117
           At/Ta  * . * . * . * . * . * . * . * . * . * . * . * . * . * . * . * . * . * . * . * . * . *
Sc_uL4A  SEKAGHQ TSAESWG TGRAVARI PRVGGG TGRS GQGF AFGNMCRGGRMFAPT KTWRKWNVK 112
Sc_uL4B  SEKAGHQ TSAESWG TGRAVARI PRVGGG TGRS GQGF AFGNMCRGGRMFAPT KTWRKWNVK 112
           All   * . * . * . * . * . * . * . * . * . * . * . * . * . * . * . * . * . * . * . * . * . *

At_uL4A  VNVNMKRHAI VSAI AATAVPAL VMARGHKI ENVPEMPL VVSDSAEAVEK T SAAIKV LKQI 179
At_uL4D  VNVNMKRHAI VSAI AATAVPAL VMARGHKI ENVPEMPL VVSDSAEAVEK T SAAIKV LKQI 180
    At    *****.* *****.* *****.* *****.* *****.* *****.* *****.*
           Ta_uL4  VNIRLRRVAVASAL AATAVPAIVTARGHR IE SVPEFPL VVSDSAEGIEK T SQAVKVLKQL 177
           At/Ta  ** . : . * * : . * . * . * . * . * . * . * . * . * . * . * . * . * . * . * . * . * . * . * . *
Sc_uL4A  VNHNEKRYAT ASAI AATAVAVASL VLARGHRVEKI PEIPLV VSTDLESIQKTKEAVAALKAV 172
Sc_uL4B  VNHNEKRYAT ASAI AATAVAVASL VLARGHRVEKI PEIPLV VSTDLESIQKTKEAVAALKAV 172
           All   ** . : . * * : . * . * . * . * . * . * . * . * . * . * . * . * . * . * . * . * . * . * . *

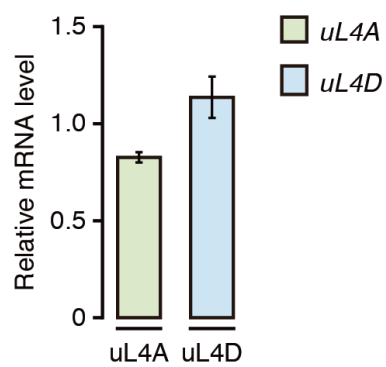
At_uL4A  GAYD DAEKAKN SIGIRP GKGMNR RRYISR KGPLVVYGT EGSKI VKAFRNL PGVELCHVE 239
At_uL4D  GAYD DAEKAKN SIGIRP GKGMNR RRYISR KGPLVVYGT EGSKI VKAFRNL PGVELCHVE 240
    At    *****.* *****.* *****.* *****.* *****.* *****.* *****.*
           Ta_uL4  GAYADADKAKDSV GIRP GKGMNR RRYINR KGPLIVYATE GSKI VKAFRNL PGVDVANVE 237
           At/Ta  *** * . * . * . * . * . * . * . * . * . * . * . * . * . * . * . * . * . * . * . * . * . *
Sc_uL4A  GAHSDLLKVLKSK KLRAG KGKYRNRRT QR RGPLV VYAED -NGIVKAL RNVP GVETANVA 231
Sc_uL4B  GAHSDLLKVLKSK KLRAG KGKYRNRRT QR RGPLV VYAED -NGIVKAL RNVP GVETANVA 231
           All   ** : * * . * * : * . * . * . * . * . * . * . * . * . * . * . * . * . * . * . *

At_uL4A  RLNLLKLAPGGHLGRFVIWTKSAFEK LESIYGS FEKPESEKKKGYVL PRAKMNADLARI I 299
At_uL4D  RLNLLKLAPGGHLGRFVIWTKSAFEK LESIYGS FEKPESEKKKGYVL PRAKMNADLARI I 300
    At    *****.* *****.* *****.* *****.* *****.* *****.* *****.*
           Ta_uL4  RLNLLD LAPGGHLGRFVIWTE SAFKKL DEVYGSFE ASSSKKGFVL PRPKMTNADLGR LI 297
           At/Ta  ***** . * . * . * . * . * . * . * . * . * . * . * . * . * . * . *
Sc_uL4A  SLNLLQLAPGAHLGRFVIWTEA AFTKLDQVWGSETV -ASSKVGYTLP SHIISTSDVTRI I 290
Sc_uL4B  SLNLLQLAPGAHLGRFVIWTEA AFTKLDQVWGSETV -ASSKVGYTLP SHIISTSDVTRI I 290
           All   **** . * . * . * . * . * . * . * . * . * . * . * . * . * . * . * . * . * . * . * . *

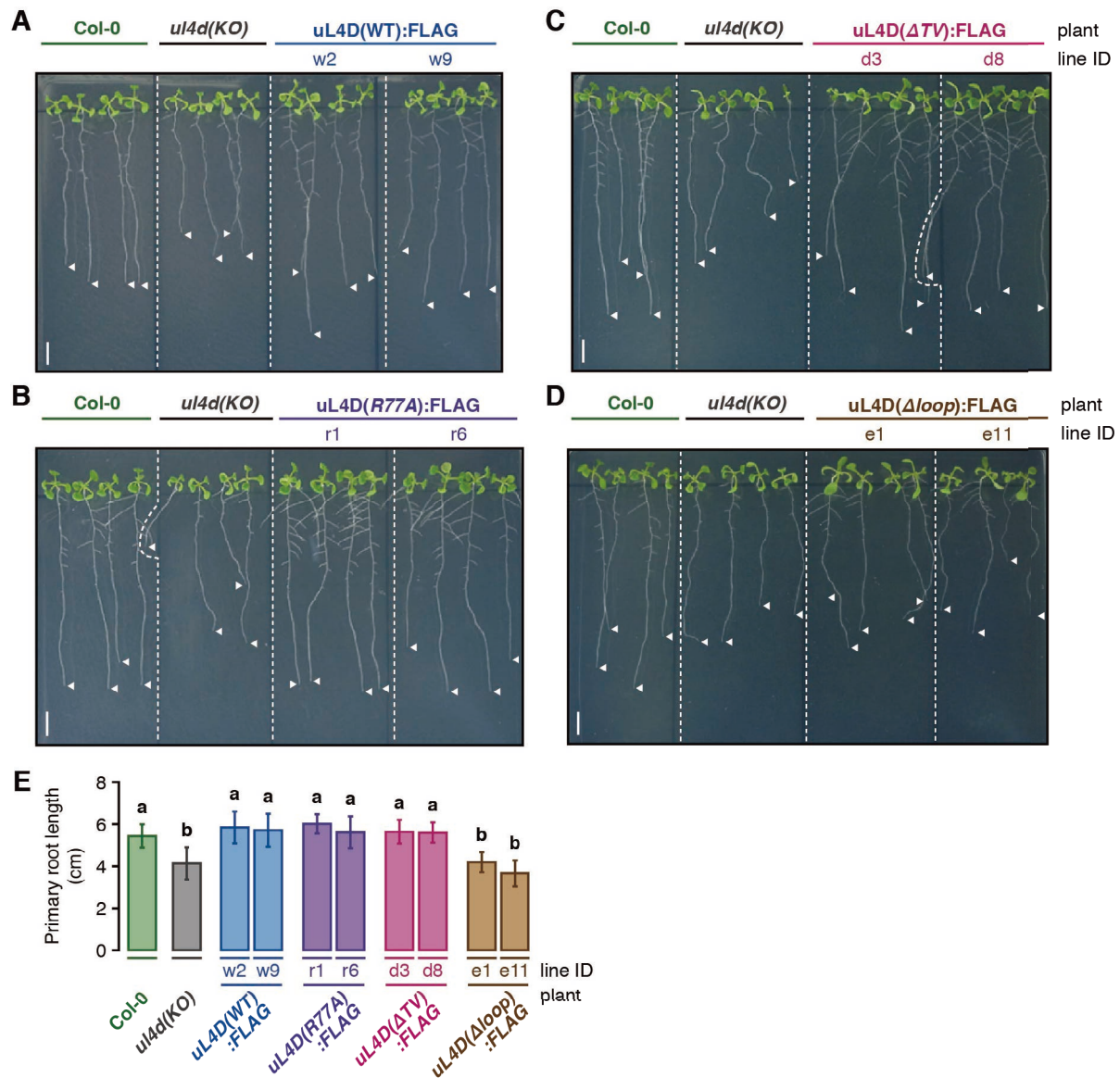
At_uL4A  NSDEIQSVVNP I KDAKRA --VLKKNPLKNLN VMLKLN PYAKTAKRMSLLAEARV KAKK 357
At_uL4D  NSDEVQSVVNP I KDGSKRA --VLKKNPLKNLN VMF KLN PYAKTAKRMSLLAEASRV KAKK 358
    At    **** . * . * . * . * . * . * . * . * . * . * . * . * . * . * . * . * . * . * . * . * . *
           Ta_uL4  NSDEVQSVVKPINKEVKRR --EARKNPLKNAAV LKLN PYFGTARRMAVLA EAARV KARK 355
           At/Ta  **** . * . * . * . * . * . * . * . * . * . * . * . * . * . * . * . * . * . * . * . * . *
Sc_uL4A  NSSEIQSAIRPAGQATQKRTHV LKKNPLKNKQVLLRL NPYAKVFA -----A 336
Sc_uL4B  NSSEIQSAIRPAGQATQKRTHV LKKNPLKNKQVLLRL NPYAKVFA -----A 336
           All   ** . * . * . * . * . * . * . * . * . * . * . * . * . * . * . * . * . * . * . * . * . *

At_uL4A  EKLAKRKT VTK EEALAIK AAGKSWYKTM ISDS DYTEFD NFTKWL GASQ 406
At_uL4D  EKLEKKR KV TKEEAQA IKAAGKAWYQ TM ISDS DYTEFD NFTKWL GASQ 407
    At    *** * . * . * . * . * . * . * . * . * . * . * . * . * . * . * . * . * . * . * . * . * . *
           Ta_uL4  DKINSRKT LSV EEASK IKAAGKAWYQ TM ISDS DYMED VFVSKWLV GSQ 404
           At/Ta  . * . * . * . * . * . * . * . * . * . * . * . * . * . * . * . * . * . * . * . * . *
Sc_uL4A  EKLGSKK ----AEKTG TKPA -AVF TETLKH D----- 362
Sc_uL4B  EKLGSKK ----AEKTG TKPA -AVFAETLKH D----- 362
           All   . * : . * : * * * : : * : *

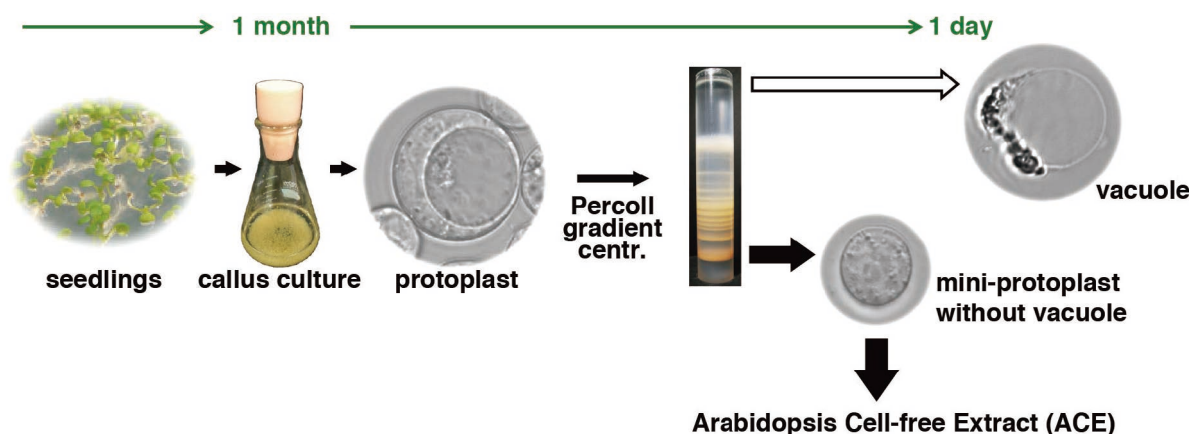
```



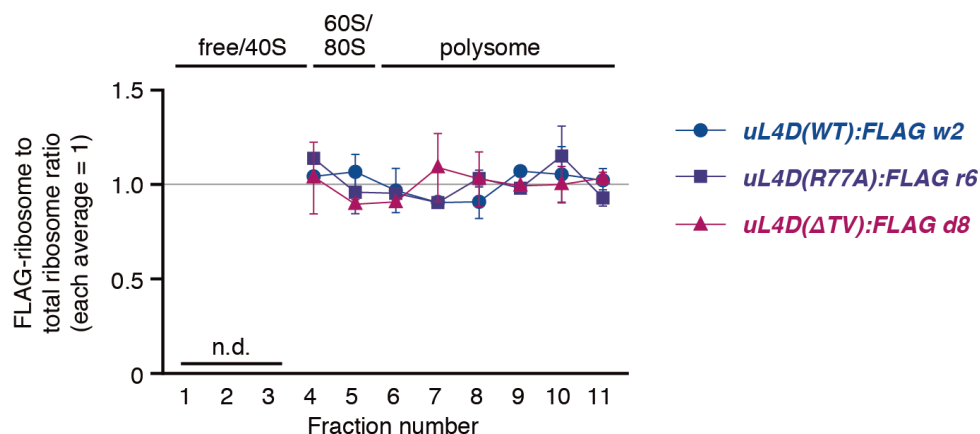
Supplementary Figure S2. Accumulation levels of *uL4A* and *uL4D* mRNAs in wild-type Col-0 plants. Total RNA was extracted from rosette leaves 4 weeks after imbibition. *uL4A* and *uL4D* mRNAs were quantified by qRT-PCR using *UBQ5* mRNA as a control. Relative amounts of *uL4A* and *uL4D* mRNAs were calculated by using known amounts of *uL4A* and *uL4D* cDNAs as standards.



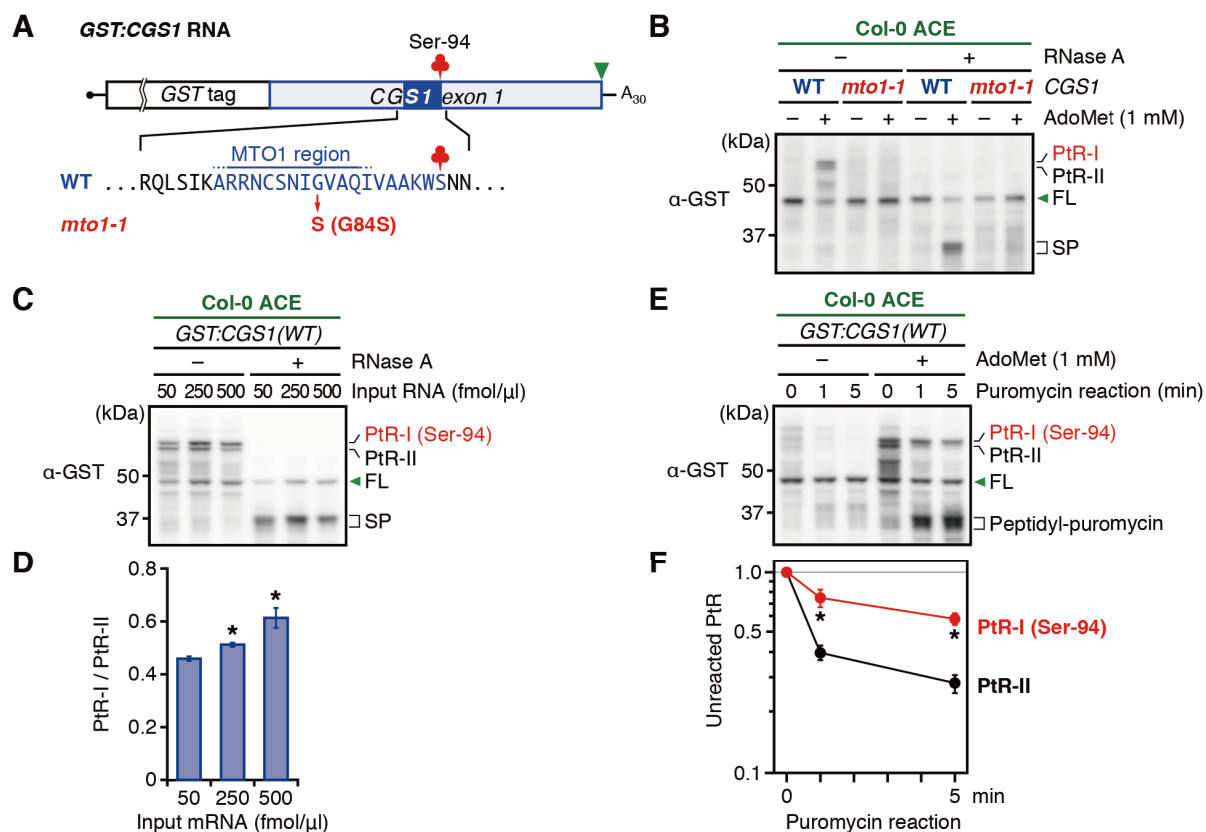
Supplementary Figure S3. FLAG-tagged uL4Ds complement the short-root phenotype of *ul4d(KO)* plants. Wild-type Col-0 plants, *ul4d(KO)*, and transgenic plants expressing FLAG-tagged uL4D(WT) (A), uL4D(R77A) (B), uL4D(ΔTV) (C), or uL4D(Δloop) (D) were grown for 10 days on half-strength MS medium plates under long-day conditions. Arrowheads indicate the tip of the primary roots. Bars = 10 mm. (E) Primary root lengths in (A–D) were measured and means ± SD ($n > 7$) are shown. Different letters indicate significant differences ($p < 0.05$, Tukey-Kramer test).



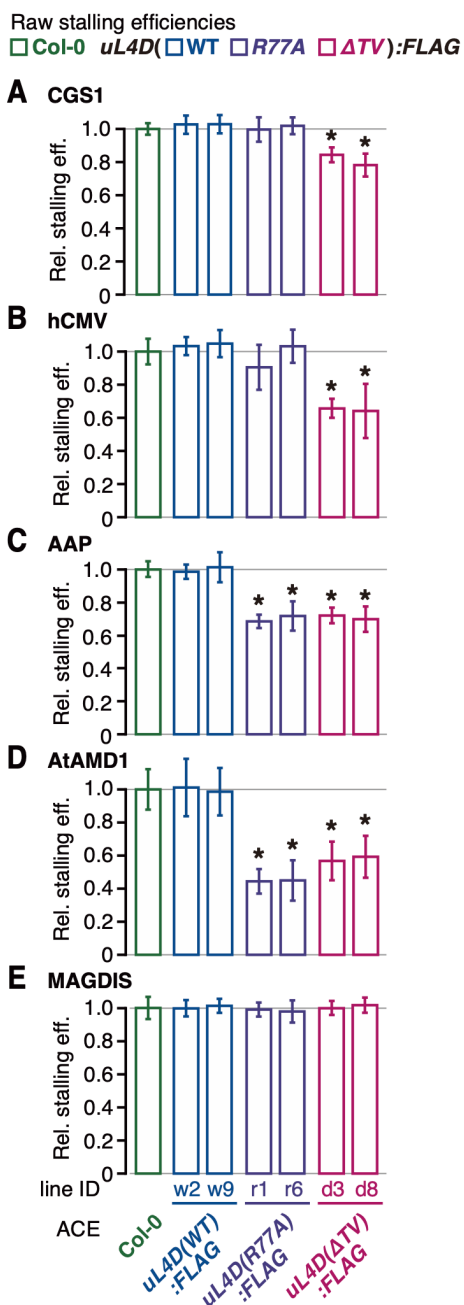
Supplementary Figure S4. Outline of the preparation of ACE *in vitro* translation system from Arabidopsis seedlings (23). One-week-old Arabidopsis seedlings were minced and were cultured with rotatory shaking in the dark. The culture medium was changed every 6 days. Three days after the third medium change, protoplasts were prepared. Plant cells have a large central vacuole that contains nucleases and proteases. The protoplasts were subjected to Percoll gradient centrifugation to obtain evacuated mini-protoplasts from which vacuoles were removed. The evacuated mini-protoplasts were disrupted using a Dounce homogenizer and the lysate was used to prepare an ACE *in vitro* translation cocktail. ACE can be prepared 1 month after sowing Arabidopsis seeds. Note that the ACE preparation protocol (23) has a typographical error of m/μ (67).



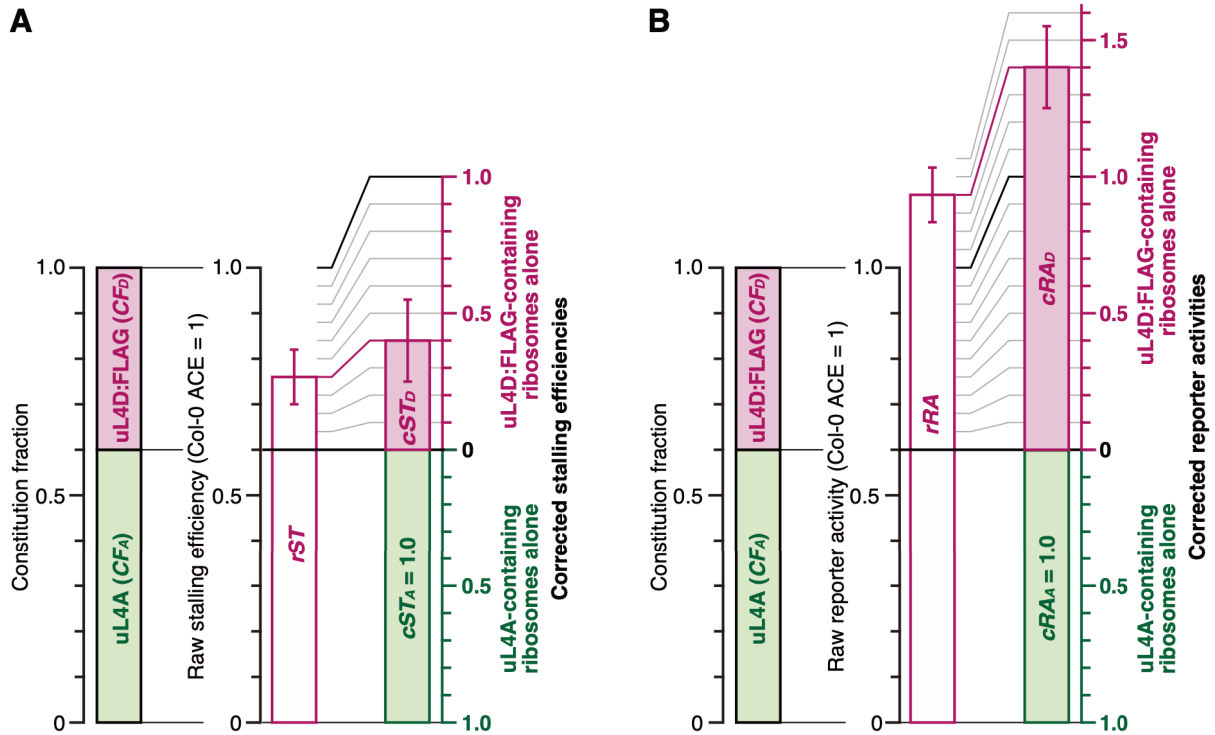
Supplementary Figure S5. Distribution of FLAG-tagged mutant uL4D-containing ribosomes in the polysome profiling. The immunoblot signals in Figure 4B were quantified and the distributions of FLAG-tagged mutant uL4D-containing ribosomes (detected by using anti-FLAG antibody) among total ribosome (detected by using anti-uL22 antiserum) were calculated. The positions of free proteins and 40S subunit, 60S subunit, 80S ribosome, and polysome fractions are indicated. The y-axis was set so that the means of *uL4D(WT):FLAG w2* line, *uL4D(R77A):FLAG r6* line, and *uL4D(ΔTV):FLAG d8* line are 1. Means \pm SD of two biological repeats are shown.



Supplementary Figure S6. The CGS1 system in Col-0 ACE. **(A)** Schematic representation of *GST:CGS1* RNA used for stalling assay (Figure 5A). The RNA carries a glutathione *S*-transferase (GST) tag sequence fused in-frame to the N-terminus of the *CGS1* exon 1 coding sequence (17,68). The amino acid sequences around the MTO1 region of the wild-type (WT) *CGS1* and *mto1-1* (G84S) mutation are shown. AdoMet-induced NPMRS occurs at Ser-94 (red clover). The MTO1 region (21) is indicated. **(B)** *GST:CGS1(WT)* and *GST:CGS1(mto1-1)* RNAs ($50 \text{ fmol } \mu\text{l}^{-1}$) were translated in Col-0 ACE for 30 min in the absence (–) or presence (+) of 1 mM AdoMet. In RNase + lanes, samples were treated with RNase A before separation by SDS-PAGE. The positions of the 45-kDa full-length product (FL), the ~55-kDa peptidyl-tRNAs (PtR-I and PtR-II), and the 35-kDa stalled peptide (SP) produced by RNase A treatment are indicated. A representative result of duplicate experiments is shown. **(C)** *GST:CGS1(WT)* RNA was translated in Col-0 ACE at different RNA concentrations for 30 min. In RNase + lanes, samples were treated with RNase A before separation by SDS-PAGE. A representative result of triplicate experiments is shown. Bands are marked as in (B). **(D)** The immunoblot signals in (C) were quantified and relative intensity of PtR-I to PtR-II was calculated. Means \pm SD of three independent experiments are shown. Asterisks indicate significant differences compared with the standard condition at $50 \text{ fmol } \mu\text{l}^{-1}$ RNA ($p < 0.05$, Welch's *t*-test). **(E)** *GST:CGS1(WT)* RNA was translated in Col-0 ACE. After 30 min of translation, puromycin was added at a final concentration of 2 mM and samples were withdrawn at the indicated time points. The position of the 35-kDa peptidyl-puromycin is indicated. A representative result of triplicate experiments is shown. **(F)** The immunoblot signals in (E) were quantified, and the intensity of unreacted peptidyl-tRNA was normalized to that at time 0. Means \pm SD of three independent experiments are shown. Asterisks indicate significant differences between PtR-I and PtR-II at each time point ($p < 0.05$, Welch's *t*-test).



Supplementary Figure S7. Raw stalling efficiencies. (A–E) The raw stalling efficiencies corresponding to the right panels of Figure 5A–E, respectively, are shown. Asterisks indicate significant differences compared with Col-0 ACE ($q < 0.05$ by Welch's t -test with FDR correction).



Supplementary Figure S8. Correction of raw values of stalling efficiencies and reporter activities for the constitution fraction of uL4D mutant ribosome.

(A) Correction of the stalling efficiency. The raw stalling efficiency relative to Col-0 ACE (rST) contains contributions from both FLAG-tagged mutant uL4D- and endogenous uL4A-containing ribosomes. To evaluate the stalling efficiencies of the mutant uL4D-containing ribosomes alone, we calculated the corrected stalling efficiencies (cST_D) by taking the constitution fraction of mutant uL4D-containing ribosomes (CF_D):

$$rST = CF_A + CF_D \times cST_D, \text{ where } CF_A = 1 - CF_D.$$

Therefore,

$$cST_D = 1 - (1 - rST) / CF_D.$$

SD values before (rSD) and after correction (cSD_D) are,

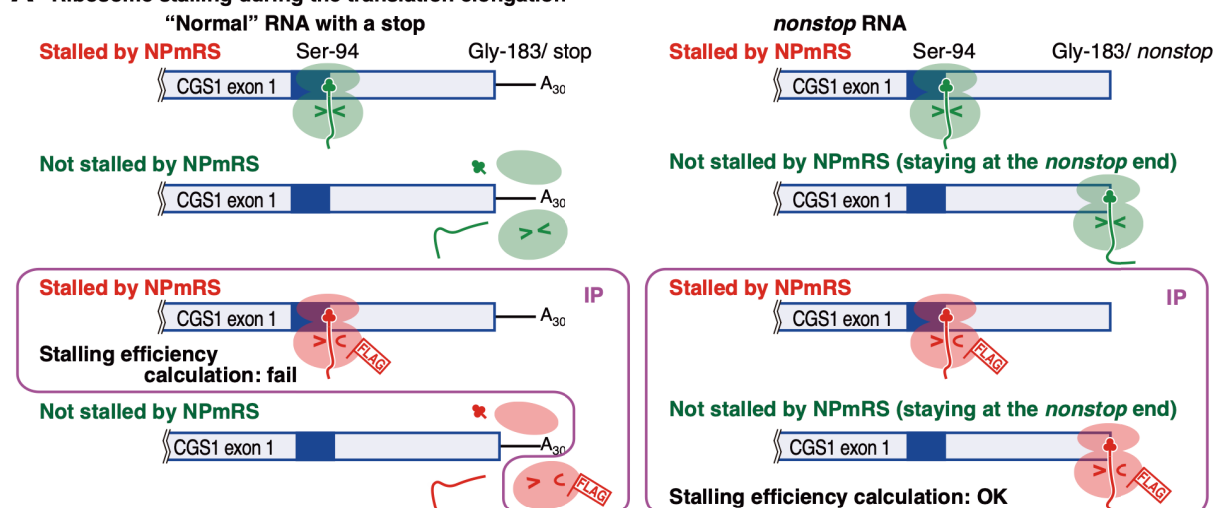
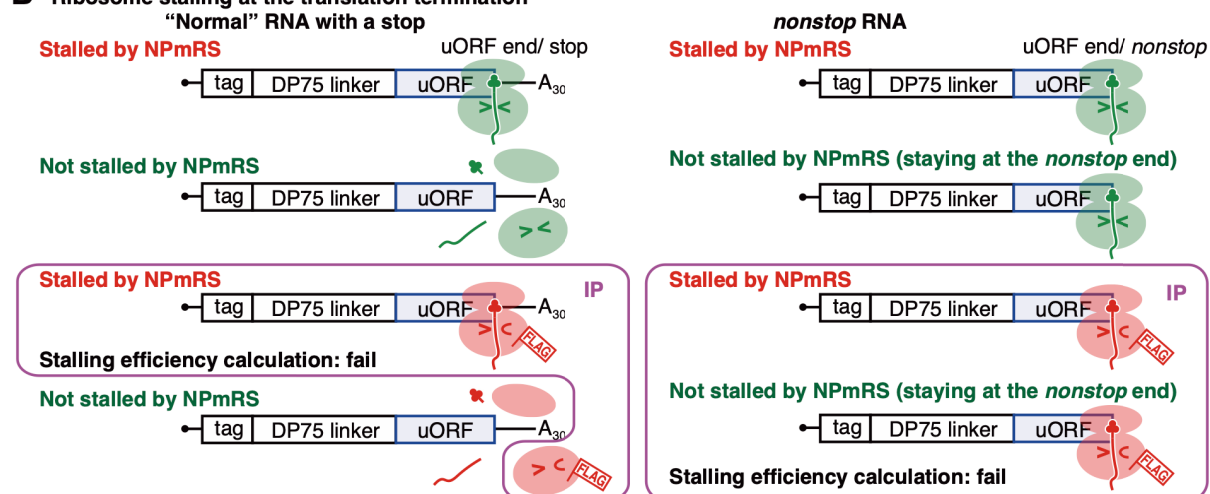
$$cSD_D = rSD / CF_D.$$

This calculation assumes that the stalling efficiency of endogenous uL4A-containing ribosomes alone (cST_A) is the same as that in Col-0 ACE (*i.e.*, $cST_A = 1$), which we believe is reasonable. The rSD value is ascribed all to cSD_D in this calculation.

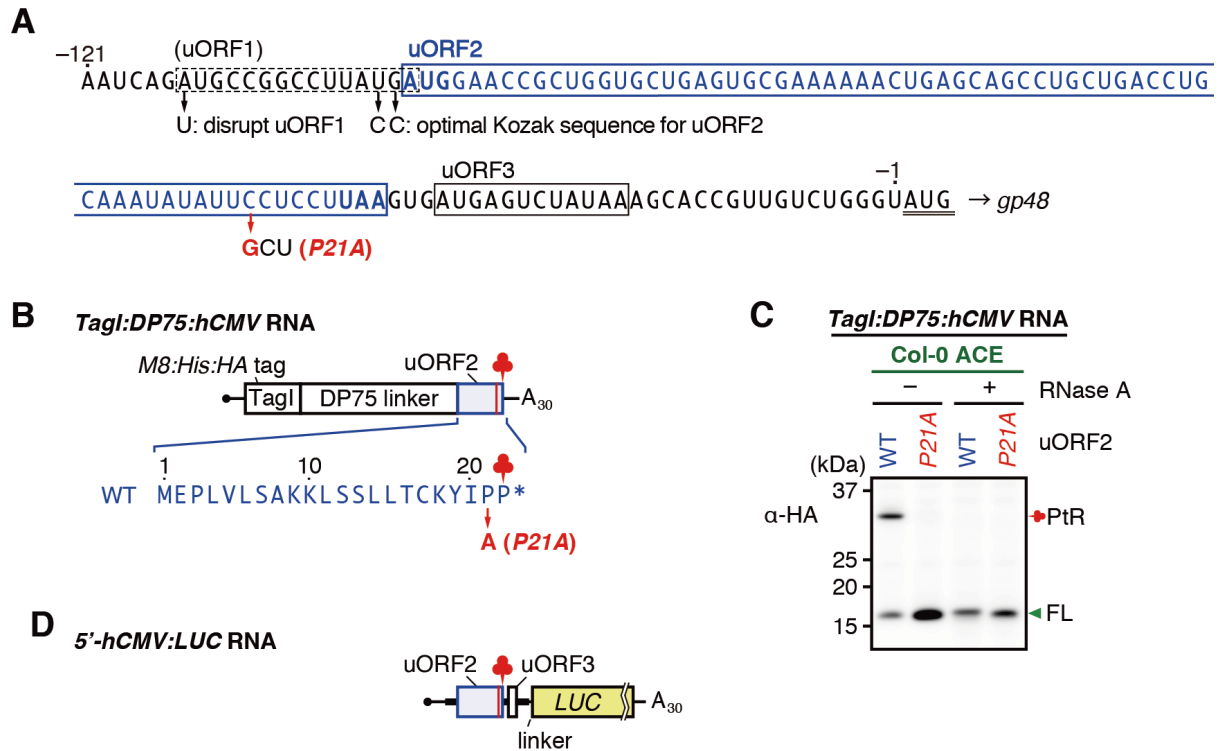
(B) Correction of the reporter activity. Likewise, the raw reporter activity relative to Col-0 ACE (rRA) and its SD values (rSD) were corrected for the constitution fraction of mutant uL4D-containing ribosomes (CF_D):

$$cRA_D = 1 - (1 - rRA) / CF_D$$

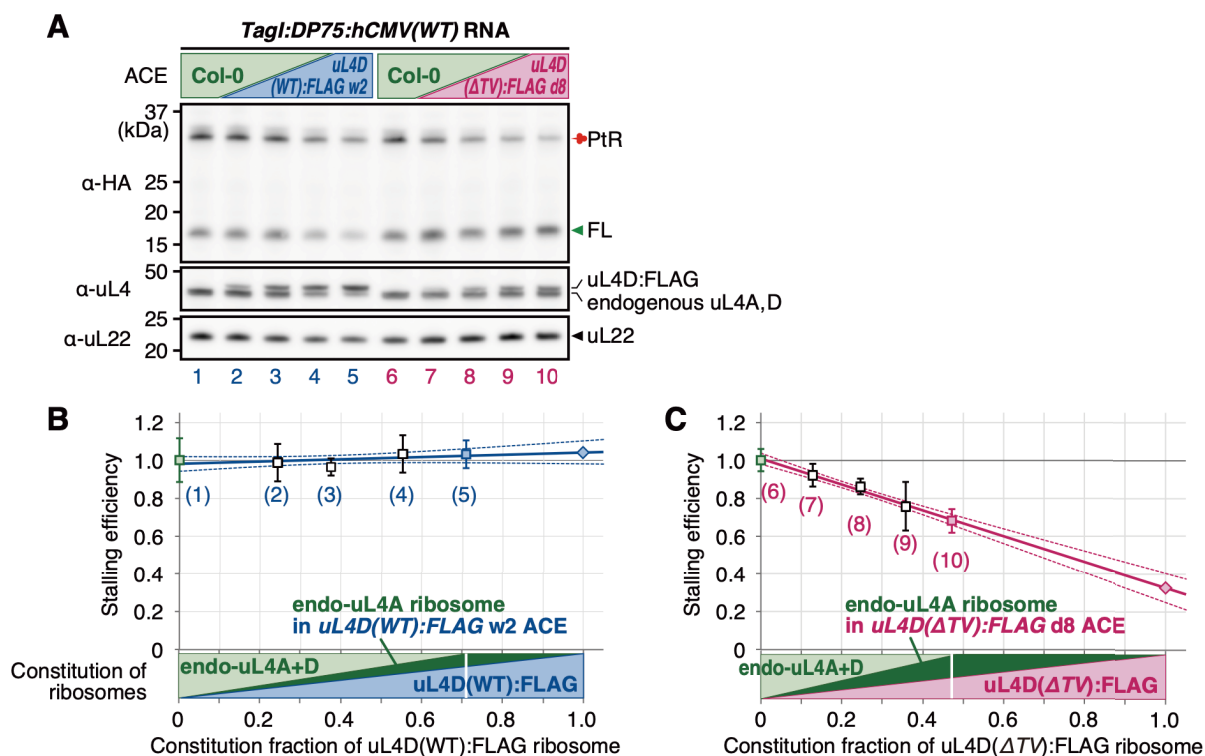
$$cSD_D = rSD / CF_D.$$

A Ribosome stalling during the translation elongation**B Ribosome stalling at the translation termination**

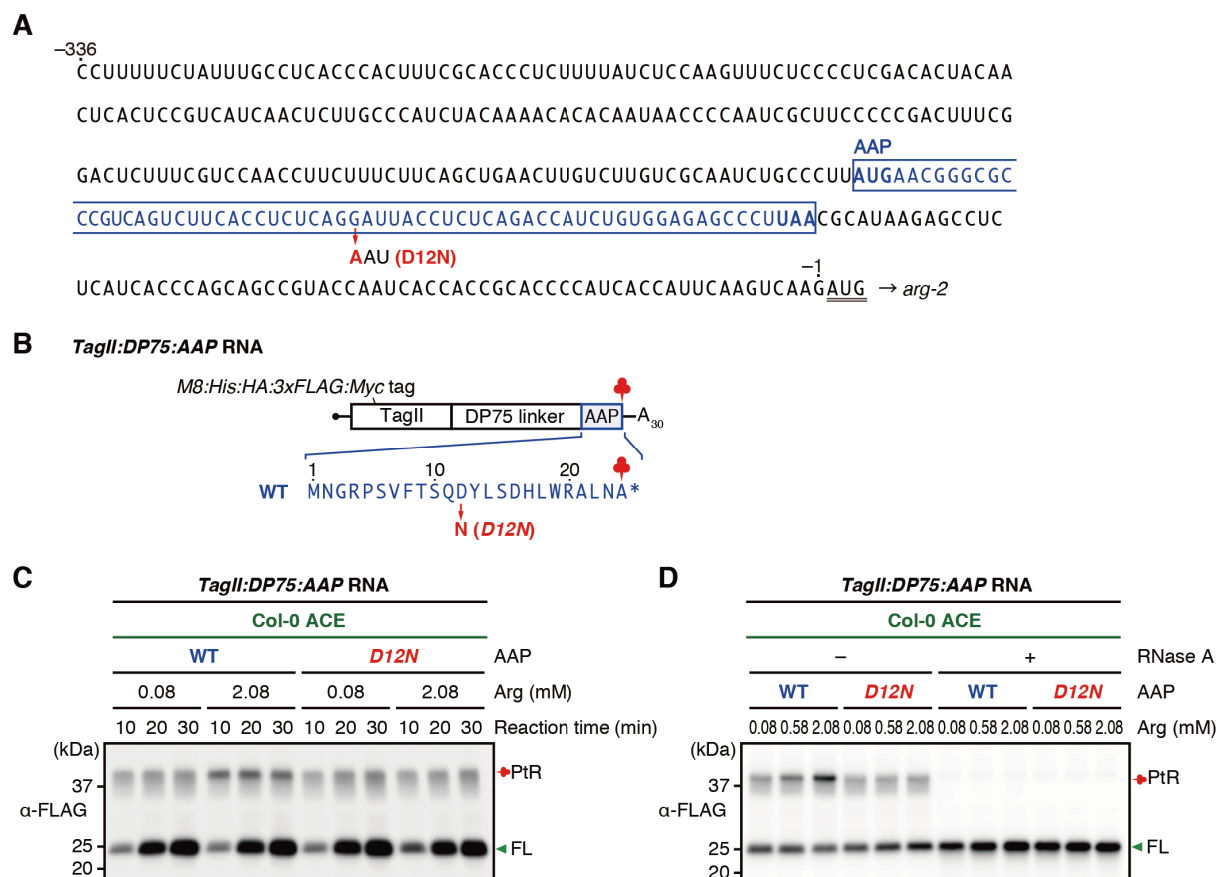
Supplementary Figure S9. Affinity purification strategy of the stalled ribosomes. The green ribosomes represent wild-type ribosomes, and the red ribosomes represent FLAG-tagged mutant ribosomes. tRNAs are represented by clovers. To calculate the stalling efficiency of FLAG-tagged mutant ribosomes alone, peptidyl-tRNAs from both stalled and non-stalled mutant ribosomes have to be purified. **(A)** Affinity purification of ribosomes stalled during the translation elongation by IP. The MTO1 region (21) is indicated by a filled blue box. *(Left)* On a “normal” RNA with a stop codon, those ribosomes that did not stall by NPmRS will translate to the stop codon and dissociate into large and small subunits and peptidyl-tRNA are hydrolyzed to tRNA and peptides. Therefore, those ribosomes that did not stall by NPmRS cannot be affinity-purified. *(Right)* On a *nonstop* RNA, those ribosomes that did not stall by NPmRS will translate to the *nonstop* RNA end and will be staying there. Therefore, both of them can be affinity-purified and stalling efficiency can be calculated. **(B)** Affinity purification of ribosomes stalled at the translation termination by IP. *(Left)* On a “normal” RNA with a stop codon, those ribosomes that did not stall by NPmRS will translate to the stop codon and dissociate into large and small subunits and peptidyl-tRNA are hydrolyzed to tRNA and peptides. Therefore, those ribosomes that did not stall by NPmRS cannot be affinity-purified. *(Right)* On a *nonstop* RNA, those ribosomes that did not stall by NPmRS will be staying at the *nonstop* RNA end. Therefore, both stalled and non-stalled ribosomes can be affinity-purified. However, stalling efficiency cannot be calculated, because these ribosomes bear the same peptidyl-tRNA species.



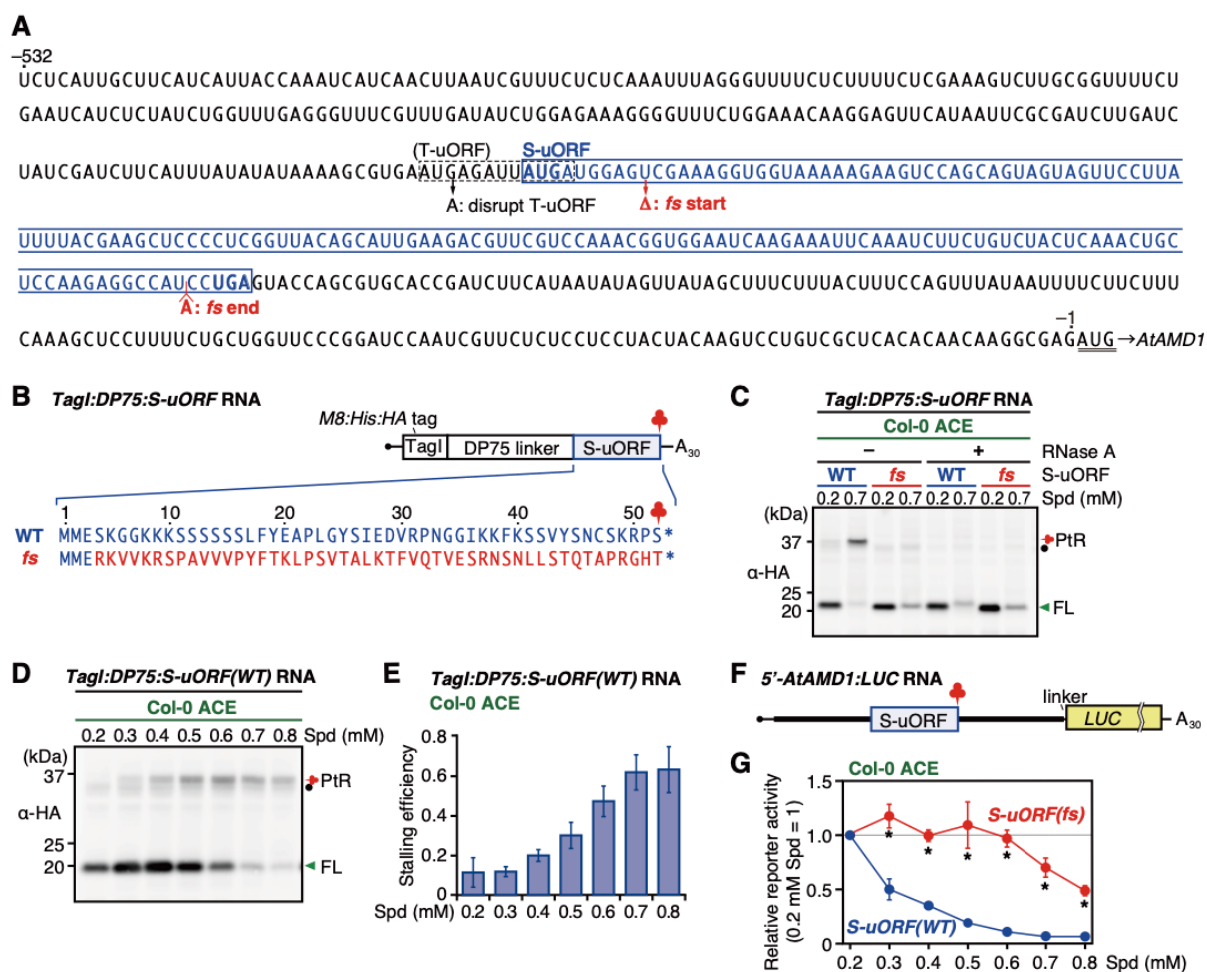
Supplementary Figure S10. The hCMV system in Col-0 ACE. (A) 5'-UTR sequence of hCMV *gp48* (46). uORFs are boxed and the start codon of *gp48* is double-underlined. uORF2 is the functional uORF for NPmRS. uORF1 (dashed box) was disrupted and the Kozak sequence for uORF2 was optimized in previous studies (27,29,46,65), and the same sequence was used in the present study. The substituted nucleotide in Pro-21 to alanine mutation (P21A) in uORF2, which abolishes the NPmRS (65), is indicated. (B) Schematic representation of *TagI:DP75:hCMV RNA* for stalling assay (Figure 5B). The uORF2 was joined in-frame to the *M8:His:HA* tags (*TagI*) and DP75 linker. The amino acid sequences of the *gp48* uORF2 and P21A mutation are shown. Ribosome stalls autonomously at the stop codon of uORF2 (red clover). (C) *TagI:DP75:hCMV(WT)* and *TagI:DP75:hCMV(P21A)* RNAs were translated in Col-0 ACE for 30 min. Translation products were separated by SDS-PAGE and analyzed by immunoblotting using anti-HA antibody. For RNase + lanes, samples were treated with RNase A before separation by SDS-PAGE. The positions of the 15-kDa full-length product (FL) and the 35-kDa peptidyl-tRNA (PtR) are indicated. A representative result of duplicate experiments is shown. (D) Schematic representation of *5'-hCMV:LUC RNA* used for reporter assay (Figure 7A). The 5'-UTR sequence (-1 to -121 nt) in (A) was joined to the *LUC* reporter gene through a linker sequence, AAGCUUCC.



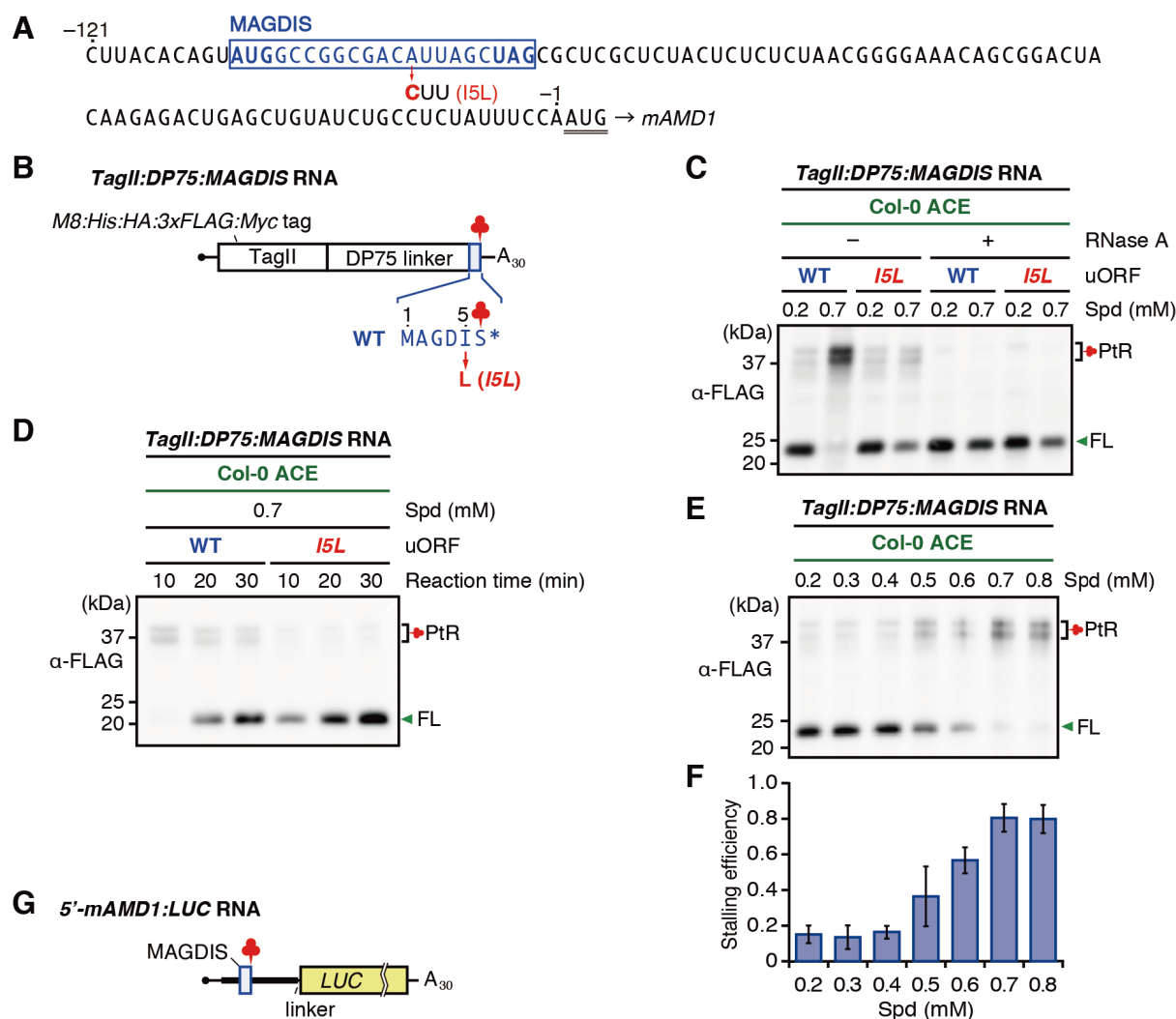
Supplementary Figure S11. Deduction of the stalling efficiencies by the mutant ribosomes alone by linear regression. (A) Col-0 ACE and uL4D(WT):FLAG line w2 ACE were mixed at 1:0, 3:1, 1:1, 1:3, and 0:1 volume ratios (lanes 1 to 5, respectively), or Col-0 ACE and uL4D(ΔTV):FLAG line d8 ACE were mixed at 1:0, 3:1, 1:1, 1:3, and 0:1 volume ratios (lanes 6 to 10, respectively). These mixtures were used to translate *Tag1:DP75:hCMV(WT)* RNA (Supplementary Figure S10B). Translation products were separated by SDS-PAGE and analyzed by immunoblotting using anti-HA antibody. Immunoblots with anti-uL4 and anti-uL22 are also shown. Positions of the full-length product (FL), peptidyl-tRNA (PtR), 48-kDa FLAG-tagged uL4Ds (uL4D:FLAG), endogenous uL4A and uL4D (uL4A, D), and 19-kDa uL22 are marked. The experiments were carried out in one of the batches of ACE preparations for each of the Col-0 and mutant lines, and a representative result of triplicate experiments is shown. (B) Linear regression (solid blue line) of stalling efficiency vs construction fraction of uL4D(WT):FLAG ribosome. Raw stalling efficiencies obtained from lanes 1–5 of (A) were plotted against the constitution fractions of the uL4D(WT):FLAG ribosome of each of the ACE mixtures (means \pm SD, $n = 3$). The constitution fraction was determined based on the intensities of the upper and lower bands of the immunoblot with anti-uL4 antibody (Figure 4C and D). The numbers in parentheses below the data refer to the lane numbers in (A). The blue diamond indicates the estimated stalling efficiency by the uL4D(WT):FLAG ribosome alone. The dashed blue curves represent the upper and lower limits of the mean prediction 95% confidence interval. (C) Linear regression (solid magenta line) of stalling efficiency vs construction fraction of uL4D(ΔTV):FLAG ribosome. Raw stalling efficiencies obtained from lanes 6–10 of (A) were plotted against the constitution fractions of the uL4D(ΔTV):FLAG ribosome of each of the ACE mixtures (means \pm SD, $n = 3$). The constitution fraction was determined as in (B). The numbers in parentheses below the data refer to the lane numbers in (A). The magenta diamond indicates the estimated stalling efficiency by the uL4D(ΔTV):FLAG ribosome alone. The dashed magenta curves represent the upper and lower limits of the mean prediction 95% confidence interval. In (B) and (C), calculated constitution fractions of endogenous uL4A- and D-containing ribosomes in Col-0 ACE (light green), endogenous uL4A-containing ribosomes in the mutant ACE (dark green), and FLAG-tagged mutant uL4D-containing ribosomes (light blue or light magenta) are shown below the graph. Note that to the right of the vertical white lines are extrapolated values. The linear regression and mean prediction 95% confidence interval were calculated using Mathematica software (Wolfram Research, Champaign, IL, USA).



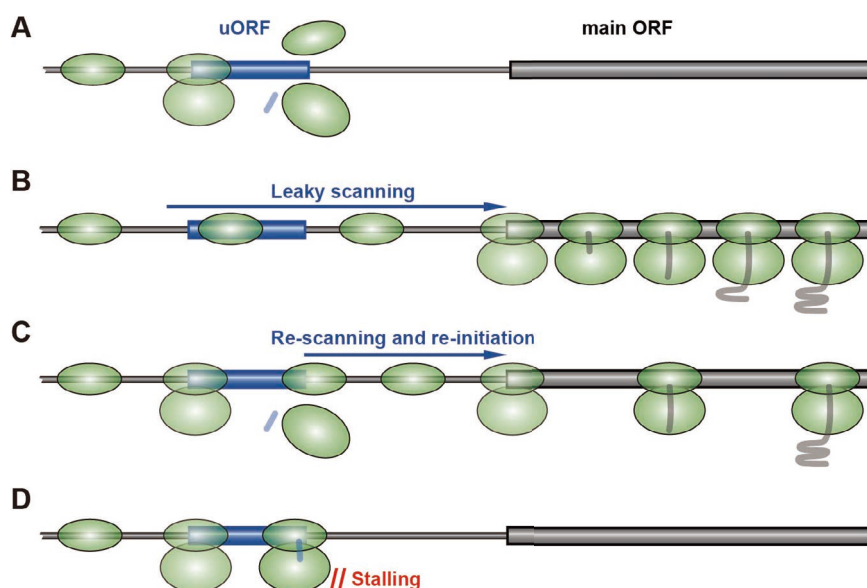
Supplementary Figure S12. The AAP system in Col-0 ACE. **(A)** The 5'-UTR sequence of *N. crassa arg-2* (24). uORF (AAP) is boxed and the start codon of *arg-2* is double-underlined. The nucleotide substituted in Asp-12 to asparagine (*D12N*) mutation is indicated. *D12N* mutation abolishes the L-arginine-dependent NPmRS of AAP (24). **(B)** Schematic representation of *TagII:DP75:AAP RNA* used for stalling assay (Figure 5C). The AAP sequence was joined in-frame to the *M8:His:HA:3xFLAG:Myc* tags (*TagII*) and DP75 linker. The amino acid sequences of AAP and *D12N* mutation are shown. L-Arginine-dependent NPmRS occurs at the stop codon (red clover). **(C)** *TagII:DP75:AAP(WT)* and *TagII:DP75:AAP(D12N)* RNAs were translated in Col-0 ACE at 0.08 or 2.08 mM L-arginine (Arg). Translation products were withdrawn at the indicated time points and analyzed by immunoblotting using anti-FLAG antibody. The positions of the 37-kDa peptidyl-tRNA (PtR) and 20-kDa full-length product (FL) are indicated. A representative result of duplicate experiments is shown. **(D)** *TagII:DP75:AAP(WT)* and *TagII:DP75:AAP(D12N)* RNAs were translated in Col-0 ACE for 10 min at different Arg concentrations. Translation products were analyzed as in (C). For RNase + lanes, samples were treated with RNase A before separation by SDS-PAGE. A representative result of duplicate experiments is shown.



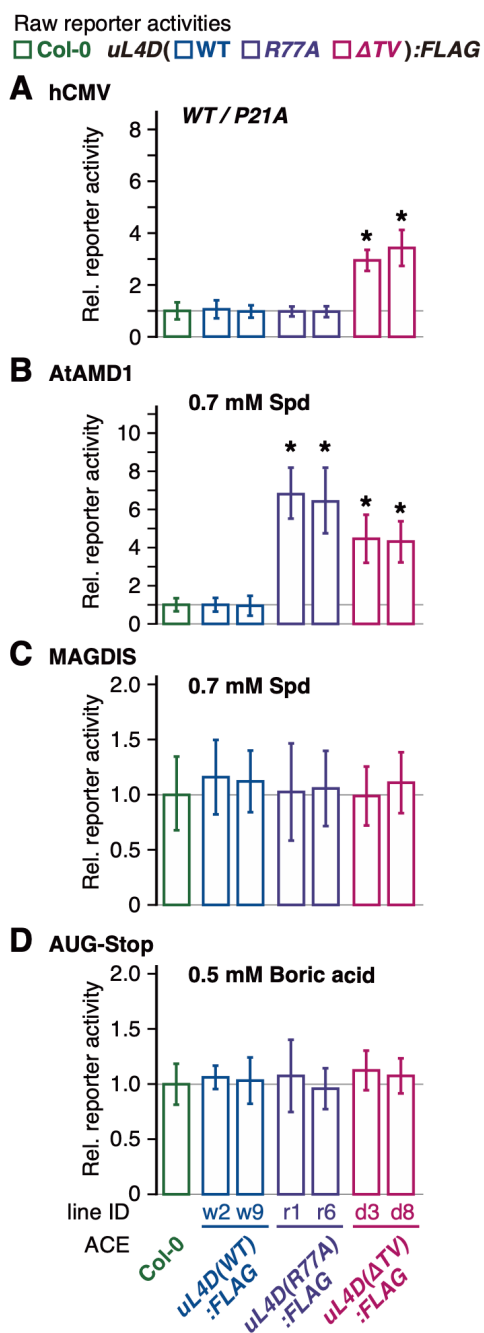
Supplementary Figure S13. The *AtAMD1* system in Col-0 ACE. (A) The 5'-UTR sequence of *AtAMD1* (31). The 5'-UTR sequence of *AtAMD1* has two uORFs, T-uORF and S-uORF (standing for Tiny-uORF and Small-uORF, respectively) (30). The S-uORF is boxed and the start codon of *AtAMD1* is double-underlined. The T-uORF was disrupted as in a previous study (31) and is marked with a dashed box. The nucleotides that are deleted and inserted to generate the frame-shift mutant are indicated. (B) Schematic representation of *TagI:DP75:S-uORF* RNA used for stalling assay (Figure 5D). The S-uORF sequence was joined in-frame to the *M8:His:HA* tags (*TagI*) and DP75 linker. The amino acid sequences of *AtAMD1* S-uORF and frame-shift (*fs*) mutation are shown. Polyamine-dependent NPMRS occurs at the stop codon of S-uORF (red clover) (31). (C) *TagI:DP75:S-uORF(WT)* and *TagI:DP75:S-uORF(fs)* RNAs were translated in Col-0 ACE for 30 min at 0.2 or 0.7 mM spermidine (Spd). Translation products were separated by SDS-PAGE and analyzed by immunoblotting using anti-HA antibody. For RNase + lanes, samples were treated with RNase A before separation by SDS-PAGE. The positions of the 37-kDa peptidyl-tRNA (PtR) and 18-kDa full-length product (FL) are indicated. A black dot indicates a nonspecific signal. A representative result of duplicate experiments is shown. (D) *TagI:DP75:S-uORF(WT)* RNA was translated in ACE at various Spd concentrations. Translation products were analyzed as in (C). A representative result of triplicate experiments is shown. (E) The immunoblot signals in (D) were quantified and the raw stalling efficiencies were calculated. Means ± SD of three independent experiments are shown. (F) Schematic representation of 5'-*AtAMD1:LUC* RNA used for reporter assay (Figure 7B). The 5'-UTR sequence (-1 to -532) in (A) was joined to the *LUC* reporter gene through a linker, CC. (G) 5'-*AtAMD1:LUC(WT)* and 5'-*AtAMD1:LUC(fs)* RNAs were translated in Col-0 ACE for 120 min at various Spd concentrations. *LUC* activity was normalized with control RLUC activity from co-translated *RLUC* RNA, and the reporter activity relative to that at 0.2 mM Spd was calculated. Means ± SD of three independent experiments are shown. Asterisks indicate significant differences at each Spd concentration ($p < 0.05$, Welch's *t*-test).



Supplementary Figure S14. The MAGDIS system in Col-0 ACE. **(A)** The 5'-UTR sequence of *mAMD1* (47,69). uORF is boxed and the start codon of *mAMD1* is double underlined. The nucleotide substituted in *I5L* mutant, which abolishes the stalling (32), is indicated. **(B)** Schematic representation of *TagII:DP75:MAGDIS* RNA used for stalling assay (Figure 5E). The uORF sequence was joined in-frame to the *M8:His:HA:3xFLAG:Myc* tags (*TagII*) and DP75 linker. The amino acid sequences of WT and *I5L* mutation are shown. **(C)** *TagII:DP75:MAGDIS(WT)* and *TagII:DP75:MAGDIS(I5L)* RNAs were translated in Col-0 ACE for 10 min at 0.2 or 0.7 mM spermidine (Spd). Translation products were analyzed by immunoblot analysis using anti-FLAG antibody. The positions of the 20-kDa full-length product (FL), and the 38-kDa peptidyl-tRNAs (PtR) are indicated. For RNase + lanes, samples were treated with RNase A before separation by SDS-PAGE. **(D)** *TagII:DP75:MAGDIS(WT)* RNA and *TagII:DP75:MAGDIS(I5L)* RNA were translated in Col-0 ACE at 0.7 mM Spd. Translation products were withdrawn at the indicated time points and analyzed by immunoblot analysis as in (C). **(E)** *TagII:DP75:MAGDIS(WT)* RNA was translated in ACE at various Spd concentrations. Translation products were analyzed as in (C). **(F)** The immunoblot signals in (E) were quantified and the raw stalling efficiencies were calculated. Means \pm SD of three independent experiments are shown. **(G)** Schematic representation of 5'-*mAMD1:LUC* RNA used for reporter assay (Figure 7C). The 5'-UTR (-1 to -121) sequence in (A) was joined to the *LUC* reporter gene through a linker, CC.



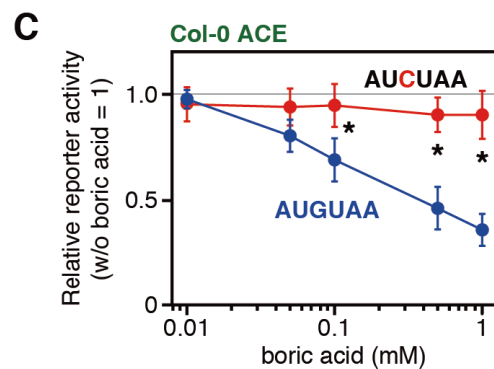
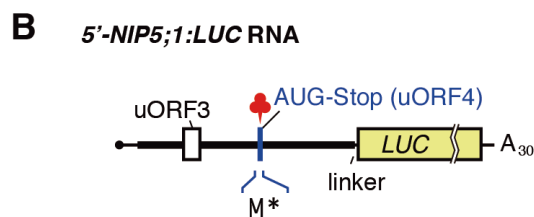
Supplementary Figure S15. Downregulation of the main ORF expression by uORF. The translation status of the uORF regulates translation of the downstream ORF, including the main ORF (59,70,71). The presence of uORF is not exceptional because 40%–50% of mRNAs in mammals and 30%–40% of mRNAs in higher plants have one or more of them (71,72). Many of the uORFs are actually translated, as evidenced by ribosome profiling analyses that showed the presence of 80S ribosomes on the uORFs (55,73). **(A)** Translation of a uORF generally downregulates the translation of the main ORF because those ribosomes that have translated the uORF will be dissociated from the mRNA (59). **(B)** The uORF may occasionally be overlooked and then translation starts at the start codon of the main ORF by a mechanism termed leaky scanning (74,75). The nucleotide sequence around the start codon, known as the Kozak sequence (70,76), of uORF plays a major role in determining the frequency of leaky scanning. **(C)** When a very short uORF is translated, the ribosome may not be fully dissociated at the termination codon and the small subunit may remain on the mRNA. The small subunit re-scans for the downstream start codon and reinitiates translation there (71,73,77). **(D)** If the ribosome stalls on the uORF, translation of the downstream ORF is severely inhibited by blocking the succeeding ribosomes (59). The ribosome stalling on uORF can occur either during translation elongation or at translation termination, while most of the known stalling events in eukaryotes occur at the termination.



Supplementary Figure S16. Raw reporter activities. (A–D) The raw reporter activities corresponding to Figure 7A–D, respectively, are shown. Asterisks indicate significant differences compared with Col-0 ACE ($q < 0.05$ by Welch's t -test with FDR correction).

A

-306
 AUUUAAGUCCUAGCUCCAUUUUCGUUUUCUUCUCUAAAAAAAAACAAAAAAAAAGUUUUUGAUCGA
 uORF3
 UUGAUGAGUUUUCUCAUUUAUUGAUCUCUCUAGUUUUAACUUGUGUUUGGUGAAACCGGUACUGGCGAAG
 UUUAAAACACAAGUGUAAACACAAAUUUAUAAAAUUUCAAAUCAUGUAAAUUUCGUCUCUAUCAUUUA
 uORF4
 AUCUAA
 UUUCCCCUCACCAAAAAAAAAACAAAAAAAAUUAGAAUUUAGUACUUUUUUUUUAAACAAAAACAAAAA
 AAAAAACAAAAAACGUUGGAAAUG
 -1



Supplementary Figure S17. The AUG-Stop system in Col-0 ACE. **(A)** The 306-nt 5'-UTR sequence of *AtNIP5;1* (34). The uORFs are boxed and the start codon of *AtNIP5;1* is double-underlined. The nucleotide substituted in *AUCUAA* mutant is indicated. **(B)** Schematic representation of *5'-NIP5;1:LUC* RNA used for reporter assay (Figure 7D). The 306-nt 5'-UTR sequence was joined to the *LUC* reporter gene through a linker, CC. **(C)** *5'-NIP5;1:LUC(AUGUAA)* and *5'-NIP5;1:LUC(AUCUAA)* RNAs were translated in Col-0 ACE for 120 min at various boric acid concentrations. LUC activity was normalized with control RLUC activity from co-translated *RLUC* RNA, and the reporter activity relative to that without boric acid was calculated. Asterisks indicate significant differences at each boric acid concentration ($p < 0.05$, Welch's *t*-test).

Supplementary Table S1. Plasmids used in this study and primers used to construct plasmids.

Name	Construct ^a	Source	Primers ^b	
			Forward	Reverse
<i>Plasmids used for construction of transgenic Arabidopsis</i>				
pYTJ10	<i>uL4D::uL4D(WT):FLAG</i>	this study	uL4Df	uL4Dr
pYTJ1	<i>uL4D::uL4D(R77A):FLAG</i>	this study	R77Af	R77Ar
pYTJ7	<i>uL4D::uL4D(ATV):FLAG</i>	this study	dTVf	dTVr
pYTJ4	<i>uL4D::uL4D(Δloop):FLAG</i>	this study	dLoopf	dLoopr
<i>Plasmids used for stalling assay</i>				
pST00	<i>SP6::M8:His:HA:DP75</i>	this study	DP75f	DP75r
pST55	<i>SP6::M8:His:HA:DP75:AAP(WT)</i>	this study	AAPf	AAPr
pST56	<i>SP6::M8:His:HA:DP75:AAP(D12N)</i>	this study	D12Nf	AAPr
pST57	<i>SP6::M8:His:HA:DP75:hCMV(WT)</i>	this study	hCMVf	hCMVr
pST58	<i>SP6::M8:His:HA:DP75:hCMV(P21A)</i>	this study	hCMVf	P21Ar
pST76	<i>SP6::M8:His:HA:DP75:S-uORF(WT)</i>	this study	SAMDC1f	SAMDC1r
pST77	<i>SP6::M8:His:HA:DP75:S-uORF(fs)</i>	this study	SAMDC1fsf	SAMDC1fsr
pST116	<i>SP6::M8:His:HA:DP75:MAGDIS(WT)</i>	this study	DP75f	MAGDISr
pST117	<i>SP6::M8:His:HA:DP75:MAGDIS(I5L)</i>	this study	DP75f	I5Lr
pTI5	<i>SP6::M8:His:HA:3xFLAG:Myc:DP75:AAP(WT)</i>	this study	3xFLAGf	3xFLAGr
pTI6	<i>SP6::M8:His:HA:3xFLAG:Myc:DP75:AAP(D12N)</i>	this study	3xFLAGf	3xFLAGr
pNU14	<i>SP6::GST:S-uORF(WT):RLUC</i>	Ref. 31		
pNU15	<i>SP6::GST:S-uORF(fs):RLUC</i>	Ref. 31		
pYF2	<i>SP6::GST:CGS1(WT)</i>	Ref. 68		
pYF3	<i>SP6::GST:CGS1(mto1-1)</i>	Ref. 68		
pYK00	<i>SP6::M8:CGS1(WT)</i>	Ref. 18		
pYY105	<i>T7::His:HA:DP75:uORF2(WT)</i>	Ref. 43		
<i>Plasmids used for reporter assay</i>				
pST118	<i>SP6::mAMD1 5'-UTR(WT):LUC</i>	this study	MAGDIS(WT)f	MAGDIS(WT)r
pST119	<i>SP6::mAMD1 5'-UTR(I5L):LUC</i>	this study	MAGDIS(I5L)f	MAGDIS(WT)r
pST120	<i>SP6::AtAMD1 5'-UTR(WT):LUC</i>	this study	SAMDC1f2	SAMDC1r2
pST121	<i>SP6::AtAMD1 5'-UTR(fs):LUC</i>	this study	SAMDC1f2	SAMDC1r2
pST122	<i>SP6::gp48 5'-UTR(WT):LUC</i>	this study	hCMVf2	hCMVr2
pST123	<i>SP6::gp48 5'-UTR(P21A):LUC</i>	this study	hCMVf2	P21Ar2
pMI21	<i>SP6::CGS1:LUC(WT)</i>	Ref. 22		
pMI27	<i>SP6::RLUC</i>	Ref. 22		
pMT131	<i>SP6::AtNIP5;1 5'-UTR(WT):LUC</i>	Ref. 34		
pMT132	<i>SP6::AtNIP5;1 5'-UTR(ATCTAA):LUC</i>	Ref. 34		
pSY209	<i>SP6::S-uORF(WT):RLUC</i>	Ref. 31		
pSY214	<i>SP6::S-uORF(fs):RLUC</i>	Ref. 31		

^aDouble colons indicate fusion of promoter sequence and an ORF, and single colons indicate an in-frame translational fusion (*i.e.*, *Promoter::ORF:ORF: ...*).

^bPrimers used for construction. Sequences of the primers are listed in Supplementary Table S2.

Supplementary Table S2. Primers used in this study.

Name	Sequence (5' to 3')	Source
<i>Plasmid construction</i> ^a		
uL4Df	CACCGGAGTATTGTTGCCCTTTGTGAA	this study
uL4Dr	CTGACTAGCGCCAAGCCACTT	this study
R77Af	ACCGGAGCTGCCGTGTCACGTA	this study
R77Ar	GTGACACGGCAGCTCCGGTT	this study
dTVf	TGGGGAGGAAGAGCCTCACGTATCCCTCGTGTT	this study
dTVr	GTGAGGCTCTTCTCCCAGGACTCGGC	this study
dLoopf	TCCGCCGAAGAGCCGGTGGTGAACCTACCG	this study
dLoopr	ACCGGCTCTTCCGGCGAGGTTTGGTGA	this study
uL4Flankf	CACCGGAGTATTGTTGCCCTTTGTGAA	this study
uL4Flankr	CTGACTAGCGCCAAGCCACTT	this study
DP75f	GATTCTAGACATCATCATCATCATTACCC	this study
DP75r	CATGGATCCGGCCATTCTGATATCCATTTCAATTTTATTGCTACT	this study
AAPf	CATGATATCATGAACGGTCGCCGTCAGTCTTCACTAGTCAGGATTACCTCTCAGACC ATC	this study
AAPr	CTAGGATCCGAGAGGCTCTCACGCGTTAAGGGCTCTCCACAGATGGTCTGAGAGG	this study
D12Nf	CATGATATCATGAACGGTCGCCGTCAGTCTTCACTAGTCAGAATTACCTCTCAGACC ATC	this study
hCMVf	CATGATATCATGGAACCGCTGGTGCTGAGTGCAGAAAACTGAGCAGCCTGCTGAC	this study
hCMVr	CTAGGATCCTCGAGTGCTTTAAGGAGGAATATTTGCAGGTCAGCAGGC	this study
P21Ar	CTAGGATCCTCGAGTGCTTTAAGGAGCAATATTTGCAGGTCAGCAGGC	this study
hCMVf2	GATTCTAGAAATCAGTTGCCGGCCTTACCATGGAACCGCTGGTGCTGAGTGCAGAAAA ACTGAGCAGCCTGCTGACCTGC	this study
hCMVr2	CATAAGCTTACCCAGACAACGGTGCTTTATAGACTCATCACTTAAGGAGGAATATATT TGCAGGTCAGCAGGC	this study
P21Ar2	CATAAGCTTACCCAGACAACGGTGCTTTATAGACTCATCACTTAAGGAGCAATATATT TGCAGGTCAGCAGGC	this study
SAMDC1f	CATGATATCATGATGGAGTCGAAAGGTG	this study
SAMDC1r	CTAGGATCCTCAGGATGGCCTCTTGGA	this study
SAMDC1fsf	CATGATATCATGATGGAGCGAAAGGTG	this study
SAMDC1fsr	CTAGGATCCTCAGGATGGCCTCTTGGA	this study
SAMDC1f2	GATTCTAGATCTCATTGCTTCATCATTACCA	this study
SAMDC1r2	CATCCATGGCTCGCCTTGTGTGTGAG	this study
MAGDISr	CATGGATCCCTAGCTAATGTCGCCGGCCATGATATCCATTT	this study
I5Lr	CATGGATCCCTAGCTAAGGTGCGCCGGCCATGATATCCATTT	this study
MAGDIS(WT)f	GATTCTAGACTTACACAGTATGGCCGGCGACATTAGCTAGCGCTCGCTCTACTCTCTC TAACGGGGAAACAG	this study
MAGDIS(I5L)r	GATTCTAGACTTACACAGTATGGCCGGCGACATTAGCTAGCGCTCGCTCTACTCTCTC TAACGGGGAAACAG	this study
MAGDIS(WT)r	CATCCATGGTGGAAATAGAGGCAGATACAGCTCAGTCTTGTAGTCCGCTGTTTCCC CGTTAG	this study
Myc:DP75f	TCAGAGGAGGACCTGGAAGGTGGCGAAGAAGAAGTTGAG	this study
HAMycr	GATCAGCTTCTGCTCAGCGTAATCTGGAACATCGTATGGG	this study
Mycf	GAGCAGAAGCTGATCTCAGAGGAG	this study
HAr	AGCGTAATCTGGAACATCGTATGGG	this study
3xFLAGf	GTTCCAGATTACGCTGACTACAAAGACCATGACGGTGATTATAAAGATCATGACATCG ACTACAAAGACG	this study
3xFLAGr	GATCAGCTTCTGCTCCTTGTGTCATCGTCTTTGTAGTCCGATGTCATGATC	this study
<i>Generating DNA templates for in vitro transcription</i>		
SP65'fp	CATCAGAGCAGATTGTAAGT	Ref. 18
G183r	ACCGCATGAACAGT	this study
poly(A)r	ACGAGCCGGAAGCATAAAG	this study
<i>Quantitative RT-PCR</i>		
RT-uL4Af	AAGAAGAAGGGGTATGTGCT	this study
RT-uL4Ar	CACCGAGCCATTTGGTGAAGT	this study
RT-uL4Df	GGGTTAAGGCTAAGAAGGAG	this study

RT-uL4Dr	<u>TCGGTGTAGTCACTGTCTGA</u>	this study
RT-FLAGf	<u>ACAGTGACTACACCGAGTTC</u>	this study
RT-FLAGr	<u>TCATCGTCATCCTTGTAGCT</u>	this study
UBQ5f	<u>GTGGTGCTAAGAAGAGGAAGA</u>	this study
UBQ5r	<u>TCAAGCTTCAACTCCTTCTTT</u>	this study

^aRestriction sites used for cloning the PCR-amplified fragments are underlined.

SUPPLEMENTARY REFERENCES

65. Geballe, A.P., Spaete, R.R. and Mocarski, E.S. (1986) A *cis*-acting element within the 5' leader of a cytomegalovirus β transcript determines kinetic class. *Cell*, **46**, 865–872.
66. International Wheat Genome Sequencing Consortium (2018) Shifting the limits in wheat research and breeding using a fully annotated reference genome. *Science*, **361**, eaar7191.
67. Murota, K., Hagiwara-Komoda, Y., Komoda, K., Onouchi, H., Ishikawa, M. and Naito, S. (2012) Corrigendum: Arabidopsis cell-free extract, ACE, a new in vitro translation system derived from Arabidopsis callus cultures. *Plant Cell Physiol.*, **53**, 602.
68. Haraguchi, Y., Kadokura, Y., Nakamoto, M., Onouchi, H. and Naito, S. (2008) Ribosome stacking defines *CGS1* mRNA degradation sites during nascent peptide-mediated translation arrest. *Plant Cell Physiol.*, **49**, 314–323.
69. Ruan, H., Shantz, L.M., Pegg, A.E. and Morris, D.R. (1996) The upstream open reading frame of the mRNA encoding *S*-adenosylmethionine decarboxylase is a polyamine-responsive translational control element. *J. Biol. Chem.*, **47**, 29576–29582.
70. Kozak, M. (1986) Point mutations define a sequence flanking the AUG initiator codon that modulates translation by eukaryotic ribosomes. *Cell*, **44**, 283–292.
71. von Arnim, A.G., Jia, Q. and Vaughn, J.N. (2014) Regulation of plant translation by upstream open reading frames. *Plant Sci.*, **214**, 1–12.
72. Crowe, M.L., Wang, X.Q. and Rothnagel, J.A. (2006) Evidence for conservation and selection of upstream open reading frames suggests probable encoding of bioactive peptides. *BMC Genomics*, **7**, 16.
73. Wethmar, K. (2014) The regulatory potential of upstream open reading frames in eukaryotic gene expression. *Wiley Interdiscip. Rev. RNA*, **5**, 765–778.
74. Kozak, M. (1999) Initiation of translation in prokaryotes and eukaryotes. *Gene*, **234**, 187–208.
75. Kozak, M. (2002) Pushing the limits of the scanning mechanism of initiation of translation. *Gene*, **299**, 1–34.
76. Joshi, C.O., Zhou, H., Huang, X. and Chiang, V.L. (1997) Context sequences of translation initiation codon in plants. *Plant Mol. Biol.*, **35**, 993–1001.
77. Kozak, M. (1987) Effects of intercistronic length on the efficiency of reinitiation by eukaryotic ribosomes. *Mol. Cell. Biol.*, **7**, 3438–3445.